Gang Lin

On the Design and Optimization of OFDM Systems

Thesis for the degree philosophiae doctor

Trondheim, October 2006

Norwegian University of Science and Technology
Faculty of Information Technology, Mathematics
and Electrical Engineering
Department of Electronics and Telecommunications

NTNU
Innovation and Creativity

NTNU
Norwegian University of Science and Technology

Thesis for the degree philosophiae doctor

Faculty of Information Technology, Mathematics and Electrical Engineering
Department of Electronics and Telecommunications

© Gang Lin

ISBN 82-471-8167-3 (printed version)
ISBN 82-471-8166-5 (electronic version)
ISSN 1503-8181

Doctoral theses at NTNU, 2006:196

Printed by NTNU-trykk

On the Design and Optimization of OFDM Systems

Gang Lin

A Dissertation Submitted in Partial Fulfillment
of the Requirements for the Degree of
Philosophiae Doctor
· 2006 ·

Department of Electronics and Telecommunications
Norwegian University of Science and Technology

NTNU
Innovation and Creativity

Abstract

In this thesis, some selected aspects of OFDM systems have been investigated. We focus on the modulation and demodulation techniques, such as efficient equalization, robustness to carrier frequency offset (CFO) and CFO estimation.

An OFDM/OQAM system with pulseshaping can achieve higher spectrum and power efficiency than conventional OFDM/QAM systems with guard interval, while it needs more complicated equalizer to counteract the multipath effects. We derive some theoretical expressions that are useful for selecting appropriate equalizer length. This allows an efficient equalization with a complexity only slightly higher than that of OFDM/QAM systems with guard interval.

OFDM systems are much more sensitive to CFO than single carrier systems. The robustness to CFO of OFDM systems can be improved by using appropriate pulseshaping. The optimal pulseshapes are found by variational calculus or numerical optimization methods. We find that even when using these optimal pulses, the effects caused by uncompensated CFO can not be completely eliminated.

Traditionally, the CFO is estimated before demodulation. For an OFDM system with many subchannels, each subchannel can be viewed as flat-fading, thus the problem of CFO estimation can be simplified based on subchannel signals. We propose several blind CFO estimation methods for OFDM/OQAM systems based on subchannel signals. Numerical simulations are performed to illustrate the performance of the suggested CFO estimation methods and validate the theoretical analysis. Simulation results show that better performance can be achieved based on estimation of subchannel signals than that based on channel signal before demodulation.

Preface

This thesis is submitted in partial fulfillment of the requirements for the degree of *Philosophiae Doctor* at the Norwegian University of Science and Technology (NTNU).

The research was carried out in the period from October 2002 to November 2006 at the Department of Electronics and Telecommunications, NTNU. The work was funded by Norwegian Research Council (NFR) through the BEATS project. Associate Professor Lars Lundheim and Professor Nils Holte, the Department of Electronics and Telecommunications, NTNU, have been main and co-supervisor respectively.

Acknowledgments

I am indebted to my two supervisors, Associate Professor Lars lundheim and Professor Nils Holte, the Department of Electronics and Telecommunications, the Norwegian University of Science and Technology (NTNU), who have initiated ideas, encouraged and given support during the course of work.

I would like to thank the manager of BEATS project, Professor Geir Øien, the Department of Electronics and Telecommunications, NTNU, for his support during this period.

I am particularly grateful to Mrs. Kirsten Marie Ekseth, the secretary of the Signal Processing Group, the Department of Electronics and Telecommunications, NTNU. She helped me with many practical matters both at my arrival and during my studies, and made my life in Trondheim much easier.

I also would like to thank Ph.D. student Saeeid Tahmasbi Oskuii, who shares the same office with me and has raised many useful discussions in study, life and culture. I would like to thank postdoctor Bojana Gajic and Ph.D. students Greg Harald Håkonsen, Fredrik Hekland, Duc Van Duong, Anna Kim and Øystein Birkenes, for their help in study and leisure time.

All the employees of the Signal Processing Group of the Department of Electronics and Telecommunications have contributed to a friendly and inspiring atmosphere which has been highly appreciated.

Finally, I would like to thank my family, especially my parents Chang-Tong Lin and Shao-Fen Zhang, and my wife Liping Huang.

Contents

Abstract iii

Preface v

Acknowledgments vii

List of Nomenclature xix

1 Introduction 1
- 1.1 Scope of the thesis 3
- 1.2 Outline of the thesis 4

2 Fundamental Principles 7
- 2.1 OFDM/QAM systems with rectangular pulseshaping 7
  - 2.1.1 Time-continuous model 7
  - 2.1.2 Time-discrete model without guard interval 9
  - 2.1.3 Time-discrete model with guard interval 9
- 2.2 OFDM/OQAM systems with pulseshaping 11
  - 2.2.1 Time-continuous model 12
  - 2.2.2 Time-discrete model 16
- 2.3 Comparison of OFDM/QAM and OFDM/OQAM 22
  - 2.3.1 Implementation complexity 22
  - 2.3.2 Transmission delay 24
  - 2.3.3 Spectrum and power efficiency 25
  - 2.3.4 Equalization over a multipath channel 26
  - 2.3.5 Summary and quantitative comparison 26

3 Efficient Equalization for OFDM/OQAM Systems 29
- 3.1 Model for OFDM/OQAM systems with single branch equalizer 30
- 3.2 Equalizer optimization 32
  - 3.2.1 Normal equation for general OFDM/OQAM systems 33

3.2.2 Normal equation for unweighted OFDM/OQAM systems . . . 34
3.3 MMSE versus equalizer length . . . 37
3.3.1 MMSE for one-tap equalizer . . . 38
3.3.2 MMSE for infinite-tap equalizer . . . 39
3.3.3 MMSE for finite-tap equalizer . . . 39
3.3.4 Example: MMSE of a two-path transmitting channel 41
3.4 Conclusion . . . 46

4 Design of Optimal Pulses Robust to CFO for OFDM Systems 51
4.1 Optimal pulse robust to CFO for OFDM/QAM systems . . 53
4.1.1 System description and interference model . . . 53
4.1.2 Optimal pulses robust to CFO . . . 54
4.1.3 Comparison of different pulses for OFDM/QAM systems . . . 58
4.2 Optimal pulse robust to CFO for OFDM/OQAM systems . 64
4.2.1 System description and interference model . . . 64
4.2.2 Design of optimal pulses robust to CFO . . . 68
4.2.3 Numerical results . . . 73
4.3 Conclusion . . . 75

5 Blind CFO Estimation for OFDM/OQAM Systems 79
5.1 System model and second- and high-order statistics of subchannel signals . . . 81
5.1.1 System description and definitions . . . 81
5.1.2 Second-order statistics of subchannel signals . . . 83
5.1.3 High-order statistics of subchannel signals . . . 85
5.2 Estimation methods . . . 86
5.2.1 Estimation methods based on null-subchannels . . . 87
5.2.2 Estimation methods based on interleaved weighting 92
5.2.3 CFO estimation methods based on high-order statistics for unweighted systems . . . 94
5.3 Asymptotic analysis . . . 95
5.3.1 Asymptotic analysis of correlation function based estimators . . . 97
5.3.2 Asymptotic analysis of conjugate correlation function based estimator . . . 99
5.4 Simulation results . . . 100
5.4.1 Comparison of null-subchannel based estimators over an AWGN channel . . . 101

5.4.2 Comparison of null-subchannel based estimators over a time-invariant multipath channel (and comparison with the modified Bölcskei's estimator) . . . 105
5.4.3 Comparison of null-subchannel based estimators over a Rayleigh multipath channel 108
5.4.4 Comparison of conjugate correlation function based estimators over an AWGN channel 109
5.4.5 Performance simulation of high-order statistics based estimation method 111
5.5 Conclusion 113

6 Conclusion 115
6.1 Contributions of the thesis 116
6.2 Future work 116

A Derivation of expressions for $c_{u_r}[\tau]$ and $c_{u_{ri}}[\tau]$ 119

B Derivation of approximate formula for MMSE versus K 123

C Series sum approximation 127

D Proof of $\sum_{m=0}^{N-1} A_{m,k}(\tau, f_e)$ to be real-valued and independent of f_e 129

E Proof of $\sum_{m=0}^{N-1} \widetilde{A}_{m,k}(\tau, f_e) = 0$ 131

F Derivation of explicit expressions for $\lim_{M\to\infty} M\,\mathbb{E}\big[\Delta c_k[\tau_1]\,\Delta c_k^*[\tau_2]\big]$ and $\lim_{M\to\infty} M\,\mathbb{E}\big[\Delta c_k[\tau_1]\,\Delta c_k[\tau_2]\big]$ 133
F.1 Time-invariant channel 134
F.2 Rayleigh fading channel 135

G Derivation of asymptotic MSE for conjugate correlation function based method 137

H Derivation of calculable expressions for $S_{e_k}(f_e + 1/2, \tau_1, \tau_2)$ and $\widetilde{S}_{e_k}(f_e + 1/2, \tau_1, \tau_2)$ 141

List of Figures

1.1 Block diagram of a digital communication system. 4

2.1 Time-continuous model for OFDM/QAM systems. 8
2.2 FFT based implementation scheme for OFDM/QAM systems with guard interval. 11
2.3 Time-continuous model for OFDM/OQAM systems. 13
2.4 Time-discrete model for OFDM/OQAM systems. 17
2.5 Filterbank based model for time-discrete OFDM/OQAM systems. 20
2.6 FFT and polyphase filterbank based scheme for OFDM/OQAM systems. 23
2.7 Block diagram of OFDM transmission systems. 24
2.8 Comparison of implementation complexity of OFDM/QAM and OFDM/OQAM. 27

3.1 Time-discrete model for OFDM/OQAM systems with a single branch equalizer. 31
3.2 Average MMSE $\overline{J_{\mathrm{min}}}(K)$ of one and infinite-tap equalizers versus second path attenuation factor α with SNR as parameter ($\tau_{\mathrm{n}} = 1/16$ for the one-tap equalizer). 42
3.3 Average MMSE $\overline{J_{\mathrm{min}}}(K)$ of one and infinite-tap equalizer versus normalized delay spread τ_{n} with attenuation factor α and SNR as parameters. 44
3.4 Average MMSE $\overline{J_{\mathrm{min}}}(K)$ versus normalized delay spread τ_{n} with equalizer length $2K + 1$ as parameter (SNR = 40 dB). 45
3.5 Average MMSE $\overline{J_{\mathrm{min}}}(K)$ versus equalizer length $2K+1$ with SNR and normalized delay spread τ_{n} as parameters ($\alpha = 0.5$). 47
3.6 Average MMSE $\overline{J_{\mathrm{min}}}(K)$ versus SNR with equalizer length $2K+1$ and normalized delay spread τ_{n} as parameters ($\alpha = 0.5$). 48

4.1 Model of OFDM transmission systems with carrier recovery and symbol synchronizer. 51

4.2 Comparison of different pulses ($\beta = 0.2$) (the optimal pulse overlaps with Franks' pulse). 60
4.3 Comparison of different pulses ($\beta = 1.0$). 61
4.4 Comparison of average ICI power and SIR versus subchannel index k for different pulses with roll-off factor β as parameter. 62
4.5 Average ICI power and SIR versus CFO of subchannel 31 for different pulses with roll-off factor β as parameter (for $\beta = 0.2$, the curves of optimal pulse and Franks' pulse overlap with the lower or upper bound). 63
4.6 Pulse shapes in time and frequency domain. 74
4.7 Comparison of total interference and SIR versus normalized CFO. 76

5.1 Time-discrete model for a critically sampled OFDM/OQAM system with carrier frequency offset and subchannel weighting. 82
5.2 Curves of $M_g(\tau, f_e)$ for $\tau = 0, 1, 2$ with square root raised cosine pulse (with a roll-off factor denoted α) as shaping filter 89
5.3 Curves of $|\widetilde{A}_{k,k}(\tau, f_e)|$ with square root raised cosine pulse (with a roll-off factor denoted α) as shaping filters. 93
5.4 Curves of $|B(\tau_1, \tau_2, \tau_3, f_e)|$ versus f_e with raised cosine pulses (with a roll-off factor denoted α) as shaping filters (the curves for $(\tau_1, \tau_2, \tau_3) = (0, 0, 1)$ and $(\tau_1, \tau_2, \tau_3) = (1, 1, 1)$ are overlapped). 96
5.5 MSE versus SNR for Method 1-3 over an AWGN channel ($M = 256$, $f_e = 0.2$ and subchannel 4 is set as the only null-subchannel). 102
5.6 MSE versus f_e for Method 1-3 over an AWGN channel ($M = 256$, SNR$=$ 40 dB and subchannel 4 is set as the only null-subchannel). 103
5.7 MSE versus data records length M for Method 1-3 over an AWGN channel with f_e and SNR as parameters (subchannel 4 is set as the only null-subchannel). 104
5.8 Magnitude response of a three-path multipath channel with attenuation factors $\begin{bmatrix}\lambda_0 & \lambda_1 & \lambda_2\end{bmatrix} = \frac{1}{\sqrt{21}}\begin{bmatrix}4 & 2 & -1\end{bmatrix}$. 106
5.9 Performance comparison of Method 1-3 and modified Bölcskei estimator over a fixed multipath (MP) channel ($M = 256$, $f_e = 0.2$ and subchannel 4 is set as the only null-subchannel). 107

5.10 Performance comparison of Method 1-3 and modified Bölcskei estimator over a random time-invariant multipath (MP) channel ($M = 256$, $f_e = 0.2$ and subchannel 1, 5, 9 ,13 are set as null-subchannels). 108
5.11 Performance comparison of Method 1-3 over a Rayleigh ($B_\lambda T = 0.01$) multipath channel ($M = 256$, $f_e = 0.2$ and subchannel 4 is set as the only null-subchannel). 110
5.12 Performance comparison of Method 3, 4 and the modified C/S estimator over an AWGN channel ($M = 512$, $f_e = 0.2$ and subchannel 4 is set as the only null-subchannel for Method 3). 111
5.13 Magnitude response of a five-path multipath channel with attenuation factors $\begin{bmatrix}\lambda_0 & \lambda_1 & \lambda_2 & \lambda_3 & \lambda_4\end{bmatrix} = \begin{bmatrix}0.8627 & 0.4313 & -0.1078 & -0.2157 & -0.1078\end{bmatrix}$. 112
5.14 Comparison of MSE versus SNR of Method 5 over an AWGN and a time-invariant multipath channel ($M = 1024$, $f_e = 0.2$).113

List of Tables

2.1 A comparison of OFDM/QAM and OFDM/OQAM. 26

5.1 A summary of different blind CFO estimation methods for OFDM/OQAM systems. 114

List of Nomenclature

CFO	carrier frequency offset
CSNR	channel signal-to-noise ratio
DFT	discrete Fourier transform
DTFT	discrete-time Fourier transform
FDM	frequency division multiplex
FFT	fast Fourier transform
FSK	frequency shift keying
ICI	interchannel interference
IFFT	inverse fast Fourier transform
ISI	intersymbol interference
LMS	least mean square
LTI	linear time-invariant
MMSE	minimum mean square error
MSE	mean square error
OFDM	orthogonal frequency division multiplex
OQAM	offset quadrature amplitude modulation
QAM	quadrature amplitude modulation
PAM	pulse amplitude modulation
PAPR	peak to average power ratio
PSK	phase shift keying
PSWFs	prolate spheroidal wave functions
SFN	single-frequency network
SIR	signal-to-interference ratio
SNR	signal-to-noise ratio
VSB	vestigial sidelobe
WSS	wide-sense stationary
α	1) roll-off factor of raised cosine pulse 2) path attenuation factor
β	roll-off factor of pulse
Δ	length of guard interval
Γ_k	interference coefficient

$\Gamma_{m,k}[n]$	interference coefficient
κ_4	fourth order cumulant
$\Lambda_{m,k}[n]$	interference coefficient
$\nu[l]$	time-discrete channel noise
$\nu^{(o)}[l]$	filtered channel noise
$\nu[s]$	down-sampled version of $\nu^{(o)}[l]$
$\psi_i(t)$	prolate spheroidal wave function number i
φ	phase shift
σ_a^2	average power of transmitted symbols
σ_{ICI}^2	average ICI power
σ_{ISI}^2	average ISI power
σ_ν^2	variance of channel noise
τ_c	path delay
τ_l	path delay
τ_n	normalized path delay

$a_k[n]$	transmitted symbol at time n and subchannel k
$\tilde{a}_k[n]$	received symbol at time n and subchannel k
$a_k^{\mathcal{R}}[n]$	real part of transmitted symbol at time n and subchannel k
$\tilde{a}_k^{\mathcal{R}}[n]$	real part of received symbol at time n and subchannel k
$a_k^{\mathcal{I}}[n]$	imaginary part of transmitted symbol at time n and subchannel k
$\tilde{a}_k^{\mathcal{I}}[n]$	imaginary part of received symbol at time n and subchannel k
c_l	path attenuation factor
$c_k(t)$	time-continuous equalizer in subchannel k at receiver side
D_T	transmission delay
$f(t)$	time-continuous receiver filter
$f[l]$	time-discrete receiver filter
$f_k[l]$	time-discrete receiver filter of subchannel k
f_e	carrier frequency offset
$\hat{f}_e$	estimated carrier frequency offset
$\mathbf{F}$	normalized DFT matrix
$F(z)$	z transform of $f[l]$
$F_k(z)$	z transform of $f_k[l]$
$g(t)$	time-continuous transmitter filter
$g[l]$	time-discrete transmitter filter
$g_k[l]$	time-discrete transmitter filter of subchannel k
G	normalized length of guard interval
$G(z)$	z transform of $g[l]$
$G_k(z)$	z transform of $g_k[l]$
$G_{m,n}$	interference coefficient

$h(t)$	time-continuous channel impulse response
$h[l]$	time-discrete channel impulse response
$H(f)$	Fourier transform of $h(t)$
$H_{m,n}$	interference coefficient
$\mathbf{H}$	Channel matrix
l	time index
L_g	length of shaping filter
M	length of data record
n	time index
N	number of subchannels
N_g	number of guard subchannels
$p_{m,k}(t)$	time-continuous equivalent overall response from subchannel m at transmitter side to subchannel k at receive side
$p^{(o)}_{m,k}[l]$	time-discrete equivalent overall response from subchannel m at transmitter side to subchannel k at receive side
$p_{m,k}[s]$	down-sampled version of $p^{(o)}_{m,k}[l]$
$p^{\mathcal{R}}_{m,k}[s]$	real part of $p_{m,k}[s]$
$p^{\mathcal{I}}_{m,k}[s]$	imaginary part of $p_{m,k}[s]$
$P_{m,k}(f)$	DTFT of $p_{m,k}[s]$
$q[l]$	time-discrete transmitted signal
$r(t)$	time-continuous received signal
$r[l]$	time-discrete received signal
$\mathbf{R}$	correlation matrix
$s(t)$	time-continuous transmitted signal
$s[l]$	time-discrete transmitted signal
$S(z)$	z transform of $s[l]$
t	time
T	OFDM symbol interval
T_s	sample interval
$u[s]$	time-discrete received subchannel signal
$\mathbf{u}_n$	vector of $u[s]$
$\mathbf{u}_{r,n}$	real part of $\mathbf{u}_n$
$\mathbf{u}_{i,n}$	imaginary part of $\mathbf{u}_n$
w_k	1) equalizer coefficient 2) subchannel weighting factor
$\mathbf{w}$	vector of w_k
$\mathbf{w}_r$	real part of $\mathbf{w}$
$\mathbf{w}_i$	imaginary part of $\mathbf{w}$
$x[l]$	time-discrete transmitted signal

Chapter 1

Introduction

The conception of orthogonal frequency division multiplex (OFDM) appeared in the end of the 1950s for the purpose of military communications [DHM57, FL61]. For a long time, the applications of OFDM systems were quite limited due to the high implementation complexity. In 1971, Weinstein and Ebert suggested an OFDM implementation based on Fast Fourier Transform (FFT) [WE71]. This milestone work dramatically reduced the implementation complexity of OFDM systems. Due to further progress in implementation technology and demand for better bandwidth efficiency, OFDM became popular for practical applications around 1990.

The basic idea of OFDM is to spread a wideband high-data-speed stream over a large number of narrow-band low-data-speed subchannels. In conventional frequency division multiplex (FDM) systems, subchannels are completely separated in the frequency domain, therefore they do not interfere with each other. For OFDM systems, there exists overlap between different subchannels and orthogonality is guaranteed by appropriately choosing transmitter and receiver filters. The advantages of OFDM are listed as follows:

- Bandwidth efficient. Because no guard band is needed between adjacent subchannels, OFDM can achieve a spectrum efficiency close to the Nyquist limit;
- Power efficient. Due to the narrow-band property of subchannels, OFDM can achieve a power efficiency close to the Shannon limit by employing water-filling power allocation;
- Robust to frequency selective fading. By mapping a high-data-speed stream into many parallel low-data-speed sequences, the symbol duration of OFDM systems is greatly extended. This makes OFDM less sensitive to time-dispersive channels due to the reduced relative

delay spread. In addition, channel coding and error correction techniques over subchannels can be easily implemented to correct the error caused by deep fading in some subchannels;

- Robust to impulse noise. The duration of OFDM symbols is much longer than that of single carrier systems. For a channel with strong impulse noise, the transmitted symbols can still be largely recovered since only a small fraction of each symbol is interfered by noise. Thus OFDM is more robust to impulse noise than single carrier systems;
- Robust to narrow-band noise. Narrow-band noise will interfere with only some subchannels. Then we can just omit these interfered subchannels, or use channel coding and error correction technique to correct the errors caused by these subchannels. Therefore OFDM is robust to narrow-band noise;
- Suited for broadcasting. Single-frequency network (SFN) is a common type of radio network for broadcasting. In such networks, all transmitters are precisely synchronized and radiate the same signal on the same frequency band. A receiver may thus receive several signals with different delays. Since the symbol duration of OFDM systems has been greatly extended, these delays will cause only a phase shift, so that reception from different transmitters will be equivalent to multipath reception from one single transmitter.

Due to these advantages, OFDM has now been adopted in many cabled and wireless communication systems:

- Broadband systems based on twisted copper cables: High-Bit-Rate Digital Subscriber Lines (HDSL) [G 998], Asymmetric Digital Subscriber Lines (ADSL) [G 999], Very-High-Speed Digital Subscriber Lines (VDSL) [G 904];
- European Digital Audio Broadcasting (DAB) [EN 01], Terrestrial Digital Video Broadcasting (DVB-T) [EN 04];
- Wireless Local Area Network (WLAN) [Std97].

One disadvantage of OFDM systems is the high peak-to-average power ratio (PAPR) since the transmitted signal is the sum of many subchannel signals. This leads to the necessity of a power amplifier with linear characteristics in a large dynamic range, otherwise the signal clipping at high levels will distort the transmitted signal and yield out-of-band emission. Another disadvantage of OFDM is the high sensitivity to carrier frequency offset (CFO). Since the bandwidth of each subchannel is only a small fraction of the total bandwidth, a small value of CFO will damage the orthogonality and yield serous interference. Thus a very precise CFO estimator is needed in OFDM systems.

There are mainly two different kinds of OFDM systems. The conventional OFDM systems are based on rectangular pulseshaping and quadrature amplitude modulation (QAM) in each subchannel, and a guard interval implemented by a cyclic prefix (or suffix). If the maximum delay of a multipath channel is shorter than the guard interval, there is no intersymbol interference (ISI) and interchannel interference (ICI) [Fau00], thus a simple multiplier in each subchannel is enough to recover the transmitted symbols. This kind of OFDM will be referred as OFDM/QAM. The insertion of a guard interval in OFDM/QAM systems will reduce the spectrum efficiency since less time is available for transmission of useful information. This also leads to reduced power efficiency. Furthermore, square pulses have large sidelobe level, so that an extra filtering at both ends of the band is needed to mitigate the out-of-band emission. This will further reduce the spectral efficiency. These drawbacks are avoided by using bandlimited pulseshapes, as first suggested in 1966 by Chang [Cha66], then generalized in 1967 by Saltzberg [Sal67]. To satisfy orthogonality, offset QAM (OQAM) is used as modulation in the subchannels. We will refer to this scheme as OFDM/OQAM. OFDM/OQAM with time-frequency well-localized pulseshapes seems an attractive alternative to conventional OFDM/QAM systems in future high-data-rate wireless applications [Bol].

It should be noted that there exists also a third type of OFDM systems that uses vestigial sideband (VSB) modulation and real symbols, and where the subchannel spacing is half of OFDM/OQAM systems [CG68]. This system has the same main properties and the same performance as OFDM/OQAM.

1.1 Scope of the thesis

A block diagram of a typical digital communication system is shown in Fig. 1.1.

The useful information signal is first processed by the source encoder to remove redundancy. Then the channel encoder adds redundancy to protect the information bit stream from errors during transmission. The modulator transforms the digital symbols into an analogue signal. Typical modulation techniques are Pulse Amplitude Modulation (PAM), Frequency Shift Keying (FSK) and Phase Shift Keying (PSK). The extension of PAM to the two-dimensional case is then QAM. In an OFDM system, each subchannel transmits one QAM sequence. Thus it can be viewed as a multiplex of

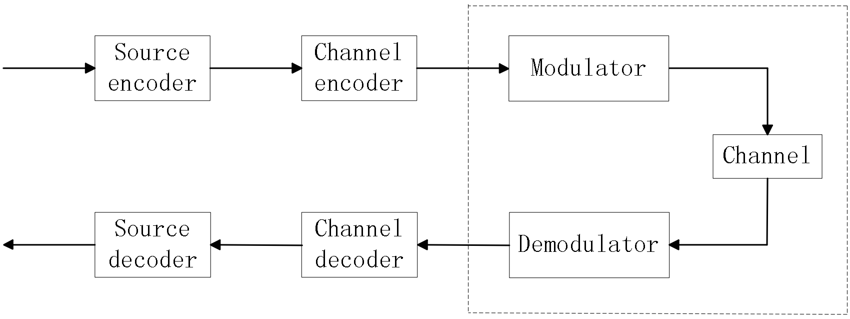

Figure 1.1: Block diagram of a digital communication system.

many parallel QAM streams. The channel distorts the transmitted signal and adds noise and interference. The demodulator transforms the analogue channel signal back to the information bit stream. The channel decoder then corrects the errors caused by the channel. At last the source decoder reconstructs the original information signal.

This thesis focuses on modulation, demodulation and the effect of the channel, i.e. the parts of the communication systems enclosed in the dashed lines in Fig. 1.1. Timing offset, finite-word-length effects and mismatch of the sampling rate in the pair of DAC and ADC are not considered. Neither the non-linear effects of power amplifier are taken into consideration.

In this thesis, we analyze and further develop OFDM systems. Different aspects of OFDM systems are considered. First the equalization problem for OFDM/OQAM systems is addressed. Due to the lack of guard interval, an equalizer in each subchannel is needed to counteract the multipath effects for OFDM/OQAM systems. We then derive some theoretical expressions that are suitable for selecting necessary equalizer length. OFDM systems are much more sensitive to CFO than single carrier systems. In order to increase the robustness to CFO for OFDM systems, we search for optimal pulseshapes. We find that the interference caused by CFO cannot be perfectly eliminated by using optimal pulseshapes. Thus the CFO should be estimated and compensated. In this thesis, we present several blind CFO estimation methods for OFDM/OQAM systems.

1.2 Outline of the thesis

The rest of this thesis is organized as follows:

- **Chapter 2:** Time-continuous and time-discrete models for OFDM systems are introduced and described. Efficient implementation based on FFT is also presented. A coarse comparison of OFDM/QAM and OFDM/OQAM is performed.

- **Chapter 3:** Some theoretical results suitable for selecting the equalizer length for OFDM/OQAM systems are derived. These theoretical expressions help to choose the necessary length of an equalizer, thus reduce the implementation complexity of OFDM/OQAM systems.

- **Chapter 4:** The sensitivity of OFDM systems to CFO is studied and optimal pulses robust to CFO are found analytically for OFDM/QAM and numerically for OFDM/OQAM. The sensitivity to CFO of OFDM/QAM and OFDM/OQAM is compared.

- **Chapter 5:** Blind CFO estimation methods for OFDM/OQAM systems are developed. Four methods are based on the second-order statistics, and one is based on the high-order statistics. The performance of proposed CFO estimation methods is compared with earlier suggested methods.

- **Chapter 6:** A conclusion of this thesis and proposals for future work are presented.

Chapter 2

Fundamental Principles

In this chapter, we introduce and describe the principles of OFDM systems. A comparison of OFDM/QAM with guard interval to OFDM/OQAM with pulseshaping is presented. This chapter establishes some notation and symbols that are used in subsequent chapters.

This chapter is organized as follows. First in section 2.1, a model for OFDM/QAM systems with rectangular pulseshaping and guard interval is described and an efficient implementation based on FFT is derived. Then, in section 2.2, we describe OFDM/OQAM systems with pulseshaping. An efficient implementation based on FFT and polyphase filterbank is derived. A simple comparison between OFDM/QAM and OFDM/OQAM is performed in section 2.3.

2.1 OFDM/QAM systems with rectangular pulseshaping

In this section, we will first describe a time-continuous model for OFDM/QAM systems with rectangular pulseshaping. Then we describe the time-discrete model and an efficient implementation based on FFT.

2.1.1 Time-continuous model

A time-continuous model for OFDM/QAM systems is shown in Fig. 2.1. In this chapter, we consider only rectangular pulseshapes. Note that smoother pulses are also suggested for OFDM/QAM systems to reduce the out-of-band emission and increase the robustness to CFO [LS95, TB04, SL05]. In this chapter, we focus on OFDM/QAM with rectangular pulseshapes.

This model has N subchannels and a subchannel spacing $1/T$. Each subchannel transmits one QAM symbol $a_k[n]$ every T seconds. The trans-

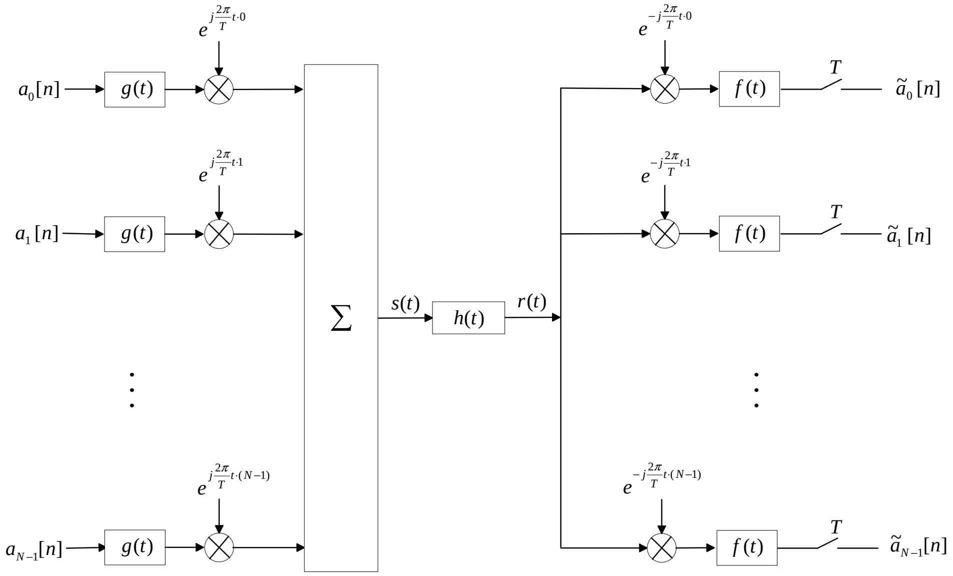
$e^{j\frac{2\pi}{T}t\cdot 0}$
$a_0[n]$
$g(t)$
$e^{j\frac{2\pi}{T}t\cdot 1}$
$a_1[n]$
$g(t)$
$e^{j\frac{2\pi}{T}t\cdot (N-1)}$
$a_{N-1}[n]$
$g(t)$
Σ
$s(t)$
$h(t)$
$r(t)$
$e^{-j\frac{2\pi}{T}t\cdot 0}$
$f(t)$
T
$\tilde{a}_0[n]$
$e^{-j\frac{2\pi}{T}t\cdot 1}$
$f(t)$
T
$\tilde{a}_1[n]$
$e^{-j\frac{2\pi}{T}t\cdot (N-1)}$
$f(t)$
T
$\tilde{a}_{N-1}[n]$

Figure 2.1: Time-continuous model for OFDM/QAM systems.

mitter $g(t)$ and receiver filter $f(t)$ are given by

$$f(t) = g(t) = \begin{cases} \frac{1}{\sqrt{T}} & -\frac{T}{2} \leq t \leq \frac{T}{2} \\ 0 & \text{otherwise.} \end{cases} \tag{2.1}$$

By summing up all symbols and all subchannels, the output signal $s(t)$ can be written as

$$s(t) = \sum_{k=0}^{N-1} \sum_{n=-\infty}^{\infty} a_k[n]\, g(t-nT)\, e^{j\frac{2\pi}{T}kt}. \tag{2.2}$$

We assume an ideal channel. Then the received signal $r(t) = s(t)$, and the received symbol can be expressed as

$$\begin{aligned} \tilde{a}_k[n] &= r(t)\, e^{-j\frac{2\pi}{T}kt} * f(t)\big|_{t=nT} \\ &= \sum_{m=0}^{N-1} \sum_{n'=-\infty}^{\infty} \int_{-\infty}^{\infty} a_m[n']\, g\big(\tau - n'T\big)\, f\big(nT-\tau\big) e^{j\frac{2\pi}{T}(m-K)\tau}\, d\tau \\ &= \sum_{m=0}^{N-1} a_m[n] \Big(\frac{1}{T} \int_{-T/2}^{T/2} e^{j\frac{2\pi}{T}(m-k)\tau}\, d\tau \Big) = a_k[n]. \end{aligned} \tag{2.3}$$

We see that the transmitted symbol $a_k[n]$ has been perfectly recovered. Thus the orthogonality is guaranteed even though there exists overlap in frequency between different subchannels.

2.1.2 Time-discrete model without guard interval

Time-continuous OFDM/QAM systems are practically prohibitive due to the high implementation complexity. On the contrary, time-discrete OFDM/QAM can be efficiently implemented based on FFT [LM94].

We consider the case of critical sampling, i.e. the systems operate at a sampling rate N/T. The time-discrete transmitter filter $g[l]$ and receiver filter $f[l]$ are given by

$$f[l] = g[l] = \begin{cases} \frac{1}{\sqrt{N}} & 0 \leq l < N \\ 0 & \text{others,} \end{cases} \tag{2.4}$$

Since there is no overlap between adjacent symbols, we consider only the nth OFDM symbol. By summing up all subchannels, the nth transmitted block can be written as

$$s[l] = \frac{1}{\sqrt{N}} \sum_{k=0}^{N-1} a_k[n]\, e^{j\frac{2\pi}{N}kl}. \tag{2.5}$$

We see clearly that $s[l]$ is the lth element of the normalized N-point IDFT of $\{a_k[n]\}_{k=0}^{N}$. The output block $s[l]$ is then transmitted over a time-discrete channel with an impulse response $h[l]$.

At the receiver side, the received sequence $r[l]$ is first down-converted by the subchannel modulator $e^{-j\frac{2\pi}{N}kl}$, then filtered by the receiver filter $f[l]$, and then sampled at instant $N-1$ to generate the recovered symbol:

$$\begin{aligned} \tilde{a}_k[n] &= r[l]\, e^{-j\frac{2\pi}{N}kl} * f[l]\big|_{l=N-1} \\ &= \frac{1}{\sqrt{N}} \sum_{l=0}^{N-1} r[N-1-l]\, e^{-j\frac{2\pi}{N}k(N-1-l)} \\ &= \frac{1}{\sqrt{N}} \sum_{l=0}^{N-1} r[l]\, e^{-j\frac{2\pi}{N}kl}. \end{aligned} \tag{2.6}$$

We see that the recovered symbol $\tilde{a}_k[n]$ is the kth element of the normalized N-point DFT of the received block $\{r[l]\}_{l=0}^{N-1}$. We assume that the channel is ideal, i.e. $h[l] = \delta[l]$ and there exists no noise. Then the received block $r[l] = s[l]$, and $\tilde{a}_k[n] = a_k[n]$ due to the invertibility of the DFT and IDFT pair.

2.1.3 Time-discrete model with guard interval

The multipath effects will cause ICI for an OFDM/QAM system without guard interval. One way to avoid ICI is to add a cyclic prefix [LM94].

Suppose we precede the output sequence $s[l]$ by G redundant symbols:

$$s_{-i} = s_{N-i}, \text{ for } 1 \leq i \leq G. \tag{2.7}$$

We assume that the length of guard interval G is longer than the length of the channel impulse response $h[l]$. Then the received sequence $r[l]$ can be expressed as the circular convolution of $s[l]$ and $h[l]$ given by

$$r[l] = s[l] \otimes h[l] = \sum_{l'=0}^{L} h[l']\, s[\mathrm{mod}(l - l', N)],\ 0 \leq l < N, \tag{2.8}$$

where L is the maximum delay of channel.

At the receiver side, the previous G symbols, i.e. $\{r[l]\}_{l=-G}^{-1}$, are discarded. The recovered symbols are obtained by taking the N-point DFT of $\{r[l]\}_{l=0}^{N-1}$. Then based on (2.5) and (2.8), we have

$$\tilde{a}_k[n] = H_k\, a_k[n], \tag{2.9}$$

where

$$H_k = \sum_{l=0}^{L} h[l]\, e^{-j\frac{2\pi}{N}kl} \tag{2.10}$$

is the kth element of the N-point DFT of $h[l]$.

We see that the received symbol $\tilde{a}_k[n]$ does not suffer from intersymbol interference (ISI) and interchannel interference (ICI) but it is attenuated by a factor H_k. Therefore only a multiplier in each subchannel is needed to recover the symbols. For a noise-free channel, the optimal multiplier is $1/H_k$ for subchannel k. This is called zero-forcing equalization. For the case of deep fading, $1/|H_k|$ becomes quite large and then the system suffers from serious noise enhancement. In this case, better performance can be obtained by using the minimum mean square error (MMSE) criterion instead of zero-forcing.

Finally, the FFT based implementation for OFDM/QAM systems with guard interval is depicted in Fig. 2.2. At the transmitter side, the transmitted symbol blocks with length N are converted to time domain by an IFFT module. Then a cyclic prefix with length G is added to the data blocks out of the IFFT module. Finally, the extended data blocks with length $N + G$ are converted to a serial sequence and sent to the channel. At the receiver side, the received serial channel signal is first converted to blocks with length $N + G$. Then the cyclic prefix is discarded and the left N symbols are converted back to frequency domain to obtain the recovered symbols.

Since not all transmitted symbols are used to convey information, there exists a certain SNR loss due to the insertion of the guard interval. For

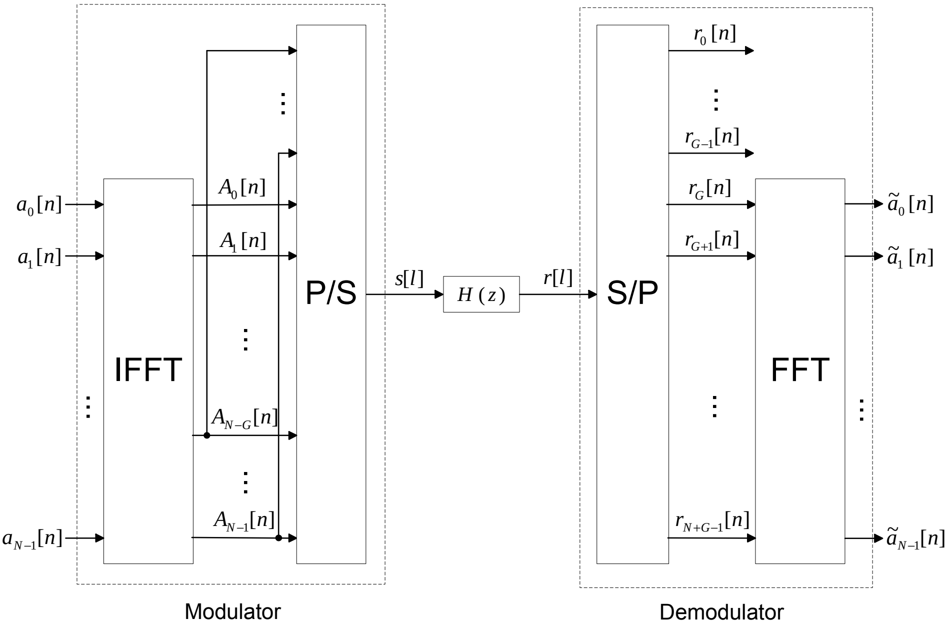
$a_0[n]$
$a_1[n]$
$a_{N-1}[n]$
IFFT
$A_0[n]$
$A_1[n]$
$A_{N-G}[n]$
$A_{N-1}[n]$
P/S
$s[l]$
$H(z)$
$r[l]$
S/P
$r_0[n]$
$r_{G-1}[n]$
$r_G[n]$
$r_{G+1}[n]$
$r_{N+G-1}[n]$
FFT
$\tilde{a}_0[n]$
$\tilde{a}_1[n]$
$\tilde{a}_{N-1}[n]$
Modulator
Demodulator

Figure 2.2: FFT based implementation scheme for OFDM/QAM systems with guard interval.

an AWGN channel, the guard interval will cause a loss (compared with a system without guard interval) in SNR given by [Vah95]

$$\mathrm{SNR}_{\mathrm{loss}} = 10\log\left(1+\frac{G}{N}\right)\ \mathrm{dB}. \tag{2.11}$$

Also due to the insertion of cyclic prefix, the symbol duration is elongated to $(1+G/N)\,T$ for the same subchannel spacing $1/T$, i.e. the data rate decreases by a factor $1+G/N$. This will cause a loss in bandwidth given by [Vah95]

$$\mathrm{BW}_{\mathrm{loss}} = 1+\frac{G}{N}. \tag{2.12}$$

2.2 OFDM/OQAM systems with pulseshaping

In the previous section, we have described both time-continuous and time-discrete models for OFDM/QAM systems. The insertion of guard interval makes OFDM/QAM immune to both ISI and ICI over a multipath channel provided the guard interval is longer than the maximum delay of channel. Then a simple multiplier in each subchannel is needed for an OFDM/QAM system with a long enough guard interval.

However, the insertion of guard interval reduces spectrum efficiency since less time is available for transmission of useful information. This also leads to lower power efficiency. Furthermore, the large sidelobe level of rectangular pulse makes the system spectrally incompact and thus an extra filter is needed to mitigate the out-of-band emissions. This additionally reduces the spectrum efficiency. These drawbacks are avoided by using bandlimited pulseshapes, as first suggested in 1966 by Chang [Cha66], then generalized to the complex constellation case in 1967 by Saltzberg [Sal67]. To satisfy orthogonality, offset QAM (OQAM) is used as modulation in the subchannels [Sal67, Hir80, VH96, BDH99]. We will refer to this scheme as OFDM/OQAM. Below we will describe this kind of OFDM systems in detail.

2.2.1 Time-continuous model

First we describe and analyze a time-continuous model for OFDM/OQAM systems.

A. System description

A time-continuous model for OFDM/OQAM systems is shown in Fig. 2.3. This model has N subchannels and a subchannel spacing $1/T$. Each subchannel transmits one QAM symbol $a_k[n] = a_k^{\mathcal{R}}[n] + j\, a_k^{\mathcal{I}}[n]$ every T seconds. The OQAM symbols are obtained by shifting the imaginary part $a_k^{\mathcal{I}}[n]$ by $T/2$. $g(t)$ and $f(t)$ are respectively the transmitter and receiver filters, and $h(t)$ is the channel impulse response.

At the transmitter side, by summing up all subchannels, the transmitted signal can be expressed as

$$s(t) = \sum_{k=0}^{N-1} \sum_{n=-\infty}^{\infty} \big(a_k^{\mathcal{R}}[n] g(t-nT) + j\, a_k^{\mathcal{I}}[n] g(t-nT-T/2)\big) e^{j(\frac{2\pi}{T}t+\frac{\pi}{2})k}. \quad (2.13)$$

Note that the phase factor $e^{j\frac{\pi}{2}k}$ in the subchannel modulator $e^{j(\frac{2\pi}{T}t+\frac{\pi}{2})k}$ is important to maintain the orthogonality between subchannels. In subchannel k at the receiver side, the received signal $r(t) = s(t) * h(t)$ is first down-converted by multiplying with $e^{-j(\frac{2\pi}{T}t+\frac{\pi}{2})k}$, then filtered by the receiver filter $f(t)$ to generate the received subchannel signal:

$$\begin{aligned} y_k(t) &= r(t)\, e^{-j(\frac{2\pi}{T}t+\frac{\pi}{2})k} * f(t) \\ &= \sum_{m=0}^{N-1} \sum_{n=-\infty}^{\infty} \big(a_m^{\mathcal{R}}[n]\, p_{m,k}(t-nT) + j\, a_m^{\mathcal{I}}[n]\, p_{m,k}(t-nT-T/2)\big), \end{aligned} \quad (2.14)$$

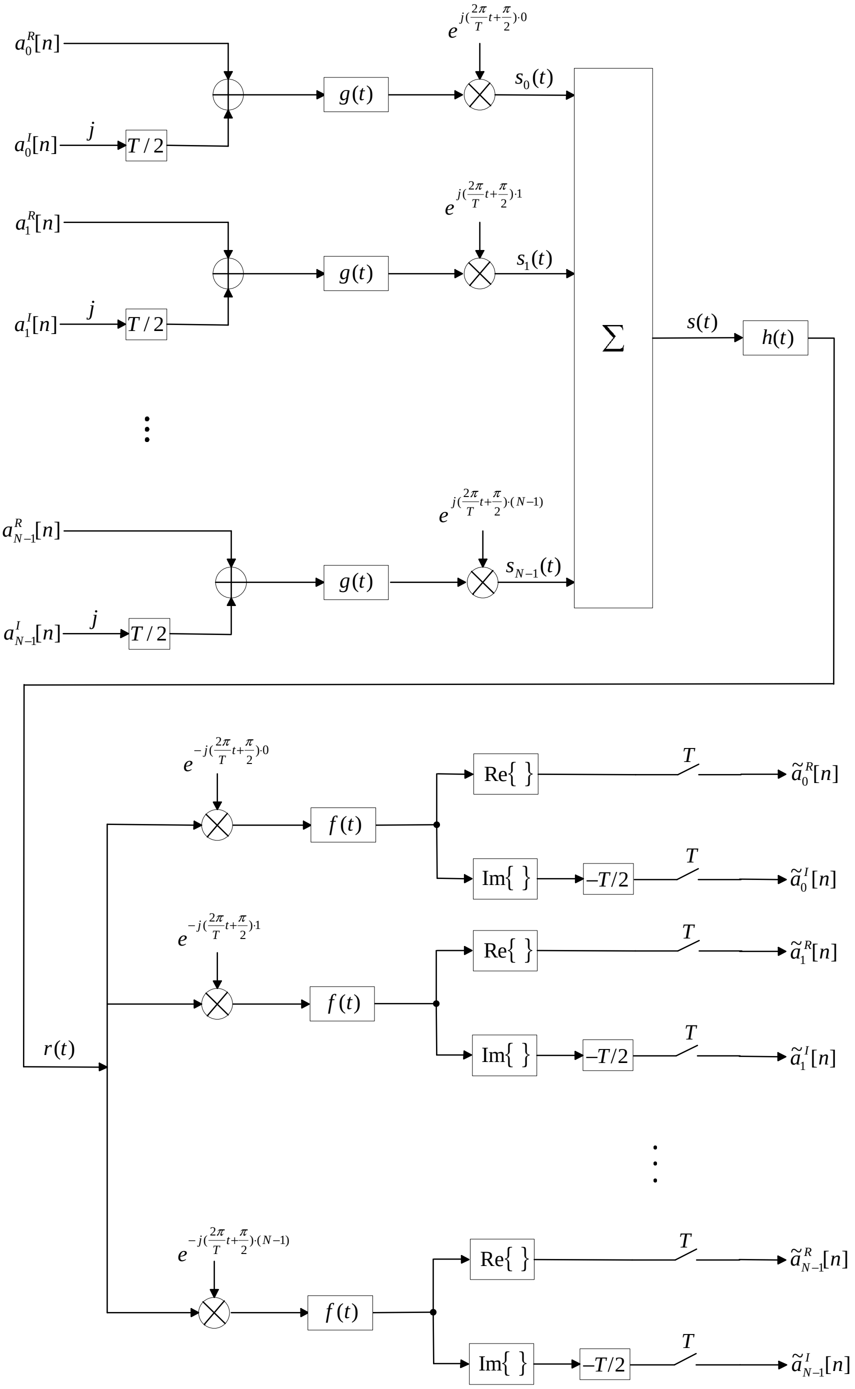
$a_0^R[n]$
$a_0^I[n]$
j
$T/2$
$g(t)$
$e^{j(\frac{2\pi}{T}t+\frac{\pi}{2})\cdot 0}$
$s_0(t)$
$a_1^R[n]$
$a_1^I[n]$
$e^{j(\frac{2\pi}{T}t+\frac{\pi}{2})\cdot 1}$
$s_1(t)$
$a_{N-1}^R[n]$
$a_{N-1}^I[n]$
$e^{j(\frac{2\pi}{T}t+\frac{\pi}{2})\cdot (N-1)}$
$s_{N-1}(t)$
Σ
$s(t)$
$h(t)$
$r(t)$
$e^{-j(\frac{2\pi}{T}t+\frac{\pi}{2})\cdot 0}$
$e^{-j(\frac{2\pi}{T}t+\frac{\pi}{2})\cdot 1}$
$e^{-j(\frac{2\pi}{T}t+\frac{\pi}{2})\cdot (N-1)}$
$f(t)$
Re{ }
Im{ }
$-T/2$
T
$\tilde{a}_0^R[n]$
$\tilde{a}_0^I[n]$
$\tilde{a}_1^R[n]$
$\tilde{a}_1^I[n]$
$\tilde{a}_{N-1}^R[n]$
$\tilde{a}_{N-1}^I[n]$

Figure 2.3: Time-continuous model for OFDM/OQAM systems.

where

$$p_{m,k}(t) = j^{m-k} g(t)\, e^{j\frac{2\pi}{T}(m-k)t} * h(t)\, e^{-j\frac{2\pi}{T}kt} * f(t) \tag{2.15}$$

is the overall response of the path from subchannel m at the transmitter side to subchannel k at the receiver side.

Finally by sampling the received subchannel signal $y_k(t)$ given in (2.14) at time instant nT and $(n+1/2)\,T$, we get the real and imaginary parts of the received symbol respectively:

$$\begin{aligned}
\tilde{a}_k^{\mathcal{R}}[n] &= \mathrm{Re}\{y_k(t)\}\big|_{t=nT} \\
&= \Lambda_{k,k}[0]\, a_m^{\mathcal{R}}[n] + \sum_{\substack{n'=-\infty \\ n'\neq n}}^{\infty} \big(\Lambda_{k,k}[n-n']\, a_k^{\mathcal{R}}[n'] - \Gamma_{k,k}[n-n']\, a_k^{\mathcal{I}}[n']\big) \\
&\quad + \sum_{\substack{m=0 \\ m\neq k}}^{N-1} \sum_{n'=-\infty}^{\infty} \big(\Lambda_{m,k}[n-n']\, a_m^{\mathcal{R}}[n'] - \Gamma_{m,k}[n-n']\, a_m^{\mathcal{I}}[n']\big) \qquad (2.16) \\
\tilde{a}_k^{\mathcal{I}}[n] &= \mathrm{Im}\{y_k(t)\}\big|_{t=(n+1/2)T} \\
&= \Lambda_{k,k}[0]\, a_m^{\mathcal{I}}[n] + \sum_{\substack{n'=-\infty \\ n'\neq n}}^{\infty} \big(\Lambda_{k,k}[n-n']\, a_k^{\mathcal{I}}[n'] + \Gamma_{k,k}[n-n'+1]\, a_k^{\mathcal{R}}[n']\big) \\
&\quad + \sum_{\substack{m=0 \\ m\neq k}}^{N-1} \sum_{n'=-\infty}^{\infty} \big(\Lambda_{m,k}[n-n']\, a_m^{\mathcal{I}}[n'] + \Gamma_{m,k}[n-n'+1]\, a_m^{\mathcal{R}}[n']\big), \qquad (2.17)
\end{aligned}$$

where the coefficients $\Lambda_{m,k}[n]$ and $\Gamma_{m,k}[n]$ are defined as

$$\begin{aligned}
\Lambda_{m,k}[n] &= \mathrm{Re}\left\{p_{m,k}(nT)\right\} \\
\Gamma_{m,k}[n] &= \mathrm{Im}\left\{p_{m,k}(nT - T/2)\right\}.
\end{aligned} \tag{2.18}$$

The right-hand sides of (2.16) and (2.17) show that the received symbol is composed of the true symbol multiplied by a constant $\Lambda_{k,k}[0]$ and a weighted sum of contributions from symbols at other instants and from other subchannels. Note that the interference from the real part of a symbol will affect both the real and imaginary parts of all other symbols. In general the quantity $\Lambda_{m,k}[n-n']$ denotes the interference from the real part of the n'th symbol of the subchannel m to the real part of desired symbol $\tilde{a}_k^{\mathcal{R}}[n]$, whereas $\Gamma_{m,k}[n-n']$ denotes the interference from the imaginary part of the sent symbols. A similar statement can be made for the imaginary part.

B. Sufficient conditions for orthogonality

In the previous section, we described the time-continuous OFDM/OQAM systems and formulated expressions for the received symbols. In this section, we will present some constraints for orthogonal pulses in OFDM/OQAM systems.

If the channel is ideal, i.e. $h(t) = \delta(t)$, the transmitted symbols should be perfectly recovered in the absence of channel noise. Based on (2.16) and (2.17), this can be formulated as

$$\Lambda_{m,k}[n] = \delta(m-k,n) \tag{2.19}$$

$$\Gamma_{m,k}[n] = 0, \tag{2.20}$$

where $\delta(k,n)$ is the two-dimensional discrete Kronecker function.

By substituting $h(t) = \delta(t)$ into (2.15) then into (2.19) and (2.20), we get the detailed necessary and sufficient conditions for orthogonal pulses:

$$\mathrm{Re}\Big\{ j^k \int_{-\infty}^{\infty} g(\tau)\, f(nT-\tau)\, e^{j\frac{2\pi}{T}k\tau}\, d\tau \Big\} = \delta(k,n) \tag{2.21}$$

$$\mathrm{Im}\Big\{ j^k \int_{-\infty}^{\infty} g(\tau)\, f(nT-T/2-\tau)\, e^{j\frac{2\pi}{T}k\tau}\, d\tau \Big\} = 0. \tag{2.22}$$

If the transmitter filter $g(t)$ and receiver filter $f(t)$ satisfy the following conditions:

- $g(t)$ and $f(t)$ are bandlimited to $[-1/T, 1/T]$,
- $g(t)$ and $f(t)$ are identical real-valued symmetric pulses,
- The cascade of $g(t)$ and $f(t)$ satisfies the Nyquist criterion,

it can be verified that (2.21) and (2.22) are fulfilled. Note that these three conditions are only sufficient conditions but *not* necessary conditions.

As shown later, the requirement of shaping filters to be bandlimited to $[-1/T, 1/T]$ helps to equalize the multipath effects. One example of such orthogonal pulses is the square root raised cosine pulse with a roll-off factor less or equal to one. In the rest of this thesis, we will assume that the shaping filters are bandlimited to $[-1/T, 1/T]$. Note that since the shaping filters are bandlimited to $[-1/T, 1/T]$, they have infinite duration in the time domain. In a practical system, such pulses must be truncated to be of finite length. Thus the pulses cannot be strictly bandlimited in frequency domain. However, for a long enough pulse duration, this spectrum leakage is negligible. It is shown in [VH96] that for a $4T$ long optimal pulse with minimum out-of-band energy, the magnitude of the main sidelobe is about 40 dB lower compared to the peak magnitude.

C. *Efficient per-subchannel equalization*

For the case of multipath fading, the orthogonality will be generally damaged for OFDM/OQAM systems since no guard interval is inserted. Therefore channel equalization is needed to counteract multipath effects. One straightforward solution is to insert the inverse filter of $h(t)$ before demodulation. Orthogonality is then guaranteed since the equivalent channel is ideal. However, such an inverse filter is generally highly complicated since it needs to equalize the whole band. Since the shaping filters are bandlimited, each subchannel can be approximated as flat-fading for OFDM/OQAM systems with a large number of subchannels. Therefore it is much easier to equalize the multipath effects per-subchannel after demodulation.

From (2.15), we see that the equivalent channel impulse response of subchannel k in the receiver side is $h(t)\, e^{-j\frac{2\pi}{T}kt}$. If we insert an equalizer $c_k(t)$ immediately after the receiver filter $f(t)$ in subchannel k, (2.15) should be revised as

$$\begin{aligned} p_{m,k}(t) &= j^{m-k} g(t)\, e^{j\frac{2\pi}{T}(m-k)t} * h(t)\, e^{-j\frac{2\pi}{T}kt} * f(t) * c_k(t) \\ &= j^{m-k} g(t)\, e^{j\frac{2\pi}{T}(m-k)t} * \big(h(t)\, e^{-j\frac{2\pi}{T}kt} * c(t)\big) * f(t). \end{aligned} \tag{2.23}$$

From (2.23), we see that the equivalent channel impulse response now becomes $h(t)\, e^{-j\frac{2\pi}{T}kt} * c_k(t)$. Since $f(t)$ is bandlimited to $[-1/T, 1/T]$, we only need to make the frequency response of $h(t)\, e^{-j\frac{2\pi}{T}kt} * c_k(t)$ flat in $[-1/T, 1/T]$. This is much easier than to equalize the whole band.

We consider a channel with an impulse response $h(t) = \sum_{l=1}^{L} \lambda_l\, \delta(t-\tau_l)$, and assume that the maximum delay τ_L is much shorter than T (as usually assumed in OFDM systems), subchannel k can be approximated as flat-fading with an attenuation factor $\beta_k = \sum_{l=1}^{L} \lambda_l\, e^{-j\frac{2\pi}{T}k\tau_l}$. In this case, a constant multiplier $1/\beta_k$ is enough to eliminate the ISI and ICI. This is similar to that in OFDM/QAM systems with guard interval.

2.2.2 Time-discrete model

Now we will describe and analyze a time-discrete model for OFDM/OQAM systems.

A. *System description*

A critically sampled time-discrete model for OFDM/OQAM systems is shown in Fig. 2.4. The time-discrete shaping filters $g[l]$ and $f[l]$ operate at the same sampling rate N/T. The digital shaping filters can either be obtained by sampling the time-continuous filters [Hir80], or be designed directly [BDH99]. Based on Fig. 2.4, by summing up all subchannels, we

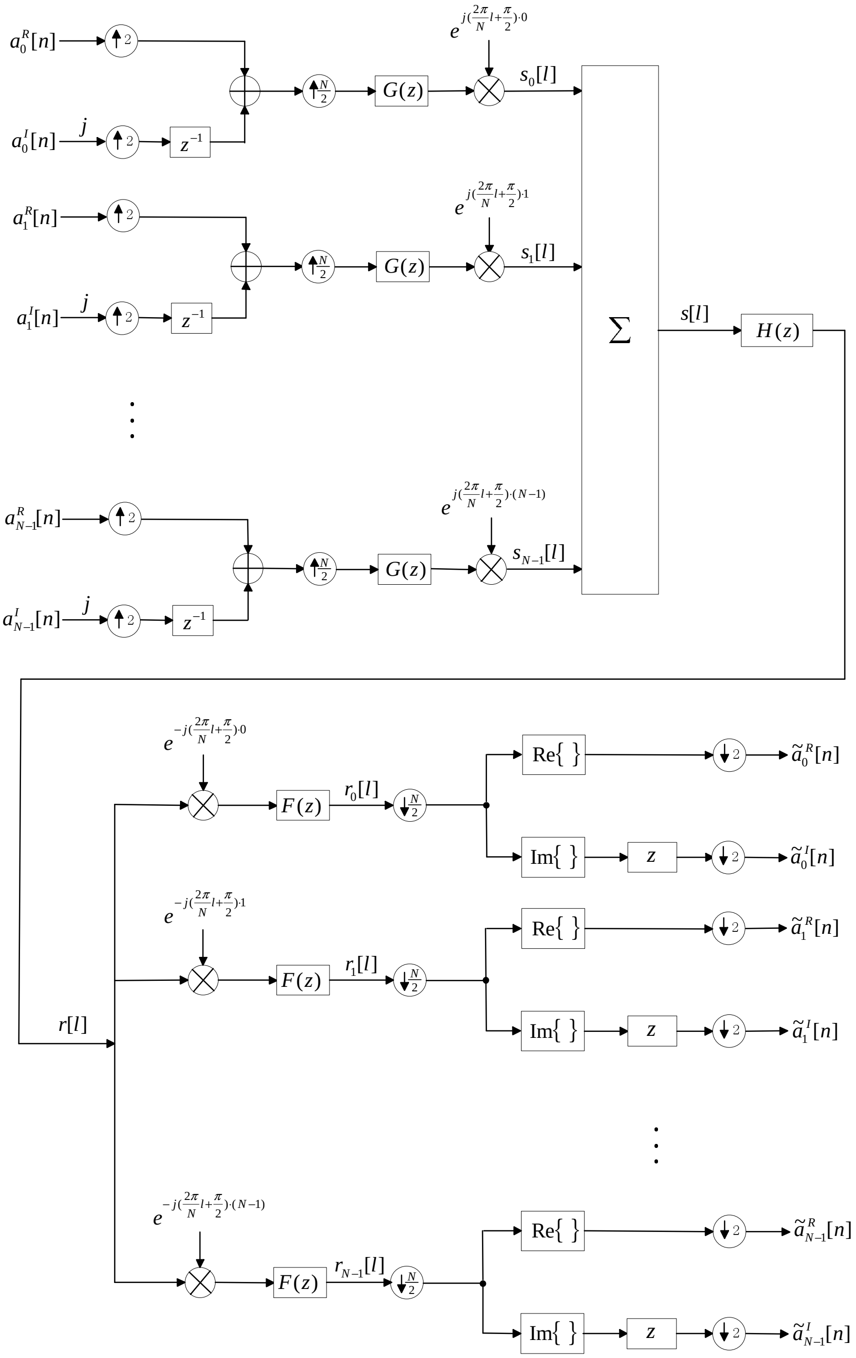
$a_0^R[n]$
2
$a_0^I[n]$
j
2
z^{-1}
$\frac{N}{2}$
$G(z)$
$e^{j(\frac{2\pi}{N}l+\frac{\pi}{2})\cdot 0}$
$s_0[l]$
$a_1^R[n]$
2
$a_1^I[n]$
j
2
z^{-1}
$\frac{N}{2}$
$G(z)$
$e^{j(\frac{2\pi}{N}l+\frac{\pi}{2})\cdot 1}$
$s_1[l]$
Σ
$s[l]$
$H(z)$
$a_{N-1}^R[n]$
2
$a_{N-1}^I[n]$
j
2
z^{-1}
$\frac{N}{2}$
$G(z)$
$e^{j(\frac{2\pi}{N}l+\frac{\pi}{2})\cdot (N-1)}$
$s_{N-1}[l]$
$r[l]$
$e^{-j(\frac{2\pi}{N}l+\frac{\pi}{2})\cdot 0}$
$F(z)$
$r_0[l]$
$\frac{N}{2}$
Re{ }
2
$\tilde{a}_0^R[n]$
Im{ }
z
2
$\tilde{a}_0^I[n]$
$e^{-j(\frac{2\pi}{N}l+\frac{\pi}{2})\cdot 1}$
$F(z)$
$r_1[l]$
$\frac{N}{2}$
Re{ }
2
$\tilde{a}_1^R[n]$
Im{ }
z
2
$\tilde{a}_1^I[n]$
$e^{-j(\frac{2\pi}{N}l+\frac{\pi}{2})\cdot (N-1)}$
$F(z)$
$r_{N-1}[l]$
$\frac{N}{2}$
Re{ }
2
$\tilde{a}_{N-1}^R[n]$
Im{ }
z
2
$\tilde{a}_{N-1}^I[n]$

Figure 2.4: Time-discrete model for OFDM/OQAM systems.

can write the transmitted sequence as

$$s[l] = \sum_{k=0}^{N-1} \sum_{n=-\infty}^{\infty} \big(a_k^{\mathcal{R}}[n]\, g[l-nN] + j\, a_k^{\mathcal{I}}[n]\, g[l-nN-N/2]\big) e^{j(\frac{2\pi}{N}l+\frac{\pi}{2})k}. \quad (2.24)$$

We assume a time-invariant channel with an impulse response $h[l]$. Then the received sequence from channel is $r[l] = s[l] * h[l]$. In subchannel k at the receiver side, the received sequence $r[l]$ is first down-converted by multiplying with $e^{-j(\frac{2\pi}{N}l+\frac{\pi}{2})k}$, then filtered by the receiver filter $f[l]$ to generate the received subchannel sequence

$$\begin{aligned} r_k[l] &= r[l]\, e^{-j(\frac{2\pi}{N}l+\frac{\pi}{2})k} * f[l] \\ &= \sum_{m=0}^{N-1} \sum_{n=-\infty}^{\infty} \big(a_m^{\mathcal{R}}[n]\, p_{m,k}^{(o)}[l-nN] + j\, a_m^{\mathcal{I}}[n]\, p_{m,k}^{(o)}[l-nN-N/2]\big), \end{aligned} \quad (2.25)$$

where $p_{m,k}^{(o)}[l]$ is the overall response from subchannel m at the transmitter side to the subchannel k at the receiver side, and it is given by

$$p_{m,k}^{(o)}[l] = j^{m-k} g[l]\, e^{j\frac{2\pi}{N}(m-k)l} * h[l]\, e^{-j\frac{2\pi}{N}kl} * f[l]. \quad (2.26)$$

Finally by $N/2$ times down-sampling the received subchannel sequence $r_k[l]$, then taking the real and imaginary parts alternately, we get the received symbol:

$$\begin{aligned} \tilde{a}_k^{\mathcal{R}}[n] &= \mathrm{Re}\{r_k[l]\}\big|_{l=nN} \\ \tilde{a}_k^{\mathcal{I}}[n] &= \mathrm{Im}\{r_k[l]\}\big|_{l=(n+1/2)N}. \end{aligned} \quad (2.27)$$

From (2.25), we see that the equivalent channel impulse response of subchannel k is $h[l]\, e^{-j\frac{2\pi}{N}kl}$. Since the shaping filters are bandlimited to $[-1/T, 1/T]$, the channel effects can be perfectly compensated by a $T/2$ spaced per-subchannel equalizer. This is similar to the time-continuous case. Such an efficient equalizer will be discussed in detail in Chapter 3.

B. Filterbank based model

Now we transform the time-discrete model shown in Fig. 2.4 into a filterbank based scheme. First we rewrite the subchannel signal $s_k[l]$ as

$$\begin{aligned} s_k[l] &= \sum_{n=-\infty}^{\infty} \big(a_k^{\mathcal{R}}[n]\, g[l-nN] + j\, a_k^{\mathcal{I}}[n]\, g[l-nN-N/2]\big) e^{j(\frac{2\pi}{N}l+\frac{\pi}{2})k} \\ &= \sum_{n=-\infty}^{\infty} \big(a_k^{\mathcal{R}}[n]\, g_k[l-nN] + j\,(-1)^k a_k^{\mathcal{I}}[n]\, g_k[l-nN-N/2]\big), \end{aligned} \quad (2.28)$$

where

$$g_k[l] \overset{\text{def}}{=} j^k\, g[l]\, e^{j\frac{2\pi}{N}kl}. \tag{2.29}$$

From (2.28), we see that $g_k[l]$ can be viewed the equivalent transmitter filter of subchannel k. Note that the multiplier $(-1)^k$ is added just to make the filterbank based model exactly identical to the original one. In a practical system, this sign factor could be omitted.

Based on Fig. 2.4, the received subchannel signal from the receiver filter can be written as

$$\begin{aligned} r_k[l] &= r[l]\, e^{-j(\frac{2\pi}{N}l+\frac{\pi}{2})k} * f[l] = (-j)^k\, e^{-j\frac{2\pi}{N}kl} \sum_{l'=-\infty}^{\infty} r[l-l']\, f[l']\, e^{j\frac{2\pi}{N}kl'} \\ &= \big(r[l] * f_k[l]\big)\, e^{-j\frac{2\pi}{N}kl}, \end{aligned} \tag{2.30}$$

where

$$f_k[l] \overset{\text{def}}{=} (-j)^k\, f[l]\, e^{j\frac{2\pi}{N}kl}. \tag{2.31}$$

From (2.30), we see that $f_k[l]$ is the equivalent receiver filter of subchannel k. We note that an additional phase factor $e^{-j\frac{2\pi}{N}kl}$ is present. However, we see from (2.27) that only the samples of $r_k[l]$ at $l = nN$ and $l = (n + 1/2)N$ are used to recover the transmitted symbols. Therefore the phase factor $e^{-j\frac{2\pi}{N}kl}$ does no effect to the real part of received symbols, whereas it results in a multiplication by $(-1)^k$ to the imaginary part of received symbols.

Finally by combining (2.28) and (2.30), we obtain a filterbank based model for OFDM/OQAM systems, which is depicted in Fig. (2.5). Based on this model, we are now ready to derive an efficient implementation based on FFT and polyphase filterbank.

C. Efficient implementation based on FFT and polyphase filterbank

Now we derive an FFT based implementation for OFDM/OQAM systems. The derivation will be performed in z domain. First we denote the $T/2$ spaced OQAM sequence as $b_k[m]$, which is given by

$$b_k[m] = \begin{cases} a_k^{\mathcal{R}}[m/2], & \text{for } m \text{ even} \\ j\,(-1)^k\, a_k^{\mathcal{I}}[(m-1)/2], & \text{for } m \text{ odd.} \end{cases} \tag{2.32}$$

We assume the z transform of $b_k[m]$ exists and is given by $B_k(z) = \sum_{m=-\infty}^{\infty} b_k[m]\, z^{-m}$. From Fig. 2.5, we see that $v_k[l]$ is the $N/2$ times oversampled version of $b_k[m]$, thus its z transform is given by

$$V_k(z) = \sum_{l=-\infty}^{\infty} v_k[l]\, z^{-l} = \sum_{m=-\infty}^{\infty} b_k[m]\, z^{-\frac{N}{2}m} = B_k(z^{N/2}). \tag{2.33}$$

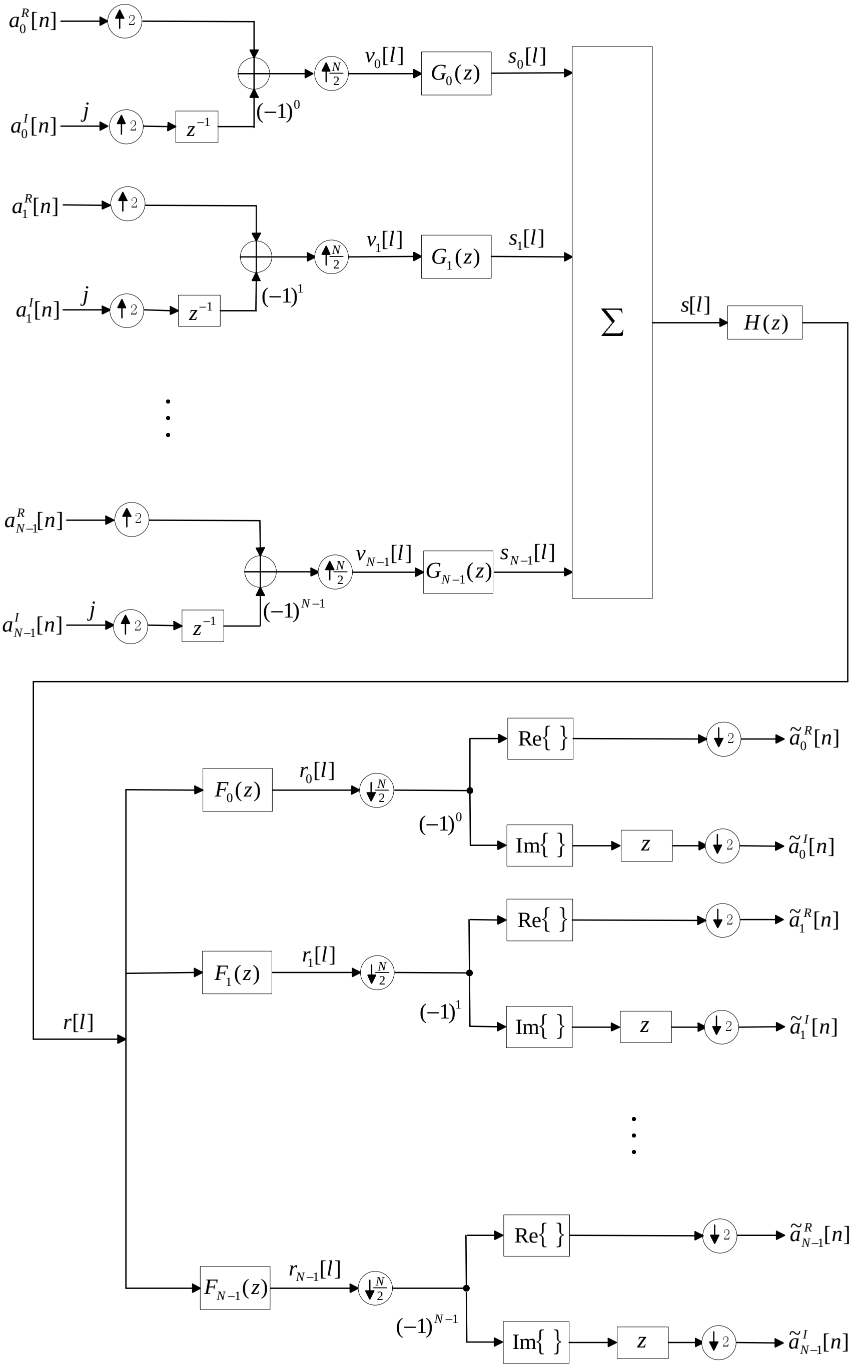
$a_0^R[n]$
$a_0^I[n]$
j
z^{-1}
$(-1)^0$
$\frac{N}{2}$
$v_0[l]$
$G_0(z)$
$s_0[l]$
$a_1^R[n]$
$a_1^I[n]$
$(-1)^1$
$v_1[l]$
$G_1(z)$
$s_1[l]$
$a_{N-1}^R[n]$
$a_{N-1}^I[n]$
$(-1)^{N-1}$
$v_{N-1}[l]$
$G_{N-1}(z)$
$s_{N-1}[l]$
$\sum$
$s[l]$
$H(z)$
$r[l]$
$F_0(z)$
$r_0[l]$
$F_1(z)$
$r_1[l]$
$F_{N-1}(z)$
$r_{N-1}[l]$
Re{ }
Im{ }
z
$\tilde{a}_0^R[n]$
$\tilde{a}_0^I[n]$
$\tilde{a}_1^R[n]$
$\tilde{a}_1^I[n]$
$\tilde{a}_{N-1}^R[n]$
$\tilde{a}_{N-1}^I[n]$

Figure 2.5: Filterbank based model for time-discrete OFDM/OQAM systems.

The z transforms of subchannel filters $g_k[l]$ and $f_k[l]$ defined in (2.29) and (2.31) are given by

$$\begin{aligned} G_k(z) &= \sum_{l=-\infty}^{\infty} j^k\, g[l]\, e^{j\frac{2\pi}{N}kl}\, z^{-l} = j^k\, G(z\, e^{-j\frac{2\pi}{N}k}) \\ F_k(z) &= \sum_{l=-\infty}^{\infty} (-j)^k\, f[l]\, e^{j\frac{2\pi}{N}kl}\, z^{-l} = (-j)^k\, F(z\, e^{-j\frac{2\pi}{N}k}), \end{aligned} \tag{2.34}$$

where $G(z) \overset{\text{def}}{=} \sum_{l=-\infty}^{\infty} g[l]\, z^{-l}$ and $F(z) \overset{\text{def}}{=} \sum_{l=-\infty}^{\infty} f[l]\, z^{-l}$ are the z transform of shaping filter $g[l]$ and $f[l]$ respectively.

Then based on Fig. 2.5, and using (2.33) and (2.34), we can write the z transform of the transmitted sequence $s[l]$ as

$$\begin{aligned} S(z) &= \sum_{k=0}^{N-1} V_k(z)\, G_k(z) = \sum_{k=0}^{N-1} j^k B_k(z^{N/2})\, G(z\, e^{-j\frac{2\pi}{N}k}) \\ &= \sum_{k=0}^{N-1} j^k B_k(z^{N/2}) \sum_{i=0}^{N-1} z^{-i}\, e^{j\frac{2\pi}{N}ik}\, G_i^{(p)}(z^N) \\ &= \sqrt{N} \sum_{i=0}^{N-1} z^{-i} G_i^{(p)}\big((z^2)^{N/2}\big) \Big(\frac{1}{\sqrt{N}} \sum_{k=0}^{N-1} j^k B_k(z^{N/2})\, e^{j\frac{2\pi}{N}ik} \Big) \end{aligned} \tag{2.35}$$

where

$$G_i^{(p)}(z) \overset{\text{def}}{=} \sum_{n=-\infty}^{\infty} g[nN+i]\, z^{-n}, \tag{2.36}$$

is the i^{th} filter of the Nth order polyphase decomposition of $G(z)$.

The sum $\frac{1}{\sqrt{N}} \sum_{k=0}^{N-1} j^k B_k(z^{N/2})\, e^{j\frac{2\pi}{N}ik}$ in (2.35) can be viewed as the i^{th} output of the normalized N-point IDFT of $\{j^k B_k(z^{N/2})\}_{k=0}^{N-1}$. Thus we get the efficient modulator of an OFDM/OQAM system based on IFFT and polyphase filterbank, which is shown in Fig. 2.6(a). Note the constant $\sqrt{N}$ is omitted in this model.

Now we derive a similar efficient implementation for the demodulator. Based on Fig. 2.5, and using (2.34), we can write the z transform of subchannel sequence $r_k[l]$ as

$$\begin{aligned} R_k(z) &= X(z)\, F_k(z) = (-j)^k X(z)\, F(e^{-j\frac{2\pi}{N}k} z) \\ &= \sqrt{N}(-j)^k \Big(\frac{1}{\sqrt{N}} \sum_{i=0}^{N-1} X(z)\, z^{-i} F_i^{(p)}\big((z^2)^{N/2}\big)\, e^{j\frac{2\pi}{N}ik} \Big), \end{aligned} \tag{2.37}$$

where

$$F_i^{(p)}(z) \overset{\text{def}}{=} \sum_{n=-\infty}^{\infty} f[nN+i]\, z^{-n}, \tag{2.38}$$

is the i^{th} filter of the Nth order polyphase decomposition of $F(z)$.

Then based on (2.37), and by noting that the received symbols are obtained by $N/2$ times down-sampling $r_k[l]$, we get the demodulator, which is shown in Fig. 2.6(b). Note that the constant $\sqrt{N}$ is omitted in this model.

Now we have obtained an efficient implementation for OFDM/OQAM systems. The implementation scheme shown in Fig. 2.6 needs an N-point complex-valued IFFT every $T/2$ seconds at both transmitter and receiver sides. From Fig. 2.2, we see that both the modulator and demodulator of OFDM/QAM systems need an N-point complex IFFT every T seconds. This implies that the implementation complexity of OFDM/OQAM is about twice as that of OFDM/QAM. It is worthwhile to mention that for OFDM/OQAM systems, more efficient implementations with approximately half complexity are possible by using the fact that the IFFT input in the transmitter are alternately pure real or imaginary-valued [CV95, VL01, Vah03]. The implementation complexity of OFDM/QAM and OFDM/OQAM will be compared in detail in the next section.

2.3 Comparison of OFDM/QAM and OFDM/OQAM

In the previous sections, we have introduced OFDM/QAM systems with rectangular pulseshapes and guard interval, and OFDM/OQAM systems with bandlimited pulseshapes. In this section, we compare these two OFDM schemes with respect to implementation complexity, transmission delay, spectrum efficiency, power efficiency and equalization complexity. In the comparison, we assume no pilot symbol has been inserted.

2.3.1 Implementation complexity

First we compare the implementation complexity of OFDM/QAM and OFDM/OQAM. The number of real multiplications performed to transmit one QAM symbol is used to evaluate the complexity. We assume that a multiplication of two complex quantities needs four real products, and that a complex-by-real product needs two real products.

From Fig. 2.2, we see that the modulator and demodulator have identical complexity disregarding other accessory modules, such as synchronizer

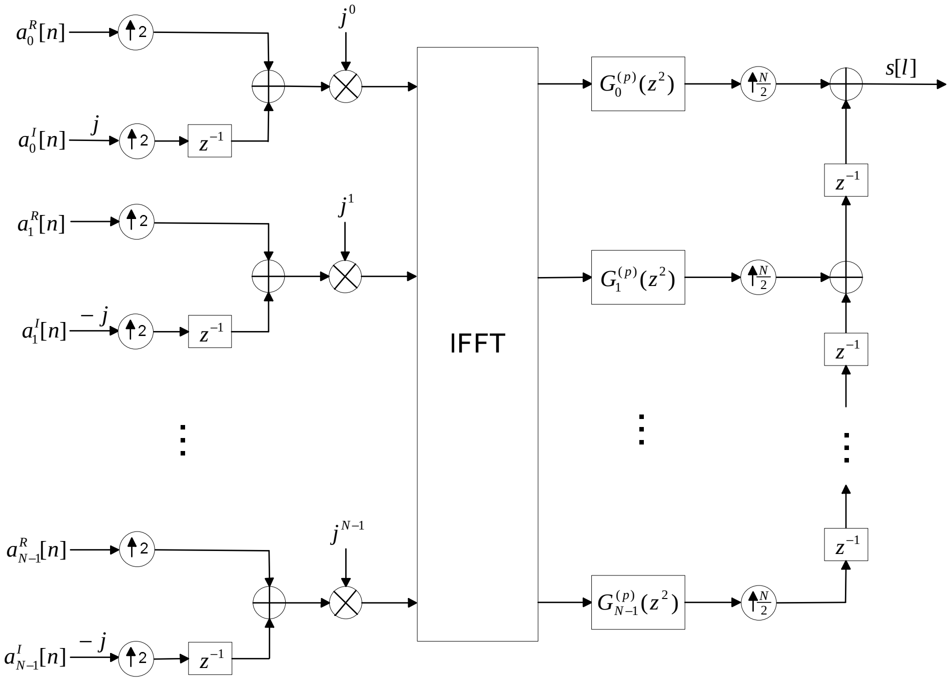
$a_0^R[n]$
$a_0^I[n]$
$a_1^R[n]$
$a_1^I[n]$
$a_{N-1}^R[n]$
$a_{N-1}^I[n]$
↑2
j
$-j$
z^{-1}
j^0
j^1
j^{N-1}
IFFT
$G_0^{(p)}(z^2)$
$G_1^{(p)}(z^2)$
$G_{N-1}^{(p)}(z^2)$
$\uparrow\frac{N}{2}$
$s[l]$

(a) Modulator

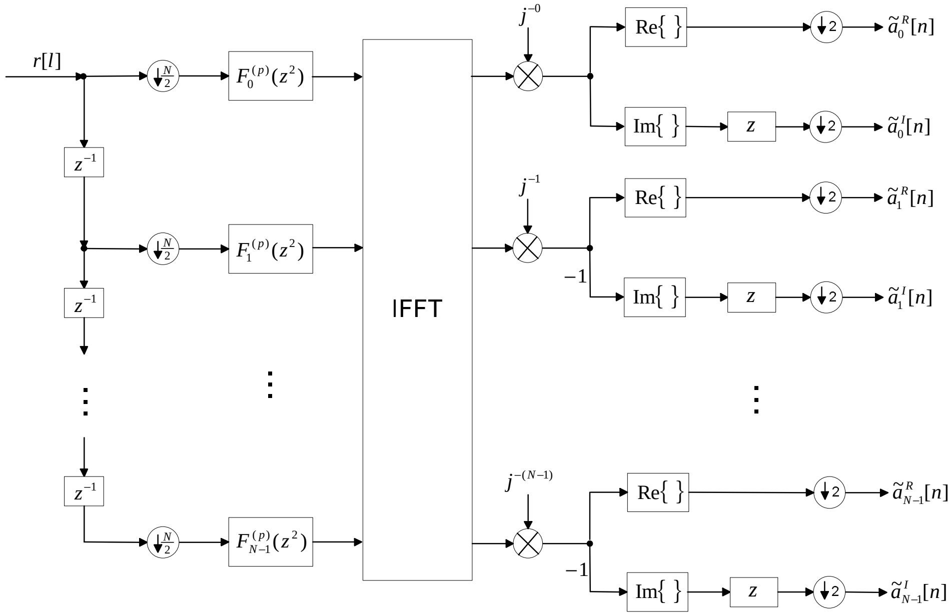
$r[l]$
$\downarrow\frac{N}{2}$
z^{-1}
$F_0^{(p)}(z^2)$
$F_1^{(p)}(z^2)$
$F_{N-1}^{(p)}(z^2)$
IFFT
j^{-0}
j^{-1}
$j^{-(N-1)}$
-1
Re{ }
Im{ }
z
↓2
$\tilde{a}_0^R[n]$
$\tilde{a}_0^I[n]$
$\tilde{a}_1^R[n]$
$\tilde{a}_1^I[n]$
$\tilde{a}_{N-1}^R[n]$
$\tilde{a}_{N-1}^I[n]$

(b) Demodulator

Figure 2.6: FFT and polyphase filterbank based scheme for OFDM/OQAM systems.

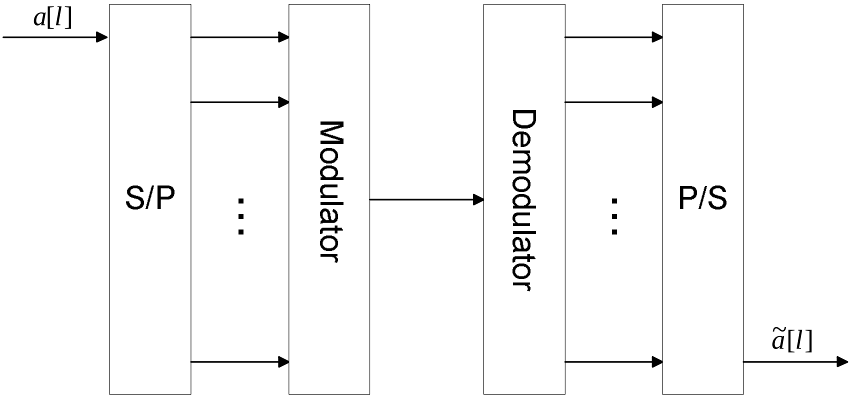

Figure 2.7: Block diagram of OFDM transmission systems.

and equalizer. To process one block of data with N symbols, we need to perform an N-point complex-valued FFT, which requires $N/2\log_2 N$ complex multiplications or $2N\log_2 N$ real multiplications. Thus the implementation complexity of OFDM/QAM is $2\log_2 N$ per QAM symbol.

From Fig. 2.6, we see that the modulator and demodulator of OFDM/OQAM also have the same implementation complexity: an N-point IFFT is performed every half OFDM symbol period, and the polyphase filterbank additionally needs L_gN complex-by-real products during this interval, where L_g is the length of shaping filters (normalized with respect to subchannel symbols period T). Therefore the complexity of the implementation scheme depicted in Fig. 2.6 for OFDM/OQAM systems is $4\log_2 N + 4L_g$ per QAM symbol.

The implementation complexity of OFDM/OQAM can be further reduced. The implementation complexity of the scheme proposed by Cariolaro is $2\log_2 N + 8L_g + 4 - 8/N$ per QAM symbol [CV95], and that of the scheme proposed by Vangelista is $2\log_2 N + 4L_g + 4 - 8/N$ per QAM symbol [VL01].

2.3.2 Transmission delay

Consider the equivalent OFDM systems depicted in Fig. 2.7, where $a[l]$ is the T_s spaced transmitted sequence of QAM symbols, and $\tilde{a}[l]$ is the corresponding received sequence of QAM symbols with the same sampling interval.

The transmission delay is caused by two sources. First the transform pair of P/S and S/P will cause a delay of $(N-1)T_s$. This delay for OFDM/QAM and OFDM/OQAM is identical. Secondly the pairs of modulator and demodulator will cause an additional delay. For OFDM/QAM systems, this delay is NT_s, no matter how long the guard interval is. For OFDM/OQAM systems, this delay is $(L_g+1/2)NT_s$, where L_g is the length of transmitter filter (or receiver filter).

Therefore the total transmission delay of OFDM/QAM system is

$$D_T = (2\,N - 1)\,T_s, \tag{2.39}$$

and that for OFDM/OQAM systems is

$$D_T = [(L_g + 3/2)\,N - 1]\,T_s. \tag{2.40}$$

Usually L_g is larger than 1, for instance, 2 to 4. Therefore the transmission delay of OFDM/OQAM systems is longer than that of OFDM/QAM systems.

2.3.3 Spectrum and power efficiency

First we define the *normalized spectrum efficiency* as the ratio of the minimum requited bandwidth to the occupied bandwidth indeed.

According to the Nyquist criterion, the minimum required bandwidth to transmit a QAM sequence with a symbols period T is $1/T$. For an OFDM/QAM system with N subchannels and a subchannel spacing $1/T$, the occupied bandwidth is then N/T. If the length of cyclic prefix is G, the symbols interval is $(1 + G/N)\,T$. We assume N_g subchannels in the each end of band are set as null-subchannels to reduce the out-of-band emission. Thus only $N - 2\,N_g$ subchannels are used to transmit useful information symbols. Therefore the minimum required bandwidth is $(N - N_g)/[(1 + G/N)\,T]$, and the normalized spectrum efficiency is then

$$\eta_{\mathrm{BW}} = \frac{N - N_g}{N + G}. \tag{2.41}$$

For an OFDM/OQAM system with the same number of subchannels N and a subchannel spacing $1/T$, the symbol interval is T and the minimum required bandwidth is N/T. If the shaping filters are bandlimited to $[-\frac{1+\alpha}{2T}, \frac{1+\alpha}{2T}]$, where α is referred to the roll-off factor, and the system is fully loaded, the occupied bandwidth is then $(N + \alpha)/T$. Thus the normalized spectrum efficiency for OFDM/OQAM systems is

$$\eta_{\mathrm{BW}} = \frac{N}{N + \alpha}. \tag{2.42}$$

We see that for large N, the spectrum efficiency of OFDM/OQAM systems with bandlimited pulseshapes is close to the Nyquist limit.

Now we analyze the power efficiency of different OFDM systems. For OFDM/QAM systems with guard interval, since the guard interval contains no information, the power efficiency (compared with systems without guard interval) is thus $N/(N+G)$. For OFDM/OQAM systems, the power efficiency is one since no guard interval is inserted.

2.3.4 Equalization over a multipath channel

From (2.9), we see that for OFDM/QAM systems with a guard interval longer than the maximum delay of the channel, there exists no ISI and ICI, while the received symbols suffer from an attenuation factor. This implies that a one-tap equalizer (or a multiplier) is enough in each subchannel to counteract the multipath effects.

For OFDM/OQAM systems, since no guard interval is inserted, the equalization is more complicated since generally both ISI and ICI are present over a multipath channel. Since the shaping filters are bandlimited to $[-1/T, 1/T]$, the ICI comes from only adjacent subchannels. The equalizer can be efficiently implemented by a single branch linear filter operating at a rate $2/T$ in each subchannel [Hir80]. Such an efficient equalizer will be discussed in detail in the next chapter.

2.3.5 Summary and quantitative comparison

The comparison of OFDM/QAM and OFDM/OQAM can be summarized as in Table 2.1 shown. Recall that N is the number of subchannels and T_s is the interval of the input serial symbols for both OFDM schemes. For OFDM/QAM, the length of the guard interval is G. For OFDM/OQAM, the length of the shaping filters is L_g (normalized with respect to subchannel symbols interval T), the roll-off factor of the shaping filters is α and the implementation complexity is based on Vangelista's algorithm [VL01].

Table 2.1: A comparison of OFDM/QAM and OFDM/OQAM.

	OFDM/QAM	OFDM/OQAM
Complexity/QAM symbol	$2\log_2 N$	$2\log_2 N + 4L_g + 4 - 8/N$
Transmission delay	$(2N-1)\,T_s$	$[(L_g+3/2)\,N-1]\,T_s$
Normalized spectrum efficiency	$(N-N_g)/(N+G)$	$N/(N+\alpha)$
Normalized power efficiency	$N/(N+G)$	1
Equalization	one-tap equalizer	multi-tap equalizer

We see that OFDM/OQAM can achieve almost full normalized spectrum efficiency and 100% normalized power efficiency. This is prohibitive in an OFDM/QAM system with guard interval. Such an improvement of normalized spectrum and power efficiency is obtained at the cost of higher implementation complexity, longer transmission delay and more complicated equalization.

Finally, we present a quantitative example. The curves of complexity versus N for different implementation schemes are shown in Fig. 2.8. For OFDM/OQAM systems, the pulse length is set to $L_g = 2$. We see that OFDM/QAM has lower implementation complexity than that of OFDM/OQAM. For large N, the complexity of the algorithms proposed by Cariolaro [CV95] or Vangelista [VL01] is quite close to that of conventional OFDM/QAM systems. We also note that among different implementation algorithms for OFDM/OQAM systems, the one proposed by Vangelista [VL01] has the lowest complexity.

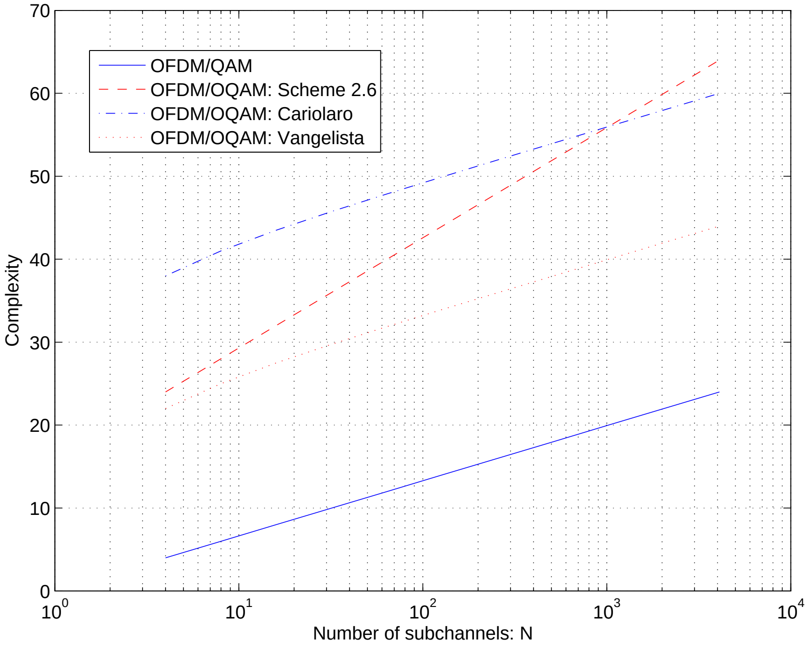

Figure 2.8: Comparison of implementation complexity of OFDM/QAM and OFDM/OQAM.

Then we fix the number of subchannels $N = 128$. For OFDM/QAM systems, $N_g = 4$ and $G = 32$. For OFDM/OQAM systems, the length of the shaping filters is $L_g = 2$ and the roll-off factor of the shaping filters is $\alpha = 1.0$.

The implementation complexity of OFDM/QAM and OFDM/OQAM is 14 and 25.9 respectively. We see that the complexity of OFDM/OQAM is about twice as that of OFDM/QAM. The transmission delay of OFDM/QAM and OFDM/OQAM is $255\,T_s$ and $447\,T_s$ respectively. The normalized spectrum efficiency of OFDM/QAM and OFDM/OQAM is 75.0% and 99.2% respectively. The normalized power efficiency is respectively 80.0% and 100%. Thus the spectrum efficiency and power efficiency of OFDM/OQAM systems are 24.2% and 20.0% higher than those of OFDM/QAM systems respectively.

Chapter 3

Efficient Equalization for OFDM/OQAM Systems

In Chapter 2, we have shown that by not using a guard interval, OFDM/OQAM can achieve higher spectrum and power efficiency. However, the increased spectrum and power efficiency of OFDM/OQAM is obtained at the cost of more complicated equalization of channel effects. For time-invariant channels, Hirosaki [Hir80] has shown that a scalar, fractionally spaced equalizer in each subchannel is sufficient to eliminate both inter-symbol interference (ISI) and inter-carrier interference (ICI). The special case of equalization of single carrier OQAM transmission systems has been investigated by Tu [Tu93]. Similar methods have also been used for echo cancellation in OFDM/OQAM systems [Ned00].

In this chapter, we restrict our scope to linear equalization for the time-invariant case. This means that the results are relevant for fixed radio communications and cabled communications. The main contribution of our investigation consists of a derivation of the normal equation for unweighted OFDM/OQAM systems, and expressions that are suitable for selecting appropriate equalizer length.

The rest of this chapter is organized as follows. In section 3.1, we present a time-discrete model for OFDM/OQAM systems with a single branch equalizer. Then, in section 3.2, we derive the objective function of the single branch equalizer for general OFDM/OQAM systems. To simplify the notation, we use one complex-valued equalizer to replace the four real-valued equalizers in Hirosaki's approach [Hir80]. Next we find that for OFDM/OQAM systems, the received $T/2$ spaced sequence is wide sense stationary. In section 3.3, we explore the relationship of MMSE versus equalizer length. Using the stationarity result in the previous section, we derive a normal equation similar to the one for a single carrier QAM transmission system. Based on this normal equation, we derive exact expressions of MMSE for one and infinite-tap equalizer. To assess how long an equalizer is needed, an expression relating MMSE as a function of equalizer length would be helpful. Although the exact MMSE for an equalizer with an arbitrary number of taps can be calculated by numerically inverting the correlation matrix, it is still interesting to derive a closed-form analytical expression. Some earlier results have been published on this problem [Hod78, RZ99], but only for special cases where the correlation matrix can be easily inverted. It has been pointed out that no clear-cut answers exist for how long the equalizer should be [TFJ96]. Circulant approximation has been suggested to get an approximate inverse of the Toeplitz-shaped correlation matrix [She85, Gra, SJB03]. Circulant approximation can work fine only for large matrix dimensions and is therefore not appropriate for our purpose since we also need to analyze an equalizer with only few taps. Some authors use gradient descent algorithms to select the optimal taps of least mean square (LMS) equalizers dynamically [RPNC01, GTC04]. To our knowledge, due to the difficulty of finding the inverse of the correlation matrix explicitly, it is still an open problem to get closed-form expressions for MMSE versus equalizer length for general cases. Then we propose an approximation of MMSE for an equalizer with an arbitrary number of taps. In the end of this section, these results are illustrated by examples based on a two-path time-invariant channel. A short conclusion is given in section 5.5.

Parts of the results of this chapter have been published in [LLH05, LLH06e].

3.1 Model for OFDM/OQAM systems with single branch equalizer

A time-discrete model for OFDM/OQAM systems with N subchannels is shown in Fig. 3.1. This scheme is a simplified version of the general model shown in Figure 2.4 in Chapter 2. At the receiver side, only subchannel k is drawn. We assume that the shaping filters $g[l]$ and $h[l]$ are bandlimited to $[-1/T, 1/T]$, where T is the period of the input QAM symbols in each subchannel. Then, in the absence of carrier frequency offset, overlap exists only between adjacent subchannels. Thus it is sufficient to consider only subchannel k and its adjacent subchannels $k \pm 1$ at the transmitter side.

Each T seconds, the transmitter takes N complex QAM symbols

$$a_k[n] = a_k^{\mathcal{R}}[n] + j\, a_k^{\mathcal{I}}[n],\ \ k = 0, 1, \cdots, N-1,$$

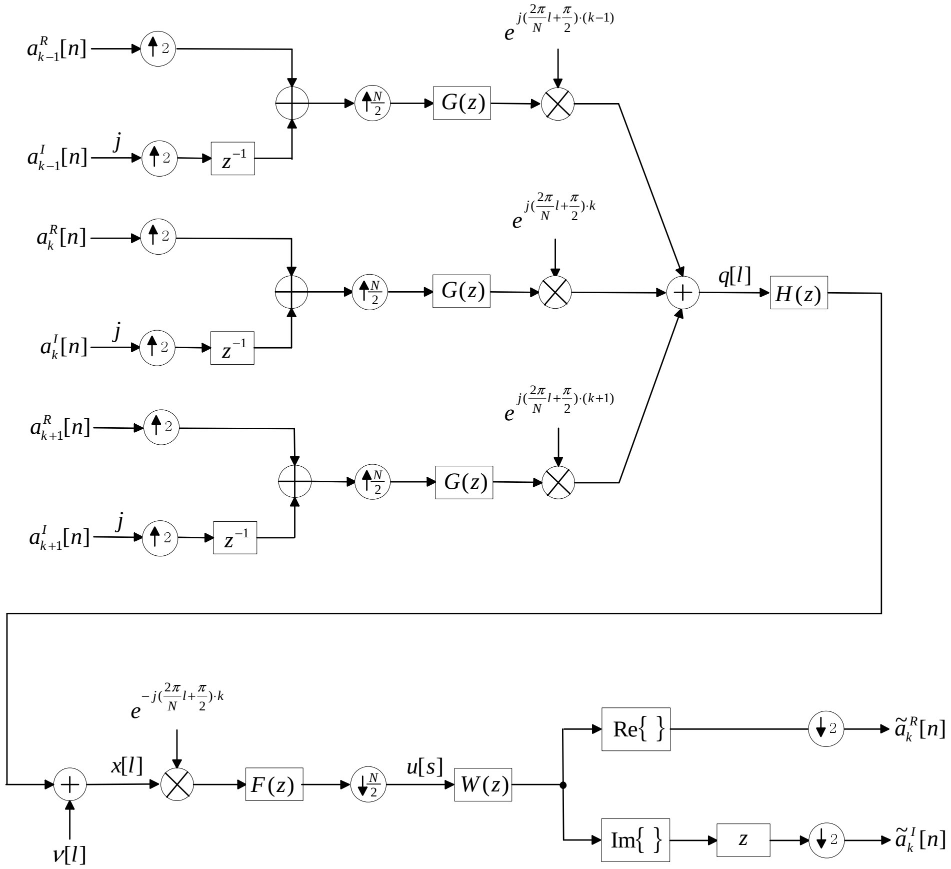
$a^R_{k-1}[n]$
$a^I_{k-1}[n]$
$a^R_k[n]$
$a^I_k[n]$
$a^R_{k+1}[n]$
$a^I_{k+1}[n]$
j
$\uparrow 2$
z^{-1}
$\uparrow \frac{N}{2}$
$G(z)$
$e^{j(\frac{2\pi}{N}l+\frac{\pi}{2})\cdot(k-1)}$
$e^{j(\frac{2\pi}{N}l+\frac{\pi}{2})\cdot k}$
$e^{j(\frac{2\pi}{N}l+\frac{\pi}{2})\cdot(k+1)}$
$q[l]$
$H(z)$
$e^{-j(\frac{2\pi}{N}l+\frac{\pi}{2})\cdot k}$
$x[l]$
$\nu[l]$
$F(z)$
$\downarrow \frac{N}{2}$
$u[s]$
$W(z)$
Re{ }
Im{ }
z
$\downarrow 2$
$\tilde{a}^R_k[n]$
$\tilde{a}^I_k[n]$

Figure 3.1: Time-discrete model for OFDM/OQAM systems with a single branch equalizer.

and generates an OFDM/OQAM waveform

$$q[l] = \sum_{m=k-1}^{k+1} \sum_{n=-\infty}^{\infty} \left(a_m^{\mathcal{R}}[n]\, g[l-nN] + j\, a_m^{\mathcal{I}}[n]\, g[l-nN-N/2]\right) e^{j(\frac{2\pi}{N}l+\frac{\pi}{2})m}.$$

The transmitter filter $g[l]$ operates with a sampling interval T/N, which is also the sampling interval of the receiver filter $f[l]$. Assuming a linear time-invariant (LTI) channel, it can be modelled as a discrete LTI system with impulse response $h[l]$ with the same sampling interval. We have also included an independent additive noise source $\nu[l]$ in the channel. Thus the received signal can be written as

$$x[l] = q[l] * h[l] + \nu[l],$$

where $*$ stands for convolution.

At the receiver side, the channel signal is demodulated by multiplying with $e^{-j(\frac{2\pi}{N}l+\frac{\pi}{2})k}$, filtered by the receiver filter $f[l]$ and down-sampled to yield a sequence with a sampling interval $T/2$:

$$\begin{aligned} u[s] &= x[l]\, e^{-j(\frac{2\pi}{N}l+\frac{\pi}{2})k} * f[l]\Big|_{l=s\frac{N}{2}} \\ &= \Big\{ \sum_{m=k-1}^{k+1} \sum_{n=-\infty}^{\infty} \big(a_m^{\mathcal{R}}[n]\, p_{m,k}^{(o)}[l-nN] + j\, a_m^{\mathcal{I}}[n]\, p_{m,k}^{(o)}[l-nN-N/2] \big) \\ &\quad + \nu_k^{(o)}[l] \Big\}\Big|_{l=s\frac{N}{2}}, \end{aligned} \tag{3.1}$$

where

$$p_{m,k}^{(o)}[l] \overset{\text{def}}{=} j^{(m-k)}\, g[l]\, e^{j\frac{2\pi}{N}(m-k)l} * h[l]\, e^{-j\frac{2\pi}{N}kl} * f[l], \tag{3.2}$$

and

$$\nu_k^{(o)}[l] \overset{\text{def}}{=} \nu[l]\, e^{-j(\frac{2\pi}{N}l+\frac{\pi}{2})k} * f[l]. \tag{3.3}$$

From (3.1), we see that $p_{m,k}^{(o)}[l]$ is actually the equivalent impulse response from subchannel m at the transmitter side to the subchannel k at the receiver side and $h[l]\, e^{-j\frac{2\pi}{N}kl}$ is the equivalent channel impulse response. Since $g[l]$ and $f[l]$ are bandlimited, the equalizer needs only to counteract the effect of non-ideal channel in the range of $[-1/T, 1/T]$, which is just the maximum equalization range of a $T/2$ spaced equalizer. Thus if the equalizer is chosen as the inverse filter (if existing) of the equivalent channel impulse response, both ISI and ICI will be eliminated. Such a zero-forcing equalizer will cause noise enhancement if subchannel k suffers from deep fading. In contrast, an MMSE equalization will result in residual ISI and ICI but the sum of all disturbances will be minimized.

3.2 Equalizer optimization

In Hirosaki's original work [Hir80], the real and imaginary parts are treated separately. Here we use one complex-valued filter instead to simplify the notation. For the equalizer $W(z)$ in Fig. 3.1, we will assume a single branch, two-sided transversal filter with complex-valued coefficients w_k, $k = -K, \cdots, K$. Then the received symbols (subscript k is omitted) before the detector can be written as

$$\begin{aligned} \tilde{a}[n] &= \operatorname{Re}\left\{\mathbf{w}^H \mathbf{u}_{2n}\right\} + j \operatorname{Im}\left\{\mathbf{w}^H \mathbf{u}_{2n+1}\right\} \\ &= \mathbf{w}_r^T \mathbf{u}_{r,2n} + \mathbf{w}_i^T \mathbf{u}_{i,2n} + j\, \left(\mathbf{w}_r^T \mathbf{u}_{i,2n+1} - \mathbf{w}_i^T \mathbf{u}_{r,2n+1}\right), \end{aligned} \tag{3.4}$$

where $\{\cdot\}^H$ represents the conjugate-transpose, and

$$\begin{aligned}\mathbf{u}_n &= \begin{bmatrix} u[n+K] & \cdots & u[n-K]\end{bmatrix}^T, \ \mathbf{u}_{r,n} = \mathrm{Re}\{\mathbf{u}_n\}, \ \mathbf{u}_{i,n} = \mathrm{Im}\{\mathbf{u}_n\} \\ \mathbf{w} &= \begin{bmatrix} w_{-K} & \cdots & w_K\end{bmatrix}^T, \ \mathbf{w}_r = \mathrm{Re}\{\mathbf{w}\}, \ \mathbf{w}_i = \mathrm{Im}\{\mathbf{w}\}.\end{aligned}$$

Now we are ready to search for the optimal equalizer coefficients based on the MMSE criterion.

3.2.1 Normal equation for general OFDM/OQAM systems

The target of the equalizer will be to reduce disturbances to a minimum. This requirement can be formulated as a mean square error (MSE) minimization problem with objective function

$$J(\mathbf{w}) = \mathbb{E}\big[|e[n]|^2\big] = \mathbb{E}\big[|a[n] - \tilde{a}[n]|^2\big]. \tag{3.5}$$

Then substituting (3.4) into (3.5), we can rewrite the objective function as

$$J(\mathbf{w}) = \begin{bmatrix}\mathbf{w}_r^T & \mathbf{w}_i^T\end{bmatrix}\begin{bmatrix}\mathbf{A}_1 & -\mathbf{B} \\ -\mathbf{B}^T & \mathbf{A}_2\end{bmatrix}\begin{bmatrix}\mathbf{w}_r \\ \mathbf{w}_i\end{bmatrix} - 2\begin{bmatrix}\mathbf{p}_1^T & \mathbf{p}_2^T\end{bmatrix}\begin{bmatrix}\mathbf{w}_r \\ \mathbf{w}_i\end{bmatrix} + \sigma_a^2, \tag{3.6}$$

where

$$\begin{aligned}\mathbf{A}_1 &= \mathbb{E}\left[\mathbf{u}_{r,2n}\mathbf{u}_{r,2n}^T + \mathbf{u}_{i,2n+1}\mathbf{u}_{i,2n+1}^T\right], \ \mathbf{A}_2 = \mathbb{E}\left[\mathbf{u}_{i,2n}\mathbf{u}_{i,2n}^T + \mathbf{u}_{r,2n+1}\mathbf{u}_{r,2n+1}^T\right] \\ \mathbf{B} &= -\mathbb{E}\left[\mathbf{u}_{r,2n}\mathbf{u}_{i,2n}^T - \mathbf{u}_{i,2n+1}\mathbf{u}_{r,2n+1}^T\right] \\ \mathbf{p}_1 &= \mathbb{E}\left[a^{\mathcal{R}}[n]\,\mathbf{u}_{r,2n} + a^{\mathcal{I}}[n]\,\mathbf{u}_{i,2n+1}\right], \ \mathbf{p}_2 = \mathbb{E}\left[a^{\mathcal{R}}[n]\,\mathbf{u}_{i,2n} - a^{\mathcal{I}}[n]\,\mathbf{u}_{r,2n+1}\right] \\ \sigma_a^2 &= \mathbb{E}\big[|a[n]|^2\big].\end{aligned} \tag{3.7}$$

The optimal equalizer can thus be found by solving the equations $\partial J(\mathbf{w})/\partial \mathbf{w}_r = 0$ and $\partial J(\mathbf{w})/\partial \mathbf{w}_i = 0$. The optimal solution of equalizer coefficients is not always practical. In particular when a time varying channel is given, an adaptive solution may be used. The partial derivative of equation (3.6) with respect to $\mathbf{w}_r$ and $\mathbf{w}_i$ can be written as

$$\begin{aligned}\frac{\partial J}{\partial \mathbf{w}_r} &= 2\big(\mathbf{A}_1\mathbf{w}_r - \mathbf{B}\mathbf{w}_i - \mathbf{p}_1\big) - 2\,\mathbb{E}\big[\mathbf{u}_{2n,r}\mathrm{Re}\{e[n]\} + \mathbf{u}_{2n+1,i}\mathrm{Im}\{e[n]\}\big] \\ \frac{\partial J}{\partial \mathbf{w}_i} &= 2\big(\mathbf{A}_2\mathbf{w}_i - \mathbf{B}^T\mathbf{w}_r - \mathbf{p}_2\big) - 2\,\mathbb{E}\big[\mathbf{u}_{2n,i}\mathrm{Re}\{e[n]\} - \mathbf{u}_{2n+1,r}\mathrm{Im}\{e[n]\}\big].\end{aligned}$$

Then

$$\frac{\partial J}{\partial \mathbf{w}} = \frac{1}{2}\Big(\frac{\partial J}{\partial \mathbf{w}_r} + j\frac{\partial J}{\partial \mathbf{w}_i}\Big) = E\big\{-\mathbf{u}_{2n}\mathrm{Re}\{e[n]\} + j\cdot\mathbf{u}_{2n+1}\mathrm{Im}\{e[n]\}\big\}. \tag{3.8}$$

If the expectation $\mathbb{E}\big\{-\mathbf{u}_{2n}^{*}\mathrm{Re}\left\{e[n]\right\} - j \cdot \mathbf{u}_{2n+1}^{*}\mathrm{Im}\left\{e[n]\right\}\big\}$ in equation (3.8) is estimated by $\big[-\mathbf{u}_{2n}^{*}\mathrm{Re}\left\{e[n]\right\} - j \cdot \mathbf{u}_{2n+1}^{*}\mathrm{Im}\left\{e[n]\right\}\big]$, the adaptive iteration based on steepest decent can be written as

$$\hat{\mathbf{w}}(k+1) = \hat{\mathbf{w}}(k) + \mu \cdot \big[\mathbf{u}_{2n}\mathrm{Re}\left\{e[n]\right\} - j \cdot \mathbf{u}_{2n+1}\mathrm{Im}\left\{e[n]\right\}\big], \tag{3.9}$$

where μ is the step-size parameter.

3.2.2 Normal equation for unweighted OFDM/OQAM systems

The expressions above are valid for both single carrier [Tu93] and multicarrier [Hir80] OQAM transmitting systems. The latter ones can even have subchannel weighting, i.e. different transmitted signal power in each subchannel. For an OFDM/OQAM system with weighting, the optimal equalizer is too complicated to be derived explicitly. For systems in which each subchannel has the same signal power, we will show in (3.15) that the optimal problem is similar to a single carrier QAM transmission system, which is much simpler. For the rest of this chapter we will assume such *unweighted* systems.

In the following we assume (as is common for OFDM/OQAM systems) that the transmitter filter $g[l]$ and receiver filter $f[l]$ are defined by identical real-valued symmetric pulses, i.e. $f[l] = g[l] = f[-l]$. We further assume that the input QAM symbols are i.i.d. between different subchannels, different instants, and between real and imaginary parts, i.e.

$$\begin{aligned} \mathbb{E}\left[a_m^{\mathcal{R}}[n_1]\, a_k^{\mathcal{R}}[n_2]\right] = \mathbb{E}\left[a_m^{\mathcal{I}}[n_1]\, a_k^{\mathcal{I}}[n_2]\right] &= \frac{\sigma_a^2}{2}\,\delta(m-k, n_1-n_2) \\ \mathbb{E}\left[a_m^{\mathcal{R}}[n_1]\, a_k^{\mathcal{I}}[n_2]\right] &= 0, \ \forall\ m, k, n_1, n_2, \end{aligned}$$

where $\delta(k,n)$ stands for the two-dimensional Kronecker delta function.

Without loss of generality, we may assume that $\sigma_a^2 = 1$. The additive noise is assumed white, zero-mean with variance σ_ν^2. Note that we make no assumption about the distribution of additive noise and input QAM symbols.

By defining the $N/2$ times down-sampled versions $p_{m,k}[s] = p_{m,k}^{(o)}[s\frac{N}{2}]$ and $\nu_k[s] = \nu_k^{(o)}[s\frac{N}{2}]$, and further defining

$$\begin{aligned} p_{m,k}^{\mathcal{R}}[s] = \mathrm{Re}\{p_{m,k}[s]\},\ p_{m,k}^{\mathcal{I}}[s] = \mathrm{Im}\{p_{m,k}[s]\} \\ \nu_k^{\mathcal{R}}[s] = \mathrm{Re}\{\nu_k[s]\},\ \nu_k^{\mathcal{I}}[s] = \mathrm{Im}\{\nu_k[s]\}, \end{aligned}$$

we can write the real and imaginary parts of $u[s]$ given by (3.1) as

$$\begin{aligned}
u_r[s] &= \sum_{m=k-1}^{k+1} \sum_{n=-\infty}^{\infty} \big(a_m^{\mathcal{R}}[n]\, p_{m,k}^{\mathcal{R}}[s-2n] - (-1)^{(m-k)}\, a_m^{\mathcal{I}}[n]\, p_{m,k}^{\mathcal{I}}[s-2n-1]\big) \\
&\quad + \nu_k^{\mathcal{R}}[s] \\
u_i[s] &= \sum_{m=k-1}^{k+1} \sum_{n=-\infty}^{\infty} \big(a_m^{\mathcal{R}}[n]\, p_{m,k}^{\mathcal{I}}[s-2n] + (-1)^{(m-k)}\, a_m^{\mathcal{I}}[n]\, p_{m,k}^{\mathcal{R}}[s-2n-1]\big) \\
&\quad + \nu_k^{\mathcal{I}}[s].
\end{aligned} \tag{3.10}$$

Then after some derivation, we can write the auto correlation functions $c_{u_r}[s,\tau]$, $c_{u_i}[s,\tau]$ and the cross correlation function $c_{u_{ri}}[s,\tau]$ as

$$\begin{aligned}
c_{u_r}[s,\tau] &\overset{\text{def}}{=} \mathbb{E}\big[u_r[s]\, u_r[s-\tau]\big] \\
&= \frac{1}{2} \sum_{m=k-1}^{k+1} \sum_{n=-\infty}^{\infty} \big(p_{m,k}^{\mathcal{R}}[s-2n]\, p_{m,k}^{\mathcal{R}}[s-\tau-2n] \\
&\quad + p_{m,k}^{\mathcal{I}}[s-2n-1]\, p_{m,k}^{\mathcal{I}}[s-\tau-2n-1]\big) + \frac{\sigma_\nu^2}{2}\, p_t[\tau] \\
c_{u_i}[s,\tau] &\overset{\text{def}}{=} \mathbb{E}\big[u_i[s]\, u_i[s-\tau]\big] \\
&= \frac{1}{2} \sum_{m=k-1}^{k+1} \sum_{n=-\infty}^{\infty} \big(p_{m,k}^{\mathcal{I}}[s-2n]\, p_{m,k}^{\mathcal{I}}[s-\tau-2n] \\
&\quad + p_{m,k}^{\mathcal{R}}[s-2n-1]\, p_{m,k}^{\mathcal{R}}[s-\tau-2n-1]\big) + \frac{\sigma_\nu^2}{2}\, p_t[\tau] \\
c_{u_{ri}}[s,\tau] &\overset{\text{def}}{=} \mathbb{E}\big[u_r[s]\, u_i[s-\tau]\big] \\
&= \frac{1}{2} \sum_{m=k-1}^{k+1} \sum_{n=-\infty}^{\infty} \big(p_{m,k}^{\mathcal{R}}[s-2n]\, p_{m,k}^{\mathcal{I}}[s-\tau-2n] \\
&\quad - p_{m,k}^{\mathcal{I}}[s-2n-1]\, p_{m,k}^{\mathcal{R}}[s-\tau-2n-1]\big),
\end{aligned} \tag{3.11}$$

where

$$p_t[\tau] \overset{\text{def}}{=} f[l] * f[-l]\big|_{l=\tau\frac{N}{2}} \tag{3.12}$$

is the $N/2$ times down-sampled version of the cascade of transmitter filter $g[l]$ and receiver filter $f[l]$ (recall that $g[l] = f[l] = f[-l]$).

It can be easily verified that $c_{u_r}[s,\tau]$, $c_{u_i}[s,\tau]$ and $c_{u_{ri}}[s,\tau]$ are periodic in s with a period 2. We also have that $c_{u_i}[s+1,\tau] = c_{u_r}[s,\tau]$, which means that $c_{u_i}[s,\tau]$ can be inferred from $c_{u_r}[s,\tau]$ directly. Therefore we deal only with $c_{u_r}[s,\tau]$ and $c_{u_{ri}}[s,\tau]$ in the following discussion.

The rest of this section is more conveniently preformed in frequency domain. It is proved in Appendix A that for an unweighted OFDM/OQAM system, $c_{u_r}[s,\tau]$ and $c_{u_{ri}}[s,\tau]$ are actually independent of time instant s, and can be expressed as

$$\begin{aligned} c_{u_r}[\tau] &= \frac{1}{8}\sum_{m=k-1}^{k+1} \mathrm{Re}\left\{S_{m,k}[\tau]\right\} + \frac{\sigma_\nu^2}{2}p_t[\tau] \\ c_{u_{ri}}[\tau] &= \frac{1}{8}\sum_{m=k-1}^{k+1} \mathrm{Im}\left\{S_{m,k}[\tau]\right\}, \end{aligned} \tag{3.13}$$

where

$$\begin{aligned} S_{m,k}[\tau] &\overset{\text{def}}{=} \int_{-0.5}^{0.5} \left(|P_{m,k}(f)|^2 + (-1)^\tau |P_{m,k}(f-1)|^2\right) e^{-j\pi f\tau}\,df \\ &= \int_{-1}^{1} |P_{m,k}(f)|^2 \, e^{-j\pi f\tau}\,df, \end{aligned}$$

and

$$P_{m,k}(f) \overset{\text{def}}{=} \sum_{s=-\infty}^{\infty} p_{m,k}[s]\, e^{-j\pi f s}.$$

Now we are ready to derive the objective function for an unweighted OFDM/OQAM system. Based on the definitions in (3.7), we have

$$\begin{aligned} \mathbf{A}_2 = \mathbf{A}_1 &= 2\begin{bmatrix} c_{u_r}[0] & \cdots & c_{u_r}[2K] \\ \vdots & \ddots & \vdots \\ c_{u_r}[2K] & \cdots & c_{u_r}[0] \end{bmatrix} \\ \mathbf{B} &= 2\begin{bmatrix} c_{u_{ri}}[0] & \cdots & -c_{u_{ri}}[2K] \\ \vdots & \ddots & \vdots \\ c_{u_{ri}}[2K] & \cdots & c_{u_{ri}}[0] \end{bmatrix}. \end{aligned} \tag{3.14}$$

By substituting (3.10) into the definitions of $\mathbf{p}_1$ and $\mathbf{p}_2$ in (3.7), we further get

$$\mathbf{p}_1 = \begin{bmatrix} p^{\mathcal{R}}_{k,k}[K] \\ \vdots \\ p^{\mathcal{R}}_{k,k}[-K] \end{bmatrix}, \; \mathbf{p}_2 = \begin{bmatrix} p^{\mathcal{I}}_{k,k}[K] \\ \vdots \\ p^{\mathcal{I}}_{k,k}[-K] \end{bmatrix}.$$

By defining $\mathbf{R} = \mathbf{A}_1 + j\,\mathbf{B}$ and $\mathbf{p} = \mathbf{p}_1 + j\,\mathbf{p}_2$, based on the facts that $\mathbf{A}_2 = \mathbf{A}_1$, $\mathbf{A}_1^T = \mathbf{A}_1$ and $\mathbf{B}^T = -\mathbf{B}$, we can rewrite the objective function (3.6) as

$$J(\mathbf{w}) = \mathbf{w}^H\mathbf{R}\mathbf{w} - 2\,\mathrm{Re}\left\{\mathbf{p}^H\mathbf{w}\right\} + 1. \tag{3.15}$$

One can easily verify that the correlation matrix $\mathbf{R}$ is a Toeplitz-shaped Hermitian matrix and semi-positive definite. Thus it can be denoted by $\big[\mathbf{R}\big]_{m,n} = r[m-n]$, where $r[\tau]$ is given by

$$\begin{aligned} r[\tau] = 2\,\left(c_{u_r}[\tau] + j\,c_{u_{ri}}[\tau]\right) &= \frac{1}{4}\sum_{m=k-1}^{k+1}\int_{-1}^{1} |P_{m,k}(f)|^2\, e^{-j\pi f\tau}\, df + \sigma_\nu^2\, p_t[\tau] \\ &= \frac{1}{4}\int_{-1}^{1} G^2(f)\,\big(G^2(f) + G^2(f-1)\big)\,|H_k(f)|^2\; e^{-j\pi f\tau}\, df + \sigma_\nu^2\, p_t[\tau] \\ &= \frac{1}{2}\int_{-1}^{1} G^2(f)\,|H_k(f)|^2\, e^{-j\pi f\tau}\, df + \sigma_\nu^2\, p_t[\tau], \end{aligned} \tag{3.16}$$

where the last step follows from the fact that $\sum_{n=0}^{1} G^2(f-n) = 2$ since the cascade of transmitter and receiver filters, i.e. $G^2(f)$, is a Nyquist pulse.

If $\mathbf{p}$ is denoted by $\big[p[K] \quad \cdots \quad p[-K]\big]^T$, its entries can be expressed as

$$\begin{aligned} p\,[\tau] = p_{k,k}[\tau] &= \frac{1}{2}\int_{-1}^{1} P_{k,k}(f)\, e^{j\pi f\tau}\, df \\ &= \frac{1}{2}\int_{-1}^{1} G^2(f)\, H_k(f)\, e^{j\pi f\tau}\, df. \end{aligned} \tag{3.17}$$

This completes the calculation of the parameters in the objective function (3.15) with complex-valued arguments for unweighted OFDM/OQAM systems. This objective function has a similar form as that for a single carrier QAM transmission system.

3.3 MMSE versus equalizer length

In order to minimize the implementation complexity and system latency, the equalizer length should not be larger than necessary. Thus it is important to know the minimum equalizer length for a given interference level.

By requiring $\partial J(\mathbf{w})/\partial \mathbf{w} = 0$, where $J(\mathbf{w})$ is given by (3.15), we obtain the normal equation

$$\mathbf{R}\mathbf{w} = \mathbf{p}. \tag{3.18}$$

It can be verified that for a noisy channel, $\mathbf{R}$ is always nonsingular. Thus the optimal coefficient vector can be expressed as $\mathbf{w}_o = \mathbf{R}^{-1}\mathbf{p}$ and the corresponding minimum mean square error (MMSE) is

$$J_{\min} = 1 - \mathbf{p}^H \mathbf{w}_o. \tag{3.19}$$

We note that $\mathbf{R}\mathbf{w}$ is a column vector with entries that can be viewed as the inner products between the rows of $\mathbf{R}$ and $\mathbf{w}$. Then by using Parseval's relation to rewrite these inner products in frequency domain, and taking DTFT of both sides of (3.18), we obtain

$$P_K(f) = \frac{1}{2}\int_{-1}^{1} R_K(f, f')\, W_K^*(f')\, df', \tag{3.20}$$

where

$$\begin{aligned} P_K(f) &\overset{\text{def}}{=} \sum_{m=-K}^{K} p\,[-m]\, e^{-j\pi f m} \\ R_K(f, f') &\overset{\text{def}}{=} \sum_{m=-K}^{K} \sum_{n=-K}^{K} r[m-n]\, e^{-j\pi f' n}\, e^{-j\pi f m} \\ W_K(f) &\overset{\text{def}}{=} \sum_{n=-K}^{K} w_n^*\, e^{-j\pi f n}. \end{aligned} \tag{3.21}$$

Note that $R_K(f, f')$ is the two-dimensional DTFT of the correlation matrix $\mathbf{R}$, and (3.20) is a Fredholm integral equation of the first kind.

By using Parseval's relation, we can also rewrite (3.19) in frequency domain as

$$J_{\min}(K) = 1 - \frac{1}{2}\int_{-1}^{1} P_K(-f)\, W_K(f)\, df. \tag{3.22}$$

If (3.20) can be solved with respect to $W_K(f)$, the result can be substituted into (3.22) to find $J_{\min}(K)$.

3.3.1 MMSE for one-tap equalizer

The simplest possible equalizer has only a single tap. This corresponds to setting $K = 0$. In this case, $\mathbf{R} = r[0]$ is a scalar and can thus be easily inverted. Then based on (3.16) and (3.17), the optimal coefficient of a one-tap equalizer can then be written as

$$w_0 = \frac{p[0]}{r[0]} = \frac{\int_{-1}^{1} G^2(f)\, H_k(f)\, df}{\int_{-1}^{1} G^2(f)\, |H_k(f)|^2\, df + 2\,\sigma_\nu^2}, \tag{3.23}$$

and using (3.19), we get

$$J_{\min}(0) = 1 - \frac{\left|\int_{-1}^{1} G^2(f)\, H_k(f)\, df\right|^2}{2\int_{-1}^{1} G^2(f)\ |H_k(f)|^2\ df + 4\,\sigma_\nu^2}. \tag{3.24}$$

This is an explicit expression of MMSE for $K = 0$. Note that the MMSE also depends on subchannel index k due to the frequency selective fading.

3.3.2 MMSE for infinite-tap equalizer

At the other extreme, we now consider the case of an infinite-tap equalizer. Substituting (3.17) into the expression for $P_K(f)$ in (3.21) and taking the limit, we get

$$\begin{aligned} P_\infty(f) &= \frac{1}{2}\int_{-1}^{1} G^2(f')\, H_k(f') \left(\lim_{K\to\infty} \sum_{m=-K}^{K} e^{-j\pi(f'+f)m} \right) df' \\ &= G^2(f)\, H_k(-f). \end{aligned} \tag{3.25}$$

Similarly by using (3.16), we write the two-dimensional DTFT of $\mathbf{R}$ for $K \to \infty$ as

$$R_\infty(f, f') = 2\, G^2(f') \left(|H_k(f')|^2 + \sigma_\nu^2 \right) \delta(f + f'). \tag{3.26}$$

Then substituting (3.25) and (3.26) into (3.20), we get

$$W_\infty(f) = \frac{H_k^*(f)}{|H_k(f)|^2 + \sigma_\nu^2}, \tag{3.27}$$

and finally by substituting (3.25) and (3.27) into (3.22), we obtain

$$\begin{aligned} J_{\min}(\infty) &= 1 - \frac{1}{2}\int_{-1}^{1} \frac{G^2(f)\, |H_k(f)|^2}{|H_k(f)|^2 + \sigma_\nu^2}\, df \\ &= \frac{\sigma_\nu^2}{2}\int_{-1}^{1} \frac{G^2(f)}{|H_k(f)|^2 + \sigma_\nu^2}\, df. \end{aligned} \tag{3.28}$$

We see that for $K \to \infty$, the optimal equalizer only depends on the channel, while the MMSE is still relative to the pulseshape $G(f)$. For the special case of noise-free channel, i.e. $\sigma_\nu^2 = 0$, we have $W_\infty(f) = 1/H_k(f)$ for $f \in [-1, 1]$, which is the inverse filter of the equivalent channel. We also have that $J_{\min}(\infty) = 0$, which means that both ISI and ICI are completely eliminated. Therefore, in the absence of noise, the MMSE equalizer is identical to a zero-forcing equalizer.

3.3.3 MMSE for finite-tap equalizer

Having found explicit expressions for the two extreme cases $K = 0$ and $K = \infty$, we will now attack the more difficult problem of finding a general expression for $J_{\min}(K)$. First we define the differences

$$\begin{aligned} \Delta W_K(f) &= W_K(f) - W_\infty(f) \\ \Delta P_K(f) &= P_K(f) - P_\infty(f) \\ \Delta R_K(f, f') &= R_K(f, f') - R_\infty(f, f'). \end{aligned} \tag{3.29}$$

Now assuming that these differences are small for large K, we can disregard the second order term $\Delta P_K(-f)\,\Delta W_K(f)$ and approximate the MMSE given in (3.22)) by

$$J_{\min}(K) \simeq J_{\min}(\infty) - \frac{1}{2}\int_{-1}^{1} \mathrm{Re}\big\{\Delta W_K(f)\,P_\infty(-f) + \Delta P_K(-f)\,W_\infty(f)\big\}\,df. \tag{3.30}$$

Note that in (3.30), only $\Delta W_K(f)$ is unknown. Substituting (3.29) into (3.20), then subtracting $P_\infty(f)$ from both sides, and using (3.26) and (3.27), we obtain

$$\Delta W_K(f) = \frac{\Delta P_K^*(-f) - \frac{1}{2}\int_{-1}^{1} \frac{\Delta R_K^*(-f,f')\,H_k^*(f')}{|H_k(f')|^2+\sigma_\nu^2}\,df'}{G^2(f)\;\left(|H_k(f)|^2+\sigma_\nu^2\right)}. \tag{3.31}$$

Finally substituting (3.25), (3.27) and (3.31) into (3.30), after some tedious but straightforward derivation, we find

$$J_{\min}(K) \simeq J_{\min}(\infty) + J_1 + J_2, \tag{3.32}$$

where

$$\begin{aligned}
J_1 &= \sum_{|m|=K+1}^{\infty} \mathrm{Re}\Big\{p^*\,[m]\int_{-1}^{1} T_k(f)\,e^{j\pi f m}\,df\Big\}\\
J_2 &= -\frac{1}{4}\sum_{m=-K}^{K}\ \sum_{|n-m|=K+1}^{\infty} \mathrm{Re}\Big\{r^*[n]\Big(\int_{-1}^{1} T_k(f)\,e^{-j\pi f m}\,df\Big)\\
&\quad\times\Big(\int_{-1}^{1} T_k^*(f)\,e^{-j\pi f(n-m)}\,df\Big)\Big\}\\
&\quad-\frac{1}{2}\sum_{m=K+1}^{\infty} \mathrm{Re}\Big\{\Big(\int_{-1}^{1} T_k(f)\,\cos(m\pi f)\,df\Big)\\
&\quad\times\Big(\int_{-1}^{1} G^2(f)\,H_k^*(f)\,\cos(m\pi f)\,df\Big)\Big\}\\
&\quad+\frac{1}{2}\sum_{m=K+1}^{\infty} \mathrm{Re}\Big\{\Big(\int_{-1}^{1} T_k(f)\,\sin(m\pi f)\,df\Big)\\
&\quad\times\Big(\int_{-1}^{1} G^2(f)\,H_k^*(f)\,\sin(m\pi f)\,df\Big)\Big\},
\end{aligned} \tag{3.33}$$

and $T_k(f) \overset{\text{def}}{=} H_k(f)/\Big(|H_k\,(f)|^2+\sigma_\nu^2\Big)$.

We have now obtained an approximate formula of the MMSE for a finite-tap optimal equalizer. We see that the MMSE for $1 \le K < \infty$ is composed of three terms. The first term is the MMSE of the infinite-tap equalizer. The second and third terms are related to $p\,[\tau]$ and $r[\tau]$ respectively.

3.3.4 Example: MMSE of a two-path transmitting channel

As an example, we assume that the transmitter and receiver filters $g[l]$ and $f[l]$ are square root raised cosine pulses with a roll-off factor equal to one, i.e. $G(f) = \sqrt{2}\ \cos(\pi f/2)$, and define $\mathrm{SNR} = \sigma_a^2/\sigma_\nu^2 = 1/\sigma_\nu^2$. We consider a two-path channel [Rum79], and assume that the main path is ideal, while the second path is τ_c seconds delayed and suffers both amplitude attenuation and phase shift. We define the normalized delay spread $\tau_\mathrm{n} = \tau_\mathrm{c}/T$. For simplicity, we assume the time-discrete delay $N\tau_\mathrm{n}$ to be an integer, and express the time-discrete channel impulse response by $h[l] = \delta[l] + \alpha\, e^{-j\varphi}\,\delta[l - N\tau_\mathrm{n}]$, where α is the attenuation factor and φ is the phase shift. Then the frequency response of the channel is $H(f) = 1 + \alpha\, e^{-j\varphi}\, e^{-j2\pi\tau_\mathrm{n} f}$ and the equivalent frequency response of subchannel k can thus be written as

$$H_k(f) = H(f+k) = 1 + \alpha\, e^{-j(2\pi\tau_\mathrm{n} f + \varphi_k)}, \tag{3.34}$$

where $\varphi_k = 2\,\pi\tau_\mathrm{n} k + \varphi$.

We now assume that the channel varies statistically, where the phase shift φ is assumed to be uniformly distributed in $[0, 2\,\pi]$, while the normalized delay spread τ_n and the attenuation factor are constants. We will denote averaging a variable x with respect to the statistical variations in the channel model by $\overline{x}$. Note that since we have assumed that $N\tau_\mathrm{n}$ is an integer, averaging MMSE over all subchannels is approximately equal to averaging over the statistical variations in the channel model. By substituting (3.34) into (3.24), and taking the statistical expectation over φ_k, we get the average MMSE for the one-tap equalizer

$$\overline{J_\mathrm{min}}(0) = \frac{\alpha^2 \left(1 - \mathrm{sinc}^2(2\,\pi\tau_\mathrm{n})/(1 - 4\,\tau_\mathrm{n}^2)^2\right) + \mathrm{SNR}^{-1}}{\sqrt{\left(1 + \alpha^2 + \mathrm{SNR}^{-1}\right)^2 - 4\,\alpha^2\ \mathrm{sinc}^2(2\,\pi\tau_\mathrm{n})/(1 - 4\,\tau_\mathrm{n}^2)^2}}. \tag{3.35}$$

Similarly by substituting (3.34) into (3.28) and taking the expectation over φ_k, we get the average MMSE for the infinite-tap equalizer

$$\overline{J_\mathrm{min}}(\infty) = \frac{\mathrm{SNR}^{-1}}{\sqrt{(1 - \alpha^2)^2 + 2\,(1 + \alpha^2)\ \mathrm{SNR}^{-1} + \mathrm{SNR}^{-2}}}. \tag{3.36}$$

We see that the average MMSE for the one-tap equalizer is a function of the normalized delay spread τ_n, while the one for an infinite-tap equalizer is independent of τ_n. The curves of $\overline{J_\mathrm{min}}(0)$ and $\overline{J_\mathrm{min}}(\infty)$ versus α for different SNR levels are shown in Fig. 3.2, with $\tau_\mathrm{n} = 1/16$ for the one-tap equalizer. We can see that both $\overline{J_\mathrm{min}}(0)$ and $\overline{J_\mathrm{min}}(\infty)$ have their maximum values at a point near $\alpha = 1$.

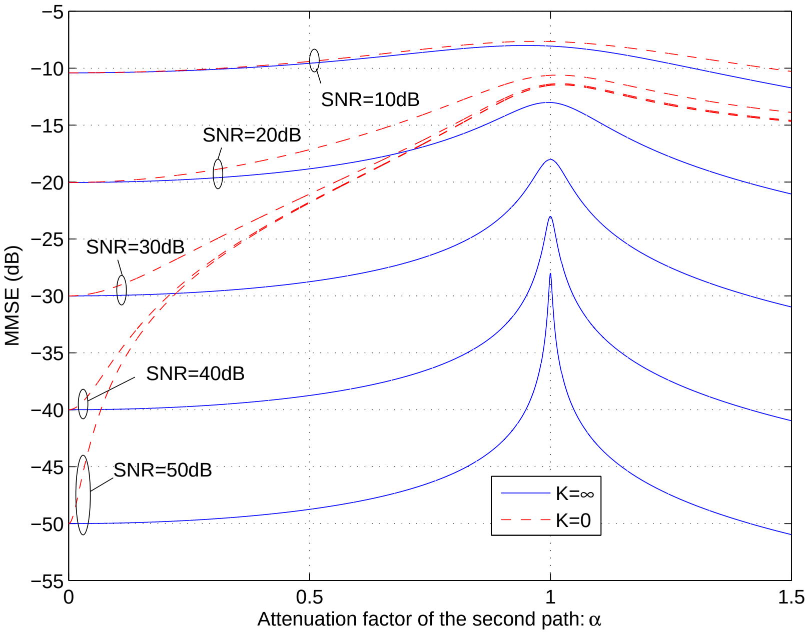

Figure 3.2: Average MMSE $\overline{J_{\min}}(K)$ of one and infinite-tap equalizers versus second path attenuation factor α with SNR as parameter ($\tau_{\mathrm{n}} = 1/16$ for the one-tap equalizer).

The curves for $\overline{J_{\min}}(0)$ and $\overline{J_{\min}}(\infty)$ versus τ_{n} for different α and SNR are shown in Fig. 3.3. We see that for τ_{n} small, the gap between $\overline{J_{\min}}(0)$ and $\overline{J_{\min}}(\infty)$ is also small, which implies that a one-tap equalizer is enough. We also note that for higher SNR, the gap is larger. This means that more taps are needed. For large τ_{n}, we note that $\overline{J_{\min}}(0)$ converges to the same value for different SNR levels. This can be explained by noting that MMSE is dominated by interference (ISI and ICI) for high SNR.

Based on formulas (3.35) and (3.36), we may give some theoretical explanation for the curves in Fig. 3.3. To determine the necessity of using a multi-tap equalizer, we define a ratio $G_{\max} = \overline{J_{\min}}(0)/\overline{J_{\min}}(\infty)$, which is the maximum obtainable gain by increasing the number of equalizer taps. By substituting (3.35) and (3.36) into the expression of $G_{\max}$, then using Taylor approximation with respect to τ_{n} and omitting the fourth order terms $O\left(\tau_{\mathrm{n}}^4\right)$, we get

$$G_{\max} \simeq 1 + C\,\tau_{\mathrm{n}}^2, \tag{3.37}$$

where

$$C = \frac{(4\,\pi^2/3 - 8)\,\alpha^2\ \mathrm{SNR}\left[(1-\alpha^2)^2 + 2\,\alpha^2\ \mathrm{SNR}^{-1} + \mathrm{SNR}^{-2}\right]}{(1+\alpha^2+\mathrm{SNR}^{-1})^2 - 4\,\alpha^2}.$$

Then for α and SNR given, $G_{\max}$ increases quadratically with increasing normalized delay spread and the rate of increase is determined by the parameter C. For $\alpha = 0$, we have $C = 0$, thus $G_{\max} = 1$. This is expected since for $\alpha = 0$, the channel is ideal and then equalization is not needed. We also note that C is approximately proportional to SNR, which implies that more precise equalization is needed for high SNR. This is in accordance with the curves in Fig. 3.3.

The curve presented for $\overline{J_{\min}}(\infty)$ represents a lower bound of what can be expected by a practical finite-tap equalizer. We will now study how close to this bound one can come by comparing $\overline{J_{\min}}(K)$ to $\overline{J_{\min}}(\infty)$. Numerical values of $\overline{J_{\min}}(K)$ are found in two steps. First the correlation matrix $\mathbf{R}$ in (3.18) is inverted numerically to find $J_{\min}(K)$ by (3.19). Then the average MMSE $\overline{J_{\min}}(K)$ is calculated by numerical integration over the phase shift φ_k. The resulting curves for $\overline{J_{\min}}(K)$ versus normalized delay spread τ_{n} with SNR$=$ 40 dB are shown in Fig. 3.4. We see that larger K means lower MMSE while the gain obtained by introducing multiple taps becomes marginal. We also note that for the worst case ($\alpha = 1.0$), more equalizer taps are needed to obtain the same equalization gain.

The discussion above is based on the numerical results. To assess how large equalizer length is required in a given situation, a closed-form expression for the MMSE versus K is needed. Due to the difficulty of explicitly inverting the correlation matrix $\mathbf{R}$, an approximate formula is suggested in

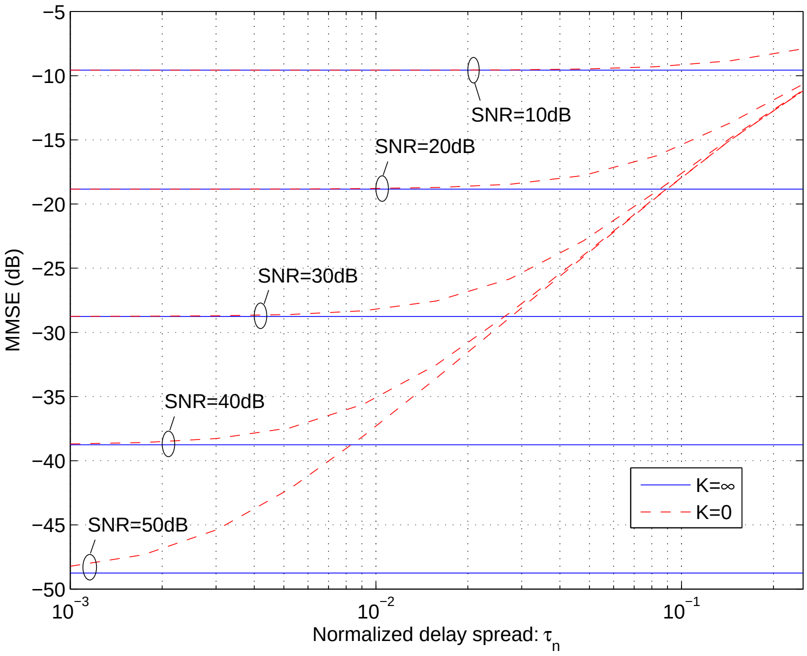

(a) $\alpha = 0.5$

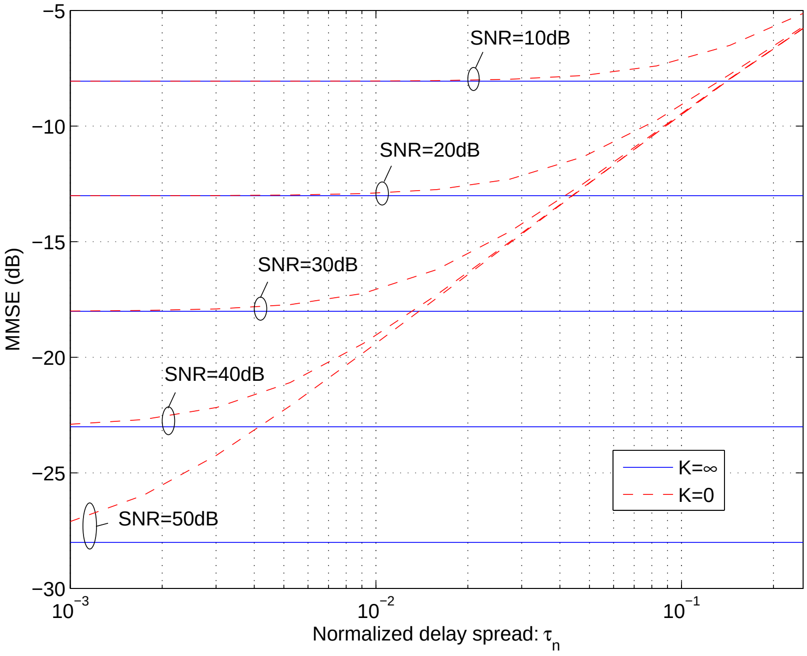

(b) $\alpha = 1.0$

Figure 3.3: Average MMSE $\overline{J_{\min}}(K)$ of one and infinite-tap equalizer versus normalized delay spread τ_{n} with attenuation factor α and SNR as parameters.

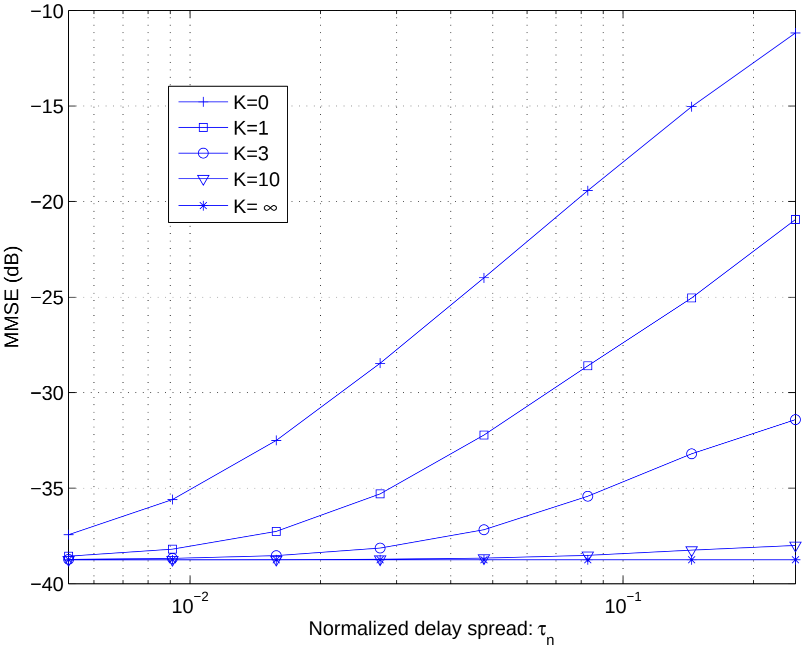

(a) $\alpha = 0.5$

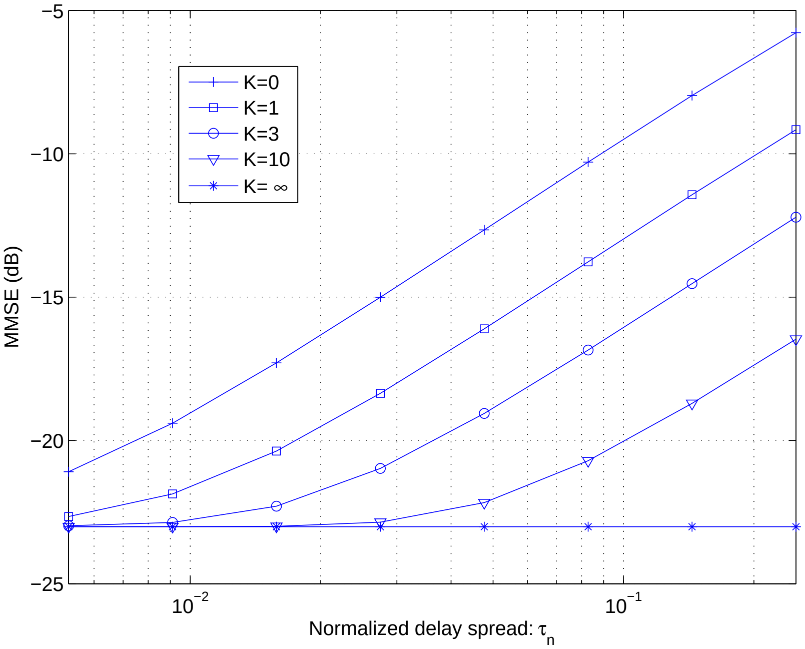

(b) $\alpha = 1.0$

Figure 3.4: Average MMSE $\overline{J_{\min}}(K)$ versus normalized delay spread τ_{n} with equalizer length $2K + 1$ as parameter (SNR = 40 dB).

Appendix B based on (3.30). It is found that

$$J_{\min}(K) \simeq J_{\min}(\infty) + \frac{B}{K\,(K+1)}, \tag{3.38}$$

where

$$B = \frac{4\,\alpha^2\,\tau_{\mathrm{n}}^2\big[\big(1+\alpha^2+2\,\alpha\,\cos(\varphi_k)+\mathrm{SNR}^{-1}\big)^2 - 4\,\sin^2(\varphi_k)\,\mathrm{SNR}^{-1}\big]}{\pi\,\big(1+\alpha^2+2\,\alpha\,\cos(\varphi_k)+\mathrm{SNR}^{-1}\big)^3}.$$

The constant B is independent of K, giving an inverse quadratic convergence towards $J_{\min}(\infty)$ with increasing K. The approximate average MMSE $\overline{J_{\min}}(K)$ can be obtained by averaging B over φ_k. The curves for average MMSE versus K for different SNR and delay spread are shown in Fig. 3.5. The attenuation factor α is set to 0.5. In the figure, the approximate curves are shown together with exact curves obtained by numerical inversion of the correlation matrix $\mathbf{R}$. Note that for $K = 0$, the average MMSE is calculated by formula (3.35). We can see that the average MMSE decreases quickly with increasing K, and saturates after a certain value of K. Higher SNR or larger delay spread τ_{n} requires larger K to reach the saturation threshold. For SNR $= 10, 20$ and 30 dB, the approximate average MMSE matches well with the exact value. For SNR $= 40$ and 50 dB, the approximation can be used as an upper bound on $\overline{J_{\min}}(K)$. We also note that the approximation error is larger for larger delay spread τ_{n}. This is because a first order approximation of the channel is used in the derivation (see formula (B.5) in Appendix B). Larger τ_{n} means worse approximation of the channel, hence worse approximation of the average MMSE.

Finally the curves for average MMSE versus SNR for different K are shown in Fig. 3.6. We can see that longer equalizers is needed for higher SNR, and the approximation formula (3.38) matches well with theoretical values for SNR less than 30 dB, especially for $\tau_{\mathrm{n}} = 1/16$.

3.4 Conclusion

In this chapter, we have derived expressions of MMSE versus equalizer length for OFDM/OQAM systems. These expressions are useful for determining how complicated equalizers are necessary in a given case. An example of a two-path channel is studied to illustrate the use of these expressions. For a two-path channel, we show that the maximum obtainable gain by introducing a multi-tap equalizer increases approximately quadratically with increasing the normalized delay spread τ_{n}. From another point of view, the need of a multi-tap equalizer decreases quadratically with increasing the number of subchannels. We also show that the average MMSE

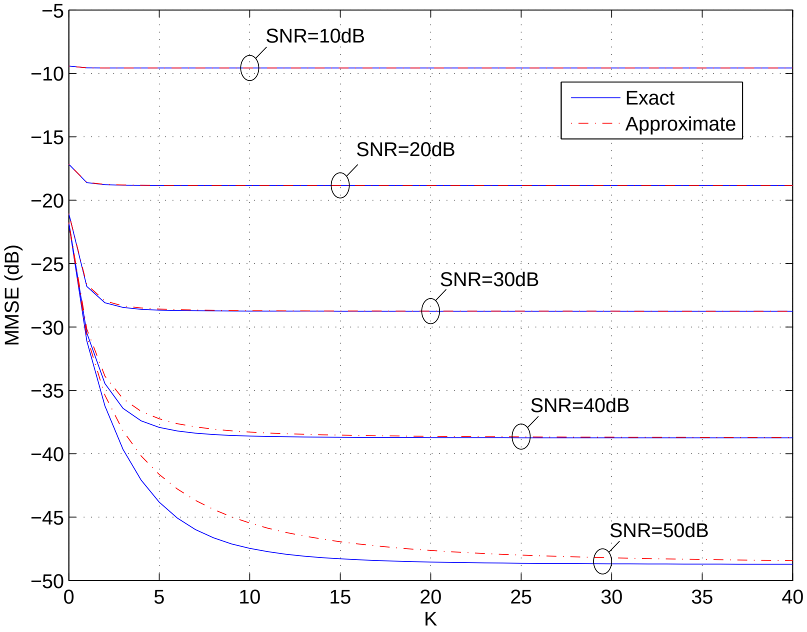

(a) $\tau_\mathrm{n} = 1/16$

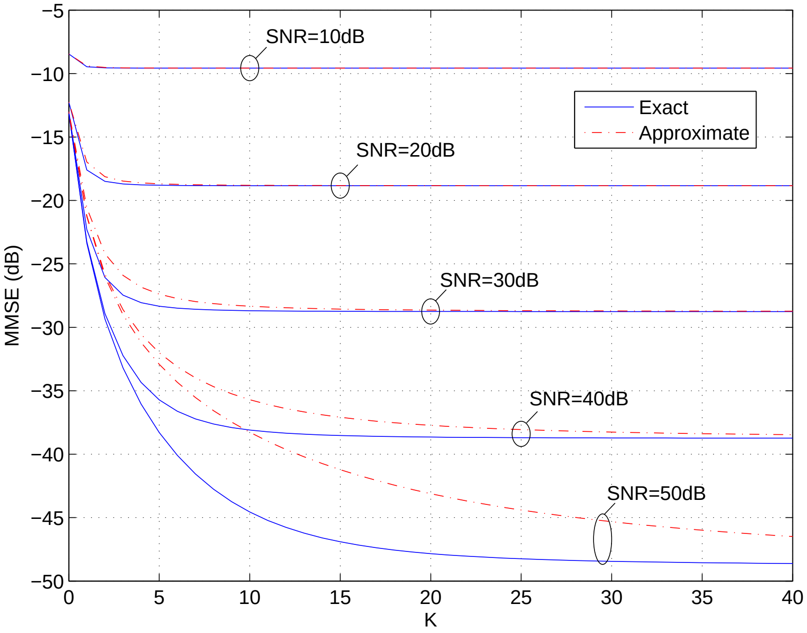

(b) $\tau_\mathrm{n} = 3/16$

Figure 3.5: Average MMSE $\overline{J_{\min}}(K)$ versus equalizer length $2K+1$ with SNR and normalized delay spread τ_n as parameters ($\alpha = 0.5$).

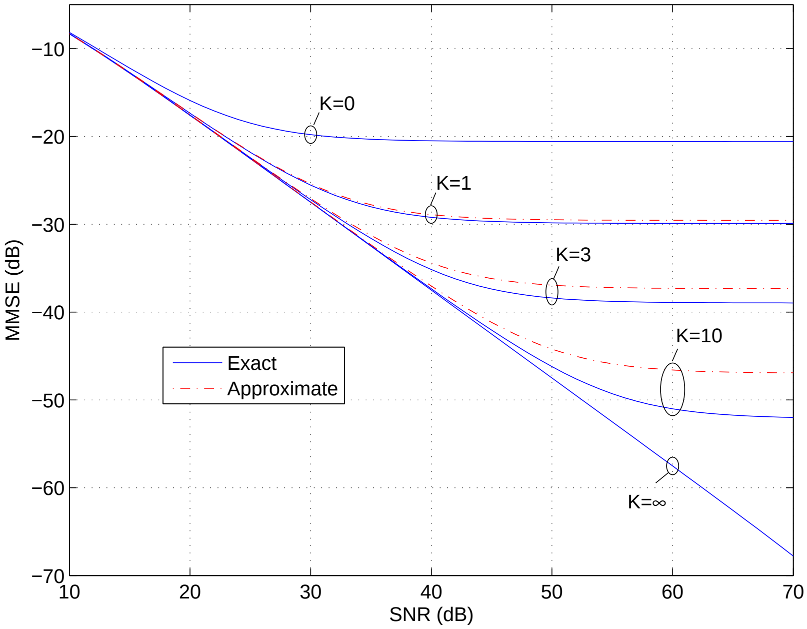

(a) $\tau_{\mathrm{n}} = 1/16$

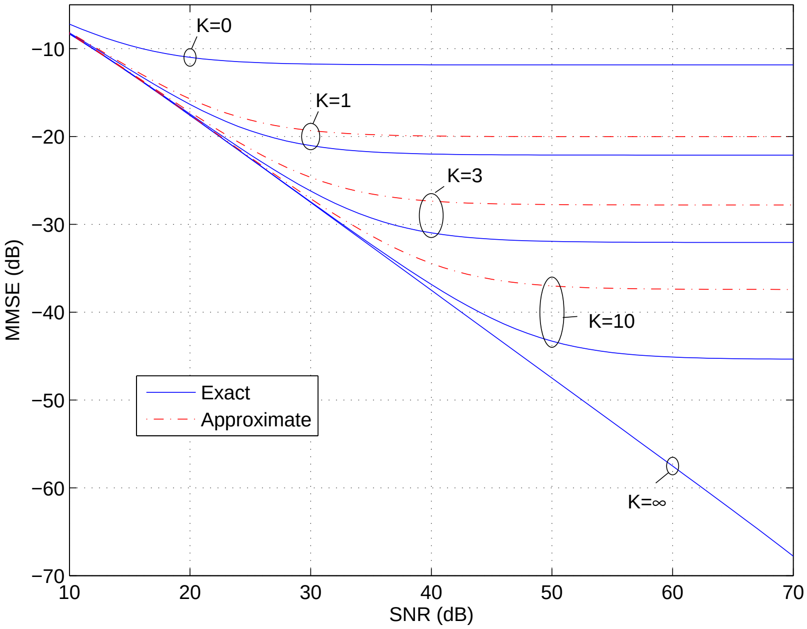

(b) $\tau_{\mathrm{n}} = 3/16$

Figure 3.6: Average MMSE $\overline{J_{\min}}(K)$ versus SNR with equalizer length $2K + 1$ and normalized delay spread τ_{n} as parameters ($\alpha = 0.5$).

converges quadratically to a floor with increasing number of equalizer taps. This implies that very long equalizers are not necessary in OFDM/OQAM systems. Numerical results show that for the case of the attenuation factor of the second path $\alpha = 0.5$ and SNR$=$ 40 dB, if we require the average MMSE to be lower than -35 dB, a one-tap ($K = 0$) equalizer is enough for $\tau_{\mathrm{n}} < 0.01$ and a seven-tap ($K = 3$) equalizer can be used up to $\tau_{\mathrm{n}} = 0.1$.

These results show that the equalization for OFDM/OQAM systems can be quite efficiently implemented. In addition, we have shown in Chapter 2 that OFDM/OQAM can be efficiently implemented with a complexity only slightly higher than conventional OFDM/QAM systems. Taking into account the increased spectrum and power efficiency and more compact spectrum, OFDM/OQAM system seems an attractive substitute for ordinary OFDM/QAM systems with guard interval.

Chapter 4

Design of Optimal Pulses Robust to CFO for OFDM Systems

A model of an OFDM system with carrier recovery and symbol synchronizer is shown in Fig. 4.1. At the transmitter side, the sequence from the OFDM modulator is multiplied with a sinusoidal signal with frequency f_c to generate the transmitted passband signal. At the receiver side, the received signal is down-converted by multiplying with the recovered carrier with frequency $\hat{f}_c$. The recovered carrier frequency $\hat{f}_c$ can be estimated based on pilot symbols or blindly. Then the down-converted baseband signal is resampled to generate the input sequence to the OFDM demodulator. The symbol synchronizer is used to eliminate the effects caused by timing offset.

Due to Doppler frequency shift and/or oscillator inaccuracy, the carrier frequency should be estimated from time to time. However, carrier

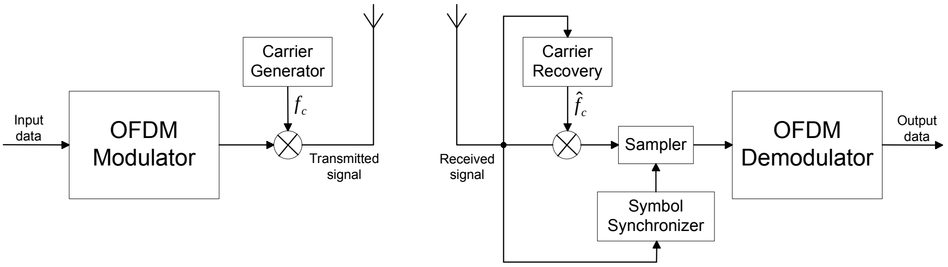
Input data
OFDM Modulator
Carrier Generator
f_c
Transmitted signal
Received signal
Carrier Recovery
$\hat{f}_c$
Sampler
Symbol Synchronizer
OFDM Demodulator
Output data

Figure 4.1: Model of OFDM transmission systems with carrier recovery and symbol synchronizer.

frequency can never be perfectly recovered.

Since the bandwidth of each subchannel is only a small fraction of the total bandwidth, OFDM systems are much more sensitive to carrier frequency offset than single carrier systems. For OFDM/QAM systems with rectangular pulseshaping, it is reported that CFO should be less than 2% of the subchannel spacing to guarantee a signal to interference ratio (SIR) higher than 30 dB [PBM95]. OFDM/OQAM systems using pulseshaping are also sensitive to CFO [RHV98, LHL05]. In this chapter, we will search for optimal pulseshapes with robustness to CFO for both OFDM/QAM and OFDM/OQAM systems.

The robustness to CFO of OFDM/QAM systems can be improved at the sacrifice of spectral efficiency. One kind of method is called self-ICI-cancellation schemes [ZH96, Arm99]. The robustness to CFO is improved by mapping data symbols to more than one adjacent subchannel, then recovering the desired symbols by using these adjacent subchannels. Another category of methods is based on using smoother pulseshapes in each subchannel. Recently, there has been an increasing interest in the design of pulses that are robust to CFO (or the dual problem of design of pulses that are robust to timing offset for bandlimited single carrier systems) [BTD01, TB04, SL05, SCC05, CSC05]. Optimal pulses in the sense of minimizing the mean square error (MSE) for small values of CFO were found in 1968 by Franks [Fra68]. Since a certain residual CFO is always present in practice, it is desirable to design a pulse with small average interchannel interference (ICI) power for CFO in a certain region around zero. In this chapter, optimal pulses with minimum ICI power at a given value of CFO are found analytically. We also show that under some conditions, such optimal pulses also minimize the maximum average ICI power over a region.

Compared to OFDM/QAM, OFDM/OQAM has more freedom in the choice of pulseshapes. In Chang's original work [Cha66], the shaping filters were strictly bandlimited, and therefore of infinite duration in time domain. Simply truncating these pulses would result in obvious spectrum leakage, or a long pulse with impractical implementation. Therefore, a compromise between pulse length and bandwidth must be sought for. One approach, carried out by Vahlin and Holte [VH96], seeks to minimize out-of-band energy while keeping the pulse length short. Similar approaches for time-discrete OFDM/OQAM systems have also been obtained [CC97, BDH99, PS01]. In this chapter, we will try to find pulseshapes that increase the robustness to CFO. Normally, as shown in Figure 4.1, a coarse frequency adjustment is done in the receiver prior to the demodulation. Remaining phase rotations are then found by the channel estimator and corrected by a simple one-tap equalizer. However, this correction will not remove intersymbol interference (ISI) and ICI introduced by the loss of orthogonality introduced by the CFO. Then similar to the OFDM/QAM case, we will search for optimal pulseshapes with minimum ICI power at given values of CFO.

The rest of this chapter is organized as follows. In section 4.1, we search for the optimal pulseshapes with minimum ICI at a given CFO point for OFDM/QAM systems analytically. Then in section 4.2, we search for optimal pulses robust to CFO for OFDM/OQAM systems numerically. At last in section 5.5, a short conclusion is given.

Parts of the results of the chapter have been published in [LHL05, LLH06d].

4.1 Optimal pulse robust to CFO for OFDM/QAM systems

First we search for optimal pulseshapes with robustness to CFO for OFDM/QAM systems. We consider the time-continuous case and assume no guard interval is inserted.

4.1.1 System description and interference model

We consider an OFDM/QAM system with N subchannels and a subchannel spacing $1/T$. The transmitter filter $g(t)$ and receiver filter $f(t)$ are assumed identical, real-valued, symmetric and time-limited to $[-\frac{(1+\beta)T}{2}, \frac{(1+\beta)T}{2}]$, where β is referred as the roll-off factor. Each $(1+\beta)\,T$ seconds, the transmitter takes N symbols $\{a_k[n]\}_{k=0}^{N-1}$, and generates a transmitted waveform

$$x(t) = \sum_{k=0}^{N-1} \sum_{n=-\infty}^{\infty} a_k[n]\, g\big(t - n(1+\beta)T\big)\, e^{j\frac{2\pi}{T}kt}.$$

The channel is assumed to be ideal. In subchannel k at the receiver side, the received signal is demodulated by the subcarrier frequency k/T minus the frequency offset f_e (normalized with respect to subchannel spacing $1/T$), then filtered by the receiver filter $f(t)$ (identical to $g(t)$) and sampled at instant $n(1+\beta)T$ to generate the received symbol

$$\begin{aligned}\tilde{a}_k[n] &= x(t)\, e^{-j\frac{2\pi}{T}(k-f_e)t} * g(t)\big|_{t=n(1+\beta)T} \\ &= e^{j2\pi n(1+\beta)f_e}\Big(a_k[n]\,\Gamma_0 + \sum_{m=0,m\neq k}^{N-1} a_m[n]\,\Gamma_{m-k}\Big),\end{aligned}$$

where $*$ stands for the convolution, and

$$\Gamma_k = e^{j2\pi k\beta n} \int_{-\frac{(1+\beta)T}{2}}^{\frac{(1+\beta)T}{2}} g^2(t)\, e^{-j\frac{2\pi}{T}(k+f_e)t}\, dt. \tag{4.1}$$

We see that no ISI is present while the desired symbol is attenuated by a factor Γ_0. The ICI comes only from the symbols at the same instant. By further assuming that the input symbols $a_k[n]$ are i.i.d. with a unit power, the average ICI power of $\tilde{a}_k[n]$ is given as

$$\sigma_{\mathrm{ICI}}^2 = \sum_{m=0, m\neq k}^{N-1} \left|\Gamma_{m-k}\right|^2, \tag{4.2}$$

and the signal to interference ratio is

$$\mathrm{SIR} = \frac{\left|\Gamma_0\right|^2}{\sum_{m=0, m\neq k}^{N-1} \left|\Gamma_{m-k}\right|^2}. \tag{4.3}$$

We see that the average ICI power is also related to the number of subchannels N and the subchannel index k. For large N, the average ICI power of most subchannels is largely independent of N and k since the ICI from far lower or higher subchannels is negligible. In the next section, we will assume the number of subchannels $N \to \infty$.

4.1.2 Optimal pulses robust to CFO

By using the transforms $t' = t/T$ and $g'(t') = \sqrt{T}\, g(tT)$, and keeping the unprimed symbols, we can normalize (4.1) as

$$\Gamma_k = e^{j2\pi k\beta n} \int_{-\frac{1+\beta}{2}}^{\frac{1+\beta}{2}} g^2(t)\, e^{-j2\pi(k+f_e)t}\, dt. \tag{4.4}$$

A. Necessary and sufficient conditions of orthogonality

To satisfy the orthogonality between subchannels, the ICI should be zero in the absence of CFO. Based on (4.4) and assuming a unit energy pulse $g(t)$, this constraint is expressed as

$$\int_{-\frac{1+\beta}{2}}^{\frac{1+\beta}{2}} g^2(t)\, e^{-j2\pi kt}\, dt = \delta[k]. \tag{4.5}$$

Since $g^2(t)$ can be viewed as the frequency response of a time domain pulse that satisfies the Nyquist criterion, the design of orthogonal pulses is equivalent to searching for bandlimited Nyquist pulses for single carrier systems. Therefore the sufficient and necessary condition is $\sum_{k=-\infty}^{\infty} g^2(t+k) \equiv 1$, and a general expression for $g^2(t)$ is given as

$$g^2(t) = \begin{cases} 1, \ |t| < \frac{1-\beta}{2} \\ \varphi(\frac{1}{2} - |t|) + \frac{1}{2}, \ \frac{1-\beta}{2} \leq |t| \leq \frac{1+\beta}{2} \\ 0, \ |t| > \frac{1+\beta}{2}, \end{cases} \tag{4.6}$$

where $\varphi(t)$ is any odd function that satisfies the constraint $\max_{t\in[0,\frac{\beta}{2}]} |\varphi(t)| \leq \frac{1}{2}$.

For the special case of $\beta = 0$, we see from (4.6) that the orthogonal pulse must fulfil $g^2(t) = 1$. By requiring $g(t)$ to be positive, the rectangular pulse is the only choice of $g(t)$.

For $\beta > 0$, there exists an infinite number of orthogonal pulses. Below we list some earlier suggested pulses by choosing different $\varphi(t)$:

- Raised Cosine (RC) pulse: $\varphi(t) = \frac{1}{2}\sin(\pi t/\beta)$;
- "Better Than" Raised Cosine (BTRC) pulse [BTD01,TB04]: $\varphi(t) = \frac{1}{2}\,\mathrm{sgn}(t)\left(4^{|t|/\beta} - 1\right)$;
- Second order polynomial pulse [SL05]: $\varphi(t) = \mathrm{sgn}(t)\left[p\left(2\,|t|/\beta\right) - \frac{1}{2}\right]$, where $p(t) = a_0 + a_1\,t + a_2\,t^2$;
- Franks' pulse [Fra68]: $\varphi(t) = t$.

We see that Franks' pulse stands for the special case of a second order polynomial pulse with $a_0 = 1/2,\ a_1 = \beta/2,\ a_2 = 0$.

We will now search for the most optimal ones with minimum average ICI power at a given CFO point among all orthogonal pulses.

B. Formulation of the optimization problem

In Franks' original work [Fra68], the optimal pulse $\varphi(t) = t$ was found by minimizing the MSE of desired symbols, i.e. minimizing $|\Gamma_0 - 1|^2 + \sum_{m=0,m\neq k}^{N-1} |\Gamma_{m-k}|^2 = |\Gamma_0 - 1|^2 + \sigma_{\text{ICI}}^2$, for small value of CFO. For practical OFDM systems, since a multiplier will correct the distortion of desired symbols, we will minimize the average ICI power instead of MSE. In addition, since a certain residual CFO is always present due to imperfect CFO estimation, we will search for optimal pulses with minimum ICI power at a given CFO point $f_e = \tilde{f}_e$. It will be shown later by **Property 2** that these optimal pulses also minimize the maximum ICI power over $[0, \tilde{f}_e]$ under certain conditions.

By substituting (4.4) into (4.2) and assuming $N \to \infty$, we get

$$\begin{aligned}
\sigma_{\text{ICI}}^2 &= \sum_{k=-\infty}^{\infty} |\Gamma_k|^2 - |\Gamma_0|^2 \\
&= \int_{-\frac{1+\beta}{2}}^{\frac{1+\beta}{2}} g^2(t) \Big(\sum_{k=-\infty}^{\infty} e^{-j2\pi(k+\tilde{f}_e)t} \int_{-\frac{1+\beta}{2}}^{\frac{1+\beta}{2}} g^2(\tau) e^{-j2\pi(k+\tilde{f}_e)\tau} d\tau \Big) dt \\
&\quad - \Big(\int_{-\frac{1+\beta}{2}}^{\frac{1+\beta}{2}} g^2(t)\, e^{-j2\pi\tilde{f}_e t}\, dt \Big)^2 \\
&= \int_{-\frac{1+\beta}{2}}^{\frac{1+\beta}{2}} g^2(t) \Big(\sum_{l=-\infty}^{\infty} e^{-j2\pi\tilde{f}_e l}\, g^2(t-l) \Big)\, dt - \Big(\int_{-\frac{1+\beta}{2}}^{\frac{1+\beta}{2}} g^2(t)\, e^{-j2\pi\tilde{f}_e t}\, dt \Big)^2,
\end{aligned} \tag{4.7}$$

where the Poisson sum formula is used to get the last equality.

Then by substituting (4.6) into (4.7), we get

$$\begin{aligned}
\sigma_{\text{ICI}}^2 = 8 \Big[&\int_0^{\frac{\beta}{2}} \varphi^2(t)\, dt - 2 \Big(\int_0^{\frac{\beta}{2}} \varphi(t)\, \sin(2\pi\tilde{f}_e t)\, dt \Big)^2 \\
&- \frac{\cos(\pi\tilde{f}_e\beta)}{\pi\tilde{f}_e} \int_0^{\frac{\beta}{2}} \varphi(t)\, \sin(2\pi\tilde{f}_e t)\, dt \Big]\, \sin^2(\pi\tilde{f}_e) \\
&+ 1 - \beta\, \sin^2(2\pi\tilde{f}_e) - \operatorname{sinc}(\pi\tilde{f}_e)\, \cos^2(\pi\tilde{f}_e\beta).
\end{aligned} \tag{4.8}$$

For $\tilde{f}_e = 0$, σ_{ICI}^2 gets the minimum value of 0 for any odd function $\varphi(t)$. For $\tilde{f}_e$ larger than 0.5, we may use subchannel $k+1$ at the receiver side to demodulate the signals from subchannel k at the transmitter side. Therefore without loss of generality, we may assume $0 < \tilde{f}_e \leq 0.5$. The minimization of σ_{ICI}^2 can be done by minimizing the functional

$$\begin{aligned}
J(\varphi) = &\int_0^{\frac{\beta}{2}} \varphi^2(t)\, dt - 2 \Big(\int_0^{\frac{\beta}{2}} \varphi(t)\, \sin(2\pi\tilde{f}_e t)\, dt \Big)^2 \\
&- \frac{\cos(\pi\tilde{f}_e\beta)}{\pi\tilde{f}_e} \int_0^{\frac{\beta}{2}} \varphi(t)\, \sin(2\pi\tilde{f}_e t)\, dt.
\end{aligned} \tag{4.9}$$

We will verify in the next section that the constraint $\max_{t\in[0,\frac{\beta}{2}]} |\varphi(t)| \leq \frac{1}{2}$ is always fulfilled for the optimal $\varphi(t)$. Therefore we will not consider it during the optimization procedure.

C. Solution of the optimization problem

The variation of functional $J(\varphi)$ in (4.9) can be written as

$$\begin{aligned}\delta J(\varphi; v) = 2\int_0^{\frac{\beta}{2}} \varphi(t)\, v(t)\, dt - 4\Big(\int_0^{\frac{\beta}{2}} \varphi(\tau)\, \sin(2\pi \tilde{f}_e \tau)\, d\tau\Big) \\ \times \Big(\int_0^{\frac{\beta}{2}} v(t)\, \sin(2\pi \tilde{f}_e t)\, dt\Big) - \frac{\cos(\pi \tilde{f}_e \beta)}{\pi \tilde{f}_e} \int_0^{\frac{\beta}{2}} v(t)\, \sin(2\pi \tilde{f}_e t)\, dt \\ = 2\int_0^{\frac{\beta}{2}} \Big[\varphi(t) - \Big(2\int_0^{\frac{\beta}{2}} \varphi(\tau)\, \sin(2\pi \tilde{f}_e \tau)\, d\tau + \frac{\cos(\pi \tilde{f}_e \beta)}{2\,\pi \tilde{f}_e}\Big) \\ \times\, \sin(2\pi \tilde{f}_e t)\Big] v(t)\, dt. \qquad (4.10)\end{aligned}$$

Now we will show that $J(\varphi)$ is strictly convex. We note that

$$\begin{aligned}& J(\varphi + v) - J(\varphi) - \delta J(\varphi; v) \\ &= \int_0^{\frac{\beta}{2}} v^2(t)\, dt - 2\Big(\int_0^{\frac{\beta}{2}} v(t)\, \sin(2\pi \tilde{f}_e t)\, dt\Big)^2 \\ &\geq \int_0^{\frac{\beta}{2}} v^2(t)\, dt - 2\Big(\int_0^{\frac{\beta}{2}} v^2(t)\, dt\Big)\Big(\int_0^{\frac{\beta}{2}} \sin^2(2\pi \tilde{f}_e t)\, dt\Big) \\ &= \big[1 - \frac{\beta}{2}\big(1 - \mathrm{sinc}(2\pi \tilde{f}_e \beta)\big)\big] \int_0^{\frac{\beta}{2}} v^2(t)\, dt \geq 0, \qquad (4.11)\end{aligned}$$

where we have first used the Cauchy-Schwarz inequality, and the last inequality follows from the fact that

$$\frac{\beta}{2}\big(1 - \mathrm{sinc}(2\pi \tilde{f}_e \beta)\big) < 1,\ \forall\, \tilde{f}_e \in \mathbb{R},\ \forall\, \beta \in [0, 1].$$

Since equality in (4.11) can be obtained if and only if $v(t) = 0$, the functional $J(\varphi)$ is strictly convex. Therefore there exists only one stationary point that is also the global minimum. Based on (4.10), the unique stationary point should satisfy

$$\varphi(t) = \Big(2\int_0^{\frac{\beta}{2}} \varphi(\tau)\, \sin(2\pi \tilde{f}_e \tau)\, d\tau + \frac{\cos(\pi \tilde{f}_e \beta)}{2\,\pi \tilde{f}_e}\Big) \sin(2\pi \tilde{f}_e t).$$

This integral equation can be easily solved since $\varphi(t)$ will have a form of $C \sin(2\pi \tilde{f}_e t)$, where C is a constant. By using the method of undermined coefficients, we get

$$\varphi(t) = \frac{\cos(\pi \tilde{f}_e \beta)}{\pi \tilde{f}_e \big[2 - \beta\big(1 - \mathrm{sinc}(2\pi \tilde{f}_e \beta)\big)\big]} \sin(2\pi \tilde{f}_e t). \qquad (4.12)$$

Finally we check if the constraint $\max_{t\in[0,\frac{\beta}{2}]}|\varphi(t)| \le \frac{1}{2}$ is satisfied. By requiring $d\varphi(t)/dt = 0$, we find that $\cos(\pi\tilde{f}_e\beta) = 0$ or $\cos(2\pi\tilde{f}_e t) = 0$. For $\cos(\pi\tilde{f}_e\beta) = 0$, the constraint is obviously satisfied. For $\cos(2\pi\tilde{f}_e t) = 0$, the minimum $\tilde{f}_e = \frac{1}{2\beta} \ge 0.5$, which is outside the interval $(0, 0.5)$. Then we only have to check the end point $t = \frac{\beta}{2}$. Assuming $\beta \le 1$, we have

$$0 \le \varphi(\frac{\beta}{2}) \le \frac{\beta\,\mathrm{sinc}(2\pi\tilde{f}_e\beta)}{1+\beta\,\mathrm{sinc}(2\pi\tilde{f}_e\beta)} \le \frac{1}{2}.$$

Therefore, the constraint $\max_{t\in[0,\frac{\beta}{2}]}|\varphi(t)| \le \frac{1}{2}$ is always satisfied for the optimal $\varphi(t)$. At last by substituting (4.12) into (4.6), we then get the optimal pulses. We note that Franks' pulses [Fra68] coincide with the optimal pulse with $\tilde{f}_e \to 0$, although a slightly different criterion was used in Franks' approach.

D. Properties of the optimal pulses

We may conclude the following two properties:

- **Property 1**: The optimal pulses given by (4.6) and (4.12) are uniquely determined by $\tilde{f}_e$, and will be distinct for different $\tilde{f}_e$;
- **Property 2**: Based on **Property 1**, if an optimal pulse obtains maximum average ICI power at the end point $f_e = \tilde{f}_e$ over $[0, \tilde{f}_e]$, it also solves the minimax optimization problem: $\min_{g^2(t)} \max_{f_e\in[0,\tilde{f}_e]} \sigma^2_{\mathrm{ICI}}$, i.e. it also minimizes the maximum average ICI power over $[0, \tilde{f}_e]$ among all orthogonal pulses.

By varying the optimized point $\tilde{f}_e$, we get a set of optimal pulses and the corresponding minimal average ICI power. By connecting these points together, we obtain a *lower bound*. Based on **Property 1**, the curves of average ICI power versus CFO for any orthogonal pulse should lie above this lower bound, and no one can touch this lower bound at more than one points in the region $f_e \in (0, 0.5]$. This lower bound shows the improvement margin of an orthogonal pulse at a given value of CFO. Similarly, we also define an SIR *upper bound*. Note that this upper bound is only an approximate result since the optimal pulses are not supposed to maximize SIR.

4.1.3 Comparison of different pulses for OFDM/QAM systems

In this section, we compare the optimal pulse to the following earlier proposed pulses: rectangular pulse, Raised Cosine (RC) pulse, "Better Than"

Raised Cosine (BTRC) pulse [BTD01] and Franks' pulse [Fra68]. In the comparison, we set the number of subchannels $N = 64$ and the roll-off factor $\beta = 0.2$ and 1.0. The optimized CFO point for optimal pulses is set to $\tilde{f}_e = 0.2$. The average ICI power of subchannel k is calculated using (4.2).

The comparison of different pulses is shown in Fig. 4.2 and 4.3. The roll-off factor are set as $\beta = 0.2$ in Fig. 4.2, and to be set as $\beta = 1.0$ in Fig. 4.3. We see that for small value of roll-off factor $\beta = 0.2$, Franks' pulse is quite close to the optimal pulse. For larger roll-off factor $\beta = 1.0$, all pulses (except for rectangular pulse) become more compact in frequency domain. We note that the optimal pulses have the lowest main sidelobes.

Recall that the average ICI power also depends on the subchannel index k for a system with finite number of subchannels. The comparison of the average ICI power versus subchannel index k for CFO = 0.2 is illustrated in Fig. 4.4. We see that the average ICI power is largely independent of subchannel index k, except for the subchannels lie in the ends of band. This verifies that the ICI from far lower or higher subchannels is negligible. For $\beta = 0.2$, the average ICI power of optimal pulse is about 0.7 dB lower than that of BTRC pulse for the middle subchannels. We also note that Franks' pulse is quite close to the optimal pulse for this case. For $\beta = 1.0$, the average ICI power of optimal pulse is about 1.3 and 2.0 dB lower than that of BTRC and Franks' pulses respectively for the middle subchannels.

The curves for the average ICI power and SIR versus CFO of subchannel 31 for different pulses are shown in Fig. 4.5. We see that the optimal pulse has the lowest average ICI power and highest SIR at the optimized point $f_e = 0.2$. Since the optimal pulses obtain the maximum average ICI power at $f_e = 0.2$ over $[0, 0.2]$, they also minimize the maximum ICI power in this region based on **Property 2**. For $\beta = 0.2$, both the optimal pulse and Franks' pulse is quite close to the lower bound. This implies that for small values of β, the optimal pulse is largely independent of the choosing of optimized CFO point $\tilde{f}_e$. For $\beta = 1.0$, the average ICI power of the optimal pulse at $f_e = 0.2$ is about 1.3 and 1.8 dB lower than that of the BTRC pulse and Franks' pulse respectively. For $\beta = 1.0$ and small values of CFO, Franks' pulse is close to the lower bound, and the optimal pulse has about the same performance as the BTRC pulse. We also note that for all pulses (except for the rectangular pulse), the robustness to CFO is improved for larger β. This is expected since we have more degree of freedom to choose pulses by using a longer transmitting interval. From another point of view, a longer transmitting interval somehow provides a wider guard-band in frequency domain, thus increases the robustness to CFO. It is worthwhile to point out that such improvement is obtained at the sacrifice of spectrum efficiency.

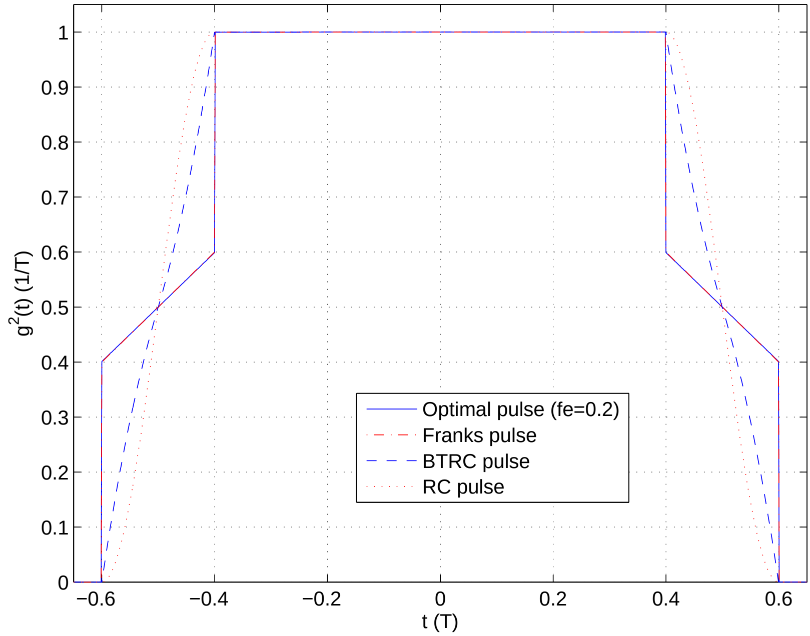

(a) Time domain pulses

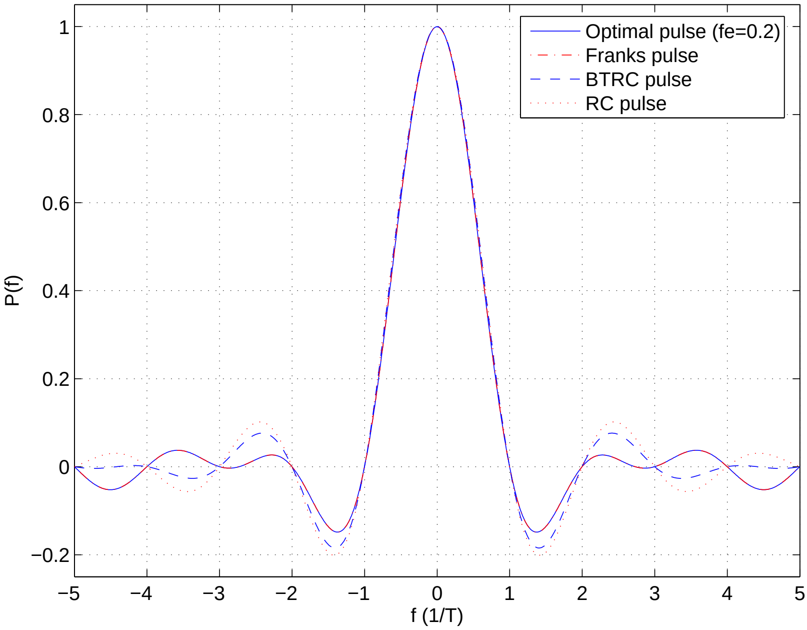

(b) Frequency domain pulses

Figure 4.2: Comparison of different pulses ($\beta = 0.2$) (the optimal pulse overlaps with Franks' pulse).

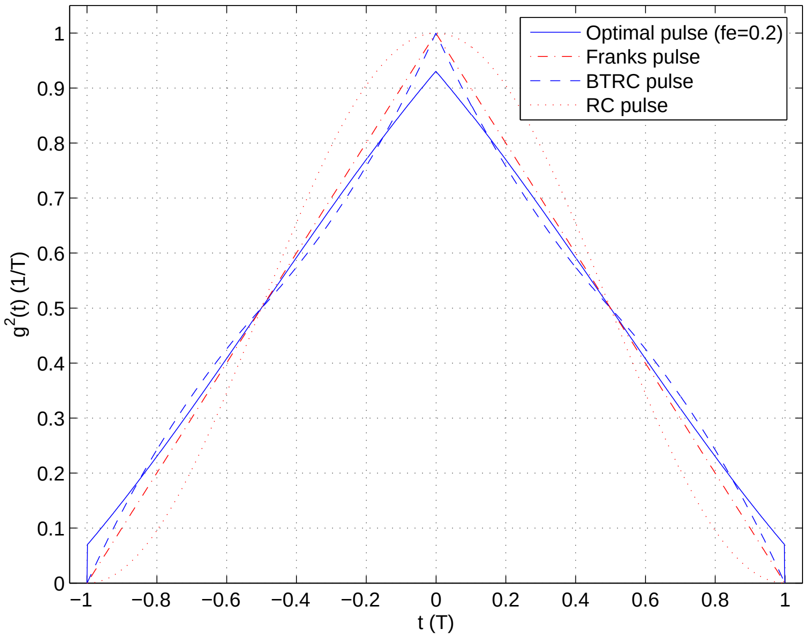

(a) Time domain pulses

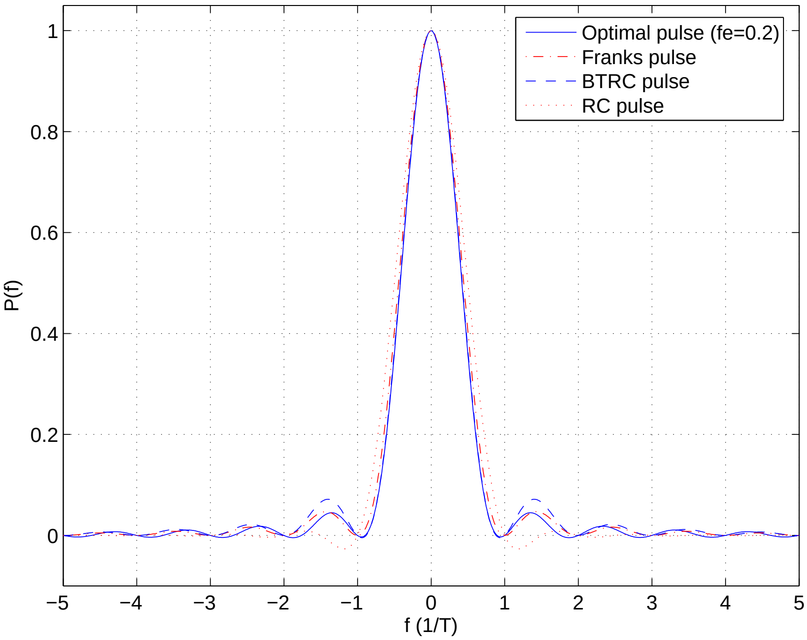

(b) Frequency domain pulses

Figure 4.3: Comparison of different pulses ($\beta = 1.0$).

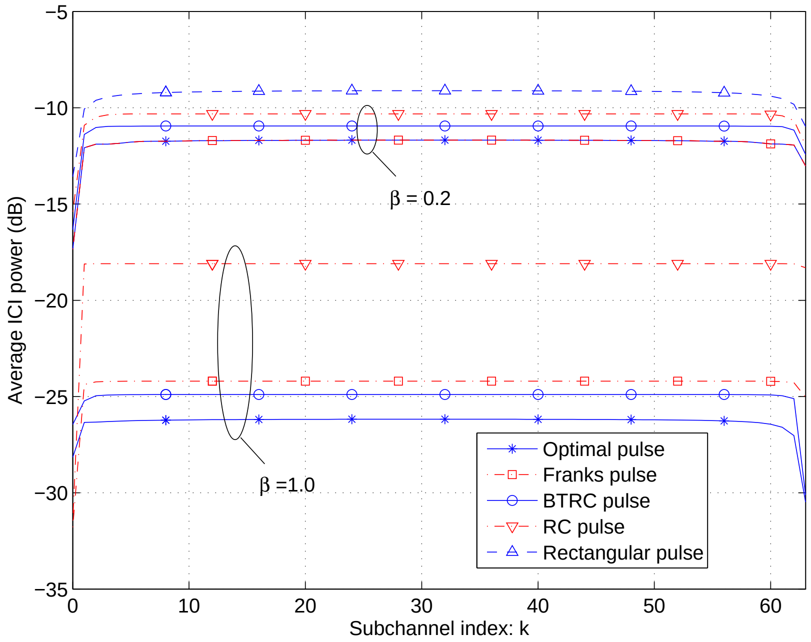

(a) Average ICI power versus subchannel index k

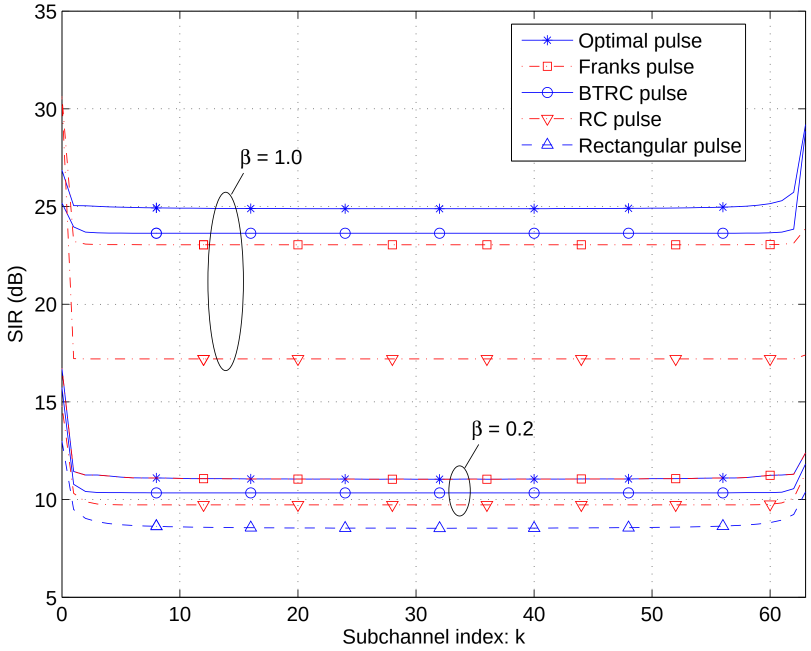

(b) SIR versus subchannel index k

Figure 4.4: Comparison of average ICI power and SIR versus subchannel index k for different pulses with roll-off factor β as parameter.

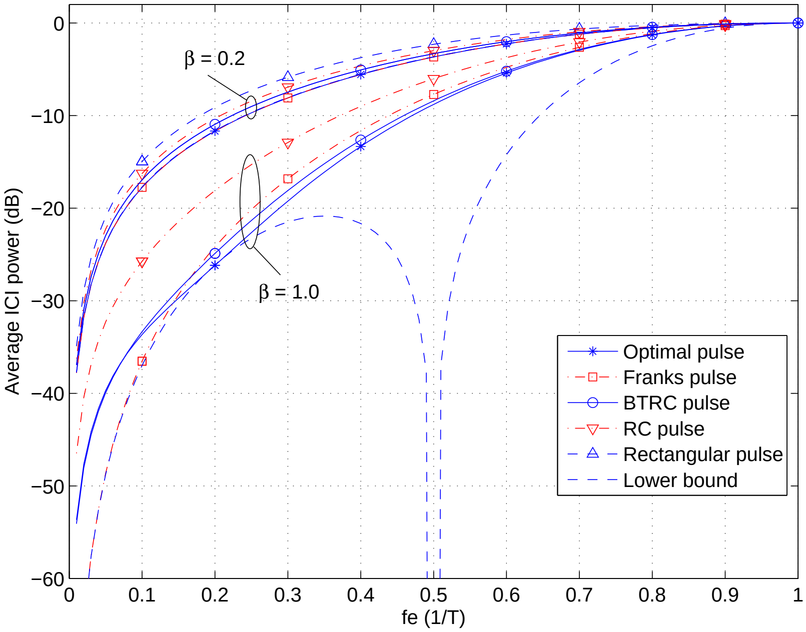

(a) Average ICI power versus CFO

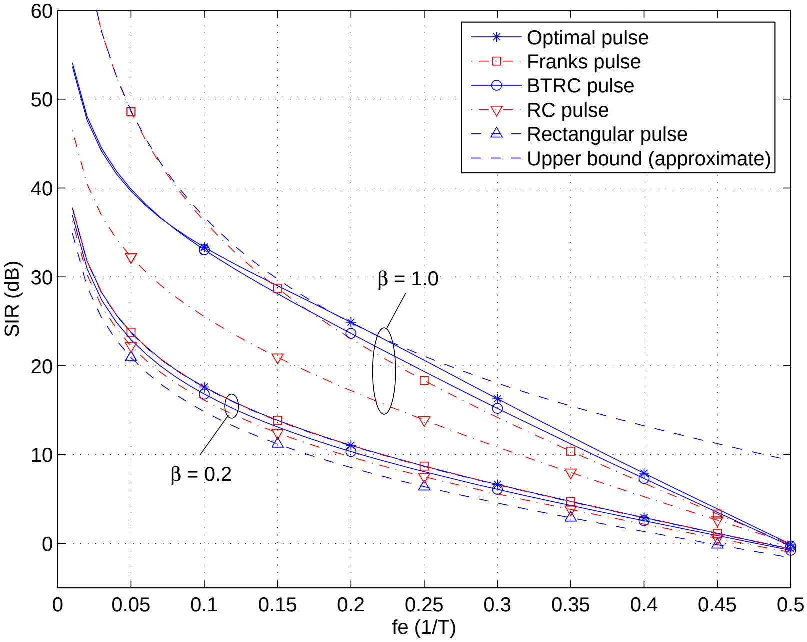

(b) SIR versus CFO

Figure 4.5: Average ICI power and SIR versus CFO of subchannel 31 for different pulses with roll-off factor β as parameter (for $\beta = 0.2$, the curves of optimal pulse and Franks' pulse overlap with the lower or upper bound).

4.2 Optimal pulse robust to CFO for OFDM/OQAM systems

In this section, we will search for the optimal pulses with minimum interference at a given CFO point for OFDM/OQAM systems. Since it is difficult to find the optimal pulse analytically for OFDM/OQAM systems, we will use numerical optimization methods instead. We assume that the transmitter filter $g(t)$ and receiver filter $f(t)$ are identical real-valued and symmetric pulses.

4.2.1 System description and interference model

A. System description

As shown above, a guard interval in frequency domain can reduce the sensitivity to CFO for pulseshaping OFDM/QAM systems. Now we check if it is feasible for OFDM/OQAM systems.

We consider an OFDM/OQAM system with N subchannels and a subchannel spacing $1/T$. Each subchannel transmits a QAM symbol $a_k[n] = a_k^{\mathcal{R}}[n] + j a_k^{\mathcal{I}}[n]$ every $(1+\beta)\,T$ seconds, where $a_k^{\mathcal{R}}[n]$ and $a_k^{\mathcal{I}}[n]$ are respectively the real and imaginary part of symbol. Offset QAM (OQAM) symbols are obtained by delaying the imaginary parts by $(1+\beta)\,T/2$. By setting $\beta = 0$, we get the critically spaced (in frequency domain) OFDM/OQAM systems described in chapter 2.

Pulseshaping of the transmitted signal is achieved by a transmitter filter $g(t)$ prior to the modulation of the subcarrier $e^{j(\frac{2\pi}{T}t+\frac{\pi}{2})k}$. By summing up all subchannels, the transmitted signal $s(t)$ can be written as

$$\begin{aligned} s(t) = \sum_{k=0}^{N-1} \sum_{n=-\infty}^{\infty} \big[& a_k^{\mathcal{R}}[n]\, g(t - n(1+\beta)\,T) \\ & + j\, a_k^{\mathcal{I}}[n]\, g(t - (n+1/2)(1+\beta)\,T)\big] e^{j(\frac{2\pi}{T}t+\frac{\pi}{2})k}. \end{aligned} \tag{4.13}$$

The channel is assumed to be ideal. In subchannel k at the receiver side, the received signal from channel is first demodulated by the subcarrier frequency minus the frequency offset f_e (normalized with respect to $1/T$), then filtered by the receiver filter $f(t)$ (identical to $g(t)$) to generate the received subchannel signal

$$\begin{aligned} y_k(t) &= s(t)\, e^{-j[(\frac{2\pi}{T}t+\frac{\pi}{2})k-\frac{2\pi}{T}f_e t]} * f(t)\\ &= e^{j\frac{2\pi}{T}f_e t}\sum_{m=0}^{N-1}\sum_{n=-\infty}^{\infty}\Big(a_m^{\mathcal{R}}[n]\int_{-\infty}^{\infty} g(t-\tau-n(1+\beta)\,T)\,g(\tau)\\ &\quad\times e^{j[(\frac{2\pi}{T}(t-\tau)+\frac{\pi}{2})(m-k)-\frac{2\pi}{T}f_e\tau]}\,d\tau\\ &\quad + j\,a_m^{\mathcal{I}}[n]\int_{-\infty}^{\infty} g(t-\tau-(n+1/2)(1+\beta)\,T)\,g(\tau)\\ &\quad\times e^{j[(\frac{2\pi}{T}(t-\tau)+\frac{\pi}{2})(m-k)-\frac{2\pi}{T}f_e\tau]}\,d\tau\Big). \end{aligned} \tag{4.14}$$

We see that as a result of the uncompensated frequency offset, the demodulated signal $y_k(t)$ is frequency shifted by f_e/T. Since the real part and imaginary parts of the received symbols are got by sampling $y_k(t)$ at $t = n(1+\beta)\,T$ and $t = (n+1/2)(1+\beta)\,T$ respectively, the received symbol $\tilde{a}_k[n]$ will then appear as rotated by an angle

$$\theta_k = \begin{cases} 2\pi n(1+\beta)f_e, & \text{for the real part} \\ 2\pi(n+\frac{1}{2})(1+\beta)f_e, & \text{for the imaginary part.} \end{cases}$$

We assume (optimistically) that this phase rotation introduced by CFO is perfectly estimated by the channel estimator and compensated for, by a multiplication by $e^{-j\,\tilde{\theta}_k}$, where $\tilde{\theta}_k = 2\pi n(1+\beta)f_e$ for the real part of symbol and $\tilde{\theta}_k = 2\pi n(1+\beta)f_e$ for the imaginary part. Then the recovered symbol can be written as

$$\begin{aligned}
\tilde{a}_k^{\mathcal{R}}[n] &= \mathrm{Re}\big\{y_k(t)\, e^{-j2\pi n(1+\beta) f_e}\big\}\big|_{t=n(1+\beta)T} \\
&= \mathrm{Re}\Big\{\sum_{m=0}^{N-1}\sum_{n'=-\infty}^{\infty}\Big[a_m^{\mathcal{R}}[n'] \int_{-\infty}^{\infty} g\big(\tau - \frac{n-n'}{2}(1+\beta)\,T\big) \\
&\quad \times g\big(\tau + \frac{n-n'}{2}(1+\beta)\,T\big) e^{-j[(\frac{2\pi}{T}\tau - \frac{\pi}{2})(m-k) + \frac{2\pi}{T} f_e \tau]}\, d\tau \\
&\quad + j\, a_m^{\mathcal{I}}[n'] \int_{-\infty}^{\infty} g\big(\tau - \frac{n-n'-1/2}{2}(1+\beta)\,T\big) \\
&\quad \times g\big(\tau + \frac{n-n'-1/2}{2}(1+\beta)\,T\big) e^{-j[(\frac{2\pi}{T}\tau - \frac{\pi}{2}(2+\beta))(m-k) + \frac{2\pi}{T} f_e \tau]}\, d\tau\Big] \\
&\quad \times e^{j\pi(n+n')(m-k)(1+\beta)}\Big\} \\
\tilde{a}_k^{\mathcal{I}}[n] &= \mathrm{Im}\big\{y_k(t)\, e^{-j2\pi f_e t}\big\}\big|_{t=(n+\frac{1}{2})(1+\beta)T} \\
&= \mathrm{Im}\Big\{\sum_{m=0}^{N-1}\sum_{n'=-\infty}^{\infty}\Big[a_m^{\mathcal{R}}[n'] \int_{-\infty}^{\infty} g\big(\tau - \frac{n-n'+1/2}{2}(1+\beta)\,T\big) \\
&\quad \times g\big(\tau + \frac{n-n'+1/2}{2}(1+\beta)\,T\big) e^{-j[(\frac{2\pi}{T}\tau - \frac{\pi}{2}(2+\beta))(m-k) + \frac{2\pi}{T} f_e \tau]}\, d\tau \\
&\quad + j\, a_m^{\mathcal{I}}[n'] \int_{-\infty}^{\infty} g\big(\tau - \frac{n-n'}{2}(1+\beta)\,T\big)\, g\big(\tau + \frac{n-n'}{2}(1+\beta)\,T\big) \\
&\quad \times e^{-j[(\frac{2\pi}{T}\tau - \frac{\pi}{2}(3+2\beta))(m-k) + \frac{2\pi}{T} f_e \tau]}\, d\tau\Big] e^{j\pi(n+n')(m-k)(1+\beta)}\Big\}. \qquad (4.15)
\end{aligned}$$

Since the received symbols are obtained by the operations of $\mathrm{Re}\{\cdot\}$ and $\mathrm{Im}\{\cdot\}$, the additional phase factor $e^{j\pi(n+n')(m-k)(1+\beta)}$ in (4.15) should be compensated, otherwise it will cause interference and then damage the orthogonality in OFDM/OQAM systems. For an arbitrary β, this phase factor is difficult to compensate. For the special cases of $\beta = 0$ and $\beta = 1$, this phase factor disappear. For $\beta = 1$, the system degenerates to a conventional FDM system. Therefore in this thesis, we will consider only the case of $\beta = 0$. For this case, we can simplify (4.15) as

$$\begin{aligned}
\tilde{a}_k^{\mathcal{R}}[n] = \sum_{m=0}^{N-1} \sum_{n'=-\infty}^{\infty} \Big[& a_m^{\mathcal{R}}[n'] \int_{-\infty}^{\infty} g(\tau - (n-n')\,T)\, g(\tau) \\
& \times \cos\big((\frac{2\pi}{T}\tau - \frac{\pi}{2})(m-k) + \frac{2\pi}{T} f_e \tau\big)\, d\tau \\
& + a_m^{\mathcal{I}}[n'] \int_{-\infty}^{\infty} g(\tau - (n-n'-1/2)\,T)\, g(\tau) \\
& \times \sin\big((\frac{2\pi}{T}\tau - \frac{\pi}{2})(m-k) + \frac{2\pi}{T} f_e \tau\big)\, d\tau \Big] \\
\tilde{a}_k^{\mathcal{I}}[n] = \sum_{m=0}^{N-1} (-1)^{m-k} \sum_{n'=-\infty}^{\infty} \Big[& -a_m^{\mathcal{R}}[n'] \int_{-\infty}^{\infty} g(\tau - (n-n'+1/2)\,T)\, g(\tau) \\
& \times \sin\big((\frac{2\pi}{T}\tau - \frac{\pi}{2})(m-k) + \frac{2\pi}{T} f_e \tau\big)\, d\tau \\
& + a_m^{\mathcal{I}}[n'] \int_{-\infty}^{\infty} g(\tau - (n-n')\,T)\, g(\tau) \\
& \times \cos\big((\frac{2\pi}{T}\tau - \frac{\pi}{2})(m-k) + \frac{2\pi}{T} f_e \tau\big)\, d\tau \Big].
\end{aligned} \tag{4.16}$$

Now we are ready to derive an interference model for OFDM/OQAM systems.

B. Interference model

We will now develop expressions for both ISI and ICI for the described system. First we can rewrite (4.16) as

$$\begin{aligned}
\tilde{a}_k^{\mathcal{R}}[n] &= a_k^{\mathcal{R}}[n] G_{0,0} + \sum_{m=0}^{N-1} \Big(\sum_{\substack{l=-\infty \\ l\neq n, \text{if}\, m=k}}^{\infty} a_m^{\mathcal{R}}[l] G_{m-k,n-l} + \sum_{l=-\infty}^{\infty} a_m^{\mathcal{I}}[l] H_{m-k,n-l} \Big) \\
\tilde{a}_k^{\mathcal{I}}[n] &= a_k^{\mathcal{I}}[n] G_{0,0} + \sum_{m=0}^{N-1} (-1)^{m-k} \Big(\sum_{\substack{l=-\infty \\ l\neq n, \text{if}\, m=k}}^{\infty} a_m^{\mathcal{I}}[l] G_{m-k,n-l} \\
&\quad - \sum_{l=-\infty}^{\infty} a_m^{\mathcal{R}}[l] H_{m-k,n-l+1} \Big),
\end{aligned} \tag{4.17}$$

where

$$\begin{aligned}
G_{m,n} &= \int_{-\infty}^{\infty} g(nT - \tau)\, g(\tau)\, \cos\big[(\frac{2\pi}{T}\tau - \frac{\pi}{2})m + \frac{2\pi}{T} f_e \tau\big]\, d\tau \\
H_{m,n} &= \int_{-\infty}^{\infty} g(nT - \frac{T}{2} - \tau)\, g(\tau) \sin\big[(\frac{2\pi}{T}\tau - \frac{\pi}{2})m + \frac{2\pi}{T} f_e \tau\big]\, d\tau.
\end{aligned} \tag{4.18}$$

Note that $G_{m,n}$ and $H_{m,n}$ are functions of the carrier frequency offset f_e.

The right hand sides of (4.17) show that the received symbol is composed of the true symbol multiplied by a constant $G_{0,0}$, and a weighted sum of contributions from symbols at other instants and from other subchannels. Note that the interference from the real part of a symbol will affect both the real and imaginary parts of all other symbols. In general the quantity $G_{m-k,n-l}$ denotes the interference from the real part of the lth symbol of the subchannel m to the real part of desired symbol $\tilde{a}_k^{\mathcal{R}}[n]$, whereas $H_{m-k,n-l}$ denotes the interference from the imaginary part of the sent symbols. A similar statement can be made for the imaginary part.

To obtain expressions for average ISI and ICI power, we now assume that the data symbols are statistically independent between different subchannels, different symbols, and between real and imaginary parts, i.e.

$$\begin{aligned} \mathrm{E}\big[a_m^{\mathcal{R}}[n_1]a_k^{\mathcal{R}}[n_2]\big] &= \mathrm{E}\big[a_m^{\mathcal{I}}[n_1]a_k^{\mathcal{I}}[n_2]\big] = \frac{\sigma_a^2}{2}\,\delta(m-k, n_1-n_2) \\ \mathrm{E}\big[a_m^{\mathcal{R}}[n_1]a_k^{\mathcal{I}}[n_2]\big] &= 0,\ \forall\ m,k,n_1,n_2, \end{aligned}$$

where σ_a^2 is the average power of the sent complex symbols, and $\delta(m,n)$ is the two-dimensional Kronecker delta function.

Without loss of generality, we may assume $\sigma_a^2 = 1$. Then based on the assumption above and (4.17), we can write the average ISI and ICI powers as

$$\begin{aligned} \sigma_{\mathrm{ISI}}^2 &= \sum_{\substack{l=-\infty \\ l\neq 0}}^{\infty} G_{0,l}^2 + \sum_{l=-\infty}^{\infty} H_{0,l}^2 \\ \sigma_{\mathrm{ICI}}^2 &= \sum_{\substack{m=0 \\ m\neq k}}^{N-1} \sum_{l=-\infty}^{\infty} \left(G_{m-k,l}^2 + H_{m-k,l}^2\right). \end{aligned} \tag{4.19}$$

By comparing (4.19) to (4.2), we find that different from OFDM/QAM systems with time-limited pulseshapes, an OFDM/OQAM system suffers from both ISI and ICI in the presence of CFO due to longer pulseshapes.

4.2.2 Design of optimal pulses robust to CFO

The expressions for average ISI and ICI power (4.19) depend on the shaping filter $g(t)$ through the factors $G_{m,n}$ and $H_{m,n}$. We are now ready to search for optimal pulseshapes with respect to minimizing the interference caused by CFO.

A. Sufficient conditions for zero ISI and ICI

First the pulse must satisfy the conditions for zero ISI and ICI when $f_e = 0$. This can be written as

$$G_{m,n}|_{f_e=0} = \delta(m,n) \tag{4.20}$$

$$H_{m,n}|_{f_e=0} = 0. \tag{4.21}$$

Recall that we have assumed that $g(t)$ is real-valued and symmetric. Then, by noting the symmetry properties of sin and cos, we see from (4.18) that (4.21) is automatically satisfied for any m and n. Furthermore, (4.20) is satisfied when m is an odd integer. Then the sufficient conditions for zero ISI and ICI can be written as

$$\begin{aligned} C_{m,n} = G_{2m,n}|_{f_e=0} &= \int_{-\infty}^{\infty} g(t-nT)\, g(t)\, \cos(\frac{2\pi}{T}2mt)\, dt \\ &= \delta(m,n). \end{aligned} \tag{4.22}$$

B. Formulation of the optimization problem

By using a transmitter filter strictly bandlimited to $[-1/T, 1/T]$, zero ISI and ICI as well as high bandwidth efficiency can be obtained [Cha66,Sal67]. The resulting pulse will, however, have infinite duration in time domain. Since this is not practically feasible, finite length pulse should be sought. One approach is to minimize out-of-band energy as proposed by Vahlin and Holte [VH96].

We will now use a similar procedure, where we also take into account robustness to carrier frequency offset. In the following, the pulse length will be restricted to L symbol intervals, i.e. $f(t) = 0$ for $|t| > LT/2$. We define an objective function consisting of a weighted sum of out-of-band energy, and ISI/ICI caused by carrier frequency offset as

$$J(g) = -\theta\, T \int_{-\frac{2\pi}{T}}^{\frac{2\pi}{T}} |G(\omega)|^2\, d\omega + (1-\theta)\,(\sigma^2_{\text{ISI}} + \sigma^2_{\text{ICI}}), \tag{4.23}$$

where

$$G(\omega) = \int_{-\infty}^{\infty} g(t)\, e^{-j\omega t}\, dt \tag{4.24}$$

is the Fourier transform of $g(t)$.

Here $0 \le \theta \le 1$ is the weight factor, and the factor T is used to make $J(g)$ dimensionless. If the weight factor $\theta = 1$, this optimization problem will degenerate to Vahlin and Holte's [VH96] result; else if $\theta = 0$, then the optimization objective will lead to minimum interference. For general case $0 < \theta < 1$, the result will lead a compromise between energy concentration and minimum interference.

Then the optimization problem can be expressed as

$$\min_{g(t)\in\mathbf{D}} J(g) \tag{4.25}$$

subject to the constraints (4.22), where the functional J is defined in (4.23) and the feasible domain

$$\mathbf{D} = \big\{g(t) \in \mathbf{C}[-\infty, \infty] : g(t) \equiv 0 \text{ for } |t| > LT/2\big\}.$$

This is a constrained optimization problem. We can write the extended Lagrangian function as

$$\mathcal{L} = J(g) - \sum_{m=-k}^{N-1-k} \sum_{n=-L}^{L} \gamma_{m,n} C_{m,n}, \tag{4.26}$$

where $\gamma_{m,n}$ are the Lagrange multipliers.

Since $g(t)$ is time limited to $[-\frac{LT}{2}, \frac{LT}{2}]$, the integrals in (4.18) will be nonzero only when $-L \le n \le L$. By substituting (4.18) into (4.19), we can expand the expression for the objective function (4.23). Using normalized time by setting $T = 1$, we get

$$\begin{aligned} J(g) = &-\theta \int_{-\frac{L}{2}}^{\frac{L}{2}} \int_{-\frac{L}{2}}^{\frac{L}{2}} g(t)\, g(\tau)\, \frac{\sin 2\pi(t-\tau)}{\pi(t-\tau)}\, dt\, d\tau \\ &+ (1-\theta) \sum_{m=-k}^{N-1-k} \Big[\sum_{\substack{n=-L \\ n\neq 0, \text{if}\, m=0}}^{L} \Big(\int_{-\frac{L}{2}}^{\frac{L}{2}} g(t-n)\, g(t) \cos(\varphi_m)\, dt \Big)^2 \\ &+ \sum_{n=-L}^{L} \Big(\int_{-\frac{L}{2}}^{\frac{L}{2}} g(t-n+\frac{1}{2})\, g(t) \sin(\varphi_m)\, dt \Big)^2 \Big], \end{aligned} \tag{4.27}$$

where

$$\varphi_m \overset{\text{def}}{=} (2\pi t - \frac{\pi}{2})m + 2\pi f_e t\,. \tag{4.28}$$

By setting $T = 1$, the constraints shown in (4.22) can also be normalized as

$$C_{m,n} = \int_{-\frac{L}{2}}^{\frac{L}{2}} g(t-n)\, g(t) \cos(4\pi m t)\, dt = \delta(m,n). \tag{4.29}$$

The feasible domain now changes to

$$\mathbf{D} = \big\{g(t) \in \mathbf{C}[-L/2, L/2] : g(t) \equiv 0 \ \text{ for } |t| > L/2\big\}.$$

Solution of the Optimization Problem

Now, the minimization of (4.27) with constraints (4.29) can be done using standard variational calculus. This requires some rather complicated functional derivatives. Instead we will exploit the fact that the integral operator

$$\int_{-\frac{L}{2}}^{\frac{L}{2}} g(\tau)\,\frac{\sin 2\pi(t-\tau)}{\pi(t-\tau)}\,d\tau$$

has a complete set of eigenfunctions $\{\psi_i(t)\}$ with corresponding eigenvalues $\{\lambda_i\}$. These functions are called *prolate spheroidal wave functions* (PSWFs), see [SP61]. We can then expand the desired pulse $g(t)$ in the basis $\{\psi_i(t)\}$ as

$$g(t) = \sum_{i=0}^{\infty} a_{2i}\,\psi_{2i}(t) \quad \text{for } |t| \le L/2. \tag{4.30}$$

By substituting (4.30) into (4.27), we can rewrite the extended Lagrangian function (4.26) as

$$\begin{aligned}\mathcal{L} = -\theta \sum_{i=0}^{\infty} a_{2i}^2\,\lambda_{2i} + (1-\theta) \sum_{m=-k}^{N-1-k} \Bigg[\sum_{\substack{n=-L\\ n\neq 0, \text{if}\, m=0}}^{L} \Big(\sum_{i,j=0}^{\infty} a_{2i}\,a_{2j}\,c^{(1)}_{i,j,m,n} \Big)^2 \\ + \sum_{n=-L}^{L} \Big(\sum_{i,j=0}^{\infty} a_{2i}\,a_{2j}\,c^{(2)}_{i,j,m,n} \Big)^2 \Bigg] - \sum_{m=-k}^{N-1-k} \sum_{n=-L}^{L} \gamma_{m,n} \Big(\sum_{i,j=0}^{\infty} a_{2i}\,a_{2j}\,b_{i,j,m,n} \Big),\end{aligned} \tag{4.31}$$

where

$$\begin{aligned} b_{i,j,m,n} &= \int_{-\frac{L}{2}}^{\frac{L}{2}} \psi_{2i}(t-n)\,\psi_{2j}(t)\,\cos(4\pi m t)\,dt \\ c^{(1)}_{i,j,m,n} &= \int_{-\frac{L}{2}}^{\frac{L}{2}} \psi_{2i}(t-n)\,\psi_{2j}(t)\,\cos(\varphi_m)\,dt \\ c^{(2)}_{i,j,m,n} &= \int_{-\frac{L}{2}}^{\frac{L}{2}} \psi_{2i}(t-n+1/2)\,\psi_{2j}(t)\,\sin(\varphi_m)\,dt. \end{aligned} \tag{4.32}$$

The constraints in (4.29) can similarly be rewritten as

$$C_{m,n} = \sum_{i=0}^{\infty} \sum_{j=0}^{\infty} a_{2i}\,a_{2j}\,b_{i,j,m,n} = \delta(m,n). \tag{4.33}$$

Now by defining

$$\mathbf{a} = \begin{bmatrix} a_0 & a_2 & \cdots \end{bmatrix}^T$$
$$\mathbf{B}_{m,n} = \begin{bmatrix} b_{0,0,m,n} & b_{0,1,m,n} & \cdots \\ b_{1,0,m,n} & b_{1,1,m,n} & \cdots \\ \vdots & \vdots & \ddots \end{bmatrix}$$
$$\mathbf{C}^{(p)}_{m,n} = \begin{bmatrix} c^{(p)}_{0,0,m,n} & c^{(p)}_{0,1,m,n} & \cdots \\ c^{(p)}_{1,0,m,n} & c^{(p)}_{1,1,m,n} & \cdots \\ \vdots & \vdots & \ddots \end{bmatrix}, \tag{4.34}$$

we can rewrite (4.31) in a matrix form as

$$\mathcal{L} = -\theta\,\mathbf{a}^T\mathbf{\Lambda}\mathbf{a} + (1-\theta)\sum_{m=-k}^{N-1-k}\Big[\sum_{\substack{n=-L\\ n\neq 0,\text{if}\, m=0}}^{L}\big(\mathbf{a}^T\mathbf{C}^{(1)}_{m,n}\mathbf{a}\big)^2 + \sum_{n=-L}^{L}\big(\mathbf{a}^T\mathbf{C}^{(2)}_{m,n}\mathbf{a}\big)^2\Big]$$
$$- \sum_{m=-k}^{N-1-k}\sum_{n=-L}^{L}\gamma_{m,n}\mathbf{a}^T\mathbf{B}_{m,n}\mathbf{a}, \tag{4.35}$$

where $\mathbf{\Lambda} = \text{diag}(\lambda_0, \lambda_2, \lambda_4, \cdots)$.

Similarly, the constraints in (4.33) can be written as

$$C_{m,n} = \mathbf{a}^T\mathbf{B}_{m,n}\mathbf{a} = \delta(m,n). \tag{4.36}$$

By requiring $\partial\mathcal{L}/\partial\mathbf{a} = \mathbf{0}$, we obtain the necessary condition

$$2(1-\theta)\sum_{m=-k}^{N-1-k}\Big[\sum_{\substack{n=-L\\ n\neq 0,\text{if}\, m=0}}^{L}\big(\mathbf{a}^T\mathbf{C}^{(1)}_{m,n}\mathbf{a}\big)\mathbf{C}^{(1)}_{m,n}\mathbf{a} + \sum_{n=-L}^{L}\big(\mathbf{a}^T\mathbf{C}^{(2)}_{m,n}\mathbf{a}\big)\mathbf{C}^{(2)}_{m,n}\mathbf{a}\Big]$$
$$= \theta\,\mathbf{\Lambda}\mathbf{a} + \sum_{m=-k}^{N-1-k}\sum_{n=-L}^{L}\gamma_{m,n}\mathbf{B}_{m,n}\mathbf{a}. \tag{4.37}$$

The matrices $\mathbf{B}_{m,n}$, $\mathbf{C}^{(1)}_{m,n}$ and $\mathbf{C}^{(2)}_{m,n}$ can be inferred from the PSWFs by (4.32), which are known. Optimal pulses can then be found by solving (4.37) subject to the constrains (4.36) and inserting the resulting coefficient values into (4.30). Note that the frequency offset f_e appears in the formulas (4.32) for $\mathbf{C}^{(1)}_{m,n}$ and $\mathbf{C}^{(2)}_{m,n}$. This means that the optimal pulses will depend on f_e.

Analytic expressions will not be pursued in this thesis. Instead, we present a numerical approach in the next section.

4.2.3 Numerical results

Looking at (4.37), we find that it is a set of third order equations in the coefficients **a**. This makes an exact solution hard to find. Fortunately, it can easily be converted into a non-linear least-squares optimization problem that can be solved by using standard numerical methods. Here we use Matlab optimization toolbox to do this work.

From [VH96] we know that pulseshapes with low sidelobes can be obtained using pulse length $L = 4$, so we will use that value in our computations also. After repeated experiments, we find that the results of the optimization are largely insensitive to the choice of f_e. This comes from the fact that our restrictions (4.36) require zero interference for $f_e = 0$. For the numerical computations of the inner products (4.32) we have assumed $f_e = 0.2$. The integrals are evaluated by Simpson's rule using a resolution of $0.0001T$.

Since the coefficients in the PSWF expansion (4.30) fall off rather rapidly, Vahlin and Holte [VH96] have found it acceptable to restrict the number of terms to $i \leq 9$. Numerical experiments confirm that this is sufficient for our case too. Furthermore, we aim at pulses essentially bandlimited to $[-1/T, 1/T]$. Then we can assume that ICI from subchannels far from subchannel k is negligible. This means that we can limit the range of values for m in (4.36) and (4.37). We find that $-6 \leq m \leq 6$ gives adequate accuracy. This also makes our results essentially independent of the number of channels N.

With these restrictions, numerical optimization has been carried out, and the resulting pulses are shown in Fig. 4.6. Apart from a rectangular pulse, included for reference, the figure contains three curves. First, we set $\theta = 1$, restricting the problem to minimizing out of band energy [VH96]. In the other extreme case $\theta = 0$, the problem amounts to finding the pulse with minimum total interference (the sum of ISI and ICI) at $f_e = 0.2$. In addition to these two, we show a curve resulting from removing the constraint of zero interference at $f_e = 0$. This latter case is discussed further below. We can see that even though $\theta = 0$ gives poorer energy concentration than $\theta = 1$, it is significantly better than the rectangular pulse in this respect.

The different pulses will now be compared with respect to total interference. This is expressed as the sum of σ^2_{ISI} and σ^2_{ICI} in (4.19). Resulting performance is shown in Fig. 4.7. Fig. 4.7(a) shows the total normalized interference level. In Fig. 4.7(b) we have the resulting SIR, which is given by $|G_{0,0}|^2/(\sigma^2_{\mathrm{ISI}} + \sigma^2_{\mathrm{ICI}})$. As expected, $\theta = 0$ gives better performance than $\theta = 1$.

For reference, we have also included a truncated square root raised cosine (SRC) pulse of the same length as the optimized ones. We see

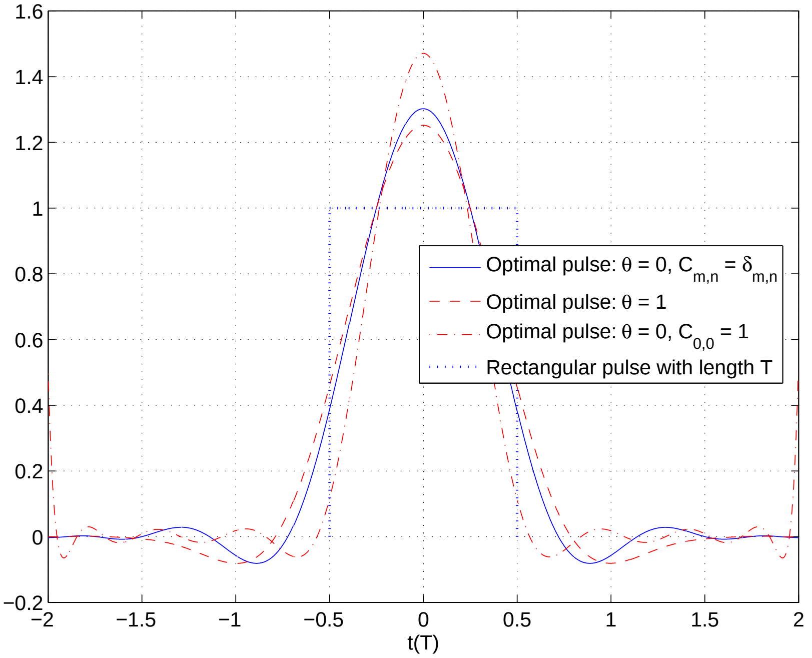

(a) Time domain pulseshapes.

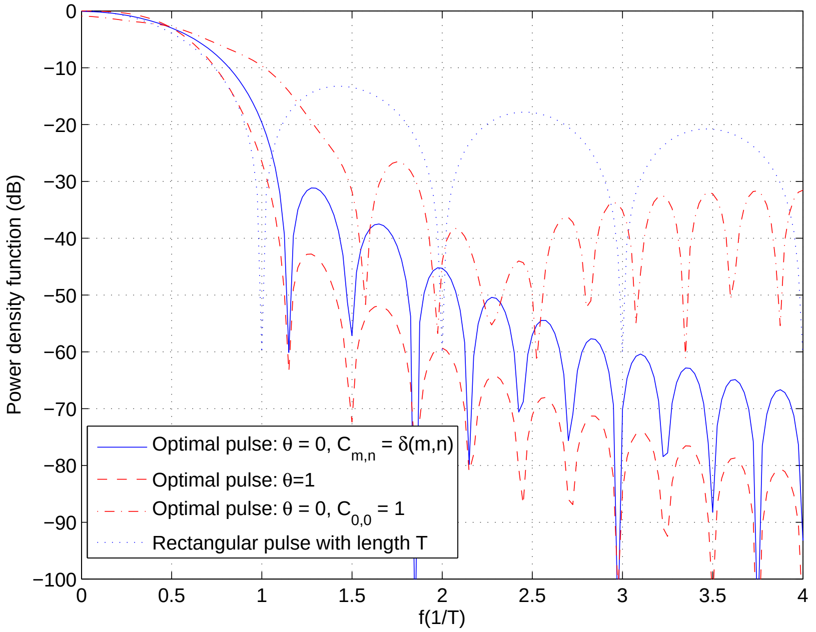

(b) Frequency domain pulseshapes.

Figure 4.6: Pulse shapes in time and frequency domain.

that for the region of f_e shown this has a performance in between the two optimized ones. However, it as less good concentration properties and a non-zero interference level at $f_e = 0$ (not visible in the figure).

Now, one could argue that the requirement of zero ISI and ICI for $f_e = 0$ is unnecessarily strict. In practice the actual f_e will fluctuate around 0, and it is more important to have a small level of interference within the most likely interval for f_e than to require exactly zero interference at one particular value. To do this, we simply release the constraints (4.36) to

$$C_{0,0} = G_{0,0} = 1. \tag{4.38}$$

This remaining constraint will keep the received signal power equal to $\sigma_a^2 = 1$ at $f_e = 0$, and thus avoid the trivial solution of $\mathbf{a} = \mathbf{0}$.

The optimization result is shown by the curve marked by * in Fig. 4.7. We see clearly that this optimal pulse gives less interference for f_e larger than 0.1 at the cost of an SIR of only 20 dB at $f_e = 0$. However, the energy concentration becomes severely reduced by this approach as seen in Fig. 4.6(b). We note that even though we don't require zero interference at $f_e = 0$, the level at this value is still at a moderate -20 dB.

The curve for the rectangular pulse in Fig. 4.7 is included to make a comparison with OFDM/QAM without guard interval. It clearly shows that the sensitivity to CFO is larger for traditional OFDM/QAM systems using rectangular pulses than using optimized pulseshapes in conjunction with OFDM/OQAM. The difference is most obvious for large values of f_e in Fig. 4.7(b).

4.3 Conclusion

In this chapter, the problem of searching for optimal pulses with minimum average ICI power at a given CFO point for pulseshaping OFDM/QAM systems is solved analytically. Based on these optimal pulses, a lower bound is introduced as a measure of robustness to CFO for a given pulse. An example of an OFDM/QAM system with 64 subchannels is studied to illustrate that the optimal pulse is more robust to CFO than previously suggested pulses. For the case of roll-off factor $\beta = 1.0$ and optimized point $\tilde{f}_e = 0.2$, the average ICI power of the optimal pulse is about 1.3 and 1.8 dB lower than that of the BTRC pulse and Franks' pulse at $f_e = 0.2$.

For OFDM/OQAM systems with pulseshaping, we present a procedure of searching for robust pulses to CFO. Numerical comparison shows that the new class of pulses is superior to previously suggested pulses in this respect. At the optimized CFO point of $f_e = 0.2$, the average interference power of the optimal pulse is about 0.5 and 0.7 dB lower than that of square

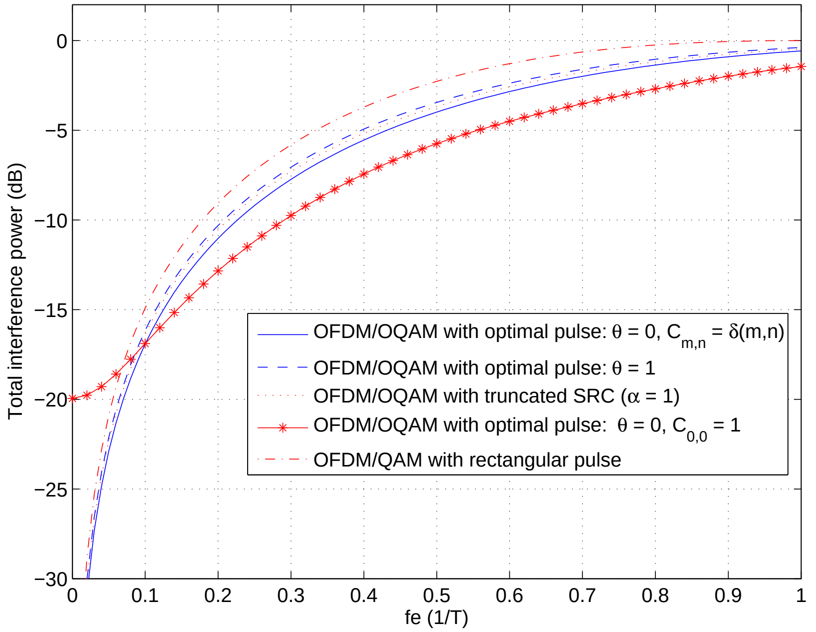

(a) Total interference versus normalized CFO.

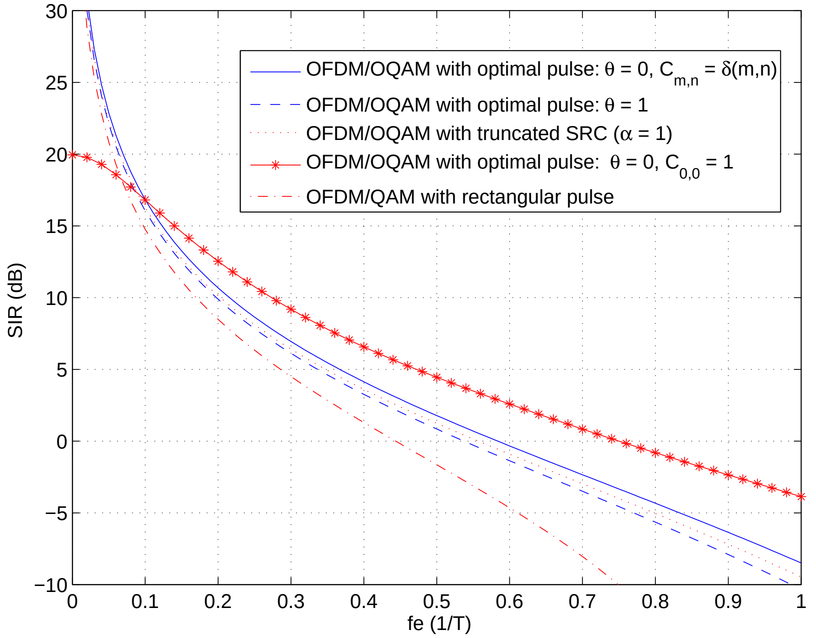

(b) SIR versus normalized CFO.

Figure 4.7: Comparison of total interference and SIR versus normalized CFO.

root raised cosine pulse and the pulse designed by Vahlin and Holte [VH96] respectively.

We also demonstrate that, with respect to robustness against CFO, OFDM/OQAM outperforms OFDM/QAM systems using rectangular pulseshaping. At the optimized CFO point of $f_e = 0.2$, the average interference power of an OFDM/OQAM system with the optimal pulse robust to CFO is about 2 dB lower than that of an OFDM/QAM system with rectangular pulseshaping.

We find that the robustness to CFO for OFDM systems can be improved by using appropriate pulseshaping, but the interference caused by CFO cannot be completely eliminated. Therefore, CFO estimation is still a crucial problem for OFDM systems. Nevertheless, the utilizing of robust pulses will help the estimation of CFO since relatively less interference is present.

Chapter 5

Blind CFO Estimation for OFDM/OQAM Systems

In Chapter 4, we have shown that both OFDM/QAM and OFDM/OQAM systems are sensitive to carrier frequency offset (CFO), even with the utilizing of optimal pulseshapes with robustness to CFO. Thus it is a crucial task to estimate and compensate the CFO caused by Doppler frequency shift or oscillator inaccuracy before demodulation.

The problem of CFO estimation for conventional OFDM/QAM systems has been intensively studied in the literature. In particular, there is now an increasing interest in blind CFO estimation. Van de Beek et al. propose a joint timing and frequency offset estimator by exploiting the redundant information contained in the cyclic prefix [vdBSB97]. Null-subchannels (or virtual subchannels) based blind CFO estimation methods are also reported [TL98, GW99, GSG01, MTGB01]. Another category of blind CFO estimation methods is based on the second-order statistics of the received signal. Bölcskei presents a blind CFO estimation algorithm based on the cyclostationarity of the received sequence before demodulation [Bol01], which is a natural extension of an estimator for single carrier QAM transmission systems [GG98]. Bölcskei's estimator has relatively large mean square error (MSE) and channel information is needed in the case of multipath fading. Park et al. have developed a similar method that does not need channel information [PCK$^+$04]. However, this method is based on the assumption of Rayleigh fading, and it requires the phase of the channel to be uniformly distributed. These conditions are not true for many practical cases like a Ricean fading channel and a time-invariant fixed radio channel. Ciblat and Vandendorpe present a blind CFO estimator based on the conjugate cyclostationarity of the received signal before demodulation [CV03]. Ciblat and Vandendorpe's method is robust to time-invariant multipath effects, while it does not work fine over a time varying channel.

CFO estimation is also an important task for OFDM/OQAM systems. In [Bol01], Bölcskei also presents a blind CFO estimator for OFDM/OQAM systems based on the correlation function of the received channel signal before demodulation. Ciblat and Serpedin [CS04] claim that the estimation accuracy can be significantly improved by using the conjugate correlation function of the received channel signal in stead of the correlation function. Both Bölcskei's and Ciblat/Serpedin's estimators are based the second-order statistics of the received signal before demodulation. The implementation complexity of Ciblat/Serpedin's estimator is much higher than Bölcskei's estimator since in addition to the estimation of conjugate correlation function, an FFT based coarse peak search and a steepest descent based fine peak search are needed. Recently, a maximum likelihood based CFO estimator for OFDM/OQAM systems is also reported [FT06].

The previously suggested blind CFO estimation methods for OFDM/OQAM systems are all based on the received channel signal before demodulation. For OFDM/OQAM systems, pulses with low sidelobes in frequency domain can be used [VH96, BDH99]. Thus for a system with many subchannels, each subchannel can be approximated as flat-fading. This motivates us to estimate CFO based on the subchannel signals. In addition, since the sampling rate of the signal from each receiver filter is $N/2$ times lower than that of the received signal before demodulation, where N is the number of subchannels, lower implementation complexity can be achieved. Such blind CFO estimation methods are based on the second-order, or high-order statistics of the subchannel signals.

The rest of this chapter is organized as follows. First, in section 5.1, a time-discrete model for OFDM/OQAM systems with subchannel weighting is introduced, then expressions for the correlation function, conjugate correlation function and a fourth-order statistics of subchannel signals are formulated. We find that subchannel weighting is needed to recover CFO for second-order statistics based methods. For the fourth-order statistics based estimation method, subchannel weighting is not necessary. Then, in section 5.2, the corresponding CFO estimation methods are presented. Asymptotical analysis is performed in section 5.3. In section 5.4, simulation results are presented to evaluate the performance of the estimators and validate the theoretical analysis. At last, a short conclusion is given in section 5.5.

Parts of the results of this chapter have been published in [LHL06, LLH06a, LLH06b, LLH06c].

5.1 System model and second- and high-order statistics of subchannel signals

5.1.1 System description and definitions

A time-discrete model for critically sampled OFDM/OQAM systems is shown in Fig. 5.1. Only subchannel k is shown at the receiver side. This model has N subchannels that are weighted by factors $\{w_k\}_{k=0}^{N-1}$. The weighting factor w_k should be real-valued to maintain the orthogonality between subchannels. By setting the weighting factor $w_k = 1$ and assuming no CFO is present, we then obtain the unweighted model depicted in Fig. 2.4 in chapter 2.

Each subchannel transmits one QAM symbol $a_k[n] = a_k^{\mathcal{R}}[n] + j\, a_k^{\mathcal{I}}[n]$ per T seconds. The OQAM symbols are formed by shifting the imaginary part of QAM symbols by $T/2$. By summing up all the subchannels, the modulator generates a T/N sampled output sequence

$$s[l] = \sum_{k=0}^{N-1} w_k \sum_{n=-\infty}^{\infty} \big(a_k^{\mathcal{R}}[n]\, g[l-nN] + j\, a_k^{\mathcal{I}}[n]\, g[l-nN-N/2]\big)\, e^{j(\frac{2\pi}{N}l+\frac{\pi}{2})k}.$$

The transmitter filter $g[l]$ and receiver filter $f[l]$ operate with the same sampling interval T/N and are bandlimited to $[-1/T, 1/T]$. We assume a time varying multipath channel, which is unchanged during one sampling interval T/N. For a large number of subchannels N, the equivalent channel response of subchannel k can be approximated as time varying flat-fading with a fading factor $\mu_k[l]$. For the special case of time-invariant channel, the factors $\mu_k[l]$ are independent of l. For a time varying channel, we assume that $\mu_k[l]$ is a stationary random process with correlation function

$$c_{\mu_k}[\tau] \overset{\text{def}}{=} \mathbb{E}\big[\mu_k[l+\tau]\mu_k^*[l]\big], \tag{5.1}$$

and variance $\sigma_{\mu_k}^2 = c_{\mu_k}[0]$.

The channel model also includes an additive circular white Gaussian noise source $\nu[l]$ with variance σ_ν^2. We further assume that input data symbols, channel and noise are mutually independent. The carrier frequency offset is normalized with respect to subchannel spacing $1/T$ and denoted f_e. Then we can write the received sequence from the channel as

$$r[l] = e^{j\frac{2\pi}{N}f_e l} \sum_{k=0}^{N-1} w_k \mu_k[l] \sum_{n=-\infty}^{\infty} \big(a_k^{\mathcal{R}}[n]\, g[l-nN] + j\, a_k^{\mathcal{I}}[n]\, g[l-nN-N/2]\big) \times e^{j(\frac{2\pi}{N}l+\frac{\pi}{2})k} + \nu[l]. \tag{5.2}$$

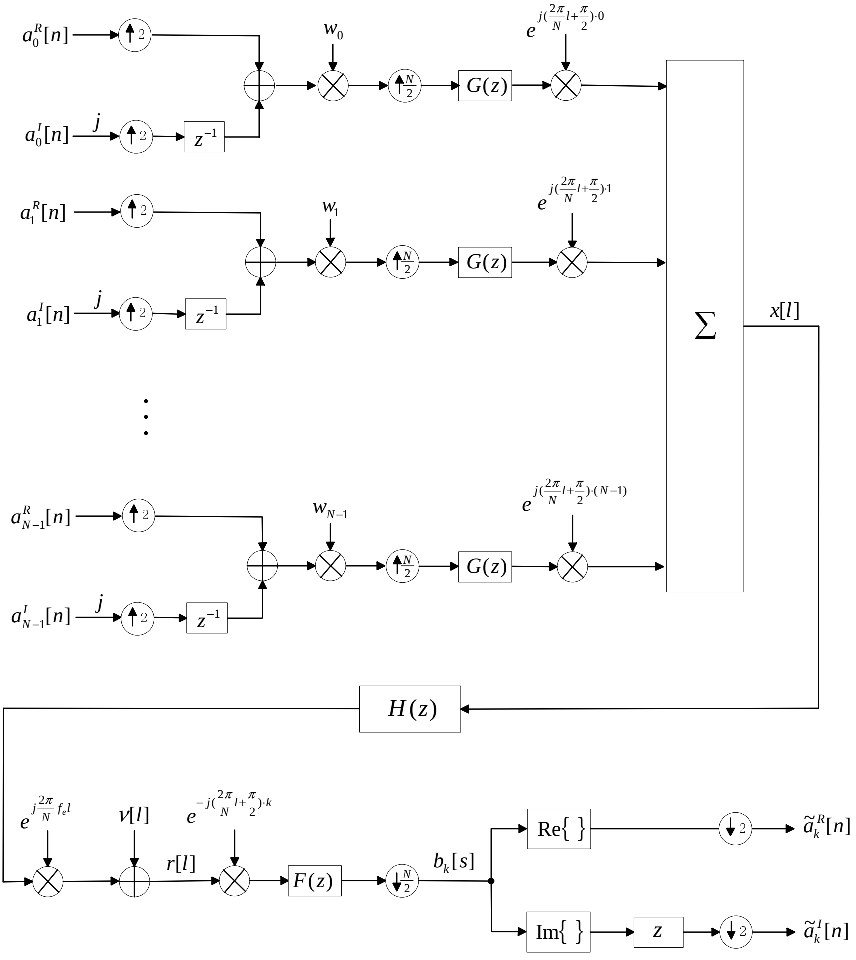
$a_0^R[n]$
$a_0^I[n]$
j
z^{-1}
w_0
$\uparrow\frac{N}{2}$
$G(z)$
$e^{j(\frac{2\pi}{N}l+\frac{\pi}{2})\cdot 0}$
$a_1^R[n]$
$a_1^I[n]$
w_1
$e^{j(\frac{2\pi}{N}l+\frac{\pi}{2})\cdot 1}$
$a_{N-1}^R[n]$
$a_{N-1}^I[n]$
w_{N-1}
$e^{j(\frac{2\pi}{N}l+\frac{\pi}{2})\cdot (N-1)}$
$\sum$
$x[l]$
$H(z)$
$e^{j\frac{2\pi}{N}f_e l}$
$v[l]$
$r[l]$
$e^{-j(\frac{2\pi}{N}l+\frac{\pi}{2})\cdot k}$
$F(z)$
$\downarrow\frac{N}{2}$
$b_k[s]$
Re{ }
Im{ }
z
$\downarrow 2$
$\tilde{a}_k^R[n]$
$\tilde{a}_k^I[n]$

Figure 5.1: Time-discrete model for a critically sampled OFDM/OQAM system with carrier frequency offset and subchannel weighting.

In subchannel k at the receiver side, the received sequence is first down-converted by multiplying with $e^{-j(\frac{2\pi}{N}l+\frac{\pi}{2})k}$, then filtered by the receiver filter $f[l]$ and $N/2$ times down-sampled to generate a $T/2$ spaced sequence

$$\begin{aligned} b_k[s] &= \left\{ \left(r[l]\, e^{-j(\frac{2\pi}{N}l+\frac{\pi}{2})k} \right) * f[l] \right\} \Big|_{l=s\frac{N}{2}} \\ &= e^{j\pi f_e s} \sum_{m=0}^{N-1} w_m\, \mu_m[s\frac{N}{2}] \sum_{n=-\infty}^{\infty} \big(a_m^{\mathcal{R}}[n]\, p_{m,k}[s-2n] \\ &\quad + j\,(-1)^{(m-k)} a_m^{\mathcal{I}}[n]\, p_{m,k}[s-2n-1] \big) + \nu_k[s], \end{aligned} \tag{5.3}$$

where $*$ stands for the convolution, and $p_{m,k}[s] \overset{\text{def}}{=} p_{m,k}^{(o)}[s\frac{N}{2}]$ and $\nu_k[s] \overset{\text{def}}{=} \nu_k^{(o)}[s\frac{N}{2}]$ are respectively the $N/2$ times down-sampled versions of $p_{m,k}^{(o)}[l]$ and $\nu_k^{(o)}[l]$ which are defined as

$$\begin{aligned} p_{m,k}^{(o)}[l] &= \left(g[l]\, e^{j(\frac{2\pi}{N}l+\frac{\pi}{2})(m-k)} \right) * \left(f[l]\, e^{-j\frac{2\pi}{N}f_e l} \right) \\ \nu_k^{(o)}[l] &= \left(\nu[l]\, e^{-j(\frac{2\pi}{N}l+\frac{\pi}{2})k} \right) * f[l]. \end{aligned} \tag{5.4}$$

Note that $p_{m,k}^{(o)}[l]$ and $\nu_k^{(o)}[l]$ herein denote slightly different meaning as those defined in (3.2) and (3.3) in Chapter 3.

It is worthy to indicate that although the sequence immediately before the decimator (or immediately after the receiver filter), i.e. $\left(r[l]\, e^{-j(\frac{2\pi}{N}l+\frac{\pi}{2})k}\right) * f[l]$, contains more information than the $N/2$ down-sampled sequence $b_k[s]$, this signal is not directly available in a receiver based on FFT and polyphase filters [CV95, VL01]. Therefore we will base our methods on $b_k[s]$.

5.1.2 Second-order statistics of subchannel signals

It has been reported that both the correlation function [Bol01] and conjugate correlation function [CS04] of the received sequence $r[l]$ are functions of f_e, and can thus be used for blind CFO estimation in OFDM/OQAM systems. We will now consider the correlation and conjugate correlation functions of the subchannel signals $b_k[s]$, and find conditions for when information about f_e is present in these. We assume that the input QAM symbols are i.i.d. between different subchannels, different instants and between real and imaginary parts, i.e.

$$\begin{aligned} &\mathbb{E}\big[a_m^{\mathcal{R}}[n_1]\, a_k^{\mathcal{R}}[n_2]\big] = \mathbb{E}\big[a_m^{\mathcal{I}}[n_1]\, a_k^{\mathcal{I}}[n_2]\big] = \frac{1}{2}\,\sigma_a^2\, \delta(m-k, n_1-n_2) \\ &\mathbb{E}\big[a_m^{\mathcal{R}}[n_1]\, a_k^{\mathcal{I}}[n_2]\big] = 0,\ \forall\ m, k, n_1, n_2, \end{aligned}$$

where $\delta(k, n)$ is the two-dimensional Kronecker delta function.

Without loss of generality, we may assume that the input QAM symbols have unit power, i.e. $\sigma_a^2 = 1$. The expressions for the correlation function and conjugate correlation function are given as below:

A. Correlation function

The correlation function of subchannel signal $b_k[s]$ is defined as $c_k[s,\tau] = \mathbb{E}\left\{b_k[s+\tau]\,b_k^*[s]\right\}$. Then, using (5.3), we find that $b_k[s]$ is wide sense stationary since $c_k[s,\tau]$ is not a function of s, and we can express the correlation function as

$$c_k[\tau] = \frac{1}{2}\sum_{m=0}^{N-1} w_m^2\, c_{\mu_m}[\tau\frac{N}{2}]\, A_{m,k}(\tau, f_e) + \sigma_\nu^2\, p_t[\tau], \tag{5.5}$$

where

$$p_t[\tau] \overset{\text{def}}{=} \left\{g[l] * f[l]\right\}\big|_{l=\tau\frac{N}{2}} \tag{5.6}$$

is the $N/2$ times down-sampled version of the overall response of the cascade of $g[l]$ and $f[l]$, and

$$\begin{aligned} A_{m,k}(\tau, f_e) &\overset{\text{def}}{=} e^{j\pi f_e \tau} \sum_{n=-\infty}^{\infty} p_{m,k}[n+\tau]\, p_{m,k}^*[n] \\ &= \frac{1}{2}\int_{-1}^{1} |P_{m,k}(f)|^2\, e^{j\pi(f+f_e)\tau}\, df, \end{aligned} \tag{5.7}$$

where the last equality follows from the Parseval's relation and the definition

$$P_{m,k}(f) = \sum_{s=-\infty}^{\infty} p_{m,k}[s]\, e^{-j\pi f s}. \tag{5.8}$$

We assume that the transmitter $f[l]$ and receiver $g[l]$ are identical real-valued and symmetric, for example, square root raised cosine pulse with a roll-off factor less or equal to one. It is proved in Appendix D that $\sum_{m=0}^{N-1} A_{m,k}(\tau, f_e)$ is real-valued and independent of f_e. Then, for the case of unweighted systems and AWGN channel, i.e. $w_k = 1$ and $\mu_k[l] \equiv 1$, the correlation function given by (5.5) is independent of f_e and thus contains no information of f_e.

B. Conjugate correlation function

The conjugate correlation function of subchannel signals $b_k[s]$ is defined as $\tilde{c}_k[s,\tau] = \mathbb{E}\left[b_k[s+\tau]\, b_k[s]\right]$. We will show in Section 5.4 by simulations that the estimation methods based on the conjugate correlation function are not robust with a time varying channel. Therefore we will assume a time-invariant channel, so that the attenuation factors $\mu_k[l]$ can be denoted as μ_k. Then based on the expression of $b_k[s]$ in (5.3), we have

$$\tilde{c}_k[s,\tau] = r_k(\tau, f_e)\, e^{j2\pi(f_e+1/2)s}, \tag{5.9}$$

where

$$r_k(\tau, f_e) = \frac{1}{2}\, e^{j\pi f_e \tau} \sum_{m=0}^{N-1} w_m^2\, \mu_m^2\, \widetilde{A}_{m,k}(\tau, f_e), \tag{5.10}$$

and

$$\widetilde{A}_{m,k}(\tau, f_e) = \sum_{n=-\infty}^{\infty} \big(p_{m,k}[2n+\tau]\, p_{m,k}[2n] - p_{m,k}[2n+\tau+1]\, p_{m,k}[2n+1]\big). \tag{5.11}$$

Since $\tilde{c}_k[s,\tau]$ is a function of f_e, it can be used for CFO estimation as long as $|r_k(\tau, f_e)| \neq 0$. In that case, we see that $\tilde{c}_k[s,\tau]$ is cyclostationary in s with a period $(f_e + 1/2)^{-1}$. Then the spectrum (with respect to s) of $\tilde{c}_k[s,\tau]$ will have a sharp peak at $f_e + 1/2$, which can be used to estimate f_e. By using the assumptions that the transmitter filter $f[l]$ and receiver filter $g[l]$ are identical real-valued and symmetric pulses, it is proved in Appendix E that $\sum_{m=0}^{N-1} \widetilde{A}_{m,k}(\tau, f_e) = 0$. Thus for the case of unweighted systems and AWGN channel, i.e. $w_k = 1$ and $\mu_k = 1$, we have $\tilde{c}_k[s,\tau] = 0$ based on (5.9) and (5.10). This implies that no information about f_e is present in $\tilde{c}_k[s,\tau]$.

5.1.3 High-order statistics of subchannel signals

In the above discussions, we have shown that for the case of unweighted systems and AWGN channel, neither the correlation function $c_k[\tau]$ nor the conjugate correlation function $\tilde{c}_k[s,\tau]$ contain information about CFO. Therefore subchannel weighting is needed for those methods. However, subchannel weighting will reduce the power efficiency. Thus it is desirable to develop a CFO estimation method without subchannel weighting.

Now we check if the high-order statistics of subchannel signals contain CFO information. We assume an unweighted system, i.e. $w_k = 1$, and consider the fourth-order statistics

$$m_{4,k}[s, \tau_1, \tau_2, \tau_3] \overset{\text{def}}{=} \mathbb{E}\big[b_k[s+\tau_3]\, b_k[s+\tau_2]\, b_k[s+\tau_1]\, b_k[s]\big]. \tag{5.12}$$

By substituting (5.3) into the definition of $m_{4,k}[s, \tau_1, \tau_2, \tau_3]$, and after some tedious but straightforward derivations, we obtain

$$m_{4,k}[s, \tau_1, \tau_2, \tau_3, f_e] = \rho_k(\tau_1, \tau_2, \tau_3, f_e)\, e^{j4\pi f_e s}, \tag{5.13}$$

where

$$\begin{aligned}
&\rho_k(\tau_1,\tau_2,\tau_3,f_e)\\
&= e^{j\pi f_e(\tau_1+\tau_2+\tau_3)}\Big\{\kappa_4\, B(\tau_1,\tau_2,\tau_3,f_e)\\
&\quad + \frac{\sigma_a^4}{4}(-1)^{\tau_2}\Big(\sum_{m=0}^{N-1}\widetilde{A}_{m,k}(\tau_3-\tau_2,f_e)\Big)\Big(\sum_{m=0}^{N-1}\widetilde{A}_{m,k}(\tau_1,f_e)\Big)\\
&\quad + \frac{\sigma_a^4}{4}(-1)^{\tau_1}\Big(\sum_{m=0}^{N-1}\widetilde{A}_{m,k}(\tau_3-\tau_1,f_e)\Big)\Big(\sum_{m=0}^{N-1}\widetilde{A}_{m,k}(\tau_2,f_e)\Big)\\
&\quad + \frac{\sigma_a^4}{4}(-1)^{\tau_1}\Big(\sum_{m=0}^{N-1}\widetilde{A}_{m,k}(\tau_2-\tau_1,f_e)\Big)\Big(\sum_{m=0}^{N-1}\widetilde{A}_{m,k}(\tau_3,f_e)\Big)\Big\}, \qquad (5.14)
\end{aligned}$$

where $\kappa_4 \overset{\text{def}}{=} \mathbb{E}\left[\left(a_m^{\mathcal{R}}[n]\right)^4\right] - \frac{3}{4}$ is the fourth-order cumulant of $a_k^{\mathcal{R}}[n]$ (or $a_k^{\mathcal{I}}[n]$), $\widetilde{A}_{m,k}(\tau,f_e)$ is defined by (5.11) and

$$B(\tau_1,\tau_2,\tau_3,f_e) \overset{\text{def}}{=} \sum_{m=0}^{N-1}\sum_{n=-\infty}^{\infty} p_{m,k}[n+\tau_3]\,p_{m,k}[n+\tau_2]\,p_{m,k}[n+\tau_1]\,p_{m,k}[n]. \qquad (5.15)$$

Since $\rho_k(\tau_1,\tau_2,\tau_3,f_e)$ is not a function of s, we see from (5.13) that $m_{4,k}[s,\tau_1,\tau_2,\tau_3,f_e]$ is periodic in s with a period $(2f_e)^{-1}$. To be useful for CFO estimation, we must in addition check that $|m_{4,k}[s,\tau_1,\tau_2,\tau_3,f_e]| \neq 0$. In that case, the spectrum (with respect to s) of $m_{4,k}[s,\tau_1,\tau_2,\tau_3,f_e]$ will have a sharp peak at $2f_e$, which can be used to estimate f_e.

For an AWGN channel, we have shown in Appendix E that $\sum_{m=0}^{N-1}\tilde{A}_{m,k}(\tau,f_e) = 0$ for unweighted systems. Thus the term $\kappa_4\, B(\tau_1,\tau_2,\tau_3,f_e)$ should be non-zero to recover f_e. By choosing appropriate constellation and symbol distribution, we can make $\kappa_4 \neq 0$. In this thesis, we assume 16OQAM constellation and uniformly distributed symbols. It can be calculated that $\kappa_4 = -0.34$. It will be shown in the next section that $B(\tau_1,\tau_2,\tau_3,f_e) \neq 0$ for some (τ_1,τ_2,τ_3). Thus it is possible to estimate f_e based on the fourth-order statistics $m_{4,k}[s,\tau_1,\tau_2,\tau_3,f_e]$ for unweighted OFDM/OQAM systems.

5.2 Estimation methods

In the previous section, we have shown that for the case of unweighted systems and AWGN channel, neither the correlation function $c_k[\tau]$ nor the conjugate correlation function $\tilde{c}_k[s,\tau]$ contain information about CFO. One method to ensure frequency offset information in the second-order statistics is subchannel weighting, i.e. distributing individual subchannel different power. Here we consider two weighting methods: null-subchannels insertion and interleaved weighting. In the case of null-subchannels insertion, we will present three estimation methods based on subchannel signals: two of them are based on the correlation function and one is based on the conjugate correlation function. For the case of interleaved weighting, we only present a method based on the conjugate correlation function.

For unweighted OFDM/OQAM systems, we have shown in the previous section that for a non-zero fourth order cumulant of transmitted symbols $\kappa_4 = \mathbb{E}\left[\left(a_m^{\mathcal{R}}[n]\right)^4\right] - \frac{3}{4}$, the fourth-order statistics of subchannel signals $m_{4,k}[s, \tau_1, \tau_2, \tau_3]$ defined in (5.12) can be used to recover the CFO blindly. In this section, we will also present a blind CFO estimation method for unweighted systems based on this fourth-order statistics.

5.2.1 Estimation methods based on null-subchannels

We set $w_k = 0$ for L selected subchannels $k_1, \; k_2, \cdots, \; k_L$, which are referred as *null-subchannels*, while the other factors are set to 1. The null-subchannels are assumed to be sparsely distributed. Below we present CFO estimation methods based on the correlation function and the conjugate correlation function respectively.

A. Correlation function based methods

If subchannel k is a null-subchannel and $0 \leq f_e < 1$, $c_{k-1}[\tau]$, $c_k[\tau]$, $c_{k+1}[\tau]$ and $c_{k+2}[\tau]$ will be functions of f_e, and thus contain information about CFO. This implies that we can estimate f_e from subchannels $k \pm 1$, k and $k+2$. In this chapter, we will base our methods only on $c_k[\tau]$. By substituting (D.1) into (5.7) and then into (5.5), and after some derivations, we obtain

$$\begin{aligned} c_k[\tau] &= \frac{1}{4} \int_{-1}^{1} \Big(\sum_{\substack{m=k-2 \\ m \neq k}}^{k+2} c_{\mu_m}[\tau \frac{N}{2}] \, |P_{m,k}(f - f_e)|^2 \Big) \, e^{j\pi f \tau} \, df + \sigma_\nu^2 \, p_t[\tau] \\ &\simeq -\frac{1}{4} \, e^{j\pi f_e \tau/2} \, c_{\mu_k}[\tau \frac{N}{2}] \, M_g\left(\tau, f_e\right) + \left(c_{\mu_k}[\tau \frac{N}{2}] + \sigma_\nu^2\right) p_t[\tau], \qquad (5.16) \end{aligned}$$

where the approximations $c_{\mu_{k\pm2}}[\tau \frac{N}{2}] \simeq c_{\mu_{k\pm1}}[\tau \frac{N}{2}] \simeq c_{\mu_k}[\tau \frac{N}{2}]$ are used during the derivations, and

$$M_g\left(\tau, f_e\right) = \int_{-1}^{1} G^2(f - \frac{f_e}{2}) \, G^2(f + \frac{f_e}{2}) \, \cos\left(\pi f \tau\right) \, df. \qquad (5.17)$$

Since we have assumed that $g(t)$ is symmetric, $M_g\left(\tau, f_e\right)$ is real-valued. For the case of $G(f)$ to be the square root raised cosine pulse with a roll-off factor equal 0.2 and 1.0, numerical results show that $M_g(\tau, f_e)$ decreases quickly towards zero with increasing τ. The curves of $M_g(\tau, f_e)$ with $\tau = 0, 1, 2$ are show in Fig. 5.2. We see that $M_g(\tau, f_e)$ also decreases with increasing $|f_e|$, while they all stay positive for $\tau = 0, 1, 2$ in the range of $|f_e| < 1$.

In practice only a finite-length data record $\{b_k[s]\}_{s=0}^{M-1}$ is available. We can estimate the correlation function by $\hat{c}_k[\tau] = \frac{1}{M}\sum_{s=0}^{M-1} b_k[s+\tau]\, b_k^*[s]$ (samples outside the data record are set to zero), which is an asymptotically unbiased estimate of $c_k[\tau]$. Below we present two estimation methods based on this estimate.

Method 1:

Since $p_t[\tau]$ defined in (5.6) is the $N/2$ times down-sampled version of the overall response of the cascade of transmitter filter $g[l]$ and receiver filter $f[l]$, it should be a two times over-sampled Nyquist pulse to guarantee the orthogonality. This implies that $p_t[\tau] = 0$ for any non-zero even τ. We further assume that $c_{\mu_k}[N]$ is positive. For a time-invariant channel, this assumption is obviously satisfied. For slow enough fading, $c_{\mu_k}[N]$ is approximately equal to $\sigma_{\mu_k}^2$ and thus also positive. From (5.16), we see that the phase of $c_k[2]$ is essentially independent of subchannel index k. Then we can estimate f_e based on the phase of the sum of $\hat{c}_{k_1}[2], \hat{c}_{k_2}[2], \cdots, \hat{c}_{k_L}[2]$ as:

$$\hat{f}_e = \frac{1}{\pi}\angle\Big(-\sum_{l=1}^{L}\hat{c}_{k_l}[2]\Big), \tag{5.18}$$

where $\angle\cdot$ stands for the operation of taking the phase in radians.

The acquisition range of Method 1 is $|f_e| < 1$. However, since $\angle c_k[2] \rightarrow \pi$ as $|f_e| \rightarrow 1$, even a small estimation error of $c_k[2]$ may cause the estimated CFO to jump to from positive to negative (or from negative to positive) due to the discontinuity of the function $\angle\cdot$, the estimation is not reliable for large values of f_e. For a fast fading channel, where $c_{\mu_k}[\tau\frac{N}{2}]$ may become negative or have a very small magnitude, this estimator fails.

Method 2:

Numerical results show that the magnitudes of $c_k[0]$ and $c_k[1]$ are higher than that of $c_k[2]$. Thus better performance is expected if we can estimate f_e based on $c_k[0]$ and $c_k[1]$. Based on (5.16), we have

$$\begin{aligned} c_k[0] &\simeq -\frac{\sigma_{\mu_k}^2}{4} M_g(0, f_e) + \big(\sigma_{\mu_k}^2 + \sigma_\nu^2\big) \\ c_k[1] &\simeq -\frac{c_{\mu_k}[N/2]}{4} e^{j\pi f_e/2} M_g(1, f_e) + \big(c_{\mu_k}[\frac{N}{2}] + \sigma_\nu^2\big)\, p_t[1]. \end{aligned}$$

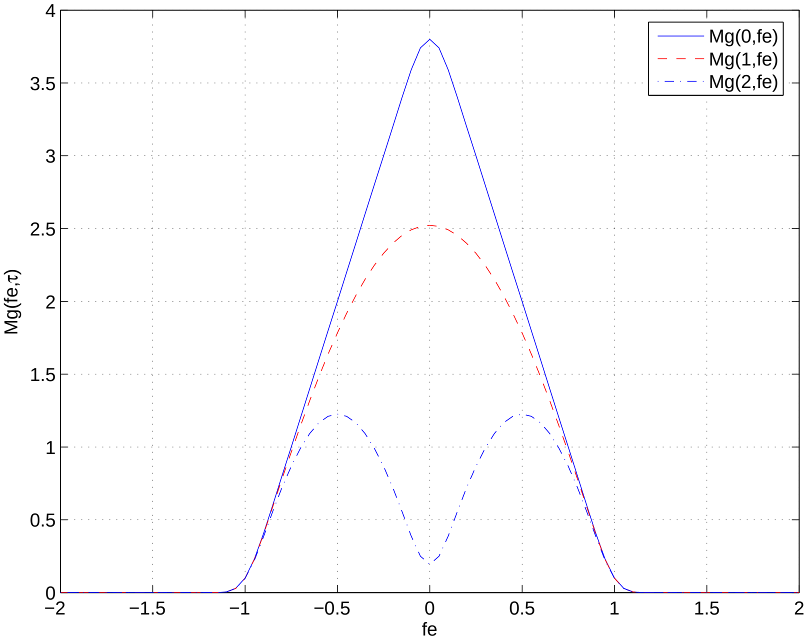

(a) $\alpha = 0.2$

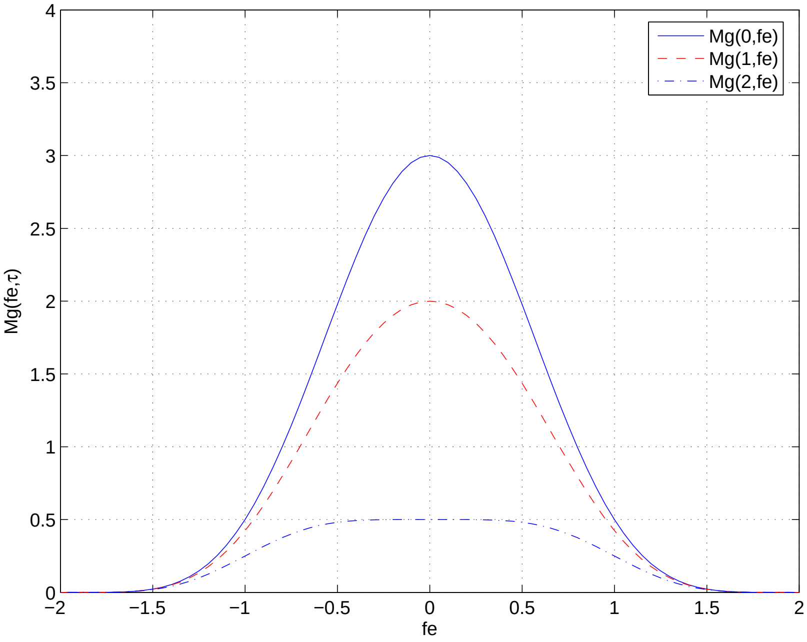

(b) $\alpha = 1.0$

Figure 5.2: Curves of $M_g(\tau, f_e)$ for $\tau = 0, 1, 2$ with square root raised cosine pulse (with a roll-off factor denoted α) as shaping filter .

We see that both $c_k[0]$ and $c_k[1]$ contain noise terms. For a slow fading channel, $c_{\mu_k}[N/2] \simeq \sigma^2_{\mu_k}$ (for a time-invariant channel they are actually equal). In that case, we may define

$$\beta_k = p_t[1]\, c_k[0] - c_k[1] \simeq \frac{\sigma^2_{\mu_k}}{4}\, M_g\left(1, f_e\right) \left(e^{j\pi f_e/2} - \frac{M_g\left(0, f_e\right)}{M_g\left(1, f_e\right)}\, p_t[1] \right).$$

By using this quantity, the noise terms have been successfully eliminated. The parameters $M_g(\tau, f_e)$ and $p_t[\tau]$ can be deferred from $G(f)$ directly. Then by summing up all null-subchannels, we can estimate CFO by

$$\hat{f}_e = \arg\left(\phi(f_e) = \hat{\phi}\right), \tag{5.19}$$

where $\phi(f_e) \overset{\text{def}}{=} \angle\left(e^{j\pi f_e/2} - \frac{M_g(0,f_e)}{M_g(1,f_e)}\, p_t[1]\right)$ and $\hat{\phi} = \angle\left(\sum_{l=1}^{L} \hat{\beta}_{k_l}\right)$, where $\hat{\beta}_k \overset{\text{def}}{=} p_t[1]\, \hat{c}_k[0] - \hat{c}_k[1]$ is an estimate of β_k.

Now the estimation problem is turned into solving the nonlinear equation $\phi(f_e) = \hat{\phi}$, and we should look closer at the properties of $\phi(f_e)$. When using a square root raised cosine pulse with a roll-off factor $\alpha = 1.0$ as pulse shapes, numerical results show that $\phi(f_e)$ increases monotonously with increasing f_e in the region of $-\pi < \phi(f_e) < \pi$. Thus $\hat{f}_e$ is uniquely determined for $-\pi < \hat{\phi} < \pi$. In practice, a look-up table may be used to solve (5.19). The acquisition range of Method 2 is $|f_e| < 2$ theoretically. However, numerical results show that both $M_g(f_e, 0)$ and $M_g(f_e, 1)$ are close to zero for $|f_e| > 1.5$, making the estimator unreliable for large CFO values.

Modified Bölcskei estimator:

To illustrate the benefit of estimation based on subchannel signals, we should compare our methods to one that is based on the received signal before demodulation. In [Bol01], Bölcskei presents an estimator based on the cyclostationarity of the received signal before demodulation assuming an AWGN channel. We will first show that the Bölcskei estimator doesn't work under the assumptions that the real and imaginary parts of input QAM symbols have the same power. Then we present a *modified Bölcskei estimator*. We will also show that subchannel weighting is needed for the modified Bölcskei estimator. We consider only the weighting case by using null-subchannels for the modified Bölcskei estimator. As in Bölcskei's original work, we assume an AWGN channel. The performance over a multipath channel will be studied by simulations.

Observing that the correlation function of the received signal before demodulation is cyclostationary with period N, Bölcskei's estimator is based on a Fourier expansion of the correlation function with Fourier coefficients given (see (15) in [Bol01]) by

$$\begin{aligned} C_r[k,\tau] = \frac{1}{N}\, e^{j2\pi\theta_e\tau}\, e^{-j\frac{2\pi}{N}kn_e}\, \Gamma_N[\tau]\, A^{(g,g)}\left[\tau, \frac{k}{N}\right) \left(\sigma_{c,R}^2 + (-1)^k\, \sigma_{c,I}^2\right) \\ + c_\rho[\tau]\, \delta[k], \end{aligned} \tag{5.20}$$

where $\sigma_{c,R}^2$ and $\sigma_{c,I}^2$ are respectively the average power of the real and imaginary parts of the input QAM symbols, $c_\rho[\tau]$ is the correlation function of the channel noise, $\Gamma_N[\tau] = \sum_{k=0}^{N-1} |w_k|^2\, e^{j\frac{2\pi}{N}k\tau}$ and

$$A^{(g,g)}\left[\tau, \frac{k}{N}\right) = \sum_{l=-\infty}^{\infty} g[l]\, g[l-\tau] e^{-j\frac{2\pi}{N}kl}. \tag{5.21}$$

Note that the frequency offset θ_e in [Bol01] is normalized with respect to N/T. By using Parseval's relation, we can rewrite $A^{(g,g)}\left[\tau, \frac{k}{N}\right)$ in frequency domain as

$$A^{(g,g)}\left[\tau, \frac{k}{N}\right) = \int_{-0.5}^{0.5} G_n(f)\, G_n(f + \frac{k}{N})\, e^{-j2\pi f\tau}\, df, \tag{5.22}$$

where $G_n(f) = \sum_{l=\infty}^{\infty} g[l]\, e^{-j2\pi fl}$.

Since $G_n(f)$ is bandlimited to $[-1/N, 1/N]$ (normalized with respect to N/T), $A^{(g,g)}\left[\tau, \frac{k}{N}\right)$ is nonzero only if $k \in \{-1, 0, 1\}$. In [Bol01], the author assumes that $\sigma_{c,R}^2 \neq \sigma_{c,I}^2$, then estimates both carrier frequency offset and timing offset based on $C_r[\pm 1, \tau]$ (see (20) and (21) in [Bol01]).

In this chapter, we have assumed that $\sigma_{c,R}^2 = \sigma_{c,I}^2$. Then we have $\sigma_{c,R}^2 + (-1)^k\, \sigma_{c,I}^2 = 0$ for $k = \pm 1$, and only $C_r[0, \tau]$ can be used for the CFO estimation. This implies that only frequency offset can be recovered. Furthermore, since the channel noise is assumed to be white, i.e. $c_\rho[\tau] = \sigma_\nu^2\, \delta[\tau]$, the effect of noise can be excluded (in theory) since only $C_r[k, \tau]$ with nonzero lag τ can be used for CFO estimation. Subchannel weighting is still needed to keep $\Gamma_N[\tau]$ nonzero for some $\tau \geq 1$. For weighting case by using null-subchannels, this can be satisfied.

In practice, the cyclic statistics $C_r[0, \tau]$ must be estimated based on a data record with finite length. Here we use the same method as Bölcskei (see (31) in [Bol01]) to get the estimate $\hat{C}_r[0, \tau]$. Finally, based on (5.20) and noting that $A^{(g,g)}[\tau, 0)$ is real-valued, we can estimate the CFO as

$$\hat{f}_e = N\hat{\theta}_e = \frac{N}{2\pi} \sum_{\substack{\tau=1 \\ \Gamma_N[\tau]\neq 0}}^{L_\tau} \frac{1}{\tau} \angle \frac{\hat{C}_r[0, \tau]}{\Gamma_N[\tau]}. \tag{5.23}$$

This expression constitutes our modified Bölcskei estimator. A practical problem is to choose the maximum lag L_τ. From (5.22), we see that

$A^{(g,g)}[\tau, 0)$ is the impulse response of the cascade of transmitter and receiver filter, which decays quickly with increasing τ. Thus the choice of L_τ depends on the decay speed of time domain pulseshapes, and too large L_τ should be avoided.

B. Conjugate correlation function based method

If subchannel k is a null-subchannel, the conjugate correlation functions $\tilde{c}_{k-1}[s,\tau]$, $\tilde{c}_k[s,\tau]$ and $\tilde{c}_{k+1}[s,\tau]$ will contain information about f_e. Simulation results show that the benefit from including contributions from subchannels $k \pm 1$ is quite marginal. Therefore we will, as in the methods above, restrict ourselves to use subchannel k.

Another practical problem is to choose the lag τ. In Appendix E, we have shown that $\sum_{m=0}^{N-1} \widetilde{A}_{m,k}(\tau, f_e) = 0$. Then by using the approximation of $\mu_{k\pm1} \simeq \mu_k$, we have $|\tilde{c}_k[s,\tau]| = |r_k(\tau, f_e)| = \frac{1}{2}|\widetilde{A}_{k,k}(\tau, f_e)|$ based on (5.9) and (5.10). Therefore the amplitude of $\widetilde{A}_{k,k}(\tau, f_e)$ is crucial to recover the CFO. The 3-D curves of $|\widetilde{A}_{k,k}(\tau, f_e)|$ for the case of square root raised cosine pulse as shaping filter are shown in Fig 5.3. We see that the amplitude of $A_{k,k}(\tau, f_e)$ is largely independent of f_e, while it approaches zero with increasing τ and is negligible for τ larger than a certain threshold $\tau_{\max}$. Note that $\tilde{c}_k[s,\tau]$ with negative τ is just a shifted version of that with positive τ and thus contains no extra information.

In practice only a finite-length data record $\{b_k[s]\}_{s=0}^{M-1}$ is available. This means that we must use a single sample estimate for $\tilde{c}_k[s,\tau]$:

$$y_k[s,\tau] = b_k[s+\tau]\, b_k[s]. \tag{5.24}$$

Recall that the spectrum of $\tilde{c}_k[s,\tau]$ with respect to s has a sharp peak at $f_e + 1/2$. Then by defining $\mathbf{y}_k[s] = \big[y_k[s,0], y_k[s,1], \cdots, y_k[s,\tau_{\max}]\big]^T$, we can write the estimation algorithm as:

Method 3:

$$\hat{f}_e = \arg\max_{f\in(0,1)} J_M(f) - \frac{1}{2}$$

$$J_M(f) = \sum_{l=1}^{L} \Big\| \frac{1}{M} \sum_{s=0}^{M-1} \mathbf{y}_{k_l}[s]\, e^{-j2\pi f s} \Big\|^2. \tag{5.25}$$

We see that $J_M(f)$ contains contributions from different τ and different null-subchannels.

5.2.2 Estimation methods based on interleaved weighting

In [CS04], Ciblat and Serpedin present a blind CFO estimation method based on the conjugate cyclostationarity of the received sequence before

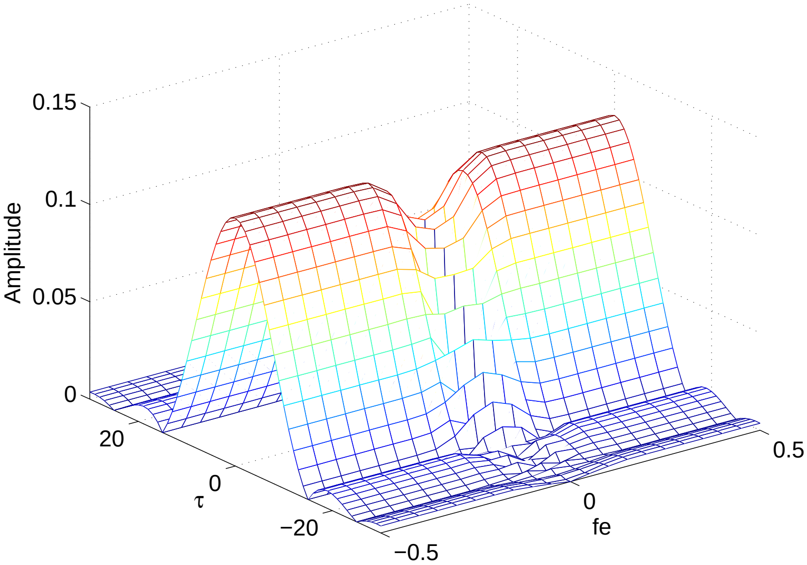

(a) $\alpha = 0.2$

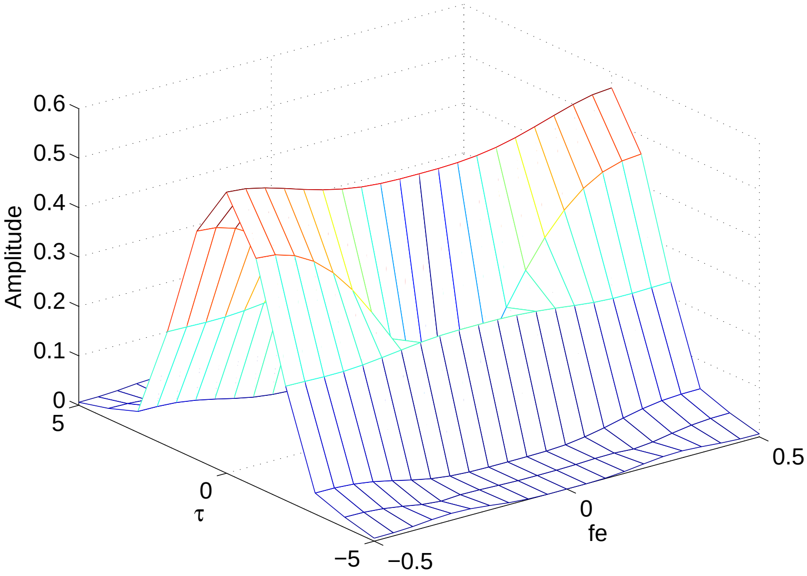

(b) $\alpha = 1.0$

Figure 5.3: Curves of $|\widetilde{A}_{k,k}(\tau, f_e)|$ with square root raised cosine pulse (with a roll-off factor denoted α) as shaping filters.

demodulation. However, they use a different modulation system that corresponds to multiplication of subchannel k by a weighting factor j^k. Application of Ciblat and Serpedin's algorithm to a standard OFDM/OQAM system is denoted *modified C/S estimator*, which will not work in an unweighted system because the conjugate correlation function of the signal before demodulation is zero [LHL06]. For a system with few null-subchannels, the conjugate correlation function is quite weak, so that the modified C/S estimator doesn't work properly (also confirmed by simulation). Therefore we implement the modified C/S estimator only for the interleaved weighting method.

Since null-subchannels are always present for practical OFDM systems, extensive investigation of estimation methods based on interleaved weighting is of less interest. Therefore for the case of interleaved weighting, we will present only the conjugate correlation function based method to show the benefit of estimation based on subchannel signals, and will not perform asymptotic analysis for the corresponding estimator in the next section.

The interleaved weighting pattern is got by setting $\mathbf{w} = \{w_1, w_2, w_1, w_2, ...\}$, where $w_1 \neq w_2$. For this case, by using the fact that $\sum_{m=0}^{N-1} \widetilde{A}_{m,k}(\tau, f_e) = 0$, and that $\widetilde{A}_{m,k}(\tau, f_e) = 0$ for $|m - k| \geq 2$ (see Appendix E), we have that $|\tilde{c}_k[s, \tau]| \simeq \frac{1}{2} \left| \mu_k^2 (w_1^2 - w_2^2) \widetilde{A}_{k,k}(\tau, f_e) \right|$ based on (5.9) and (5.10) and the approximation of $\mu_{k\pm 1}^2 \simeq \mu_k^2$. Therefore the CFO can be estimated over all subchannels, and we can express the estimation problem as:

Method 4:

$$\hat{f}_e = \arg \max_{f \in (0,1)} J_M(f) - \frac{1}{2}$$

$$J_M(f) = \sum_{k=0}^{N-1} \left\| \frac{1}{M} \sum_{s=0}^{M-1} \mathbf{y}_k[s] \, e^{-j2\pi f s} \right\|^2. \tag{5.26}$$

We see that the conjugate correlation function based Method 3 and 4 have the same acquisition range $(-0.5, 0.5)$. Method 3 uses only the signals of null-subchannels, while Method 4 includes the contribution of all subchannels.

5.2.3 CFO estimation methods based on high-order statistics for unweighted systems

The previously suggested CFO estimators based on second-order statistics all need subchannel weighting. This will lead lower power efficiency. Now we present a CFO estimation method based on fourth-order statistics for unweighed OFDM/OQAM systems.

Based on (5.13) and using the approximation $\mu_{k\pm 1} \simeq \mu_k$, we have that $|m_4(s, \tau_1, \tau_2, \tau_3, f_e)| = |\rho_k(\tau_1, \tau_2, \tau_3, f_e)| \simeq |\kappa_4\, B(\tau_1, \tau_2, \tau_3, f_e)|$. Since we have assumed that $\kappa_4 \neq 0$, CFO can be recovered by searching the peak of the spectrum (with respect to s) of $m_4(s, \tau_1, \tau_2, \tau_3, f_e)$ if $|B(\tau_1, \tau_2, \tau_3, f_e)| \neq 0$. Numerical results show that $|B(\tau_1, \tau_2, \tau_3, f_e)|$ decreases quickly with increasing τ_m. In this thesis, we will estimate f_e based on the set $\mathbb{S} = \{(\tau_1, \tau_2, \tau_3) : (0,0,0), (0,0,1), (0,1,1), (1,1,1)\}$. The curves of $|B(\tau_1, \tau_2, \tau_3, f_e)|$ versus f_e are shown in Fig. 5.4, in which the square root raised cosine pulses are used as the pulseshapes.

In practice, only one finite-length data record $\{b_k[s]\}_{s=0}^{M-1}$ is available. A one-sample estimate of $m_{4,k}[s, \tau_1, \tau_2, \tau_3, f_e]$ can be expressed as

$$\hat{m}_{4,k}[s, \tau_1, \tau_2, \tau_3, f_e] = \frac{1}{M} \sum_{n=0}^{M-1} b_k[s+\tau_3]\, b_k[s+\tau_2]\, b_k[s+\tau_1]\, b_k[s]. \tag{5.27}$$

From (5.13), we see that the amplitude of DTFT of $m_{4,k}[s, \tau_1, \tau_2, \tau_3, f_e]$ (with respect to time instant s) should has a sharp peak at $f = 2f_e$. Then by defining a row vector

$$\hat{\mathbf{m}}_k[s] = \begin{bmatrix} \hat{m}_{4,k}[s,0,0,0,f_e] \\ \hat{m}_{4,k}[s,0,0,1,f_e] \\ \hat{m}_{4,k}[s,0,1,1,f_e] \\ \hat{m}_{4,k}[s,1,1,1,f_e] \end{bmatrix}, \tag{5.28}$$

we can express the estimation problem as:

Method 5:

$$\hat{f}_e = \frac{1}{2} \arg \max_{f \in (-0.5, 0.5)} J_M(f)$$
$$J_M(f) = \sum_{k=0}^{N-1} \left\| \frac{1}{M} \sum_{s=0}^{M-1} \hat{\mathbf{m}}_k[s]\, e^{-j2\pi f s} \right\|^2. \tag{5.29}$$

It is obviously that the acquisition range of estimator (5.29) is $f_e \in (-0.25, 0.25)$.

5.3 Asymptotic analysis

In the previous section, we have suggested two weighting methods with corresponding Method 1-4, where the first three are based on null-subchannels, and the last one is based on interleaved weighting. We have also suggested the high-order statistics based Method 5 for unweighted systems.

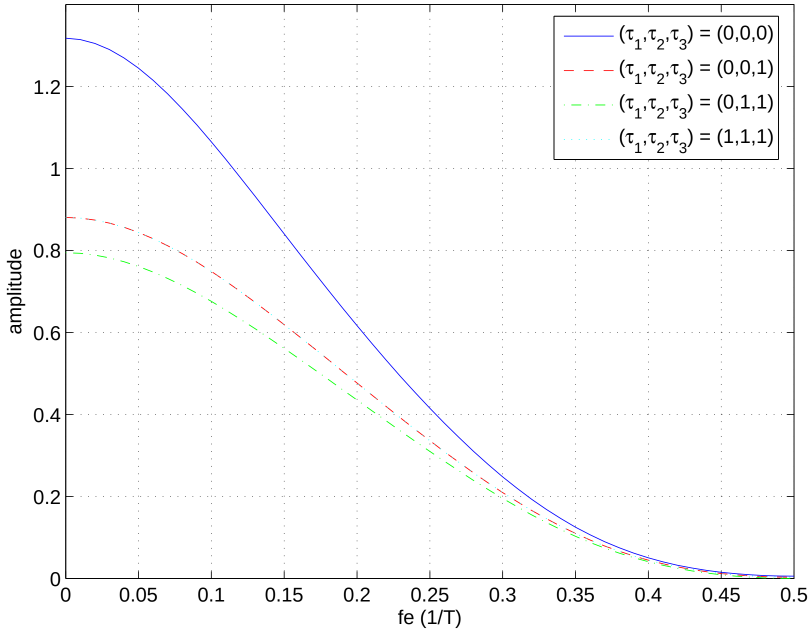

(a) $\alpha = 0.2$

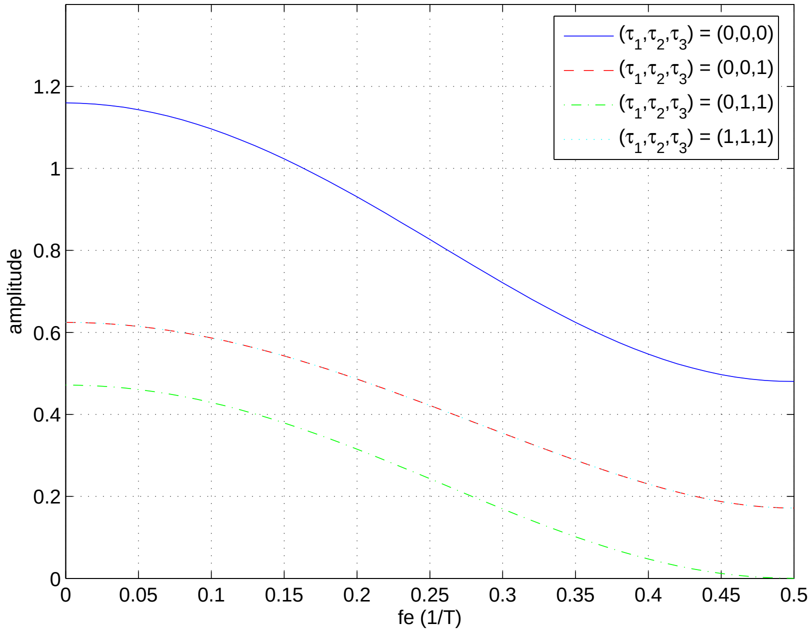

(b) $\alpha = 1.0$

Figure 5.4: Curves of $|B(\tau_1, \tau_2, \tau_3, f_e)|$ versus f_e with raised cosine pulses (with a roll-off factor denoted α) as shaping filters (the curves for $(\tau_1, \tau_2, \tau_3) = (0, 0, 1)$ and $(\tau_1, \tau_2, \tau_3) = (1, 1, 1)$ are overlapped).

In this section, we will present asymptotic analysis only for the null-subchannels based Method 1-3. The CFO estimation error is defined as $\Delta f_e = \hat{f}_e - f_e$ and the Mean Square Error (MSE) is given by $\mathbb{E}\big[|\Delta f_e|^2\big]$.

5.3.1 Asymptotic analysis of correlation function based estimators

We first analyze the correlation function based Method 1 and 2 by using a reasoning similar to the one in [WCSL02]. We assume that the transmitter filter $g[l]$ is truncated to be of finite length. Then $b_k[s+\tau]\, b_k^*[s]$ satisfies a so called mixing condition ([Bri75]: Theorem 2.3.1 (iii), p.19). By Lemma 1 in [CLSG02] we then have that $\lim_{M\to\infty} |\hat{c}_k[\tau] - c_k[\tau]|^2 \to 0$ with probability 1. Thus the estimate error $\Delta c_k[\tau] \overset{\text{def}}{=} \hat{c}_k[\tau] - c_k[\tau]$ should be small for large values of data record length M.

By using a first order Taylor expansion of (5.18), we can approximate the the CFO estimate by

$$\begin{aligned}\hat{f}_e &= \frac{1}{\pi}\,\mathrm{Im}\Big\{\ln\Big(-\sum_{l=1}^{L}\hat{c}_{k_l}[2]\Big)\Big\} \simeq \frac{1}{\pi}\,\mathrm{Im}\left\{\ln\Big(-\sum_{l=1}^{L} c_{k_l}[2]\Big) + \frac{\sum_{l=1}^{L}\Delta c_{k_l}[2]}{\sum_{l=1}^{L} c_{k_l}[2]}\right\}\\ &= f_e + \frac{\Big(\sum_{l=1}^{L}\Delta c_{k_l}[2]\Big)\Big(\sum_{l=1}^{L} c_{k_l}^*[2]\Big) - \Big(\sum_{l=1}^{L}\Delta c_{k_l}^*[2]\Big)\Big(\sum_{l=1}^{L} c_{k_l}[2]\Big)}{2\,j\,\pi\,\big|\sum_{l=1}^{L} c_{k_l}[2]\big|^2}.\end{aligned} \tag{5.30}$$

Since $\lim_{M\to\infty}\mathbb{E}\left[\Delta c_k[\tau]\right] = \mathbb{E}\left[\hat{c}_k[\tau]\right] - c_k[\tau] = 0$, we see that $\lim_{M\to\infty}\mathbb{E}\big[\hat{f}_e - f_e\big] = 0$ from (5.30). This implies that the estimated f_e is asymptotically unbiased. Since the null-subchannels are sparsely distributed, the terms $\mathbb{E}\big[\Delta c_{k_1}[\tau_1]\,\Delta c_{k_2}^*[\tau_2]\big]$ and $\mathbb{E}\big[\Delta c_{k_1}[\tau_1]\,\Delta c_{k_2}[\tau_2]\big]$ for $k_1 \neq k_2$ will be of order $O(\sigma_\nu^4)$, which is negligible for high SNR. Therefore $\Delta c_{k_1}[\tau_1]$ and $\Delta c_{k_2}[\tau_2]$ are approximately uncorrelated for $k_1 \neq k_2$. Then based on (5.30), we can write the MSE of Method 1 as

$$\mathrm{MSE}_1 \simeq \frac{\sum_{l=1}^{L}\Big(\mathbb{E}\big[\big|\Delta c_{k_l}[2]\big|^2\big] - \mathrm{Re}\big\{e^{-j2\pi f_e}\,\mathbb{E}\big[\big(\Delta c_{k_l}[2]\big)^2\big]\big\}\Big)}{2\,\pi^2\,\big|\sum_{l=1}^{L} c_{k_l}[2]\big|^2}. \tag{5.31}$$

Explicit calculable expressions for $\mathbb{E}\big[\big|\Delta c_k[2]\big|^2\big]$ and $\mathbb{E}\big[\big(\Delta c_k[2]\big)^2\big]$ are given by (5.33). Now we turn to the analysis of Method 2.

By defining $\Delta\beta_k = \hat{\beta}_k - \beta_k = p_t[1]\,\Delta c_k[0] - \Delta c_k[1]$, we can write the nonlinear equation in (5.19) as

$$\phi(f_e + \Delta f_e) = \mathrm{Im}\Big\{\ln\Big(\sum_{l=1}^{L}\left(\beta_{k_l} + \Delta\beta_{k_l}\right)\Big)\Big\}.$$

Then by using a first order Taylor approximation at both sides and the fact that $\phi(f_e) \simeq \mathrm{Im}\big\{\ln\big(\sum_{l=1}^{L}\beta_{k_l}\big)\big\}$ (they are actually equal for a time-invariant channel), we obtain

$$\begin{aligned}\phi'(f_e)\,\Delta f_e &= \mathrm{Im}\left\{\frac{\sum_{l=1}^{L}\Delta\beta_{k_l}}{\sum_{l=1}^{L}\beta_{k_l}}\right\}\\ &= \frac{\big(\sum_{l=1}^{L}\Delta\beta_{k_l}\big)\big(\sum_{l=1}^{L}\beta^*_{k_l}\big) - \big(\sum_{l=1}^{L}\Delta\beta^*_{k_l}\big)\big(\sum_{l=1}^{L}\beta_{k_l}\big)}{2\,j\,\big|\sum_{l=1}^{L}\beta_{k_l}\big|^2},\end{aligned}$$

where $\phi'(f_e)$ stands for the derivative of $\phi(f_e)$.

Since $\lim_{M\to\infty}\mathbb{E}\left[\Delta\beta_k\right] = 0$, the estimated f_e is asymptotically unbiased. By using the assumption that $\Delta c_{k_1}[\tau_1]$ and $\Delta c_{k_2}[\tau_2]$ are approximately uncorrelated for $k_1 \neq k_2$, and after some straightforward derivations, the MSE of Method 2 can be written as

$$\mathrm{MSE}_2 \simeq \frac{\sum_{l=1}^{L}\Big(\mathbf{p}^T\mathbf{\Gamma}_{k_l}\mathbf{p} - \mathrm{Re}\big\{e^{-j2\phi(f_e)}\,\mathbf{p}^T\widetilde{\mathbf{\Gamma}}_{k_l}\mathbf{p}\big\}\Big)}{2\,\left|\phi'(f_e)\right|^2\,\big|\sum_{l=1}^{L}\beta_{k_l}\big|^2}, \tag{5.32}$$

where $\mathbf{p} = \begin{bmatrix}p_t[1] & -1\end{bmatrix}^T$ and

$$\begin{aligned}\mathbf{\Gamma}_k &= \begin{bmatrix}\mathbb{E}\big[|\Delta c_k[0]|^2\big] & \mathbb{E}\big[\Delta c_k[0]\,\Delta c_k^*[1]\big]\\ \mathbb{E}\big[\Delta c_k[1]\,\Delta c_k^*[0]\big] & \mathbb{E}\big[|\Delta c_k[1]|^2\big]\end{bmatrix}\\ \widetilde{\mathbf{\Gamma}}_k &= \begin{bmatrix}\mathbb{E}\big[(\Delta c_k[0])^2\big] & \mathbb{E}\big[\Delta c_k[0]\,\Delta c_k[1]\big]\\ \mathbb{E}\big[\Delta c_k[1]\,\Delta c_k[0]\big] & \mathbb{E}\big[(\Delta c_k[1])^2\big]\end{bmatrix}.\end{aligned}$$

From (5.31) and (5.32), we see that the MSE is inversely proportional to the number of null-subchannels over an AWGN channel, and that we need to derive explicit calculable expressions for $\mathbb{E}\big[\Delta c_k[\tau_1]\,\Delta c_k^*[\tau_2]\big]$ and $\mathbb{E}\big[\Delta c_k[\tau_1]\,\Delta c_k[\tau_2]\big]$. It is shown in Appendix F that

$$\begin{aligned}\lim_{M\to\infty} M\,\mathbb{E}\big[\Delta c_k[\tau_1]\,\Delta c_k^*[\tau_2]\big] &= S_{d_k}(0,\tau_1,\tau_2)\\ \lim_{M\to\infty} M\,\mathbb{E}\big[\Delta c_k[\tau_1]\,\Delta c_k[\tau_2]\big] &= \widetilde{S}_{d_k}(0,\tau_1,\tau_2).\end{aligned} \tag{5.33}$$

where the detailed expressions for $S_{d_k}(0,\tau_1,\tau_2)$ and $\widetilde{S}_{d_k}(0,\tau_1,\tau_2)$ over a time-invariant channel and a Rayleigh fading channel are given by (F.3) and (F.4) in Appendix F respectively.

By comparing (F.3) and (F.4), we find that the MSE floor (obtained when $\sigma_\nu^2 \to 0$) for both Method 1 and 2 over a Rayleigh fading channel with $\sigma_{\mu_k}^2 = 1$ is about 2 times (3 dB) higher than that over an AWGN channel ($\mu_k = 1$). Based on the expressions given by (F.3) and (F.4), we can rewrite the asymptotic MSE for Method 1 and 2 as

$$\begin{aligned} \mathrm{MSE}_1 &\simeq \left[A_1(f_e) + B_1(f_e)/\mathrm{SNR} + C_1(f_e)/\mathrm{SNR}^2\right]/M \\ \mathrm{MSE}_2 &\simeq \left[A_2(f_e) + B_2(f_e)/\mathrm{SNR} + C_2(f_e)/\mathrm{SNR}^2\right]/M, \end{aligned} \tag{5.34}$$

where $\mathrm{SNR} \stackrel{\mathrm{def}}{=} \sigma_a^2/\sigma_\nu^2 = 1/\sigma_\nu^2$, and the quantities $A_1(f_e)$, $B_1(f_e)$, $C_1(f_e)$ and $A_2(f_e)$, $B_2(f_e)$, $C_2(f_e)$ are independent of SNR and data record length M.

We see that the MSE decreases as $O(M^{-1})$ for both Method 1 and 2. Even for the case of noise-free channel, a non-zero $A_1(f_e)$ and $A_2(f_e)$ will cause a certain MSE floor. For the case of AWGN channel, it can be proven that $A_1(0) = 0$, thus no MSE floor is present for Method 1 at $f_e = 0$. This will be verified by simulations.

5.3.2 Asymptotic analysis of conjugate correlation function based estimator

Now we will derive the asymptotic MSE for the conjugate correlation function based Method 3. From the definition of $y_k[s,\tau]$ in (5.24), we see that $\mathbb{E}\left[y_k[s,\tau]\right] = \tilde{c}_k[s,\tau]$. Thus we can write $y_k[s,\tau]$ as

$$y_k[s,\tau] = \tilde{c}_k[s,\tau] + e_k[s,\tau],$$

where $e_k[s,\tau]$ is error of the one sample estimation.

Since the transmitter filter $g[l]$ is of finite length, $e_k[s,\tau]$ satisfies the same kind of mixing condition as mentioned in the previous subsection. In [CLSG02], Ciblat et al. have shown how to apply this property to derive the asymptotic MSE. Using a similar reasoning, we find (see Appendix G) that $\hat{f}_e$ is an asymptotically unbiased estimation for f_e, and the asymptotic variance is given by

$$\mathrm{MSE}_3 = \frac{3}{2\,\pi^2\,M^3}\,\frac{\sum_{l=1}^{L} \mathrm{Re}\left\{\Psi_{k_l}(f_e) - \widetilde{\Psi}_{k_l}(f_e)\right\}}{\left(\sum_{l=1}^{L} \Phi_{k_l}(f_e)\right)^2}, \tag{5.35}$$

where

$$\begin{aligned} \Psi_k(f_e) &= \mathbf{r}_k^H(f_e)\,\mathbf{P}_k\,\mathbf{r}_k(f_e) \\ \widetilde{\Psi}_k(f_e) &= \mathbf{r}_k^H(f_e)\,\widetilde{\mathbf{P}}_k\,\mathbf{r}_k^*(f_e) \\ \Phi_k(f_e) &= \mathbf{r}_k^H(f_e)\,\mathbf{r}_k(f_e). \end{aligned} \tag{5.36}$$

Here $\mathbf{r}_k(f_e)$ is a vector given by $\mathbf{r}_k(f_e) = \left[r_k(0,f_e), r_k(1,f_e), \cdots, r_k(\tau_{\max},f_e)\right]^T$ and $\mathbf{P}_k$, $\widetilde{\mathbf{P}}_k$ are matrices with entries given by

$$\begin{aligned} \left[\mathbf{P}_k\right]_{\tau_1,\tau_2} &= S_{e_k}(f_e + 1/2, \tau_1, \tau_2) \\ \left[\widetilde{\mathbf{P}}_k\right]_{\tau_1,\tau_2} &= \widetilde{S}_{e_k}(f_e + 1/2, \tau_1, \tau_2) \end{aligned}$$

respectively.

Explicit expressions for $S_{e_k}(f_e+1/2,\tau_1,\tau_2)$ and $\widetilde{S}_{e_k}(f_e+1/2,\tau_1,\tau_2)$ are given by (H.1) and (H.2) in Appendix H. Based on these expressions, we can rewrite the theoretical MSE of Method 3 as

$$\mathrm{MSE}_3=\left[A_3(f_e)+B_3(f_e)/\mathrm{SNR}+C_3(f_e)/\mathrm{SNR}^2\right]/M^3, \tag{5.37}$$

where $A_3(f_e), B_3(f_e), C_3(f_e)$ are related to f_e but independent of SNR and data records length M.

We see that the theoretical MSE decreases as $O(M^{-3})$ for Method 3, thus it has a much lower MSE than that of Method 1 and 2 for large M. This improvement is obtained by greatly increasing the implementation complexity since a fine peak searching procedure is needed. The MSE floor is determined by $A_3(f_e)$. For AWGN channel, it can be verified that $A_3(0)=0$ based on (H.1) and (H.2), this implies that no MSE floor is present at $f_e=0$ for Method 3.

5.4 Simulation results

The following conditions apply to all simulations:

- The number of subchannels N is set to 16;
- 16OQAM modulation is used in all subchannels, and the input symbols are uniformly distributed;
- $g[l]$ and $p[l]$ are square root raised cosine pulses with a roll-off factor $\alpha=1.0$, giving $\tau_{\max}=2$ for Method 3 and 4;
- Each result is obtained by averaging over 1000 Monte Carlo trials.

For Method 1 and 2, we need only to estimate the correlation function based on the data record $\{b_k[s]\}_{s=0}^{M-1}$. For Method 3 and 4, a peak searching procedure is also needed after the estimating of the conjugate correlation function. In addition to an expected peak at $f_e+0.5$, the objective function $J_M(f)$ for these methods will have local maxima caused by noise. If the desired peak around $f_e+0.5$ is lower than other peak(s) caused by noise, *false detection* occurs. The peak is found in two steps: first a coarse search is made using FFT with four times oversampling accomplished by zero padding (simulations show that only marginal improvement is attained by using larger oversampling rate), then the simplex method is used to find the precise maximum point.

5.4.1 Comparison of null-subchannel based estimators over an AWGN channel

In the first three simulations, we compare the performance of different estimation methods based on null-subchannels with an AWGN channel. We find that the correlation function based Method 1 and 2 have much larger MSE than the conjugate correlation function based Method 3. Thus Method 1 and 2 can be used as coarse CFO estimators while Method 3 can be used as a fine CFO estimator.

Simulation 1: *performance comparison of Method 1-3 versus SNR over an AWGN channel*

In this simulation, we set the data record length $M = 256$, $f_e = 0.2$ and subchannel 4 is set as the only null-subchannel. The curves of MSE versus SNR are shown in Fig. 5.5. We see that for all estimation methods, the simulated results match well with the theoretical predictions, except for SNR below a certain threshold for Method 3. The threshold effect of Method 3 is caused by false peak detection in $J_M(f)$. We also note that for Method 3, the simulated results deviate from theoretical predictions for high SNR. This is due to the asymptotical approach of the theoretical analysis. It will be illustrated in Simulation 3 that both the threshold effect in low SNR region and the deviation in high SNR region of Method 3 disappear asymptotically with increasing M. We also note that as expected, the MSE of Method 3 is much lower than Method 1 and 2, except for the low SNR region. However, we should note that the implementation complexity of Method 3 is much higher than Method 1 and 2.

Simulation 2: *performance comparison of Method 1-3 versus f_e over an AWGN channel*

Now we study the performance of Method 1-3 versus f_e. We set $M = 256$, $\text{SNR} = 40$ dB, and subchannel 4 is set as the only null-subchannel. The simulation results are shown in Fig. 5.6. Since the acquisition range of Method 3 is $|f_e| < 0.5|$, it is simulated only in $f_e \in [0, 0.5)$. We see that for $f_e < 0.5$, the MSE of Method 3 is much lower than that of Method 1 and 2. Next we compare the two correlation function based methods. Since no MSE floor is present at $f_e = 0$ for Method 1, it has much smaller MSE than that of Method 2 for small values of f_e. This implies that Method 1 could be better than Method 2 if closed-loop estimation is used. For $f_e > 0.15$, Method 2 outperforms Method 1. We also note that the performance of Method 2 and 3 is largely independent of f_e. For Method 1, the simulated results deviate from theoretical predictions for $f_e > 0.6$. This is because the estimate becomes unreliable as $f_e \to 1$ for Method 1 due to the discontinuity of the function $\angle\cdot$. We will show in Simulation 3 that the threshold effect of Method 1 for large f_e, and the gap between

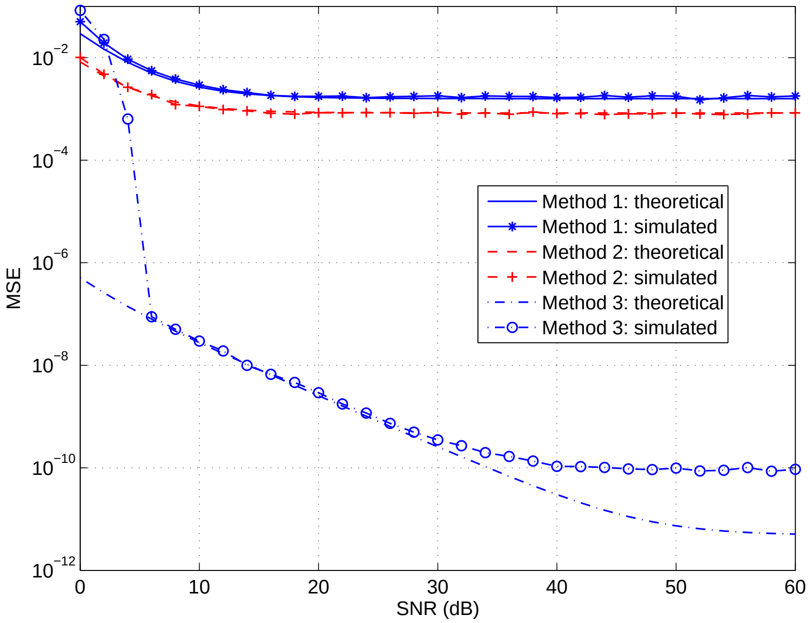

Figure 5.5: MSE versus SNR for Method 1-3 over an AWGN channel ($M = 256$, $f_e = 0.2$ and subchannel 4 is set as the only null-subchannel).

simulated results and theoretical predictions for Method 3 disappear with increasing the data record length M.

Simulation 3: *performance comparison of Method 1-3 versus data record length M over an AWGN channel*

In this simulation, we still set subchannel 4 as the only null-subchannel. For Method 1 and 2, SNR is fixed as 40 dB, and we simulate two cases of CFO: $f_e = 0.2$ and 0.8. For Method 3, CFO is fixed as $f_e = 0.2$, while we simulate two cases of SNR: 0 and 40 dB. The simulation results are shown in Fig. 5.7. We see that the MSE of Method 3 decreases faster than that of Method 1 and 2 with increasing data record length M. This is expected since the MSE of Method 1 and 2 decreases as $O(M^{-1})$ according to (5.34), while the MSE of Method 3 decreases as $O(M^{-3})$ according to (5.37). We also note that for $f_e = 0.8$ and SNR$= 40$ dB, the threshold effect of Method 1 disappears for $M > 2600$. For Method 3 with $f_e = 0.2$ and SNR$= 0$ dB, the threshold effect caused by false detection of peaks disappears for $M > 1800$. For Method 3 with $f_e = 0.2$ and SNR$= 40$ dB, the small gap between simulated results and theoretical predictions, which is due to the asymptotic approach of the theoretical analysis, disappears asymptotically with increasing M.

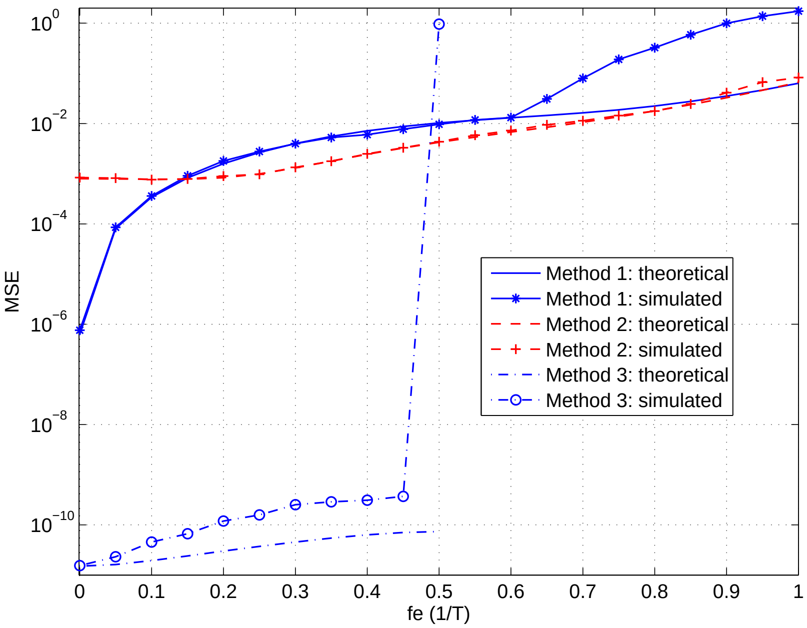

Figure 5.6: MSE versus f_e for Method 1-3 over an AWGN channel ($M = 256$, SNR$=$ 40 dB and subchannel 4 is set as the only null-subchannel).

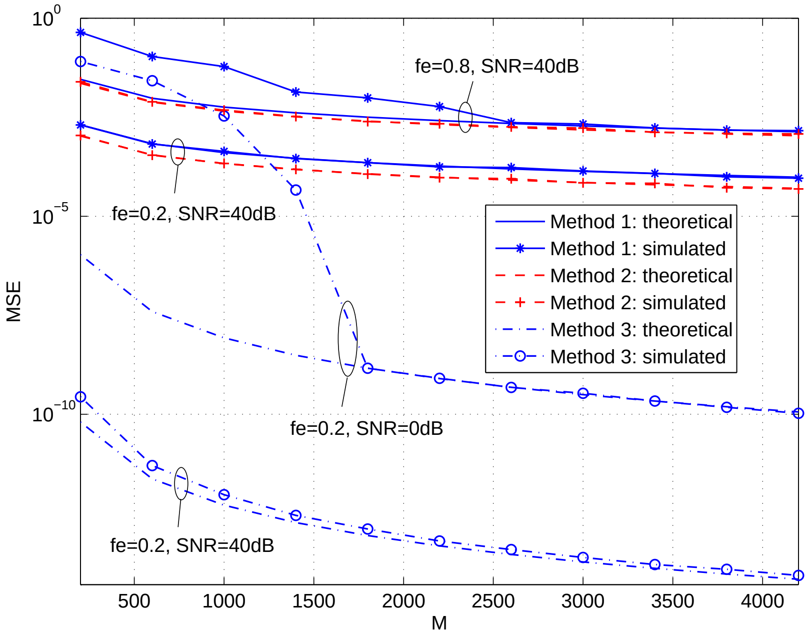

Figure 5.7: MSE versus data records length M for Method 1-3 over an AWGN channel with f_e and SNR as parameters (subchannel 4 is set as the only null-subchannel).

5.4.2 Comparison of null-subchannel based estimators over a time-invariant multipath channel (and comparison with the modified Bölcskei's estimator)

In this simulation, we will find that Method 1-3, which are based on subchannel signals, are robust to time-invariant multipath effects. The modified Bölcskei estimator, which is based on the signals before demodulation, is not robust in that respect.

The modified Bölcskei estimator, which is given in (5.23), is included to illustrate the benefit of estimation based on subchannel signals. Note that the modified Bölcskei estimator was derived assuming an AWGN channel. Its performance over a multipath channel will be studied by simulations.

Simulation 4: *performance comparison of Method 1-3 and modified Bölcskei estimator over a fixed time-invariant multipath channel*

In this comparison, we set $M = 256, f_e = 0.2$. First we consider a three-path time-invariant channel with impulse response

$$h[l] = \sum_{d=0}^{2} \lambda_d \, \delta[l-d], \tag{5.38}$$

where λ_d are the path attenuation factors.

We set subchannel 4 as the only null-subchannel and simulate over a fixed time-invariant channel with attenuation factors $\begin{bmatrix}\lambda_0 & \lambda_1 & \lambda_2\end{bmatrix} = \frac{1}{\sqrt{21}}\begin{bmatrix}4 & 2 & -1\end{bmatrix}$. The magnitude response of this channel is shown in Fig. 5.8.

To calculate the theoretical MSE of Method 1-3, the fading factor μ_k cross subchannel k is approximated as $\sum_{d=0}^{2} \lambda_d \, e^{-j\frac{2\pi}{N}kd}$. For the case of AWGN channel, only the simulated results are shown since the theoretical predictions have been illustrated in Fig. 5.5 in Simulation 1. The performance of the modified Bölcskei estimator is evaluated only by simulations. The simulation results are shown in Fig. 5.9. We see that the simulated curves match well with theoretical predictions for all of Method 1-3 over a fixed multipath channel, except for SNR below a certain threshold for Method 3. This verifies that the flat-fading approximation of each subchannel is reasonable, and the theoretical predictions given by (5.31), (5.32) and (5.35) are also valid for time-invariant multipath channel. We also note that the performance of Method 1-3 over the multipath channel is quite close to that over the AWGN channel. The performance over the multipath channel is even better than that over an AWGN for low SNR. This is because the magnitude response around subchannel 4 over the multipath channel is slightly higher 1 (see Fig. 5.8). For the modified Bölcskei estimator, the multipath effects will cause an obvious performance degradation.

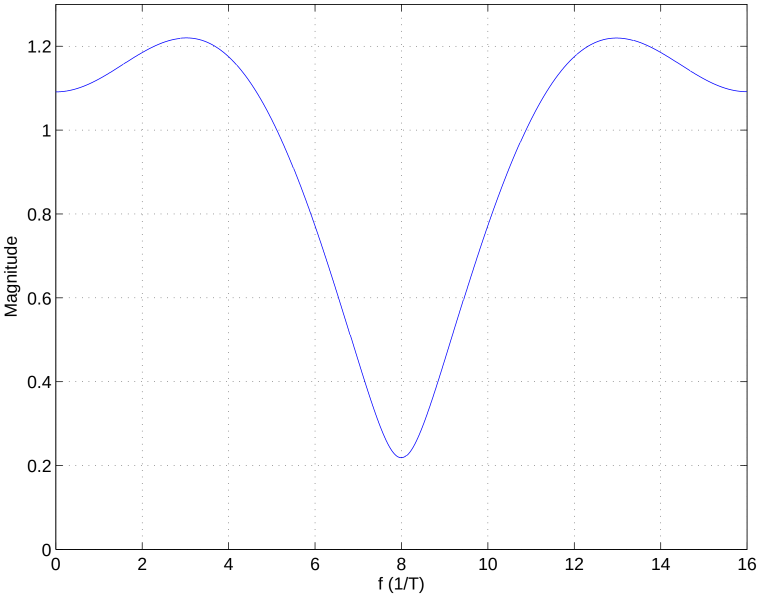

Figure 5.8: Magnitude response of a three-path multipath channel with attenuation factors $\begin{bmatrix}\lambda_0 & \lambda_1 & \lambda_2\end{bmatrix} = \frac{1}{\sqrt{21}}\begin{bmatrix}4 & 2 & -1\end{bmatrix}$.

Simulation 5: *performance comparison of Method 1-3 and modified Bölcskei estimator over a random time-invariant multipath channel*

Now we study the performance of CFO estimators over a random time-invariant multipath channel. We still use the three-path channel model (5.38), but we change the coefficients λ_d for each trial (the coefficients are unchanged during one trial). For the purpose of simulation, we set the path attenuation factors λ_d to be circular Gaussian and independently distributed, and with a variance 1/3 so that the average received power is identical to the AWGN case. To make the estimator work fine even when some subchannels suffer deep fading, multiple null-subchannels are used. In the simulation subchannels 1, 5, 9 and 13 are used for this purpose.

The simulation results are shown in Fig. 5.10. We see that for Method 1-3 over an AWGN channel, the simulated results match well with the theoretical predictions, except for SNR below a certain threshold for Method 3. This validates that disregarding dependency between different null-subchannels during the derivation of theoretic MSE is reasonable. We also see that the unknown random multipath effects will cause a slightly higher MSE for all estimators, and a higher SNR threshold for Method 3. We also note that the performance of the modified Bölcskei estimator is closer

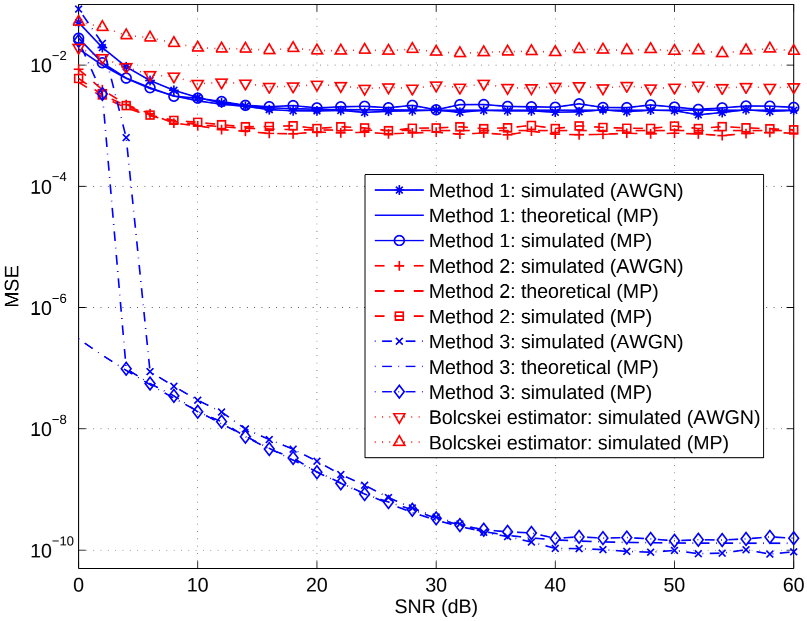

Figure 5.9: Performance comparison of Method 1-3 and modified Bölcskei estimator over a fixed multipath (MP) channel ($M = 256,\ f_e = 0.2$ and subchannel 4 is set as the only null-subchannel).

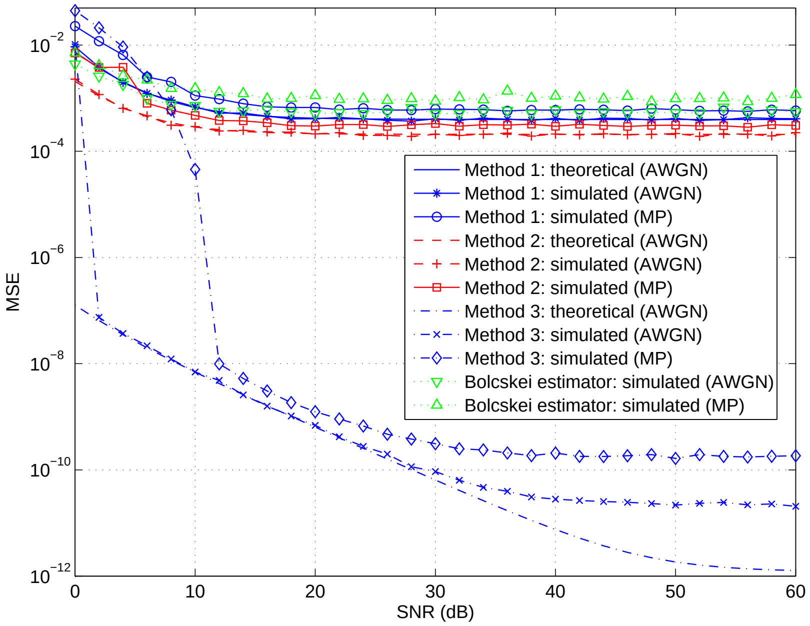

Figure 5.10: Performance comparison of Method 1-3 and modified Bölcskei estimator over a random time-invariant multipath (MP) channel ($M = 256$, $f_e = 0.2$ and subchannel 1, 5, 9 ,13 are set as null-subchannels).

to Method 1 and 2 for a system with four null-subchannels. This is expected. Null-subchannels will cause a non-flat spectrum of the received signal, which can be used for blind CFO estimation. The improved performance of CFO estimation based on subchannel signals are actually got by removing the flat section of the spectrum of received signal by receiver filters. This improvement will become not so obvious for larger number of null-subchannels since less flat section of spectrum is removed.

5.4.3 Comparison of null-subchannel based estimators over a Rayleigh multipath channel

In this simulation, we will find that the correlation function based Method 1 and 2 are robust to slow Rayleigh multipath fading. This is not the case for the conjugate correlation function based Method 3. The modified Bölcskei estimator is not included, since it is derived assuming a time-invariant channel.

Simulation 6: *performance comparison of Method 1-3 over a Rayleigh multipath channel*

We still use the channel model (5.38), but now the factors are time varying and denoted $\lambda_d[l]$. In the simulations, the factors $\lambda_d[l]$ are i.i.d. for different paths and modelled as autoregressive processes, which are generated by filtering a circular white Gaussian noise source by lowpass filters with a frequency response $H(f) = 1/(1-\rho\, e^{-j2\pi f})^5$ and a 3 dB bandwidth denoted $B_\lambda T$. The power of the driving noise source is set to let $\sum_{d=0}^{2} \sigma_{\lambda_d}^2 = 1$. The attenuation factors $\mu_k[l]$ are approximated as $\sum_{d=0}^{2} \lambda_d[l]\, e^{-j\frac{2\pi}{N}kd}$. Then it can be verified that $\sigma_{\mu_k}^2 = 1$.

Furthermore, we set $M = 256$, $f_e = 0.2$ and subchannel 4 as the only null-subchannel. The fading speed parameter is set as $B_\lambda T = 0.01$ (slow fading). We leave out the theoretical predictions over an AWGN channel since they have been shown in Fig. 5.5. For Method 3, we illustrate only the simulated results over a Rayleigh multipath channel since no theoretical predictions are available. The simulation results are shown in Fig. 5.11. We see that for Method 1 and 2, the simulated results match well with the theoretical predictions over a Rayleigh multipath channel, and that the Rayleigh multipath effects will cause approximately a 3 dB (2 times) higher MSE than that over an AWGN channel. Thus, the correlation based methods (1 and 2) seem fairly robust to time varying multipath effects. This can not be said about Method 3, which exhibits a significant performance degradation compared to the AWGN case.

5.4.4 Comparison of conjugate correlation function based estimators over an AWGN channel

Now we will show that for the case of interleaved weighting, the subchannel signals based Method 4 outperforms the modified Ciblat/Serpedin estimator based on the signal before demodulation.

Simulation 7: *performance comparison of Method 3, 4 and the modified Ciblat/Serpedin estimator over an AWGN channel*

In this simulation, we study the performance of conjugate correlation function based estimation methods. The modified Ciblat/Serpedin estimator [LHL06] is also included to show the benefit of estimation based on subchannel signals. Since interleaved weighting is less practical than the weighing method of null-subchannel insertion, we study only the AWGN channel case.

In the simulation, we set $M = 512$, $f_e = 0.2$. For the null-subchannels based Method 3, subchannel 4 is set as the only null-subchannel. For the interleaved weighting based Method 4 and modified C/S estimator, two weighting cases are simulated: $w_1 = \sqrt{3}/2$, $w_2 = \sqrt{5}/2$ and $w_1 = \sqrt{2}/2$, $w_2 = \sqrt{6}/2$. This corresponds to 1.25 and 3.0 dB attenuation of the weakest subchannels respectively. The simulation results are shown

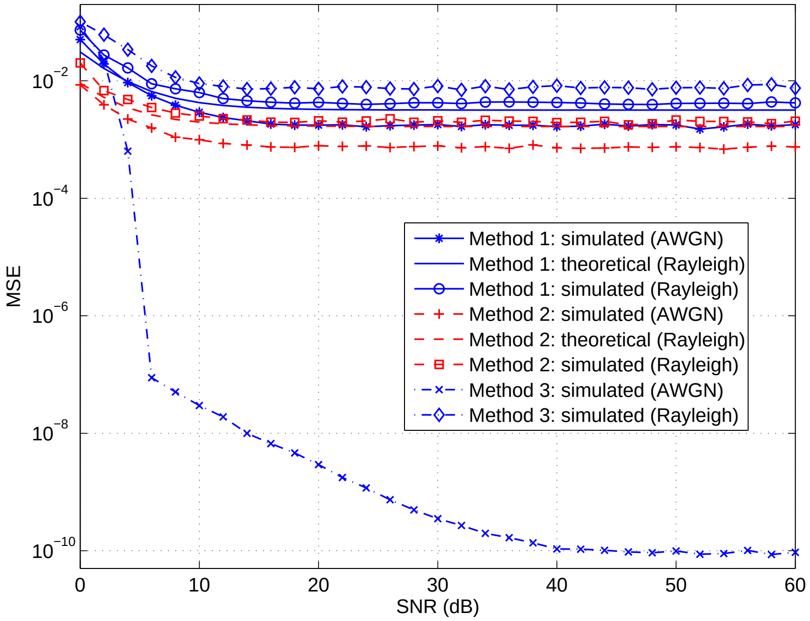

Figure 5.11: Performance comparison of Method 1-3 over a Rayleigh ($B_\lambda T = 0.01$) multipath channel ($M = 256$, $f_e = 0.2$ and subchannel 4 is set as the only null-subchannel).

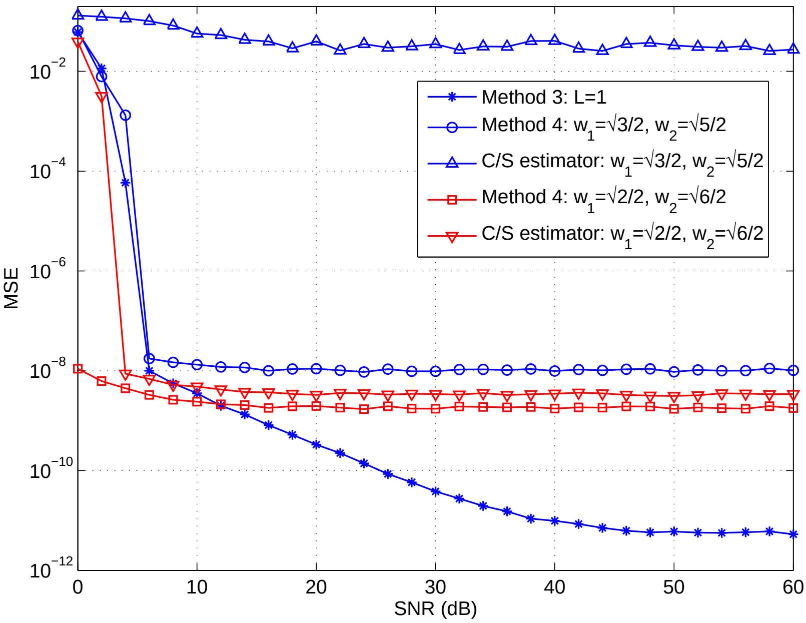

Figure 5.12: Performance comparison of Method 3, 4 and the modified C/S estimator over an AWGN channel ($M = 512$, $f_e = 0.2$ and subchannel 4 is set as the only null-subchannel for Method 3).

in Fig. 5.12. For the modified C/S estimator with $w_1 = \sqrt{3}/2$, $w_2 = \sqrt{5}/2$, the self-noise, which arises from the estimation of statistics based on a finite length data record, will cause a false detection ratio about 4%, resulting in a high MSE floor. For the case of $w_1 = \sqrt{3}/2$, $w_2 = \sqrt{5}/2$, both Method 4 and the modified C/S estimator can work properly, while Method 4 has lower SNR threshold and MSE floor than the modified C/S estimator. Thus better performance is achieved when the estimation is based on subchannel signals. We also note that Method 3 outperforms Method 4 and the modified C/S estimator for SNR$>$ 12 dB. This can be partly explained by noting that the loss caused by interleaved weighting decreases with increasing SNR, while the spectral loss caused by inserting L null-subchannels is fixed as L/N, which is essentially independent of SNR.

5.4.5 Performance simulation of high-order statistics based estimation method

Finally, we will simulate the fourth-order statistics based Method 5 for unweighted OFDM/OQAM systems. Simulation results show that such

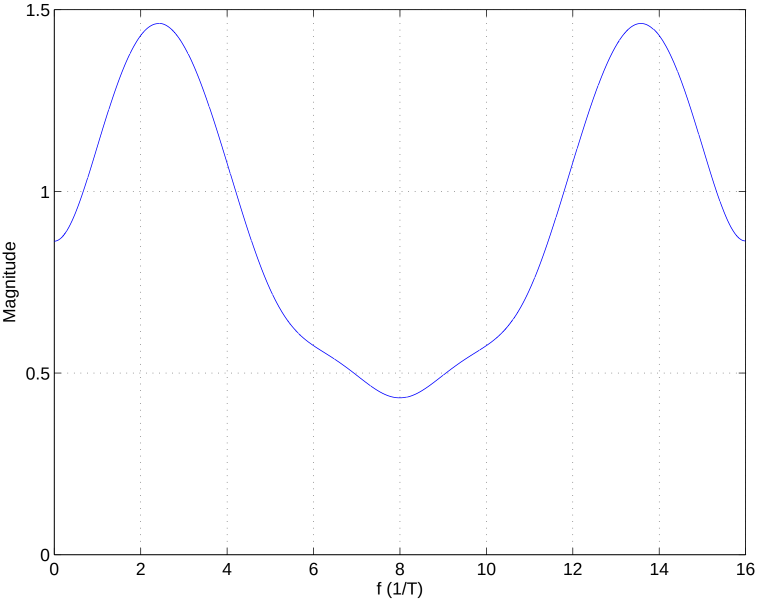

Figure 5.13: Magnitude response of a five-path multipath channel with attenuation factors $\begin{bmatrix}\lambda_0 & \lambda_1 & \lambda_2 & \lambda_3 & \lambda_4\end{bmatrix} = \begin{bmatrix}0.8627 & 0.4313 & -0.1078 & -0.2157 & -0.1078\end{bmatrix}$.

estimator is robust to time-invariant multipath effects.

Simulation 8: *performance of Method 5 over an AWGN and multipath channel*

In this simulation, we simulate the performance of the high-order statistics based Method 5. No subchannel weighting is used. Since more samples are needed to estimate high-order statistics, we set the number of OFDM symbols to $M = 1024$. The CFO is set as $f_e = 0.2$.

We simulate only the case of AWGN and static multipath channel. Here we consider a five paths channel with an impulse response $h[l] = \sum_{d=0}^{4} \lambda_d \, \delta[l-d]$, where the path attenuation factors $\begin{bmatrix}\lambda_0 & \lambda_1 & \lambda_2 & \lambda_3 & \lambda_4\end{bmatrix} = \begin{bmatrix}0.8627 & 0.4313 & -0.1078 & -0.2157 & -0.1078\end{bmatrix}$. The magnitude response of this channel is shown in Fig. 5.13.

The curves of MSE versus SNR are shown in Fig. 5.14. We see that as expected, the proposed estimator is largely robust to multipath effect. The multipath effect will cause a slightly higher threshold and floor mse. We also note that estimator (5.29) has similar performance to estimator (5.25) and (5.26). Since is do not need subchannel weighting, full spectral efficiency is achieved. We see that for SNR higher than a certain threshold, the MSE of estimator (5.29) is very low. This implies that estimator (5.29) can also be used as a fine CFO estimator.

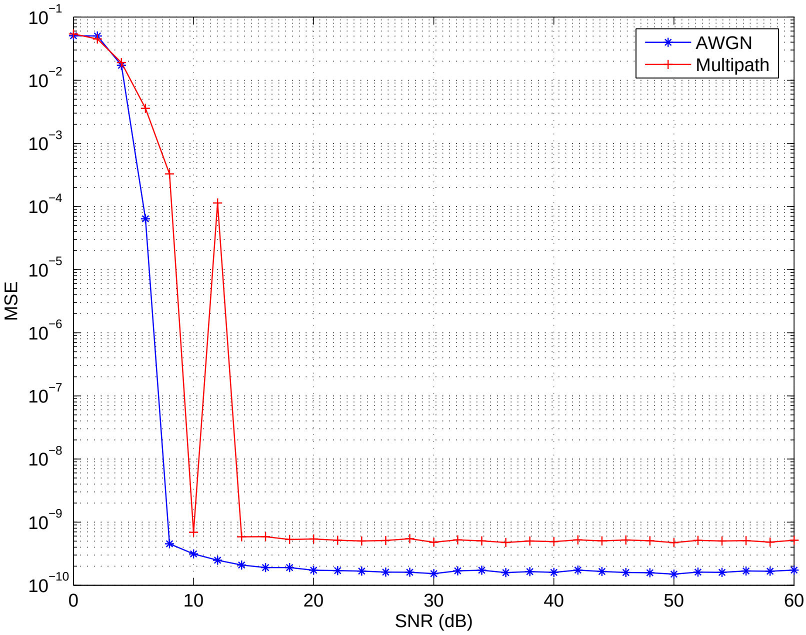

Figure 5.14: Comparison of MSE versus SNR of Method 5 over an AWGN and a time-invariant multipath channel ($M = 1024$, $f_e = 0.2$).

5.5 Conclusion

In this chapter, we have shown how to estimate CFO based on subchannel signals for OFDM/OQAM systems.

For second-order statistics based estimation methods, we show that non-uniform power distribution (weighting) is needed to retain the information about CFO. Two different weighting patterns are suggested. For the case of null-subchannels, we present two estimators based on the correlation function of the subchannel signals and one estimator based on the conjugate correlation function of the subchannel signals, which are all robust to time-invariant multipath effects. Asymptotic analysis, which matches well with simulation results, shows that the MSE of the correlation function based estimators decreases as $O(M^{-1})$ and that of the conjugate correlation function based estimator decreases as $O(M^{-3})$, where M is the length of data record. For slow Rayleigh multipath fading with the same signal power, only 3 dB MSE degradation is observed compared to that of AWGN case for the correlation function based methods, while the conjugate correlation function based method is not robust to time varying multipath effects. For the case of interleaved weighting, we present one estimator based on the conjugate correlation function of subchannel signals, which outperforms the previously suggested estimator based on the conjugate correlation function of the received signal before demodulation over an AWGN channel.

To achieve full power efficiency, we also suggest a blind CFO estimator for unweighted OFDM/OQAM systems based on the high-order statistics of subchannel signals. Simulation results show that this estimator can be used as a fine CFO estimator and is also robust to static multipath effects.

Finally, a summary of different blind CFO estimators are shown in Table 5.1.

Table 5.1: A summary of different blind CFO estimation methods for OFDM/OQAM systems.

	Implementation complexity	Estimation accuracy	Subchannel weighting needed?
Bölcskei estimator	Low	Coarse	Yes
Ciblat estimator	High	Precise	Yes
Method 1	Low	Coarse	Yes
Method 2	Low	Coarse	Yes
Method 3	High	Precise	Yes
Method 4	High	Precise	Yes
Method 5	High	Precise	No

Chapter 6

Conclusion

In this thesis, we have carried out an analysis and optimization of some important aspects of OFDM systems with main emphasis on systems with OQAM modulation and pulseshaping.

In Chapter 2, we have made a comparison between OFDM/QAM with guard interval and OFDM/OQAM with pulseshaping. It is shown that by not using a guard interval, OFDM/OQAM with pulseshaping can achieve higher spectrum and power efficiency. The disadvantage is slightly higher implementation complexity and longer transmission delay.

In Chapter 3, we have derived theoretical expressions that are useful for selecting appropriate equalizer length for OFDM/OQAM systems. By using these expressions, we find that an equalizer with few taps (typically $3-7$ taps) in each subchannel is enough to counteract the multipath effects. This allows an efficient equalization with a complexity only slightly higher than that of conventional OFDM/QAM systems with guard interval.

In Chapter 4, we have found optimal pulses with robustness to CFO for both OFDM/QAM and OFDM/OQAM systems. Our results show that the robustness to CFO can be improved by using these optimal pulses. We have found that OFDM/OQAM with pulseshaping is more robust to CFO than OFDM/QAM with rectangular pulseshapes.

In Chapter 5, we have developed five blind CFO estimation methods for OFDM/OQAM systems based on the subchannel signals. Numerical simulations are performed to illustrate the performance of the suggested CFO estimation methods and validate the theoretical analysis.

6.1 Contributions of the thesis

The main original contributions of this thesis are listed as follows:

- Explicit analytical expressions of MMSE versus equalizer length have been derived for OFDM/OQAM systems;
- Optimal pulses with minimum interference power at a given CFO point have been found for both OFDM/QAM and OFDM/OQAM systems;
- Blind methods for CFO estimation based on subchannel signals have been developed for OFDM/OQAM systems.

6.2 Future work

In this thesis, we present only a simple comparison between OFDM/QAM with guard interval and OFDM/OQAM with pulseshaping. A more quantitative comparison of these two OFDM schemes is surely of interest, and one of the most relevant comparisons would be to perform a detailed and optimized design of both systems for one or more practical applications. A quantitative comparison would be most straightforward for a time-invariant case, and a potential application would be the WiMAX (IEEE 802.16) systems [Std04] used for fixed radio access. One relevant criterion of comparison would be the bandwidth efficiency, assuming that all other parameters like channel SNR (CSNR), available bandwidth, delay spread etc are same for both systems. However, complexity and latency should also be considered.

Channel estimation in OFDM systems is usually accomplished using training or pilot symbols. This will result in a reduction of spectral efficiency. A subspace-based algorithm for the blind estimation of time-dispersive channels for OFDM/OQAM systems is presented by Bolcskei [Bol01]. Bolcskei's algorithm is based on the received channel signal. For an OFDM system with many subchannels, each subchannel can be approximated as flat-fading. This motivates us to estimate channel based on subchannel signals. Furthermore, for a multipath channel with L paths, the path attenuation factors can be uniquely determined by L points of frequency response of the channel. Usually L is much smaller than the number of subchannels, thus we can use only few subchannels for channel estimation. This implies that lower implementation complexity can be achieved since the data rate of subchannels is much lower than that of received signal before demodulation.

In chapter 5, we develop blind CFO estimation methods based on the conjugate correlation function of subchannel signals. In such methods, a coarse peak search based on FFT is needed. When the amplitude of peak(s) caused by noise is higher than the expected peak, false detection occurs and leads to high estimation error. The false detection ratio decreases quickly for SNR higher than a certain threshold. In chapter 5, we have only performed a theoretical analysis by assuming perfect coarse peak search. To design a reliable CFO estimation method, such threshold effects caused by false peak detection should be analyzed. Some earlier theoretical analysis about such kind of threshold effects has been reported [RB74, CG06]. However, these earlier results deal only with some special cases. To the best of our knowledge, a general analysis has not been presented in the literature.

We have only considered the case of time-invariant channels. For a double-dispersive radio channel, both the time-dispersion and Doppler frequency spreading will destroy the orthogonality in OFDM systems, and then cause a certain amount of ISI and ICI. An OFDM system with a large number of subchannels is less sensitive to time-dispersion, but very sensitive to Doppler spreading. On the contrary, an OFDM system with only a few subchannels is less sensitive to Doppler spreading, whereas it is very sensitive to time-dispersion. Some earlier results about the robustness to double-dispersive effects for have been reported for OFDM/OQAM systems [ATP05]. We would like to analyze the interference power versus the number of subchannel over a double-dispersive channel, which is useful for selecting the optimal number of subchannels. We also would like to search for optimal pulseshapes that are robust to double-dispersive channel for OFDM/OQAM systems.

Appendix A

Derivation of expressions for $c_{u_r}[\tau]$ and $c_{u_{ri}}[\tau]$

First based on (3.2), we can write the equivalent overall frequency response from subchannel m to subchannel k as

$$P^{(o)}_{m,k}(f) = j^{(m-k)}\, G_0(f-m+k)\, G_0(f)\, H_k(f), \tag{A.1}$$

where $G_0(f) \overset{\text{def}}{=} \sum_{l=-\infty}^{\infty} g[l]\, e^{-j\frac{2\pi}{N}fl}$ is the frequency response of shaping filter $g[l]$, and $H_k(f) \overset{\text{def}}{=} \sum_{l=-\infty}^{\infty} h[l]\, e^{-j\frac{2\pi}{N}(f+k)l}$ is the equivalent frequency response of subchannel k. Note that f is normalized with respect to $1/T$.

Since $G_0(f)$ is bandlimited to $[-1,1]$, so is $P^{(o)}_{m,k}(f)$ based on (A.1). Therefore $P_{m,k}(f)$ has the same shape as $P^{(o)}_{m,k}(f)$ in the interval $[-1,1]$. Now we will express $p^{\mathcal{R}}_{m,k}[s]$ and $p^{\mathcal{I}}_{m,k}[s]$ in frequency domain. Since $p^{\mathcal{R}}_{m,k}[s] = \big(p_{m,k}[s] + p^*_{m,k}[s]\big)/2$ and $p^{\mathcal{I}}_{m,k}[s] = \big(p_{m,k}[s] - p^*_{m,k}[s]\big)/(2j)$, we have

$$\begin{aligned} P^{\mathcal{R}}_{m,k}(f) &\overset{\text{def}}{=} \sum_{s=-\infty}^{\infty} p^{\mathcal{R}}_{m,k}[s]\, e^{-j\pi fs} = \frac{P_{m,k}(f) + P^*_{m,k}(-f)}{2} \\ P^{\mathcal{I}}_{m,k}(f) &\overset{\text{def}}{=} \sum_{s=-\infty}^{\infty} p^{\mathcal{I}}_{m,k}[s]\, e^{-j\pi fs} = \frac{P_{m,k}(f) - P^*_{m,k}(-f)}{2j}. \end{aligned} \tag{A.2}$$

Then we can use the decimator formula (4.1.13) in [Vai93] to get

$$\begin{aligned} P1^{\mathcal{R}}_{m,k}(f) &\overset{\text{def}}{=} \sum_{n=-\infty}^{\infty} p^{\mathcal{R}}_{m,k}[2n]\, e^{-j2\pi fn} = \frac{1}{2}\big[P^{\mathcal{R}}_{m,k}(f) + P^{\mathcal{R}}_{m,k}(f-1)\big] \\ &= \frac{1}{4}\left[P_{m,k}(f) + P^*_{m,k}(-f) + P_{m,k}(f-1) + P^*_{m,k}(1-f)\right]. \end{aligned} \tag{A.3}$$

Note here f is normalized with respect to $1/T$ while the frequency ω in [Vai93] is normalized with respect to the sampling radius frequency.

We can view $p^{\mathcal{R}}_{m,k}[2n-1]$ as the 2 times decimated version of $p^{\mathcal{R}}_{m,k}[s-1]$, while $\sum_{s=-\infty}^{\infty} p^{\mathcal{R}}_{m,k}[s-1]\, e^{-j\pi f s} = e^{-j\pi f}\, P^{\mathcal{R}}_{m,k}(f)$, then we have

$$\begin{aligned}
P2^{\mathcal{R}}_{m,k}(f) &\overset{\text{def}}{=} \sum_{n=-\infty}^{\infty} p^{\mathcal{R}}_{m,k}[2n-1]\, e^{-j2\pi f n} = \frac{e^{-j\pi f}}{2}\left[P^{\mathcal{R}}_{m,k}(f) - P^{\mathcal{R}}_{m,k}(f-1)\right] \\
&= \frac{e^{-j\pi f}}{4}\left[P_{m,k}(f) + P^*_{m,k}(-f) - P_{m,k}(f-1) - P^*_{m,k}(1-f)\right].
\end{aligned} \tag{A.4}$$

Similarly, we have

$$\begin{aligned}
P1^{\mathcal{I}}_{m,k}(f) &\overset{\text{def}}{=} \sum_{n=-\infty}^{\infty} p^{\mathcal{I}}_{m,k}[2n]\, e^{-j2\pi f n} \\
&= \frac{1}{4j}\left[P_{m,k}(f) - P^*_{m,k}(-f) + P_{m,k}(f-1) - P^*_{m,k}(1-f)\right] \\
P2^{\mathcal{I}}_{m,k}(f) &\overset{\text{def}}{=} \sum_{n=-\infty}^{\infty} p^{\mathcal{I}}_{m,k}[2n-1]\, e^{-j2\pi f n} \\
&= \frac{e^{-j\pi f}}{4j}\left[P_{m,k}(f) - P^*_{m,k}(-f) - P_{m,k}(f-1) + P^*_{m,k}(1-f)\right].
\end{aligned} \tag{A.5}$$

Now we are ready to calculate $c_{u_r}[s,\tau]$ and $c_{u_{ri}}[s,\tau]$. Since they are periodic in s with a period 2, we only need to calculate $c_{u_r}[0,\tau]$, $c_{u_r}[1,\tau]$, $c_{u_{ri}}[0,\tau]$, and $c_{u_{ri}}[1,\tau]$. First we consider $c_{u_r}[0,\tau]$. For $\tau = 2\,q$ (i.e. τ is even), we can write the summation in the expression of $c_{u_r}[s,\tau]$ in (3.11) as

$$\begin{aligned}
&\sum_{n=-\infty}^{\infty} \left(p^{\mathcal{R}}_{m,k}[2n]\, p^{\mathcal{R}}_{m,k}[2n-\tau] + p^{\mathcal{I}}_{m,k}[2n-1]\, p^{\mathcal{I}}_{m,k}[2n-\tau-1]\right) \\
&= \sum_{n=-\infty}^{\infty} \left(p^{\mathcal{R}}_{m,k}[2n]\, p^{\mathcal{R}}_{m,k}[2n-2q] + p^{\mathcal{I}}_{m,k}[2n-1]\, p^{\mathcal{I}}_{m,k}[2n-2q-1]\right) \\
&\overset{(a)}{=} \int_{-0.5}^{0.5} \left(P1^{\mathcal{R}}_{m,k}(f)\, P1^{\mathcal{R}}_{m,k}(-f) + P2^{\mathcal{I}}_{m,k}(f)\, P2^{\mathcal{I}}_{m,k}(-f)\right) e^{j2\pi f q}\, df \\
&= \frac{1}{4}\int_{-0.5}^{0.5} \Big(\left|P_{m,k}(f)\right|^2 + \left|P_{m,k}(f-1)\right|^2 \\
&\quad + 2\,\mathrm{Re}\left\{P_{m,k}(f) P_{m,k}(1-f)\right\}\Big) \cos(\pi f \tau)\, df,
\end{aligned} \tag{A.6}$$

where the step (a) follows from the Parseval's relation.

Similarly for τ odd, we have

$$\begin{aligned}
&\sum_{n=-\infty}^{\infty} \left(p^{\mathcal{R}}_{m,k}[2n]\, p^{\mathcal{R}}_{m,k}[2n-\tau] + p^{\mathcal{I}}_{m,k}[2n-1]\, p^{\mathcal{I}}_{m,k}[2n-\tau-1]\right) \\
&= \frac{1}{4}\int_{-0.5}^{0.5} \Big[\left(\left|P_{m,k}(f)\right|^2 - \left|P_{m,k}(f-1)\right|^2\right)\cos(\pi f\tau) \\
&\quad + 2\,\mathrm{Im}\left\{P_{m,k}(f)P_{m,k}(1-f)\right\}\sin(\pi f\tau)\Big]\, df. \qquad \text{(A.7)}
\end{aligned}$$

Then we consider $c_{u_r}[1,\tau]$. For τ even, we can write the summation in the expression of $c_{u_r}[s,\tau]$ in (3.11) as

$$\begin{aligned}
&\sum_{n=-\infty}^{\infty} \left(p^{\mathcal{R}}_{m,k}[2n-1]\, p^{\mathcal{R}}_{m,k}[2n-\tau-1] + p^{\mathcal{I}}_{m,k}[2n]\, p^{\mathcal{I}}_{m,k}[2n-\tau]\right) \\
&= \frac{1}{4}\int_{-0.5}^{0.5} \Big(\left|P_{m,k}(f)\right|^2 + \left|P_{m,k}(f-1)\right|^2 \\
&\quad - 2\,\mathrm{Re}\left\{P_{m,k}(f)P_{m,k}(1-f)\right\}\Big)\cos(\pi f\tau)\, df. \qquad \text{(A.8)}
\end{aligned}$$

For τ odd, we have

$$\begin{aligned}
&\sum_{n=-\infty}^{\infty} \left(p^{\mathcal{R}}_{m,k}[2n-1]\, p^{\mathcal{R}}_{m,k}[2n-\tau-1] + p^{\mathcal{I}}_{m,k}[2n]\, p^{\mathcal{I}}_{m,k}[2n-\tau]\right) \\
&= \frac{1}{4}\int_{-0.5}^{0.5} \Big[\left(\left|P_{m,k}(f)\right|^2 - \left|P_{m,k}(f-1)\right|^2\right)\cos(\pi f\tau) \\
&\quad - 2\,\mathrm{Im}\left\{P_{m,k}(f)P_{m,k}(1-f)\right\}\sin(\pi f\tau)\Big]\, df. \qquad \text{(A.9)}
\end{aligned}$$

By combining (A.6), (A.7), (A.8), and (A.9), then substituting the results into (3.11), we obtain

$$c_{u_r}[s,\tau] = \frac{1}{8}\sum_{m=k-1}^{k+1} S1_{m,k}[s,\tau] + \frac{\sigma_\nu^2}{2} p_t[\frac{N}{2}\tau], \qquad \text{(A.10)}$$

where

$$S1_{m,k}[s,\tau] = \begin{cases} \int_{-0.5}^{0.5} \Big(\left|P_{m,k}(f)\right|^2 + \left|P_{m,k}(f-1)\right|^2 \\ +2\,(-1)^s\,\mathrm{Re}\left\{P_{m,k}(f)P_{m,k}(1-f)\right\}\Big)\cos(\pi f\tau)\, df, & \text{for } \tau \text{ even} \\ \\ \int_{-0.5}^{0.5} \Big[\left(\left|P_{m,k}(f)\right|^2 - \left|P_{m,k}(f-1)\right|^2\right)\cos(\pi f\tau) \\ +2\,(-1)^s\,\mathrm{Im}\left\{P_{m,k}(f)P_{m,k}(1-f)\right\}\sin(\pi f\tau)\Big]\, df, & \text{for } \tau \text{ odd.} \end{cases}$$

Through similar argument, we have

$$c_{u_{ri}}[s,\tau] = \frac{1}{8}\sum_{m=k-1}^{k+1} S2_{m,k}[s,\tau], \tag{A.11}$$

where

$$S2_{m,k}[s,\tau] = \begin{cases} \int_{-0.5}^{0.5}\Big[\Big(\big|P_{m,k}(-f)\big|^2 + \big|P_{m,k}(1-f)\big|^2\Big)\sin(\pi f\tau) \\ +2\,(-1)^s\,\mathrm{Im}\left\{P_{m,k}(f)P_{m,k}(1-f)\right\}\cos(\pi f\tau)\Big]\,df, \text{ for } \tau \text{ even} \\ \\ \int_{-0.5}^{0.5}\Big(\big|P_{m,k}(-f)\big|^2 + \big|P_{m,k}(f-1)\big|^2 \\ +2\,(-1)^s\,\mathrm{Re}\left\{P_{m,k}(-f)P_{m,k}(f-1)\right\}\Big)\sin(\pi f\tau)\,df, \text{ for } \tau \text{ odd.} \end{cases}$$

Formula (A.10) and (A.11) can be further simplified. Based on (A.1), we get

$$\begin{aligned} P_{k+1,k}(f) &= \begin{cases} j\,G(f-1)\,G(f)\,H_k(f), \text{ for } f\in[0,1] \\ 0, \text{ otherwise} \end{cases} \\ P_{k-1,k}(f) &= \begin{cases} -j\,G(f+1)\,G(f)\,H_k(f), \text{ for } f\in[-1,0] \\ 0, \text{ otherwise} \end{cases} \\ P_{k,k}(f) &= G^2(f)\,H_k(f), \text{ for } f\in[-1,1], \end{aligned}$$

where $G(f)$ is the $N/2$ times down-sampling version of $G_0(f)$, thus it has the same shape as $G_0(f)$ in $[-1,1]$, while its period with respect to f is 2.

Based on the facts that $G(f)$ and $P_{m,k}(f)$ are periodic in f with a period 2, it can be verified that $\sum_{m=k-1}^{k+1} P_{m,k}(f)\,P_{m,k}(1-f) \equiv 0$ for any $H_k(f)$. At last by substituting this result into (A.10) and (A.11), we can then get (3.13) after some manipulations.

Appendix B

Derivation of approximate formula for MMSE versus K

First by substituting (3.34) into (3.16) and (3.17) respectively, we have

$$p\,[\tau] \simeq 2\,(-1)^{\tau}\,\alpha\,\tau_{\mathrm{n}}\,e^{-j\varphi_k}/\tau^3, \;\text{ for } |\tau| \geq 2, \tag{B.1}$$

and

$$r[\tau] \simeq \begin{cases} \big(1+\alpha^2+2\,\alpha\,\cos(\varphi_k)\big)+\sigma_\nu^2, \;\text{ for } \tau=0 \\ \big(1+\alpha^2+2\,\alpha\,\cos(\varphi_k)+6\,j\,\alpha\,\tau_{\mathrm{n}}\,\sin(\varphi_k)+\sigma_\nu^2\big)/2, \;\text{ for } \tau=1 \\ 4\,j\,(-1)^{\tau}\,\alpha\,\tau_{\mathrm{n}}\,\sin\left(\varphi_k\right)/\tau^3, \;\text{ for } |\tau|\geq 2. \end{cases} \tag{B.2}$$

Note that τ_{n} represents the normalized delay spread of a two-path channel and has completely different physical meaning from τ. By substituting (B.1) into the expression of J_1 in (3.33), we get

$$J_1 = \mathrm{Re}\left\{2\,\alpha\,\tau_{\mathrm{n}}\,e^{j\varphi_k}\sum_{|m|=K+1}^{\infty}\frac{(-1)^m}{m^3}\,I[m]\right\}, \tag{B.3}$$

where

$$I[m] = \int_{-1}^{1} T_k(f)\,e^{j\pi f m}\,df. \tag{B.4}$$

We can't get closed-form expression for $I[m]$ even for a simple two-path channel response $H_k(f) = 1+\alpha\,e^{-j(2\pi\tau_{\mathrm{n}}f+\varphi_k)}$. While for small value of τ_{n}, the variation of $H_k(f)$ in $[-1,1]$ is also small. This inspires us to use polynomial approximation. By using the first order Taylor expanding, we can approximate $T_k(f)$ as

$$T_k(f) \simeq c_0 + c_1\,f, \tag{B.5}$$

where

$$\begin{aligned} c_0 &= \frac{1+\alpha\, e^{-j\varphi_k}}{1+2\,\alpha\,\cos(\varphi_k)+\alpha^2+\sigma_\nu^2} \\ c_1 &= \frac{2\,\pi\,\alpha\,\tau_{\mathrm{n}}\, e^{-j(\varphi_k+\pi/2)}}{\left(1+2\,\alpha\,\cos(\varphi_k)+\alpha^2+\sigma_\nu^2\right)^2} \\ &\quad \times \left[\cos(2\,\varphi_k)+\alpha^2+2\,\alpha\,\cos(\varphi_k)+\sigma_\nu^2+j\left(\sin(2\,\varphi_k)+2\,\alpha\,\sin(\varphi_k)\right)\right]. \end{aligned} \tag{B.6}$$

Then $I[m]$ can be approximated as

$$I[m] \simeq \begin{cases} 2\,c_0, \text{ for } m=0 \\ -\frac{2\,j\,c_1\,(-1)^m}{m\,\pi}, \text{ for } m \neq 0. \end{cases} \tag{B.7}$$

By substituting (B.7) into (B.3), we get

$$\begin{aligned} J_1 &\simeq \frac{8\,\alpha\,\tau_{\mathrm{n}}\,\mathrm{Re}\left\{c_1\, e^{j(\varphi_k-\pi/2)}\right\}}{\pi} \left(\sum_{m=K+1}^{\infty} \frac{1}{m^4}\right) \\ &\simeq \frac{8\,\alpha\,\tau_{\mathrm{n}}\,\mathrm{Re}\left\{c_1\, e^{j(\varphi_k-\pi/2)}\right\}}{3\,\pi\,(K+0.57)^3}, \end{aligned} \tag{B.8}$$

where the last step follows from the series sum approximation formula (C.1) shown in Appendix C.

Now we will try to get the expression for J_2. By substituting (B.2), (B.5) and (B.7) into the expression of J_2 shown in (3.33), through some tedious but similar manipulation, we get

$$\begin{aligned} J_2 \simeq\; & \frac{\left[1+\alpha^2+2\,\alpha\,\cos(\varphi_k)+\sigma_\nu^2\right]\,|c_1|^2}{\pi^2\,K\,(K+1)} \\ & -\frac{4\,\alpha\,\tau_{\mathrm{n}}\,\mathrm{Re}\left\{2\,c_0\,c_1^*\,\sin(\varphi_k)+c_1\, e^{j(\varphi_k+\pi/2)}\right\}}{3\,\pi\,(K+0.57)^3}. \end{aligned} \tag{B.9}$$

At last by substituting (B.6) into (B.8) and (B.9) then into (3.32) and omitting the third order smallness term, we get

$$J_{\min}(K) \simeq J_{\min}(\infty) + \frac{B}{K\,(K+1)},\ K \geq 1, \tag{B.10}$$

where

$$B = \frac{4\,\alpha^2\,\tau_{\mathrm{n}}^2\left[\left(1+\alpha^2+2\,\alpha\,\cos(\varphi_k)+\sigma_\nu^2\right)^2 - 4\,\sin^2(\varphi_k)\,\sigma_\nu^2\right]}{\left(1+\alpha^2+2\,\alpha\,\cos(\varphi_k)+\sigma_\nu^2\right)^3}. \tag{B.11}$$

By comparing with the coefficients got by least square (LS) method, we find that B is about π times larger than the coefficients got by LS method. The reason is that the omitting of term $\int_{-1}^{1} \Delta R_K(f, f') \, \Delta W_K(f') \, df'$ in (3.30) will cause an error of $O(1/K^2)$. By dividing B by π and replacing σ_ν^2 by SNR^{-1}, we can then get (3.38).

Appendix C

Series sum approximation

It is shown in [Col92] that for an integrable, positive and monotonously decreasing function f on $[1, \infty]$, if $f''(x)$ is positive, then

$$\int_{K+1}^{\infty} f(x)\,dx \le \sum_{m=K+1}^{\infty} f(m) \le \int_{K}^{\infty} f(x)\,dx,$$

which implies that

$$\sum_{m=K+1}^{\infty} f(m) = \int_{K+\xi}^{\infty} f(x)\,dx,$$

where $0 \le \xi \le 1$.

We find that for $f(m) = \frac{1}{m^p}$, good approximation can be got by choosing $\xi = 0.57$ for $p > 1$. Hence we have

$$\sum_{m=K+1}^{\infty} \frac{1}{m^p} \simeq \frac{1}{(p-1)\,(K+0.57)^{p-1}}. \tag{C.1}$$

Appendix D

Proof of $\sum_{m=0}^{N-1} A_{m,k}(\tau, f_e)$ to be real-valued and independent of f_e

Proof: From the definition of $p_{m,k}[l]$ shown in (5.4) and the relationship of $p_{m,k}[s] = p^{(o)}_{m,k}[s\frac{N}{2}]$, we can write the frequency domain response $P_{m,k}(f)$ defined in (5.8) as

$$P_{m,k}(f) = G(f-(m-k))\, G(f+f_e)\, e^{j\frac{\pi}{2}(m-k)} \quad \text{for } -1 \le f \le 1, \tag{D.1}$$

where $G(f) = \sqrt{2/N}\,\sum_{l=-\infty}^{\infty} g[l]\, e^{-j\frac{2\pi}{N}fl}$.

Then by substituting (D.1) into (5.7), and using the fact that $P_{m,k}(f)$ is periodic in f with a period 2, we have

$$\begin{aligned}
\sum_{m=0}^{N-1} A_{m,k}(\tau, f_e) &= \frac{1}{2}\int_{-1}^{1}\Big(\sum_{m=0}^{N-1} |P_{m,k}(f-f_e)|^2\Big) e^{j\pi f\tau}\, df \\
&= \frac{1}{2}\int_{-1}^{1}\Big(\sum_{m=0}^{N-1} G^2(f-(m-k)-f_e)\Big) G^2(f)\, e^{j\pi f\tau}\, df \\
&\overset{(a)}{=} \int_{-1}^{1} G^2(f)\, e^{j\pi f\tau}\, df = \int_{-1}^{1} G^2(f)\, \cos(\pi f\tau)\, df,
\end{aligned} \tag{D.2}$$

where (a) follows from the fact that $\sum_{m=0}^{N-1} G^2(f-(m-k)) \equiv 2$ since $G^2(f)$ is a Nyquist pulse.

Then we can conclude that $\sum_{m=0}^{N-1} A_{m,k}(\tau, f_e)$ is real-valued and to be independent of f_e. ■

Appendix E

Proof of $\sum_{m=0}^{N-1} \widetilde{A}_{m,k}(\tau, f_e) = 0$

Proof: By recalling the definition of $P_{m,k}(f)$ in (5.8) and using the decimator formula (see formula 4.1.13 in [Vai93]), we have

$$
\begin{aligned}
P1_{m,k}(f) &\overset{\text{def}}{=} \sum_{n=-\infty}^{\infty} p_{m,k}[2n]\, e^{-j2\pi nf} = \frac{1}{2}\big[P_{m,k}(f) + P_{m,k}(f-1)\big] \\
P2_{m,k}(f) &\overset{\text{def}}{=} \sum_{n=-\infty}^{\infty} p_{m,k}[2n+1]\, e^{-j2\pi nf} = \frac{1}{2}\, e^{j\pi f}\big[P_{m,k}(f) - P_{m,k}(f-1)\big].
\end{aligned}
\tag{E.1}
$$

Then by using (E.1) and Parseval's relation, we can rewrite (5.11) in frequency domain as

$$
\begin{aligned}
\widetilde{A}_{m,k}(\tau, f_e) &= \frac{1}{2}\int_{-0.5}^{0.5} \Big[P_{m,k}(f)\, P_{m,k}(1-f)\, e^{j\pi f\tau} \\
&\quad + P_{m,k}(-f)\, P_{m,k}(f-1)\, e^{j\pi(f+1)\tau}\Big]\, df \\
&= \frac{1}{2}\int_{-1}^{1} T_{m,k}(f)\, e^{j\pi f\tau}\, df,
\end{aligned}
\tag{E.2}
$$

where $T_{m,k}(f) \overset{\text{def}}{=} P_{m,k}(f)\, P_{m,k}(1-f)$.

From the definition of $p^{(o)}_{m,k}[l]$ shown in (5.4) and the relationship of $p_{m,k}[s] = p^{(o)}_{m,k}[s\frac{N}{2}]$, we have

$$
P_{m,k}(f) = e^{j\frac{\pi}{2}(m-k)} \sum_{n=-\infty}^{\infty} G_0(f-(m-k)-2n)\, G_0(f+f_e-2n), \tag{E.3}
$$

where $G_0(f)$ is the prototype filter and bandlimited to $[-1, 1]$, i.e. $G_0(f) = 0$ for $|f| \geq 1$.

We see that $P_{m,k}(f)$ is a periodic extension of $G_0(f-(m-k))\,G_0(f+f_e)$. Note that (E.3) is equivalent to (D.1) for $f \in [-1,1]$. Then by substituting (E.3) into the definition of $T_{m,k}(f)$, we have

$$\begin{aligned} T_{m,k}(f) = (-1)^{m-k} \sum_{n_1=-\infty}^{\infty} \sum_{n_2=-\infty}^{\infty} &\big[G_0(f-(m-k)-2n_1)\,G_0(f+f_e-2n_1) \\ &\times G_0(f+(m-k)+2n_2+1)\,G_0(f+2n_2+1-f_e)\big]. \end{aligned}$$

Without loss of generality, we may assume $0 \le f_e < 0.5$ (we will show later that the acquisition range for conjugate correlation function based methods is $|f_e| < 0.5$). Then $P_{m,k}(f)$ is nonzero only if $m \in \{k-2, k-1, k, k+1\}$. Based on the facts that $G_0(f)$ is bandlimited to $[-1,1]$, we have

$$\begin{aligned} T_{k-2,k}(f) &= 0 \\ T_{k-1,k}(f) &= -\sum_{n=-\infty}^{\infty} G_0(f-2n)\,G_0(f+f_e-2n)\,G_0(f-2n+1) \\ &\quad\times G_0(f-2n+1-f_e) \\ T_{k,k}(f) &= \sum_{n=-\infty}^{\infty} \Big[G_0(f-2n)\,G_0(f+f_e-2n)\,G_0(f-2n-1) \\ &\quad\times G_0(f-2n-1-f_e) + G_0(f-2n)\,G_0(f+f_e-2n) \\ &\quad\times G_0(f-2n+1)\,G_0(f-2n+1-f_e)\Big] \\ T_{k+1,k}(f) &= -\sum_{n=-\infty}^{\infty} G_0(f-2n)\,G_0(f+f_e-2n)\,G_0(f-2n-1) \\ &\quad\times G_0(f-2n-1-f_e). \end{aligned}$$

Then we can conclude that $\sum_{m=0}^{N-1} T_{m,k}(f) = 0$, which implies that $\sum_{m=0}^{N-1} \widetilde{A}_{m,k}(\tau, f_e) = 0$ based on (E.2). ■

Appendix F

Derivation of explicit expressions for $\lim_{M\to\infty} M\,\mathbb{E}\big[\Delta c_k[\tau_1]\,\Delta c_k^*[\tau_2]\big]$ and $\lim_{M\to\infty} M\,\mathbb{E}\big[\Delta c_k[\tau_1]\,\Delta c_k[\tau_2]\big]$

First by defining $d_k[s,\tau] = b_k[s+\tau]\,b_k^*[s] - c_k[\tau]$, which is the estimation deviation by one sample, we have $\Delta c_k[\tau] = \frac{1}{M}\sum_{s=0}^{M-1} d_k[s,\tau]$. It can be verified that both the (cross) correlation function $R_{d_k}[\lambda,\tau_1,\tau_2] = \mathbb{E}\big[d_k[s+\lambda,\tau_1]\,d_k^*[s,\tau_2]\big]$ and the conjugate (cross) correlation function $\widetilde{R}_{d_k}[\lambda,\tau_1,\tau_2] = \mathbb{E}\big[d_k[s+\lambda,\tau_1]\,d_k[s,\tau_2]\big]$ are not functions of time instant s. Then since $d_k[s,\tau]$ satisfies the mixing conditions, we have

$$\begin{aligned}\lim_{M\to\infty} M\,\mathbb{E}\big[\Delta c_k[\tau_1]\,\Delta c_k^*[\tau_2]\big] &= S_{d_k}(0,\tau_1,\tau_2)\\ \lim_{M\to\infty} M\,\mathbb{E}\big[\Delta c_k[\tau_1]\,\Delta c_k[\tau_2]\big] &= \widetilde{S}_{d_k}(0,\tau_1,\tau_2),\end{aligned} \tag{F.1}$$

where

$$\begin{aligned}S_{d_k}(f,\tau_1,\tau_2) &\overset{\text{def}}{=} \sum_{\lambda=-\infty}^{\infty} R_{d_k}[\lambda,\tau_1,\tau_2]\,e^{-j2\pi f\lambda}\\ \widetilde{S}_{d_k}(f,\tau_1,\tau_2) &\overset{\text{def}}{=} \sum_{\lambda=-\infty}^{\infty} \widetilde{R}_{d_k}[\lambda,\tau_1,\tau_2]\,e^{-j2\pi f\lambda}.\end{aligned} \tag{F.2}$$

By using the expression of $b_k[s]$ in (5.3), we can first calculate $R_{d_k}[\lambda,\tau_1,\tau_2]$ and $\widetilde{R}_{d_k}(\lambda,\tau_1,\tau_2)$, then derive the calculable expressions for $S_{d_k}[f,\tau_1,\tau_2]$

and $\widetilde{S}_{d_k}(f,\tau_1,\tau_2)$ based on (F.2). The explicit expressions for $S_{d_k}(0,\tau_1,\tau_2)$ and $\widetilde{S}_{d_k}(0,\tau_1,\tau_2)$ over a time-invariant channel and a Rayleigh fading channel are as below shown.

F.1 Time-invariant channel

After some tedious but straightforward derivations, we find that

$$
\begin{aligned}
&S_{d_k}(0,\tau_1,\tau_2) = \\
&\frac{\kappa_4\, e^{j\pi f_e(\tau_1-\tau_2)}}{4} \sum_{m=0}^{N-1} |w_m\,\mu_m|^4 \Big(\int_{-1}^{1} |P_{m,k}(f)|^2\; e^{j\pi f \tau_1}\, df\Big)\Big(\int_{-1}^{1} |P_{m,k}(f)|^2\; e^{-j\pi f \tau_2}\, df\Big) \\
&+ \frac{1}{8}\,(-1)^{\tau_1}\, e^{j\pi f_e(\tau_1-\tau_2)} \int_{-1}^{1} \Big|\sum_{m=0}^{N-1} (w_m\,\mu_m)^2\, P_{m,k}(f)\, P_{m,k}(1-f)\Big|^2 e^{-j\pi f(\tau_1+\tau_2)}\, df \\
&+ \frac{1}{8}\, e^{j\pi f_e(\tau_1-\tau_2)} \int_{-1}^{1} \Big(\sum_{m=0}^{N-1} |w_m\,\mu_m|^2\; |P_{m,k}(f)|^2\Big)^2 e^{j\pi f(\tau_1-\tau_2)}\, df \\
&+ \frac{\sigma_\nu^2}{2} \int_{-1}^{1} \Big(\sum_{m=0}^{N-1} |w_m\,\mu_m|^2\; |P_{m,k}(f-f_e)|^2\Big)\, G^2(f)\, e^{j\pi f(\tau_1-\tau_2)}\, df \\
&+ \frac{\sigma_\nu^4}{2} \int_{-1}^{1} G^4(f)\, e^{j\pi f(\tau_1-\tau_2)}\, df \\
&\widetilde{S}_{d_k}(0,\tau_1,\tau_2) = \\
&\frac{\kappa_4\, e^{j\pi f_e(\tau_1+\tau_2)}}{4} \sum_{m=0}^{N-1} |w_m\,\mu_m|^4 \Big(\int_{-1}^{1} |P_{m,k}(f)|^2\; e^{j\pi f \tau_1}\, df\Big)\Big(\int_{-1}^{1} |P_{m,k}(f)|^2\; e^{j\pi f \tau_2}\, df\Big) \\
&+ \frac{1}{8}\,(-1)^{\tau_2}\, e^{j\pi f_e(\tau_1+\tau_2)} \int_{-1}^{1} \Big|\sum_{m=0}^{N-1} (w_m\,\mu_m)^2\, P_{m,k}(f)\, P_{m,k}(1-f)\Big|^2 e^{j\pi f(\tau_1-\tau_2)}\, df_1 \\
&+ \frac{1}{8}\, e^{j\pi f_e(\tau_1+\tau_2)} \int_{-1}^{1} \Big(\sum_{m=0}^{N-1} |w_m\,\mu_m|^2\; |P_{m,k}(f)|^2\Big)^2 e^{j\pi f(\tau_1+\tau_2)}\, df \\
&+ \frac{\sigma_\nu^2}{2} \int_{-1}^{1} \Big(\sum_{m=0}^{N-1} |w_m\,\mu_m|^2\; |P_{m,k}(f-f_e)|^2\Big) G^2(f)\, e^{j\pi f(\tau_1+\tau_2)}\, df \\
&+ \frac{\sigma_\nu^4}{2} \int_{-1}^{1} G^4(f)\, e^{j\pi f(\tau_1+\tau_2)}\, df,
\end{aligned}
\tag{F.3}
$$

where $\kappa_4 \overset{\text{def}}{=} \mathbb{E}\Big[\big(a_k^{\mathcal{R}}[n]\big)^4\Big] - \frac{3}{4}$ is the fourth order cumulant of $a_k^{\mathcal{R}}[n]$ (or $a_k^{\mathcal{I}}[n]$).

F.2 Rayleigh fading channel

We assume that $\mu_k[l]$ is a circular zero-mean complex-valued Gaussian process with variance $\sigma^2_{\mu_k}$, i.e. Rayleigh fading channel. After some tedious derivations, we get

$$
\begin{aligned}
&S_{d_k}(0,\tau_1,\tau_2) = \\
&\frac{\sigma^4_{\mu_k}\,\kappa_4\, e^{j\pi f_e(\tau_1-\tau_2)}}{2}\sum_{m=0}^{N-1} w_m^4 \Big(\int_{-1}^{1}|P_{m,k}(f)|^2\, e^{j\pi f\tau_1}\,df\Big)\Big(\int_{-1}^{1}|P_{m,k}(f)|^2\, e^{-j\pi f\tau_2}\,df\Big) \\
&+\frac{\sigma^4_{\mu_k}}{4}(-1)^{\tau_1}\, e^{j\pi f_e(\tau_1-\tau_2)}\int_{-1}^{1}\Big|\sum_{m=0}^{N-1} w_m^2\, P_{m,k}(f)\, P_{m,k}(1-f)\Big|^2 e^{-j\pi f(\tau_1+\tau_2)}\,df \\
&+\frac{\sigma^4_{\mu_k}}{4}\, e^{j\pi f_e(\tau_1-\tau_2)}\int_{-1}^{1}\Big(\sum_{m=0}^{N-1} w_m^2\, |P_{m,k}(f)|^2\Big)^2 e^{j\pi f(\tau_1-\tau_2)}\,df \\
&+\frac{\sigma^2_{\nu}\,\sigma^2_{\mu_k}}{2}\int_{-1}^{1}\Big(\sum_{m=0}^{N-1} w_m^2\, |P_{m,k}(f-f_e)|^2\Big)G^2(f)\, e^{j\pi f(\tau_1-\tau_2)}\,df \\
&+\frac{\sigma^4_{\nu}}{2}\int_{-1}^{1} G^4(f)\, e^{j\pi f(\tau_1-\tau_2)}\,df \\
&\widetilde{S}_{d_k}(0,\tau_1,\tau_2) = \\
&\frac{\sigma^4_{\mu_k}\,\kappa_4\, e^{j\pi f_e(\tau_1+\tau_2)}}{2}\sum_{m=0}^{N-1} w_m^4 \Big(\int_{-1}^{1}|P_{m,k}(f)|^2\, e^{j\pi f\tau_1}\,df\Big)\Big(\int_{-1}^{1}|P_{m,k}(f)|^2\, e^{j\pi f\tau_2}\,df\Big) \\
&+\frac{\sigma^4_{\mu_k}}{4}(-1)^{\tau_2}\, e^{j\pi f_e(\tau_1+\tau_2)}\int_{-1}^{1}\Big|\sum_{m=0}^{N-1} w_m^2\, P_{m,k}(f)\, P_{m,k}(1-f)\Big|^2 e^{j\pi f(\tau_1-\tau_2)}\,df_1 \\
&+\frac{\sigma^4_{\mu_k}}{4}\, e^{j\pi f_e(\tau_1+\tau_2)}\int_{-1}^{1}\Big(\sum_{m=0}^{N-1} w_m^2\, |P_{m,k}(f)|^2\Big)^2 e^{j\pi f(\tau_1+\tau_2)}\,df \\
&+\frac{\sigma^2_{\nu}\,\sigma^2_{\mu_k}}{2}\int_{-1}^{1}\Big(\sum_{m=0}^{N-1} w_m^2\, |P_{m,k}(f-f_e)|^2\Big)G^2(f)\, e^{j\pi f(\tau_1+\tau_2)}\,df \\
&+\frac{\sigma^4_{\nu}}{2}\int_{-1}^{1} G^4(f)\, e^{j\pi f(\tau_1+\tau_2)}\,df.
\end{aligned}
\tag{F.4}
$$

Since $P_{m,k}(f)$ can be inferred from the shaping pulse $G(f)$ and f_e based on (D.1), we now get the explicit calculable expressions for $S_{d_k}(0,\tau_1,\tau_2)$ and $\widetilde{S}_{d_k}(0,\tau_1,\tau_2)$.

Appendix G

Derivation of asymptotic MSE for conjugate correlation function based method

The following derivations follow a argument similar to that in [CLSG02]. First since $\mathbf{e}_k[s]$ satisfies the mixing condition (see [Bri75]: Theorem 2.3.1 (iii), p.19), by defining $\mathbf{s}_{M,k}^{(K)}(f) = \frac{1}{M^{K+1}} \sum_{s=0}^{M-1} s^K \, \mathbf{e}_k[s] \, e^{-j2\pi f s}$, we have the below theorem:

Theorem 1 *$\hat{f}_e - f_e \xrightarrow{a.s.} 0$ and $M\,(\hat{f}_e - f_e) \xrightarrow{a.s.} 0$ as $M \to \infty$, where a.s. stands for 'almost sure' (or in probability 1).*

Proof: Recalling that $y_k[s,\tau] = \hat{c}_k[s,\tau] + e_k[s,\tau]$, we immediately have $\mathbf{y}_k[s] = \mathbf{r}_k(f_e)\, e^{j2\pi(f_e+1/2)s} + \mathbf{e}_k[s]$ and can write the objective function in (5.25) as

$$J_M(f) = \sum_{l=1}^{L} \left\| \mathbf{r}_{k_l}(f_e) \Big(\frac{1}{M} \sum_{s=0}^{M-1} e^{j2\pi(f_e+1/2-f)s} \Big) + \mathbf{s}_{M,k_l}^{(0)}(f) \right\|^2.$$

As $M \to \infty$, $\frac{1}{M} \sum_{s=0}^{M-1} e^{j2\pi(f_e+1/2-f)s} \to \delta[f_e + 1/2 - f]$; and by Lemma 1, $\mathbf{s}_{M,k_l}^{(0)}(f) \xrightarrow{a.s.} \mathbf{0}$. Then $\arg\max_{f\in(0,1)} J_M(f) \xrightarrow{a.s.} f_e + 1/2$, $\hat{f}_e - f_e \xrightarrow{a.s.} 0$. Also based on the Lemma 3 in [CLSG02], $M\,(\hat{f}_e - f_e) \xrightarrow{a.s.} 0$ as $M \to \infty$; otherwise $\frac{1}{M} \sum_{s=0}^{M-1} e^{j2\pi(f_e+1/2-f)s}$ will not converge to $\delta[f_e + 1/2 - f]$. ■

Theorem 2 *$M^{3/2}\,(\hat{f}_e - f_e)$ is asymptotically Gaussian.*

Proof: Since $\hat{f}_e = \arg\max_{f\in(0,1)} J_M(f) - \frac{1}{2}$, we have $\left.\frac{dJ_M(f)}{df}\right|_{f=\hat{f}_e+\frac{1}{2}} = 0$. Then using the first order Taylor expansion of $\frac{dJ_M(f)}{df}$ around $f_e + \frac{1}{2}$, we have

$$\left.\frac{dJ_M(f)}{df}\right|_{f=\hat{f}_e+\frac{1}{2}} = \left.\frac{dJ_M(f)}{df}\right|_{f=f_e+\frac{1}{2}} + (\hat{f}_e - f_e)\left.\frac{d^2J_M(f)}{df^2}\right|_{f=f_\xi+\frac{1}{2}},$$

where f_ξ lies between f_e and $\hat{f}_e$.

Then we have

$$M^{3/2}\,(\hat{f}_e - f_e) = -\mathcal{A}_M^{-1}\,\mathcal{B}_M, \tag{G.1}$$

where $\mathcal{A}_M = \frac{1}{M^2}\left.\frac{d^2J_M(f)}{df^2}\right|_{f=f_\xi+\frac{1}{2}}$ and $\mathcal{B}_M = \frac{1}{\sqrt{M}}\left.\frac{dJ_M(f)}{df}\right|_{f=f_e+\frac{1}{2}}$.

Now we try to calculate $\mathcal{A}_M$ as $M \to \infty$. First we define $\mathbf{Y}_{k_l}(f) = \frac{1}{M}\sum_{s=0}^{M-1}\mathbf{y}_{k_l}[s]\,e^{-j2\pi fs}$, then $J_M(f) = \sum_{l=1}^{L}\|\mathbf{Y}_{k_l}(f)\|^2$ and

$$\frac{d^2J_M(f)}{df^2} = 2\sum_{l=1}^{L}\left(\left\|\frac{\partial\mathbf{Y}_{k_l}(f)}{\partial f}\right\|^2 + \mathrm{Re}\left\{\mathbf{Y}_{k_l}^H(f)\,\frac{\partial^2\mathbf{Y}_{k_l}(f)}{\partial f^2}\right\}\right).$$

It can be easily calculated that $\frac{\partial^K\mathbf{Y}_{k_l}(f)}{\partial f^K} = \frac{1}{M}\sum_{s=0}^{M-1}(-j2\pi s)^K\,\mathbf{y}_{k_l}[s]\,e^{-j2\pi fs}$. Then by using the Lemma 1 introduced in [CLSG02], we have

$$\mathcal{A}_M \xrightarrow{a.s.} -\frac{2\,\pi^2}{3}\sum_{l=1}^{L}\|\mathbf{r}_{k_l}(f_e)\|^2 \;\text{ as } M \to \infty. \tag{G.2}$$

Now we will show that $\mathcal{B}_M$ is asymptotically Gaussian distributed as $M \to \infty$. First after some tedious while straightforward derivation, we get

$$\begin{aligned}\mathcal{B}_M \;&=\; \sum_{l=1}^{L}\frac{2}{\sqrt{M}}\,\mathrm{Re}\left\{\mathbf{Y}_{k_l}^H(f)\frac{\partial\mathbf{Y}_{k_l}(f)}{\partial f}\right\}\Bigg|_{f=f_e+\frac{1}{2}}\\ &\xrightarrow{a.s.} j\,2\,\pi\sum_{l=1}^{L}\mathbf{R}_{k_l}^H\,\mathbf{E}_{M,k_l} \;\text{ as } M \to \infty,\end{aligned} \tag{G.3}$$

where

$$\begin{aligned}\mathbf{R}_k &= \begin{bmatrix}\frac{\mathbf{r}_k^H(f_e)}{2} & -\mathbf{r}_k^H(f_e) & -\frac{\mathbf{r}_k^T(f_e)}{2} & \mathbf{r}_k^T(f_e)\end{bmatrix}^H\\ \mathbf{E}_{M,k} &= \begin{bmatrix}\mathbf{E}_{M,k}^{(0)T}(f_e+\frac{1}{2}) & \mathbf{E}_{M,k}^{(1)T}(f_e+\frac{1}{2}) & \mathbf{E}_{M,k}^{(0)H}(f_e+\frac{1}{2}) & \mathbf{E}_{M,k}^{(1)H}(f_e+\frac{1}{2})\end{bmatrix}^T,\end{aligned} \tag{G.4}$$

and

$$\mathbf{E}_{M,k}^{(K)}(f) = \frac{1}{M^K\sqrt{M}} \sum_{s=0}^{M-1} s^K\, \mathbf{e}_k[s]\, e^{-j2\pi f s}. \tag{G.5}$$

It can be proved that $\mathbf{E}_{M,k}^{(K)}(f_e+\frac{1}{2})$ is asymptotically zero-mean Gaussian distributed (ref. [CLSG02] for more details). Then $\mathcal{B}_M \xrightarrow{a.s.} \mathcal{N}(0,\sigma_{\mathcal{B}}^2)$ as $M \to \infty$, where $\sigma_{\mathcal{B}}^2$ is asymptotic covariance of $\mathcal{B}_M$. At last by substituting (G.2) and (G.3) into (G.1), we can conclude that $M^{3/2}\,(\hat{f}_e - f_e) \xrightarrow{a.s.} \mathcal{N}(0,\sigma^2)$, where $\sigma^2 = \frac{9\,\sigma_{\mathcal{B}}^2}{4\,\pi^4\ \sum_{l=1}^{L}\left\|\mathbf{r}_{k_l}(f_e)\right\|^2\ {}^2}$. ■

From the proof of Theorem 2, we see that the MSE of estimated $\hat{f}_e$ is given by

$$\mathrm{MSE}_3 = \frac{9\,\sigma_{\mathcal{B}}^2}{4\,\pi^4\, M^3\left(\sum_{l=1}^{L}\|\mathbf{r}_{k_l}(f_e)\|^2\right)^2}. \tag{G.6}$$

We still need to calculate $\sigma_{\mathcal{B}}^2$. Based on the approximation that $\{b_{k_l}[s]\}_{l=1}^{L}$ are mutually independent and the expression of $\mathcal{B}_M$ shown in (G.3), we have

$$\sigma_{\mathcal{B}}^2 = 4\,\pi^2 \sum_{l=1}^{L} \mathbf{R}_{k_l}^H\, \mathbb{E}\left[\mathbf{E}_{M,k_l}\mathbf{E}_{M,k_l}^H\right]\, \mathbf{R}_{k_l}. \tag{G.7}$$

The matrix $\mathbb{E}\big[\mathbf{E}_{M,k}\mathbf{E}_{M,k}^H\big]$ can be expressed as

$$\mathbb{E}\left[\mathbf{E}_{M,k}\mathbf{E}_{M,k}^H\right] = \begin{bmatrix} \mathbf{P}_{M,k}(0,0) & \mathbf{P}_{M,k}(0,1) & \widetilde{\mathbf{P}}_{M,k}(0,0) & \widetilde{\mathbf{P}}_{M,k}(0,1) \\ \mathbf{P}_{M,k}(1,0) & \mathbf{P}_{M,k}(1,1) & \widetilde{\mathbf{P}}_{M,k}(1,0) & \widetilde{\mathbf{P}}_{M,k}(1,1) \\ \widetilde{\mathbf{P}}_{M,k}^*(0,0) & \widetilde{\mathbf{P}}_{M,k}^*(0,1) & \mathbf{P}_{M,k}^*(0,0) & \mathbf{P}_{M,k}^*(0,1) \\ \widetilde{\mathbf{P}}_{M,k}^*(1,0) & \widetilde{\mathbf{P}}_{M,k}^*(1,1) & \mathbf{P}_{M,k}^*(1,0) & \mathbf{P}_{M,k}^*(1,1) \end{bmatrix}, \tag{G.8}$$

where

$$\begin{aligned} \mathbf{P}_{M,k}(K_1,K_2) &= \mathbb{E}\left[\mathbf{E}_{M,k}^{(K_1)}(f_e+\frac{1}{2})\,\mathbf{E}_{M,k}^{(K_2)H}(f_e+\frac{1}{2})\right] \\ \widetilde{\mathbf{P}}_{M,k}(K_1,K_2) &= \mathbb{E}\left[\mathbf{E}_{M,k}^{(K_1)}(f_e+\frac{1}{2})\,\mathbf{E}_{M,k}^{(K_2)T}(f_e+\frac{1}{2})\right]. \end{aligned}$$

We then define $R_{e_k}[\lambda,\tau_1,\tau_2] = \mathbb{E}\left[e_k[s+\lambda,\tau_1]\, e_k^*[s,\tau_2]\right]$, $\widetilde{R}_{e_k}[\lambda,\tau_1,\tau_2] = \mathbb{E}\left[e_k[s+\lambda,\tau_1]\, e_k[s,\tau_2]\right]\, e^{-j4\pi f_e s}$ (It can be verified that $R_{e_k}[\lambda,\tau_1,\tau_2]$, $\widetilde{R}_{e_k}[\lambda,\tau_1,\tau_2]$ are not a function of s). By using the mixing conditions, we can write the entries of $\mathbf{P}_{M,k}(K_1, K_2)$ and $\widetilde{\mathbf{P}}_{M,k}(K_1, K_2)$ as

$$\begin{aligned}\lim_{M\to\infty}\big[\mathbf{P}_{M,k}(K_1, K_2)\big]_{\tau_1,\tau_2} &= \frac{1}{K_1+K_2+1} S_{e_k}(f_e + \frac{1}{2}, \tau_1, \tau_2)\\ \lim_{M\to\infty}\big[\widetilde{\mathbf{P}}_{M,k}(K_1, K_2)\big]_{\tau_1,\tau_2} &= \frac{1}{K_1+K_2+1} \widetilde{S}_{e_k}(f_e + \frac{1}{2}, \tau_1, \tau_2), \quad \text{(G.9)}\end{aligned}$$

where

$$\begin{aligned}S_{e_k}(f, \tau_1, \tau_2) &\stackrel{\text{def}}{=} \sum_{\lambda=-\infty}^{\infty} R_{e_k}[\lambda, \tau_1, \tau_2]\, e^{-j2\pi f\lambda}\\ \widetilde{S}_{e_k}(f, \tau_1, \tau_2) &\stackrel{\text{def}}{=} \sum_{\lambda=-\infty}^{\infty} \widetilde{R}_{e_k}[\lambda, \tau_1, \tau_2]\, e^{-j2\pi f\lambda}. \quad \text{(G.10)}\end{aligned}$$

The explicit calculable expressions for $S_{e_k}(f, \tau_1, \tau_2)$ and $\widetilde{S}_{e_k}(f, \tau_1, \tau_2)$ will be shown in Appendix H. From (G.9), we see that $\mathbf{P}_{M,k_l}(0, 1) = \mathbf{P}_{M,k_l}(1, 0) = \frac{1}{2}\,\mathbf{P}_{M,k_l}(0, 0)$, $\mathbf{P}_{M,k_l}(1, 1) = \frac{1}{3}\,\mathbf{P}_{M,k_l}(0, 0)$ and $\widetilde{\mathbf{P}}_{M,k_l}(0, 1) = \widetilde{\mathbf{P}}_{M,k_l}(1, 0) = \frac{1}{2}\,\widetilde{\mathbf{P}}_{M,k_l}(0, 0)$, $\widetilde{\mathbf{P}}_{M,k_l}(1, 1) = \frac{1}{3}\,\widetilde{\mathbf{P}}_{M,k_l}(0, 0)$ as $M \to \infty$. Then by substituting (G.8) into (G.7), we have

$$\sigma_{\mathcal{B}}^2 = \frac{2\,\pi^2}{3} \sum_{i=1}^{L} \operatorname{Re}\left\{\mathbf{r}_{k_l}^H(f_e)\,\mathbf{P}_{M,k_l}(0, 0)\,\mathbf{r}_{k_l}(f_e) - \mathbf{r}_{k_l}^H(f_e)\,\widetilde{\mathbf{P}}_{M,k_l}(0, 0)\,\mathbf{r}_{k_l}^*(f_e)\right\}.$$

By shortening the denotements $\mathbf{P}_{M,k}(0, 0)$, $\widetilde{\mathbf{P}}_{M,k}(0, 0)$ to $\mathbf{P}_k$, $\widetilde{\mathbf{P}}_k$ respectively, and substituting the expression of $\sigma_{\mathcal{B}}^2$ into (G.6), we then get (5.35).

Appendix H

Derivation of calculable expressions for $S_{e_k}(f_e + 1/2, \tau_1, \tau_2)$ and $\widetilde{S}_{e_k}(f_e + 1/2, \tau_1, \tau_2)$

Recall that $e_k[s,\tau] = y_k[s,\tau] - \tilde{c}_k[s,\tau] = b_k[s+\tau]\, b_k[s] - r_k(\tau, f_e)\, e^{j2\pi(f_e+1/2)s}$. Based on the expression of $b_k[s]$ in (5.3), we can derive the expressions for $R_{e_k}[\lambda, \tau_1, \tau_2]$ and $\widetilde{R}_{e_k}[\lambda, \tau_1, \tau_2]$. Finally taking the DTFT of $R_{e_k}[\lambda, \tau_1, \tau_2]$

and $\widetilde{R}_{e_k}[\lambda, \tau_1, \tau_2]$ with respect to λ, we get

$$
\begin{aligned}
& S_{e_k}(f_e + \frac{1}{2}, \tau_1, \tau_2) \\
= {} & \frac{\kappa_4 \, e^{j\pi f_e(\tau_1 - \tau_2)}}{4} \sum_{m=0}^{N-1} |w_m \, \mu_m|^4 \left(\int_{-1}^{1} P_{m,k}(f) \, P_{m,k}(1-f) \, e^{j\pi f \tau_1} \, df \right) \\
& \times \left(\int_{-1}^{1} P_{m,k}(f) \, P_{m,k}(1-f) \, e^{j\pi f \tau_2} \, df \right)^{*} \\
& + \frac{(-1)^{\tau_2} e^{j\pi f_e(\tau_1 - \tau_2)}}{8} \int_{-1}^{1} \Big(\sum_{m=0}^{N-1} |w_m \mu_m|^2 \, |P_{m,k}(f)|^2 \Big) \\
& \times \Big(\sum_{m=0}^{N-1} |w_m \mu_m|^2 \, |P_{m,k}\,(1-f)|^2 \Big) e^{j\pi f(\tau_1 + \tau_2)} \, df \\
& + \frac{e^{j\pi f_e(\tau_1 - \tau_2)}}{8} \int_{-1}^{1} \Big(\sum_{m=0}^{N-1} |w_m \mu_m|^2 \, |P_{m,k}(f)|^2 \Big) \\
& \times \Big(\sum_{m=0}^{N-1} |w_m \mu_m|^2 \, |P_{m,k}\,(1-f)|^2 \Big) e^{j\pi f(\tau_1 - \tau_2)} \, df \\
& + \frac{\sigma_\nu^2}{4} \int_{-1}^{1} \Big(\sum_{m=0}^{N-1} |w_m \mu_m|^2 \, |P_{m,k}(1 + f_e - f)|^2 \Big) G^2\,(f) \;\, e^{j\pi f(\tau_1 - \tau_2)} \, df \\
& + \frac{\sigma_\nu^2 \, e^{-j\pi(2f_e+1)\tau_2}}{4} \\
& \times \int_{-1}^{1} \Big(\sum_{m=0}^{N-1} |w_m \mu_m|^2 \, |P_{m,k}(1 + f_e - f)|^2 \Big) G^2\,(f) \;\, e^{j\pi f(\tau_1 + \tau_2)} \, df \\
& + \frac{\sigma_\nu^2 \, e^{j\pi(2f_e+1)\tau_1}}{4} \\
& \times \int_{-1}^{1} \Big(\sum_{m=0}^{N-1} |w_m \mu_m|^2 \, |P_{m,k}(1 + f_e - f)|^2 \Big) G^2\,(f) \;\, e^{-j\pi f(\tau_1 + \tau_2)} \, df \\
& + \frac{\sigma_\nu^2 \, e^{j\pi(2f_e+1)(\tau_1 - \tau_2)}}{4} \\
& \times \int_{-1}^{1} \Big(\sum_{m=0}^{N-1} |w_m \mu_m|^2 \, |P_{m,k}(1 + f_e - f)|^2 \Big) G^2\,(f) \;\, e^{-j\pi f(\tau_1 - \tau_2)} \, df \\
& + \frac{\sigma_\nu^4}{2} \int_{-1}^{1} G^2(f) \, G^2(2f_e + 1 - f) \left(e^{j\pi f(\tau_1 - \tau_2)} + e^{j\pi(2f_e+1)\tau_1} \, e^{-j\pi f(\tau_1 + \tau_2)} \right) df,
\end{aligned}
\tag{H.1}
$$

and

$$
\begin{aligned}
&\widetilde{S}_{e_k}(f_e + \frac{1}{2}, \tau_1, \tau_2) \\
&= \frac{\kappa_4\, e^{j\pi f_e(\tau_1+\tau_2)}}{4} \sum_{m=0}^{N-1} (w_m\, \mu_m)^4 \Big(\int_{-1}^{1} P_{m,k}(f)\, P_{m,k}(1-f)\, e^{j\pi f \tau_1}\, df \Big) \\
&\quad \times \Big(\int_{-1}^{1} P_{m,k}(f)\, P_{m,k}(1-f)\, e^{j\pi f \tau_2}\, df \Big) \\
&\quad + \frac{(-1)^{\tau_2} e^{j\pi f_e(\tau_1+\tau_2)}}{8} \\
&\quad \times \int_{-1}^{1} \Big(\sum_{m=0}^{N-1} (w_m\, \mu_m)^2\ P_{m,k}(f)\, P_{m,k}(1-f) \Big)^2\ e^{j\pi f(\tau_1-\tau_2)} df \\
&\quad + \frac{e^{j\pi f_e(\tau_1+\tau_2)}}{8} \int_{-1}^{1} \Big(\sum_{m=0}^{N-1} (w_m\, \mu_m)^2\ P_{m,k}(f)\, P_{m,k}(1-f) \Big)^2 e^{j\pi f(\tau_1+\tau_2)}\, df,
\end{aligned}
\tag{H.2}
$$

where $\kappa_4 \overset{\text{def}}{=} \mathbb{E}\left[\left(a_k^{\mathcal{R}}[n] \right)^4 \right] - \frac{3}{4}$ is the fourth order cumulant of $a_k^{\mathcal{R}}[n]$ (or $a_k^{\mathcal{I}}[n]$).

Since $P_{m,k}(f)$ can be inferred from the shaping pulse $G(f)$ and f_e based on (D.1), we now get the explicit calculable expressions for $S_{e_k}(f_e + 1/2, \tau_1, \tau_2)$ and $\widetilde{S}_{e_k}(f_e + 1/2, \tau_1, \tau_2)$.

Bibliography

[Arm99] J. Armstrong. Analysis of new and existing methods of reducing intercarrier interference due to carrier frequency offset in OFDM. *IEEE Trans. Commun.*, 47:365–369, Mar. 1999.

[ATP05] A. Assalini, M. Trivellato, and S. Pupolin. Performance analysis of OFDM-OQAM systems. In *Proc. Wireless Personal Multimedia Communications WPMC '05*, Sept. 17-22 2005.

[BDH99] H. Bolcskei, P. Duhamel, and R. Hleiss. Design of pulse shaping OFDM/OQAM systems for high data-rate transmission over wireless channels. In *Proc. IEEE International Conference on Communications, ICC '99*, volume 1, pages 559–564, 6-10 Jun. 1999.

[Bol] H. Bolcskei. Orthogonal frequency division multiplexing based on offset QAM. *Book chapter in "Advances in Gabor Analysis"*, pages 321–352.

[Bol01] H. Bolcskei. Blind estimation of symbol timing and carrier frequency offset in wireless OFDM systems. *IEEE Trans. Commun.*, 49:988–999, Jun. 2001.

[Bri75] D. R. Brillinger. *Time series: data analysis and theory.* Holt, Rinehart and Winston, Inc., New York, 1975.

[BTD01] N. C. Beaulieu, C. C. Tan, and M. O. Damen. A "better than" Nyquist pulse. *IEEE Communications Letters*, 5:367–368, Sept. 2001.

[CC97] H. H. Chen and X. D. Cai. Waveform Optimization for OQAM-OFDM Systems by Using Nonlinear Programming Algorithms. In *Proc. IEEE Vehicular Technology Conference, VTC '97*, volume 3, pages 1385–1389, 4-7 May 1997.

[CG68] R. W. Chang and R. A. Gibby. A theoretical study of performance of an orthogonal multiplexing data transmission systems. *IEEE Trans. Commun. Technol.*, COM-16:529–540, Aug. 1968.

[CG06] P. Ciblat and M. Ghogho. Blind NLLS carrier frequency-offset estimation for QAM, PSK, and PAM modulations : performance at low SNR. *accepted for publication in IEEE Trans. Commun.*, Feb. 2006.

[Cha66] R. W. Chang. Synthesis of band-limited orthogonal signals for multichannel data transmission. *Bell Syst. Tech. J.*, 45:1775–1796, Dec. 1966.

[CLSG02] P. Ciblat, P. Loubaton, E. Serpedin, and G.B. Giannakis. Performance analysis of blind carrier frequency offset estimators for noncircular transmissions through frequency-selective channels. *IEEE Trans. SP*, 50:130–140, Jan. 2002.

[Col92] R. J. Collins. Approximating Series. *The College Mathematics Journal*, 23:153–157, Mar. 1992.

[CS04] P. Ciblat and E. Serpedin. A fine blind frequency offset estimator for OFDM/OQAM systems. *IEEE Trans. SP*, 52:291–296, Jan. 2004.

[CSC05] S. Chandan, P. Sandeep, and A. K. Chaturvedi. A family of ISI-free polynomial pulses. *IEEE Communications Letters*, 9:496–498, Jun. 2005.

[CV95] G. Cariolaro and F. C. Vagliani. An OFDM scheme with a half complexity. *IEEE J. Select. Areas Commun.*, 13:1586–1599, Dec. 1995.

[CV03] P. Ciblat and L. Vandendorpe. Blind carrier frequency offset estimation for noncircular constellation-based transmissions. *IEEE Trans. SP*, 51:1378–1389, May. 2003.

[DHM57] M. L. Doelz, E. T. Heald, and D. L. Martin. Binary transmission techniques for linear systems. In *Pro. IRE' 1957*, volume 45, pages 656–661, May 1957.

[EN 01] ETSI EN 300 401. *Radio Broadcasting Systems; Digital Audio Broadcasting (DAB) to mobile, portable and fixed receivers.* ETSI, May 2001.

[EN 04] ETSI EN 300 744. *Digital Video Broadcasting (DVB); Framing structure, channel coding and modulation for digital terrestrial television.* ETSI, Nov. 2004.

[Fau00] M. Faulkner. The effect of filtering on the performance of OFDM systems. *IEEE Trans. VT*, 49:1877–1884, Sept. 2000.

[FL61] G. A. Franco and G. Lachs. An orthogonal coding technique for communications. In *Pro. IRE' 1961*, volume 9, pages 126–133, 1961.

[Fra68] L. E. Franks. Futher results on Nyquist's problem in pulse transmission. *IEEE Trans. Commun. Technol.*, COM-16:337–340, Apr. 1968.

[FT06] T. Fusco and M. Tanda. Blind CFO estimation for OFDM/OQAM systems. In *Proc. IEEE International Conference on Acoustics, Speech, and Signal Processing, ICASSP '06*, 14-19 May 2006.

[G 998] ITU-T G 991.1. *High bit rate Digital Subscriber Line (HDSL) transceivers.* ITU, Oct. 1998.

[G 999] ITU-T G 992.1. *Asymmetric digital subscriber line (ADSL) transceivers.* ITU, Jul. 1999.

[G 904] ITU-T G 993.1. *Very high speed digital subscriber line transceivers.* ITU, Jun. 2004.

[GG98] F. Gini and G.B. Giannakis. Frequency offset and symbol timing recovery in flat-fading channels: a cyclostationary approach. *IEEE Trans. Commun.*, 46:400–411, Mar. 1998.

[Gra] R. M. Gray. Toeplitz and circulant matrices: A review. Technical report, Information Systems Lab., Center for Systems Research, Stanford Univ., Stanford, CA, 2002.

[GSG01] M. Ghogho, A. Swami, and G. B. Giannakis. Optimized null-subcarrier selection for CFO estimation in OFDM over frequency-selective fading channels. In *Proc. Global Telecommunications Conference, GLOBECOM '01*, volume 1, pages 202–206, 25-29 Nov. 2001.

[GTC04] Y. Gu, K. Tang, and H. Cui. LMS algorithm with gradient descent filter length. *IEEE Signal Processing Letters*, 11:305–307, Mar. 2004.

[GW99] H. Ge and K. Wang. Efficient method for carrier offset correction in OFDM system. In *Proc. IEEE International Conference on Acoustics, Speech, and Signal Processing, ICASSP '99*, volume 5, pages 2467–2470, 15-19 Mar. 1999.

[Hir80] B. Hirosaki. An Analysis of Automatic Equalizers for Orthogonally Multiplexed QAM Systems. *IEEE Trans. Commun.*, 28:73–83, Jan. 1980.

[Hod78] W. Hodgkiss. Selecting the length of an adaptive transversal filter. In *Proc. IEEE International Conference on Acoustics, Speech, and Signal Processing (ICASSP '78)*, volume 3, pages 96–99, Apr. 1978.

[LHL05] G. Lin, N. Holte, and L. Lundheim. Design of robust pulses to carrier frequency offset for OFDM/OQAM system. In *Proc. 48th IEEE Global Telecommunications Conference, GLOBECOM '05*, volume 3, pages 1423–1428, 28 Nov. - 2 Dec. 2005.

[LHL06] G. Lin, N. Holte, and L. Lundheim. Internal note 10: Comment to "A fine blind frequency offset estimator for OFDM/OQAM systems". Technical report, 2006.

[LLH05] G. Lin, L. Lundheim, and N. Holte. On efficient equalization for OFDM/OQAM systems. In *Proc. 10th International OFDM-Workshop*, Hamburg, Germany, 31 Aug. - 1 Sept. 2005.

[LLH06a] G. Lin, L. Lundheim, and N. Holte. Blind Carrier Frequency Offset Estimation for OFDM/OQAM Systems based on Second-Order Statistics. *to submit to IEEE Trans. SP*, 2006.

[LLH06b] G. Lin, L. Lundheim, and N. Holte. Blind carrier frequency offset estimation for OFDM/OQAM systems based on subchannel signals. *to appear in Proc. 49th IEEE Global Telecommunications Conference, Globecom '06*, 2006.

[LLH06c] G. Lin, L. Lundheim, and N. Holte. New methods for blind fine estimation of carrier frequency offset in OFDM/OQAM systems. *in Proc. International Workshop on Signal Processing Advances in Wireless Communications, SPAWC '06*, 2-5 Jul. 2006.

[LLH06d] G. Lin, L. Lundheim, and N. Holte. Optimal pulses robust to carrier frequency offset for OFDM/QAM systems. *to submit to IEEE Communications Letters*, 2006.

[LLH06e] G. Lin, L. Lundheim, and N. Holte. Some theoretical results on selecting the equalizer length for OFDM/OQAM systems. *submitted to IEEE Trans. Commun.*, Feb. 2006 (revised Sep. 2006).

[LM94] Edward A. Lee and David G. Messerschmitt. *Digital communication (second edition).* Kluwer Academic Publishers, 3300 AH Dordrecht, Netherlands, 1994.

[LS95] R. Li and G. Stette. Time-limited orthogonal multicarrier modulation schemes. *IEEE Trans. Commun.*, 43:1269–1272, Feb./Mar./Apr. 1995.

[MTGB01] X. Ma, C. Tepedelenlioglu, G. B. Giannakis, and S. Barbarossa. Non-data aided carrier-offset estimators for OFDM with null subcarriers: identifiability, algorithms, and performance. *IEEE J. Select. Areas Commun.*, 19:2504–2515, Dec. 2001.

[Ned00] S. Nedic. An approach to data-driven echo cancellation in OQAM-based multicarrier data transmission. *IEEE Trans. Commun.*, 48:1077–1082, Jul. 2000.

[PBM95] T. Pollet, M. Van Bladel, and M. Moeneclaey. BER sensitivity of OFDM systems to carrier frequency offset and Wiener phase noise. *IEEE Trans. Commun.*, 43:191–193, Feb./Mar./Apr. 1995.

[PCK$^+$04] B. Park, H. Cheon, E. Ko, C. Kang, and D. Hong. A blind OFDM synchronization algorithm based on cyclic correlation. *IEEE Signal Processing Letters*, 11:83–85, Feb. 2004.

[PS01] S. Pfletschinger and J. Speidel. Optimized Impulses for Multicarrier Offset-QAM. In *Proc. IEEE Global Telecommunications Conference, GLOBECOM '01*, volume 1, pages 207–211, 25-29 Nov. 2001.

[RB74] D. Rife and R. Boorstyn. Single tone parameter estimation from discrete-time observations. *IEEE Trans. IT*, 20:591–598, Sept. 1974.

[RHV98] P. K. Remvik, N. Holte, and A. Vahlin. Fading and carrier frequency offset robustness for different pulse shaping filters in OFDM. In *Proc. 48th IEEE Vehicular Technology Conference, VTC '98*, volume 2, pages 777–781, 18-21 May 1998.

[RPNC01] F. Riera-Palou, J. M. Noras, and D. G. M. Cruickshank. Segmented equalizers with dynamic length selection. In *Conference Record of the Thirty-Fifth Asilomar Conference on Signals, Systems and Computers*, volume 2, pages 951–955, 4-7 Nov. 2001.

[Rum79] W. D. Rummler. A new selective fading model: Application to propagation data. *Bell Syst. Tech. J.*, 58:1037–1071, May-Jun. 1979.

[RZ99] M. Reuter and J. R. Zeidler. Nonlinear effects in LMS adaptive equalizers. *IEEE Trans. SP*, 47:1570–1579, Jun. 1999.

[Sal67] B. Saltzberg. Performance of an Efficient Parallel Data Transmission System. *IEEE Trans. Commun.*, 15:805–811, Dec. 1967.

[SCC05] P. Sandeep, S. Chandan, and A. K. Chaturvedi. ISI-free pulses with reduced sensitivity to timing errors. *IEEE Communications Letters*, 9:292–294, Apr. 2005.

[She85] P. Sherman. Circulant approximations of the inverses of Toeplitz matrices and related quantities with applications to stationary random processes. *IEEE Trans. ASSP*, 33:1630–1632, Dec. 1985.

[SJB03] F.-W. Sun, Y. Jiang, and J. S. Baras. On the convergence of the inverses of Toeplitz matrices and its applications. *IEEE Trans. IT*, 49:180–190, Jan. 2003.

[SL05] R. Song and S.-H. Leung. A novel OFDM receiver with second order polynomial Nyquist window function. *IEEE Communications Letters*, 9:391–393, May 2005.

[SP61] D. Slepian and H. O. Pollak. Prolate spheroidal wave functions, Fourier analysis and uncertainty - I. *Bell Syst. Tech. J.*, 40:43–63, Jan. 1961.

[Std97] IEEE Std. 802.11. *Wireless Local Area Networks Standard.* IEEE, Nov. 1997.

[Std04] IEEE Std. 802.16. *Local and metropolitan area networks, Part 16: Air Interface for fixed broadband wireless access systems.* IEEE, Oct. 2004.

[TB04] P. Tan and N. C. Beaulieu. Improved BER performance in OFDM systems with frequency offset by novel pulse-shaping. In *Proc. Global Telecommunications Conference, GLOBECOM '04*, volume 1, pages 230–236, 29 Nov.-3 Dec. 2004.

[TFJ96] J. R. Treichler, I. Fijalkow, and C. R. Johnson. Fractionally spaced equalizers: How long should they really be? *IEEE Signal Processing Magazine*, 13:65–81, May 1996.

[TL98] U. Tureli and H. Liu. Blind carrier synchronization and channel identification for OFDM communications. In *Proc. IEEE International Conference on Acoustics, Speech, and Signal Processing, ICASSP '98*, volume 6, pages 3509–3512, 12-15 May 1998.

[Tu93] J. C. Tu. Optimum MMSE equalization for staggered modulation. In *Conference Record of The Twenty-Seventh Asilomar Conference on Signals, Systems and Computers*, volume 2, pages 1401–1406, Nov. 1993.

[Vah95] A. Vahlin. *Optimisation and analysis of OFDM communication systems.* Dr.ing thesis. NTNU (former NTH), N-7491, Trondheim, Norway, 1995.

[Vah03] A. Vahlin. Efficient algorithms for modulation and demodulation in OFDM-systems. In *Proc. Norsig 2003*, 2-4 Oct. 2003.

[Vai93] P. P. Vaildyanathan. *Multirate systems and filter banks.* Prentice Hall, Upper Saddle River, NJ, USA, 1993.

[vdBSB97] J. J. van de Beek, M. Sandell, and P. O. Borjesson. ML estimation of time and frequency offset in OFDM systems. *IEEE Trans. SP*, 45:1800–1805, Jul. 1997.

[VH96] A. Vahlin and N. Holte. Optimal finite duration pulses for OFDM. *IEEE Trans. Commun.*, 44:10–14, Jan. 1996.

[VL01] L. Vangelista and N. Laurenti. Efficient implementations and alternative architectures for OFDM-OQAM systems. *IEEE Trans. Commun.*, 49:664–675, Apr. 2001.

[WCSL02] Y. Wang, P. Ciblat, E. Serpedin, and P. Loubaton. Performance analysis of a class of nondata-aided frequency offset and symbol timing estimators for flat-fading channels. *IEEE Trans. SP*, 50:2295–2305, Sept. 2002.

[WE71] S. B. Weinstein and P. M. Ebert. Data Transmission by Frequency Division Multiplexing Using the Discrete Fourier Transform. *IEEE Trans. Commun.*, 19:628–634, Oct. 1971.

[ZH96] Y. Zhao and S.-G. Haggman. Sensitivity to Doppler shift and carrier frequency errors in OFDM systems-the consequences and solutions. In *Proc. IEEE 46th Vehicular Technology Conference, VTC '96*, volume 3, pages 1564–1568, 28 Apr.-1 May 1996.